

Binary Mixtures of Ultracold Quantum Gases in Optical Lattices

A thesis submitted in partial fulfilment of
the requirements for the degree of

Doctor of Philosophy

by

Kuldeep Suthar

(Roll No. 11330018)

Under the supervision of

Prof. Angom Dilip Kumar Singh

Professor

Theoretical Physics Division

Physical Research Laboratory, Ahmedabad, India.



DISCIPLINE OF PHYSICS

INDIAN INSTITUTE OF TECHNOLOGY GANDHINAGAR

2016

to

my family

Declaration

I declare that this written submission represents my ideas in my own words and where others' ideas or words have been included, I have adequately cited and referenced the original sources. I also declare that I have adhered to all principles of academic honesty and integrity and have not misrepresented or fabricated or falsified any idea/data/fact/source in my submission. I understand that any violation of the above will be cause for disciplinary action by the Institute and can also evoke penal action from the sources which have thus not been properly cited or from whom proper permission has not been taken when needed.

Signature

Name: Kuldeep Suthar

(Roll No: 11330018)

Date:

CERTIFICATE

It is certified that the work contained in the thesis titled **“Binary Mixtures of Ultracold Quantum Gases in Optical Lattices”** by Mr. Kuldeep Suthar (Roll No. 11330018), has been carried out under my supervision and that this work has not been submitted elsewhere for a degree.

Prof. Angom Dilip Kumar Singh
Professor
Theoretical Physics Division,
Physical Research Laboratory,
Ahmedabad, India.
(Thesis Supervisor)

Date:

Thesis Approval

The thesis entitled

Binary Mixtures of Ultracold Quantum Gases in Optical Lattices

by

Kuldeep Suthar

(Roll No. 11330018)

is approved for the degree of

Doctor of Philosophy

Examiner

Examiner

Supervisor

Chairman

Date: _____

Place: _____

Acknowledgments

The end of my journey as a graduate student is approaching, and there are many people who have influenced my path, and contributed in one way or another to make this endeavor a successful one, after all. It has been a period of intense learning for me, not only in the scientific arena, but also on a personal level. I would like to reflect on the people whose consistent support and encouragement made this thesis possible. It gives me a great pleasure to acknowledge all of them.

First and foremost, I wish to express sincere gratitude to my advisor Prof. Angom Dilip Kumar Singh for the continuous support during my thesis work and related research, for his patience, motivation, and immense knowledge. I am thankful to him for assigning me thesis problem and giving due importance to my thesis work. His far-sighted guidance and the broad scientific experience helped me during the time of research and writing of this thesis. I am indebted to him for teaching me the basics of the subject and the programming skills. I respect his views towards ethics in scientific activities and thankful to him for teaching me the same.

I acknowledge the help from Dr. Sandeep Gautam and Dr. Arko Roy during my PhD tenure. I must thank them for improving my understanding of the subject and related numerical techniques. More importantly, the preliminary discussions on DNLSE helped me enormously in the code development. I am grateful for their thorough help and the encouragement during research work. I am also thankful to Dr. Siddhartha Chattopadhyay and Dr. Shashi Prabhakar for their constant assistance and cooperation in the computational issues. I express my hearty thanks to my colleagues Sukla, Rukmani and Soumik for the useful and stimulating discussions on various topics.

I express my gratitude to the Director, Dean, academic committee members and the area chairman Prof. H. Mishra for providing the necessary facilities to carry out the research work. I am thankful to academic head Dr. Bhushit G. Vaishnav for his continual support. My debt of gratitude goes to the DSC members Prof. J. R. Bhatt and Prof. B. K. Sahoo for reviewing the work and motivating constantly during these five years. I would also like to thank other faculty members of Theoretical Physics Division, especially Prof. U. Sarkar, Prof. N. Mahajan, Prof. R. Rangarajan, Prof. N. Singh, Prof. S. Mohanty, Prof. S. Goswami, and Prof. P. Konar. Along these lines, I also thank to Prof. R. P. Singh, Prof. J. Banerji, and Prof. K. P. Subramanian for encouraging me during this period. I thank all the instructors for the interesting courses during my course-work at PRL. I am grateful to all the faculty members of the Department of Physics, MLSU, Udaipur, especially Prof. B. L. Ahuja, Prof. R. Pandey and Prof. S. Kumar for inspiring me towards higher studies.

It is my pleasure to acknowledge the help from computer center; in particular the high performance computing (HPC) and Vikram-100 facility which I have used throughout the research work. I am thankful to all members of computer center, especially Mr. Jigar Raval, Mr. Samuel Johnson, Mr. Tejas Sarvaiya and Mr. H. D. Mishra for their sincere support. I am also thankful to the staff members of our division, Administration, Dispensary, Canteen, Workshop and Maintenance section of PRL for their assistance and support. I am grateful to the PRL and IIT-GN Library staff for all the facilities. I thank Dr. T. S. Kumbar of IIT-GN

for mailing interesting articles, and allowing me to access the journals subscribed by IIT-GN. I take this moment to express my gratitude to IIT-GN for registration and PRL for providing research facility.

My stay at PRL will always be memorable due to the presence of wonderful friends. I take this opportunity to appreciate and express my sincere gratitude to my batch-mates Abhaya, Alok, Anirban, Arun, Chithrabhanu, Gaurava, Girish, Guruprasad, Ikshu, Manu, Sanjay, Shraddha and Tanmoy for the good times we have shared together, without you all it would have been dreary. I would also like to thank my PRL friends Avdhesh, Damodar, Dillip, Girish, Gulab, Monojit, Nabyendu, Naveen, Ravi, Sudip, and Yashpal for creating an enjoyable environment. I must not forget the support from my junior friends with whom I spent time during this period. I wish to thank Aman, Apurv, Ashim, Bharti, Bhavesh, Bivin, Chandan, Newton, Nijil, Pankaj, Pradeep, Rahul, Venkatesh, and Vishnu for the same. I sincerely thank to all the research scholars and PDFs of PRL. The festival celebration, table tennis game till late night hours, and many other activities will always be unforgettable moments in PRL.

Of course, I would not have been able to reach this position without the love, unflinching support and encouragement of my family over the years. I have no words to express immeasurable gratitude to my parents and family members. I am also indebted to my (late) grandmother, grandfather, brothers, sister, uncle and aunt for their infinite love, unquestioning belief, heartfelt blessings, and unconditional care. Last but not the least, I am indebted to Pooja for her love, immense understanding and companionship. She has been a great source of motivation and I would like to thank her for cheering me up in the final period of writing.

Kuldeep Suthar

Abstract

The stationary state, and dynamics of the ultracold bosons in optical lattices at zero temperature are well described by the discrete nonlinear Schrödinger equation (DNLSE). This equation is valid in the tight-binding limit, and used for the superfluid (SF) phase of bosons or Bose-Einstein condensate (BEC) in optical lattices. The recent experimental realizations of the binary mixtures of ultracold bosons in optical lattices provide the motivation to study the effects of finite temperatures in the lattice system. We report the development of the coupled DNLSEs, and the Hartree-Fock-Bogoliubov formalism with the Popov (HFB-Popov) approximation for the two-component BECs (TBECs) or binary condensate mixtures of dilute atomic gases in optical lattices. This method is ideal to study the ground state density profiles, and the evolution of the low-lying quasiparticle modes at zero as well as finite temperatures. The thesis can be broadly divided into three parts. The first two parts are results of the zero temperature calculations, which examine the quasiparticle excitation spectra of the TBECs in quasi-1D and quasi-2D optical lattices. The third part deals with the finite temperature results, and pertains to the investigation of the finite temperature effects on the quasiparticle mode evolution of the TBECs. The spontaneous symmetry breaking of $U(1)$ global gauge symmetry results into two Nambu-Goldstone (NG) modes corresponding to each of the species in quasi-1D TBECs. However, at phase separation an extra NG mode emerges with *sandwich* type density profile in the immiscible phase. We investigate the role of quantum fluctuations on the quasiparticle mode evolution for quasi-1D TBECs. In the presence of the fluctuations, an extra NG mode which appears at phase separation gets hardened, and a symmetry broken *side-by-side* density profile appears in the immiscible phase. Furthermore, we examine the ground state geometry, and the quasiparticle spectra of quasi-2D TBECs. We observe that the TBECs acquire the side-by-side geometry when it is tuned from miscible to the immiscible phase. The energies of the quasiparticle modes are softened as the system is tuned towards the phase separation, and harden after phase separation. In the miscible domain the quasiparticle modes are degenerate, and this degeneracy is lifted after the phase separation. Furthermore, in the miscible domain, the quasiparticles have well-defined azimuthal quantum numbers, and hence shows a clear structure in the dispersion curve. On the other hand,

the dispersion curve of the immiscible phase does not have a discernible trend due to the presence of the mode mixing. We also report the enhancement in the miscibility of the condensates of quasi-2D TBEC in the presence of the thermal fluctuations.

Keywords: Bose-Einstein condensation, Multicomponent condensates, Optical lattice, Bose-Hubbard model, Phase separation, Quantum fluctuations.

Abbreviations

BEC	Bose-Einstein condensate
BCS	Bardeen-Cooper-Schrieffer
SF	Superfluid
MI	Mott insulator
ODLRO	Off-diagonal long-range order
TBEC	Two-component Bose-Einstein condensate
BZ	Brillouin zone
BH	Bose-Hubbard
DMRG	Density matrix renormalization group
QMC	Quantum Monte Carlo
DNLSE	Discrete nonlinear Schrödinger equation
BdG	Bogoliubov-de Gennes
HFB	Hartree-Fock-Bogoliubov
GPE	Gross-Pitaevskii equation
TBA	Tight-binding approximation
SSB	Spontaneous symmetry breaking
NG	Nambu-Goldstone
RTI	Rayleigh-Taylor instability
IC	Iteration cycle

Contents

Acknowledgements	i
Abstract	iii
Abbreviations	v
Contents	vii
List of Figures	xi
1 Introduction	1
1.1 Bose-Einstein condensation	3
1.1.1 Theory of a Bose-Einstein condensate	3
1.1.2 Two-component Bose-Einstein condensates	5
1.2 Optical lattices	6
1.2.1 Atom-light interaction : dipole potentials	8
1.2.2 Lattice geometry	10
1.2.3 Band structure	12
1.3 Quantum phase transition	15
1.4 Binary mixtures in optical lattices	18
1.5 Objectives of the present study	20
1.6 Overview of the chapters	22
2 Finite temperature theory of bosons in optical lattices	25
2.1 Hartree-Fock-Bogoliubov theory	26
2.2 Single-component BEC	30

2.2.1	Optical lattice and tight-binding approximation	30
2.2.2	Bose-Hubbard Hamiltonian	32
2.2.3	Bogoliubov approximation	33
2.2.4	Bogoliubov-de Gennes (BdG) equations	34
2.2.5	Hartree-Fock-Bogoliubov (HFB) equations	37
2.2.6	HFB-Popov approximation	39
2.3	Two-component BEC	39
2.3.1	Two-component Bose-Hubbard Hamiltonian	41
2.3.2	HFB-Popov approximation for the TBEC	41
2.3.3	TBEC in quasi-2D optical lattices	47
3	Topological transition of quasi-1D binary condensates	51
3.1	Zero temperature mode evolution of trapped TBEC	54
3.1.1	Third Goldstone mode in ^{87}Rb - ^{85}Rb TBEC	55
3.1.2	Third Goldstone mode in ^{133}Cs - ^{87}Rb TBEC	59
3.2	Position exchange of species	61
3.3	Effect of quantum fluctuations	63
3.4	Conclusions	66
4	Quasiparticle spectra and dispersion curves of quasi-2D binary BECs	67
4.1	Mode evolution of trapped TBEC at $T = 0$ K	69
4.1.1	^{87}Rb - ^{85}Rb TBEC	70
4.1.2	^{133}Cs - ^{87}Rb TBEC	74
4.2	Dispersion relations	77
4.2.1	Miscible domain	79
4.2.2	Immiscible domain	81
4.3	Conclusions	82
5	Thermal fluctuations enhanced miscibility of condensate mixtures	85
5.1	Overlap integral and correlation function	87
5.2	Quasiparticle spectra of trapped TBEC	88
5.2.1	Zero temperature	90
5.2.2	Finite temperatures	90

5.3	Correlation function of TBEC	96
5.4	Conclusions	97
6	Summary and future directions	99
A	Numerical Details	101
	Bibliography	103
	List of publications	133
	Publications attached with thesis	135

List of Figures

1.1	Absorption images of momentum distribution of the ultracold bosons in optical lattice potential.	2
1.2	Absorption images of ^{87}Rb - ^{85}Rb TBEC at two different scattering lengths of ^{85}Rb	7
1.3	Schematical drawing of the multidimensional optical lattice potential formed by superimposing counter-propagating laser beams.	12
1.4	Band structure in an optical lattice for different depths $V_0 = \{0, 5, 10\} E_R$	14
1.5	Zero temperature mean-field phase diagram of SF-MI transition for the homogeneous and inhomogeneous system.	16
1.6	Interference pattern of ^{87}Rb for different optical lattice depths $V_0 = \{6, 11, 16\} E_R$	19
3.1	The low-lying quasiparticle amplitudes for ^{87}Rb condensate trapped in quasi-1D optical lattices.	52
3.2	The evolution of the low-lying mode energies as a function of the intraspecies interaction of the ^{85}Rb (U_{22}) in the ^{87}Rb - ^{85}Rb TBEC held in quasi-1D optical lattices.	56
3.3	The evolution of the quasiparticle amplitudes corresponding to the Kohn mode as the intraspecies interaction of ^{85}Rb (U_{22}) is decreased from $0.25E_R$ to $0.062E_R$	57
3.4	The geometry of the condensate density profiles and its transition from the miscible to the immiscible regime.	58

3.5	The evolution of the energies of the low-lying modes as a function of the interspecies interaction (U_{12}) in Cs-Rb TBEC held in a quasi-1D lattice potential.	60
3.6	The evolution of the quasiparticle amplitudes corresponding to the Kohn mode as the interspecies interaction is increased from $0.2E_R$ to $0.35E_R$ for a Cs-Rb TBEC in quasi-1D lattice potential at $T = 0$ K.	61
3.7	The evolution of the quasiparticle amplitudes corresponding to the Kohn mode for ^{87}Rb - ^{85}Rb TBEC in the presence of the fluctuations as the intraspecies interaction of ^{85}Rb (U_{22}) is decreased from $0.2E_R$ to $0.05E_R$	62
3.8	The fluctuation-induced transition in the geometry of the total density profile (condensate + quantum fluctuations) of a TBEC at $T = 0$ K in a quasi-1D lattice potential.	64
3.9	The evolution of the quasiparticle amplitudes corresponding to the Kohn mode for the Cs-Rb TBEC in the presence of quantum fluctuations at $T = 0$ K.	65
4.1	The geometry of the condensate density profiles and its transition from the miscible to the immiscible domain for the ^{87}Rb - ^{85}Rb TBEC.	70
4.2	The evolution of the low-lying quasiparticle mode energies as a function of the intraspecies interaction U_{22} for the ^{87}Rb - ^{85}Rb TBEC held in quasi-2D optical lattices.	71
4.3	The evolution of the quasiparticle amplitudes corresponding to the slosh mode of the ^{87}Rb - ^{85}Rb TBEC as U_{22} is decreased from $0.30E_R$ to $0.05E_R$	72
4.4	The evolution of the quasiparticle amplitudes corresponding to the other slosh mode, which is degenerate to the mode shown in Fig. 4.3 in the miscible domain.	73
4.5	The geometry of the condensate density profiles and its transition from the miscible to the immiscible domain in the ^{133}Cs - ^{87}Rb TBEC.	74

4.6	The evolution of the low-lying mode energies as a function of the interspecies interaction in the ^{133}Cs - ^{87}Rb TBEC held in quasi-2D optical lattices.	75
4.7	The evolution of the quasiparticle amplitudes corresponding to the slosh mode of the ^{133}Cs - ^{87}Rb TBEC as U_{12} is increased from $0.5E_R$ to $1.2E_R$	76
4.8	The evolution of the quasiparticle amplitudes corresponding to the slosh mode, which is degenerate with the mode shown in Fig. 4.7 in the miscible domain.	77
4.9	The discrete BdG quasiparticle dispersion curve of the ^{87}Rb - ^{85}Rb TBEC.	78
4.10	The quasiparticle amplitudes in the miscible domain of a TBEC.	80
4.11	The quasiparticle amplitudes in the immiscible domain of a TBEC.	81
5.1	The condensate density profiles at different temperatures in the phase-separated domain of ^{87}Rb - ^{85}Rb TBEC.	89
5.2	The noncondensate density profile at different temperatures in the phase-separated domain of ^{87}Rb - ^{85}Rb TBEC.	90
5.3	The overlap integral as a function of the temperature.	91
5.4	The quasiparticle energies of the low-lying modes as a function of the temperature in the phase-separated domain of ^{87}Rb - ^{85}Rb TBEC.	92
5.5	The mode function of the first excited mode (slosh mode) as a function of the temperature in the phase-separated domain of ^{87}Rb - ^{85}Rb TBEC.	93
5.6	The mode function of the second excited mode (slosh mode) for ^{87}Rb - ^{85}Rb TBEC, which at $T/T_c \geq 0.185$ becomes degenerate to the mode shown in Fig. 5.5.	93
5.7	The mode function corresponding to the Kohn mode as a function of the temperature in the phase-separated domain of ^{87}Rb - ^{85}Rb TBEC.	94
5.8	The mode function of the Kohn mode for ^{87}Rb - ^{85}Rb TBEC which is degenerate to the mode shown in Fig. 5.7.	94
5.9	The evolution of the interface mode in the phase-separated domain of ^{87}Rb - ^{85}Rb TBEC with temperature.	95

- 5.10 The normalized first-order off-diagonal correlation function $g_k^{(1)}(0, \mathbf{r})$ of ^{87}Rb (upper panel) and ^{85}Rb (lower panel) at $T/T_c = 0, 0.08, 0.17,$ and 0.2 96

Chapter 1

Introduction

The achievement of Bose-Einstein condensation in dilute atomic gases [1–3] in 1995 has served to create an ideal test bed for a myriad of many-body quantum phenomena. The experimental milestone of laser cooling and trapping [4–6], and the observation of the Bose-Einstein condensate (BEC) of ^{87}Rb , ^{23}Na , and ^7Li were recognized with the Nobel prizes in 1997 and 2001, respectively. Since the first ever realization of BEC, the field of ultracold atoms has completed two decades in 2015 [7]. The investigation on BECs have lead to a studies on a variety of processes that represent the intersection of many research fields, ranging from quantum optics to condensed matter physics. The subsequent achievements of BECs in optical lattice potential [8–12], quantum degeneracy in atomic Fermi gases [13], and in ultracold molecular gases [14–16] made the physics of ultracold quantum gases even more wider and diverse. The ultracold quantum gases allow for, to mention a few, the investigation of hydrodynamics, superfluidity, topological defects, exotic phases, transport in lattice [17], and the BEC-BCS crossover [18–20]. In addition to this, the optical lattices allow for the study of interacting matter waves and strongly correlated systems [21]. The pioneering experiments with optical lattices initiated the growing field of quantum simulation using ultracold atoms [22].

The ability to load ultracold atoms in periodic light field, represented by the optical lattices, is a versatile system which connects atomic and condensed matter physics [23, 24]. Indeed, the motion of an electron in a crystal can be interpreted as motion of a single quantum particle in a periodic potential, and this is equivalent to an ultracold

atom moving in an optical lattice. In recent years, the experiments in optical lattices have grown from cubic to more complex geometries [25, 26]. However, these experiments are performed at finite temperatures. Therefore, the presence of quantum or thermal fluctuations, and their interactions with the condensate atoms play a vital role in the study of such systems. A remarkable significance of BEC in an optical lattice is that it shows a quantum phase transition [27, 28]. When a BEC is subjected to a lattice potential, atoms can be in one of the two phases depending on the depth of the lattices. A superfluid (SF) phase appears for small interatomic interactions compared to the tunnel coupling and the system is in Mott insulator (MI) phase for the opposite limit. It is possible to drive the system from one phase to the other by tuning the ratio of the interaction to the tunneling energy, and hence by changing the depth of the potential [29, 30]. In Fig. 1.1, the diffraction images from the first experimental realization of the superfluid-to-insulator transition is shown. In the figure, the images are obtained after suddenly releasing the atoms from optical lattice with different potential depths. As the depth of the lattice potential increases, the resulting interference pattern changes markedly. In the superfluid regime [Fig. 1.1(a-d)], a narrow interference maxima is visible, exhibiting the long-range phase coherence across the lattice. The interference pattern completely vanishes for the lattice with depth $20E_R$.

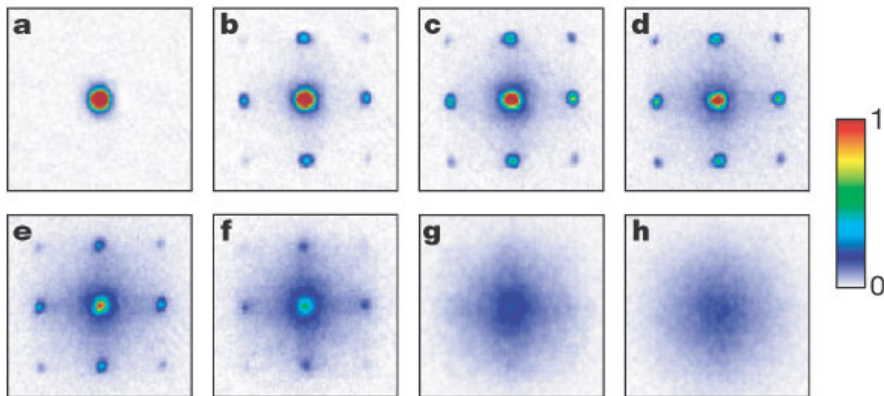


Figure 1.1: Absorption images of momentum distribution of the ultracold bosons in optical lattice potential. The values of the lattice depths (a-h) are 0, 3, 7, 10, 13, 14, 16, and 20 in terms of the recoil energy E_R . Reprinted from Macmillan Publishers Ltd: [Greiner et al., Nature (London) **415**, 39 (2002)], copyright © 2002.

1.1 Bose-Einstein condensation

The Bose-Einstein condensation is a quantum phenomenon relying on the indistinguishability of the bosonic particles composing the atomic ensemble. The quantum statistics of bosons was first proposed in 1924, when Satyendra Nath Bose examined the nature of photons, and he was able to deduce the Planck's law for black-body radiation from the statistical properties of photons. This work was subsequently extended to an ideal gas of bosons by Albert Einstein who found that below a critical temperature T_c all the atoms would occupy the ground state of the system. The behaviour of a classical gas is described by the Maxwell-Boltzmann distribution where the thermal energy is much higher than the intrinsic level spacing of the system. At temperatures below T_c , spatial extent of atomic wave function is of the order of the interatomic separation. It is to be mentioned that the mean physical extent of wave packet at temperature T is defined by the thermal de Broglie wavelength $\lambda_{\text{dB}} = h/\sqrt{2\pi mk_B T}$ with m being mass of the atomic species. A significant deviation occurs from the Maxwell-Boltzmann statistics when the interparticle separation $n^{-1/3} \simeq \lambda_{\text{dB}}$, where n is density of the system, and then the system is described by the Bose-Einstein statistics. In this case, the coherence among the atomic wave packets grows, and a macroscopic occupation of the ground state appears. At BEC phase transition, the *phase-space density* for an ideal and homogeneous Bose gas is $n\lambda_{\text{dB}}^3 \approx 2.612$. For alkali atoms, the typical density of the Bose-condensed atomic cloud is $10^{13} - 10^{15} \text{ cm}^{-3}$ with critical temperatures in the range from 100 nK to a few μK .

1.1.1 Theory of a Bose-Einstein condensate

Consider a non-interacting Bose gas of N atoms in the grand canonical ensemble at temperature T . The population of atoms in the i th energy level with energy ϵ_i is given by

$$N_i = \frac{1}{e^{(\epsilon_i - \mu)/k_B T} - 1}, \quad (1.1)$$

where μ is the chemical potential which is kept less than the ground state energy (ϵ_0) to avoid the unphysical negative population. When the chemical potential approaches ϵ_0 , the number of atoms in the ground state N_0 then diverges, and for a fixed number

of atoms $N = \sum_i N_i$, the ground state has macroscopic occupation of atoms.

To determine T_c for bosons trapped in the confining potential of harmonic oscillator potential we separate the number of atoms in the lowest level to the total sum

$$N - N_0 = \zeta(3) \left(\frac{k_B T}{\hbar \bar{\omega}} \right)^3, \quad (1.2)$$

where $\bar{\omega}$ is the geometric mean of the three oscillator frequencies of the three-dimensional (3D) harmonic oscillator. Here $\zeta(\alpha) = \sum_{k=1}^{\infty} k^{-\alpha}$ is the Riemann zeta function, where $\alpha = 3$ for a 3D harmonic oscillator. At $T = T_c$, the ground state population is zero, and hence the critical temperature to achieve BEC is

$$T_c = \frac{\hbar \bar{\omega}}{k_B} \left(\frac{N}{\zeta(3)} \right)^{1/3} = 0.94 \frac{\hbar \bar{\omega}}{k_B} N^{1/3}. \quad (1.3)$$

Below this temperature the ground state is macroscopically populated and the condensate fraction increases with decrease in temperature [31]. In terms of temperature, it is given by

$$\frac{N_0}{N} = 1 - \left(\frac{T}{T_c} \right)^3. \quad (1.4)$$

Another important characteristic of BEC is the off-diagonal long-range order (ODLRO). A system of non-interacting atoms possess an ODLRO, if the single-particle density matrix $\rho_1(\mathbf{r}, \mathbf{r}')$ has a large eigenvalue, i.e., an eigenvalue proportional to the total number of particles N . In the presence of the BEC, $\rho_1(\mathbf{r}, \mathbf{r}')$ does not vanish over large distances $|\mathbf{r} - \mathbf{r}'|$, but approaches a finite value. The condition for a BEC to exist is given by the Penrose-Onsager criterion [32]

$$\frac{n_M}{N} = e^{O(1)}, \quad (1.5)$$

where n_M is the maximum eigenvalue which represents the number of condensed bosons and $e^{O(1)}$ is a positive number of the order unity. The ratio n_M/N is referred to as the condensate fraction. This definition is applicable irrespective of the presence or absence of the interactions. When the system is not spatially uniform, the condition of ODLRO is given by

$$\rho_1(\mathbf{r}, \mathbf{r}') \rightarrow \psi^*(\mathbf{r})\psi(\mathbf{r}') \quad \text{as} \quad |\mathbf{r} - \mathbf{r}'| \rightarrow \infty, \quad (1.6)$$

where $\psi(\mathbf{r})$ is the *condensate wave function* or the *order parameter* of the system. The coherent properties of the many-body system can be determined using the order parameter of the BEC.

In addition to the ground state, the collective modes are also of importance. The elementary excitations of the condensate were investigated by Bogoliubov using a theory of small fluctuations around the ground state. The Bogoliubov excitation spectrum of a homogeneous system is given by

$$\epsilon_q = \sqrt{(\epsilon_q^0)^2 + 2gn\epsilon_q^0}, \quad (1.7)$$

where $\epsilon_q = \pm\hbar\omega$ with ω is the frequency of the excitation, $\epsilon_q^0 = \hbar^2q^2/2m$ is the free-particle energy, and g is the strength of the interatomic interaction. The dispersion law corresponds to the phonon excitations $\omega \propto q$ for low momenta, and free-particle excitations $\omega \propto q^2$ for large momenta. The velocity of sound for the low momenta is $c = \sqrt{gn/m}$. It is worth noting that this velocity coincides with the hydrodynamic expression $c = [(1/m)\partial p/\partial n]^{1/2}$ for a gas with pressure p and density n . In addition, the excitations due to finite temperature and the interactions which lead to depletion of the condensate can be studied. At zero temperature, the condensate fraction with the interatomic interactions is reduced to [33]

$$\frac{N_0}{N} = 1 - \frac{8}{3\sqrt{\pi}} \sqrt{na_s^3}. \quad (1.8)$$

The depletion of the condensate becomes larger as the parameter na_s^3 increases, where a_s is the s-wave scattering length. In superfluid helium, the high density and strong interactions lead to a Bose-condensed fraction of only $\approx 10\%$ [34]. For the harmonically trapped dilute atomic gases, an important role is played by the ratio Na_s/a_{osc} , where a_{osc} is harmonic oscillator length. A comprehensive study of the collective excitations is essential to examine the quantum many-body system. The idea of BEC is also exploited in other field of physics, to name a few are understanding the phenomena of superconductivity [35, 36], Hawking radiation [37–39], and quantum processes of the early universe [40–42].

1.1.2 Two-component Bose-Einstein condensates

Two-component Bose-Einstein condensates (TBECs) are the mixture of two condensates of two different atomic species or two isotopes of the same element or two different hyperfine states of the same atomic species. This field is currently the focus

of intensive experimental and theoretical research, exhibiting rich physics, inaccessible to single-component BEC experiments. The first TBEC composed of ^{87}Rb atoms in the states $|F = 2, m_F = 2\rangle$ and $|F = 1, m_F = -1\rangle$ was produced in an Ioffe-type magnetic trap by sympathetic cooling [43]. Over the last two decades, the TBECs have been realized in two different atomic species [44–49], in two different isotopes [50–52], and in two different hyperfine states of the same species [43, 53–61]. TBECs have been used to explore diverse phenomena such as pattern formation [62–65], nonlinear dynamical excitations [59, 66, 67], phase separation [46, 48–50, 61], Kibble-Zurek mechanism [68], collective excitations [56], the production of dipolar molecules [69–71], etc. Among these the phenomena of phase separation is a unique property of TBECs. For the TBECs with same trap center three different types of density profiles have been observed. A miscible phase where both components overlap at the trap center; a symmetric sandwich profile where one component forms a shell structure around the other; and an asymmetric side-by-side immiscible phase where the center of mass of the two components do not coincide. With the experimental advances of Feshbach resonance, it is possible to tune the interatomic interactions, and drive the TBECs from miscible to the immiscible phase. The experimental observation of the miscible and immiscible phase for ^{87}Rb - ^{85}Rb TBEC is shown in Fig. 1.2. In the figure, Δ is the immiscibility parameter, which is positive ($\Delta > 0$) for the miscible phase and negative ($\Delta < 0$) for the immiscible phase. These density profiles of the TBECs are the important platforms to understand the rethermalization rate [57], structure of the vortex lattice [72, 73], coarse-graining dynamics [62, 74, 75], and various instabilities in the fluid dynamics [76–78].

1.2 Optical lattices

Neutral atoms interact with the laser light field in both a conservative and a dissipative ways. The conservative interaction of atoms with the laser field involves a modification of the energy levels of the atoms. This arises due to the interaction of the light field with the light-induced dipole moment of the atoms which leads to a shift in the energy called *ac-stark shift*. For large detuning of the light with respect to the atomic resonance, the

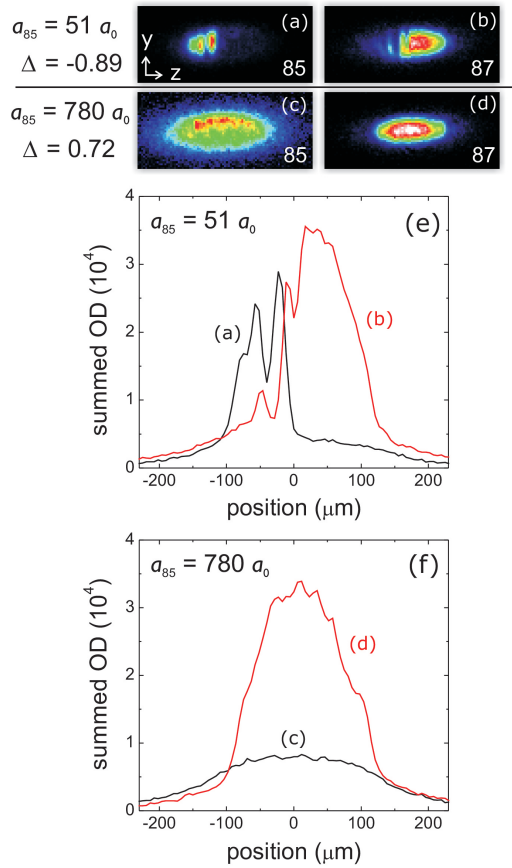


Figure 1.2: Absorption images of ^{87}Rb - ^{85}Rb TBEC at two different scattering lengths of ^{85}Rb . (a), (b) Show immiscible phase with side-by-side geometry and (c), (d) show miscible phase at $a_{85} = 51a_0, 780a_0$, respectively. (e), (f) The optical density (OD) of ^{87}Rb (red) and ^{85}Rb (black) in the radial direction. Reprinted from [Papp et al., Phys. Rev. Lett. **101**, 040402 (2008).] Copyright © 2008 by the American Physical Society.

spontaneous emission can be neglected, and the energy shift can be used for trapping neutral atoms in the conservative potential [79, 80].

In contrast to this, the dissipative interaction arises due to the absorption of photons followed by subsequent spontaneous emission. It results in a dissipative force on the atoms caused by the momentum transfer to the atoms by the absorbed and spontaneously emitted photons. This force is widely used for laser-cooling and magnetic-optical trapping of atoms [81]. By shining a spatially modulated light onto a cloud of cold atoms an energy landscape can be formed, where the local potential energy is proportional to the light intensity [82].

1.2.1 Atom-light interaction : dipole potentials

We consider a two-level atomic system consisting of a ground state $|g\rangle$ and an excited state $|e\rangle$ with energy separation $\hbar\omega_0 = E_e - E_g$, where ω_0 is the frequency of the atomic resonance. When an atom is placed into a laser light, it interacts with the monochromatic electric field $\mathbf{E}(\mathbf{r}, t) = E(\mathbf{r})\hat{e}\cos(\omega t - kz)$ which is propagating along the z direction with polarization vector \hat{e} . Here, E is the electric field amplitude, k is the wave vector, and $\omega = 2\pi\nu$ is the angular frequency of the oscillation of the field. The atom-light interaction induces an electric dipole moment \mathbf{p} which is proportional to the electric field, i.e.

$$\mathbf{p} = \alpha(\omega)\mathbf{E}. \quad (1.9)$$

Here, $\alpha(\omega)$ is the complex polarizability which depends on the laser frequency. The resulting dipole potential is

$$V_{\text{dip}} = -\frac{1}{2}\langle \mathbf{p} \cdot \mathbf{E} \rangle = -\frac{1}{2\epsilon_0 c} \text{Re}(\alpha)I, \quad (1.10)$$

where $\langle \rangle$ is the time average over one oscillation period. This average takes into account that the light field is rapidly oscillating. The $1/2$ factor arises from the fact that the dipole is only induced and not permanent. Here, $I = \epsilon_0 c |E|^2/2$ is the intensity of the laser light with c as the speed of light, and ϵ_0 is the electric permittivity. The potential energy of the atom is thus proportional to the intensity of the laser and on the real part of the polarizability. The dipole force acting on the atoms by the laser light field is

$$F_{\text{dip}}(\mathbf{r}) = -\nabla V_{\text{dip}} = -\frac{1}{2\epsilon_0 c} \text{Re}(\alpha)\nabla I. \quad (1.11)$$

The dipole force vanishes for atoms moving in an uniform field, and is stronger where the inhomogeneity of the field is large. Another quantity of interest is the scattering rate Γ_{sc} , that describes the rate at which photons from the laser beams are absorbed and re-emitted, causing heating of the atoms. This rate is defined as the ratio of the average energy absorbed by the atom per unit time to the photon energy $\hbar\omega$, which is given by

$$\Gamma(\mathbf{r}) = \frac{\frac{d\mathbf{p}}{dt} \cdot \mathbf{E}}{\hbar\omega} = \frac{1}{\hbar\epsilon_0 c} \text{Im}(\alpha)I(\mathbf{r}). \quad (1.12)$$

The dynamic polarizability can be approximately calculated using the Lorentz's model of a classical damped oscillator [83]

$$\alpha(\omega) = 6\pi\epsilon_0 c^3 \frac{\Gamma/\omega_0^2}{\omega_0^2 - \omega^2 + i(\omega^3/\omega_0^2)\Gamma}, \quad (1.13)$$

where Γ is the line-width of the atomic transition with frequency ω_0 . A more appropriate approach to calculate the atomic polarizability is given by a semi-classical model, where the line-width is determined by the dipole matrix element between the ground state $|g\rangle$ and the excited state $|e\rangle$ as

$$\Gamma = \frac{\omega_0^3}{3\pi\epsilon_0\hbar c^3} |\langle e|\boldsymbol{\mu}|g\rangle|^2, \quad (1.14)$$

with $\boldsymbol{\mu} = -e\mathbf{r}$ is the electric dipole operator. Using the above expressions, strength of the dipole potential and the scattering rate can be written as

$$V_{\text{dip}} = -\frac{3\pi c^2}{2\omega_0^3} \left(\frac{\Gamma}{\omega_0 - \omega} + \frac{\Gamma}{\omega_0 + \omega} \right) I(\mathbf{r}), \quad (1.15)$$

$$\Gamma_{\text{sc}} = \frac{3\pi c^2}{2\hbar\omega_0^3} \left(\frac{\omega}{\omega_0} \right)^3 \left(\frac{\Gamma}{\omega_0 - \omega} + \frac{\Gamma}{\omega_0 + \omega} \right)^2 I(\mathbf{r}), \quad (1.16)$$

where $\omega - \omega_0 = \Delta$ is the detuning of the laser light at frequency ω from the atomic resonance frequency ω_0 and $\omega + \omega_0 = \Delta_+$ represents the fast rotating term. In most of the experiments the laser frequency ω is tuned such that $|\Delta| \ll \omega_0$. In this limit, the rotating-wave approximation is employed, where the fast rotating term is neglected, which results in

$$V_{\text{dip}} = \frac{3\pi c^2}{2\omega_0^3} \frac{\Gamma}{\Delta} I(\mathbf{r}), \quad (1.17)$$

$$\Gamma_{\text{sc}} = \frac{3\pi c^2}{2\hbar\omega_0^3} \left(\frac{\Gamma}{\Delta} \right)^2 I(\mathbf{r}). \quad (1.18)$$

These equations describe the main characteristics of the atom-light interaction. The dipole force is proportional to I/Δ , while the scattering rate is proportional to I/Δ^2 . For blue detuned laser light ($\Delta > 0$), the dipole force acts on atoms towards the region of low intensity and results in a repulsive potential. On the other hand, for red detuned laser light ($\Delta < 0$), the dipole force attracts the atoms toward the region of high intensity and results in an attractive potential. It is therefore possible to minimize the inelastic scattering processes by detuning the laser light far from the atomic resonance.

The corresponding reduction in the dipole potential can be compensated by higher laser intensity.

Since the real atoms exhibit much more complicated structure and are insufficiently described by a two-level approach. In the case of multilevel alkali atoms, such as Rb and K, the more complex structure can approximately be taken into account by the calculation of the dipole potential, and the scattering rate for each individual transitions. The results are then summed, and weighted by their corresponding oscillator strengths [83, 84]. The line-width of the $J \rightarrow J'$ fine-structure transition is given by

$$\Gamma = \frac{e^2 \omega_0^2}{2\pi \epsilon_0 m_e c^3} \frac{2J+1}{2J'+1} f, \quad (1.19)$$

where e and m_e are the charge and mass of the electron. The oscillator strength f describes how the energy of the classical dipole is distributed among different transitions [85]. For ^{87}Rb the fine-structure splitting of the 5P state leads to two D_1 and D_2 transition lines. For large detunings the hyperfine splitting of the level can be neglected. In the case of linearly polarized light, the dipole potential is then given by [83]

$$V_{\text{dip}} = \frac{3\pi c^2}{2\omega_0^3} \left(\frac{2}{3} \frac{\Gamma_{D_2}}{\Delta_{D_2}} + \frac{1}{3} \frac{\Gamma_{D_1}}{\Delta_{D_1}} \right) I(\mathbf{r}), \quad (1.20)$$

where Γ_{D_i} and Δ_{D_i} are the line-width and detuning of the transition line D_i ($i = 1, 2$).

1.2.2 Lattice geometry

The dipole force makes it possible to realize many lattice geometries by using different laser configurations. In experiments, a Gaussian laser beam is used to create such interference pattern and a far red detuned laser beam creates an attractive potential for the atoms. The intensity profile of a Gaussian beam is

$$I(\mathbf{r}, z) = \frac{2P}{\pi w^2(z)} \exp\left(-\frac{2r^2}{w^2(z)}\right), \quad (1.21)$$

where P is the total power of the laser beam, $w(z) = w_0 \sqrt{1 + (z/z_R)^2}$ is the radius of the beam at z with w_0 is the beam waist and $z_R = \pi w_0^2 / \lambda_L$ is the Rayleigh length, defined as the distance from the beam waist at which the radius and the cross-sectional area are increased by a factor of $\sqrt{2}$ and 2, respectively. Here, λ_L is the wavelength of the laser beam. The simplest possible geometry is the one-dimensional (1D) lattice,

which is created by retro-reflected laser beam, such that it creates a standing wave pattern. The resulting intensity distribution is

$$I(z) = I_0 \sin^2(k_L z), \quad (1.22)$$

where I_0 is the maximum intensity and $k_L = 2\pi/\lambda_L$ is the wave number of the laser beam. The corresponding dipole potential due to the constructive interference of the laser beams is

$$V_{\text{latt}}(z) = V_0 \sin^2(k_L z), \quad (1.23)$$

where V_0 is four times the depth of a single laser beam without retro-reflection. Depending on the detuning of the laser light, the intensity pattern [Eq. (1.22)] causes a force that pulls atoms towards the minima or the maxima of the standing wave. The location where the atoms accumulate are called the *sites* of the lattice. In the case of retro-reflected beam, the sites are separated by a lattice spacing also known as lattice constant $a = \lambda_L/2$. In general, for two laser beams which interfere at an angle θ , $a = \lambda_L/2 \sin(\theta/2)$. Periodic potential in higher dimensions are created by superimposing additional laser beams. To create a two-dimensional (2D) optical lattice two orthogonal sets of counter-propagating laser beams are used. A 2D lattice potential is then

$$V_{\text{latt}}(x, y) = V_0 [\cos^2(k_L x) + \cos^2(k_L y) + 2\hat{e}_1 \cdot \hat{e}_2 \cos \phi \cos(k_L x) \cos(k_L y)], \quad (1.24)$$

where \hat{e}_1 and \hat{e}_2 are polarization vectors of the horizontal and vertical standing wave laser fields, respectively and ϕ is the relative phase between them. If the polarization vectors are not orthogonal, but the frequencies of the laser beams are same, then the interference of the lasers result in a potential which depends on the relative phase. The variation in phase leads to chequerboard like pattern for a 2D optical lattice. A square lattice is created by the laser beams with orthogonal polarizations ($\phi = 90^\circ$). In this case, the resulting potential is the sum of two superimposed 1D lattice potentials. The interference term can be suppressed by choosing different laser frequencies for the standing waves. A similar arrangement can be extended in three dimension to create a cubic lattice [86]. The schematic representations of 2D and 3D optical lattice geometries are shown in Fig. 1.3. In optical lattice experiments, in order to suppress

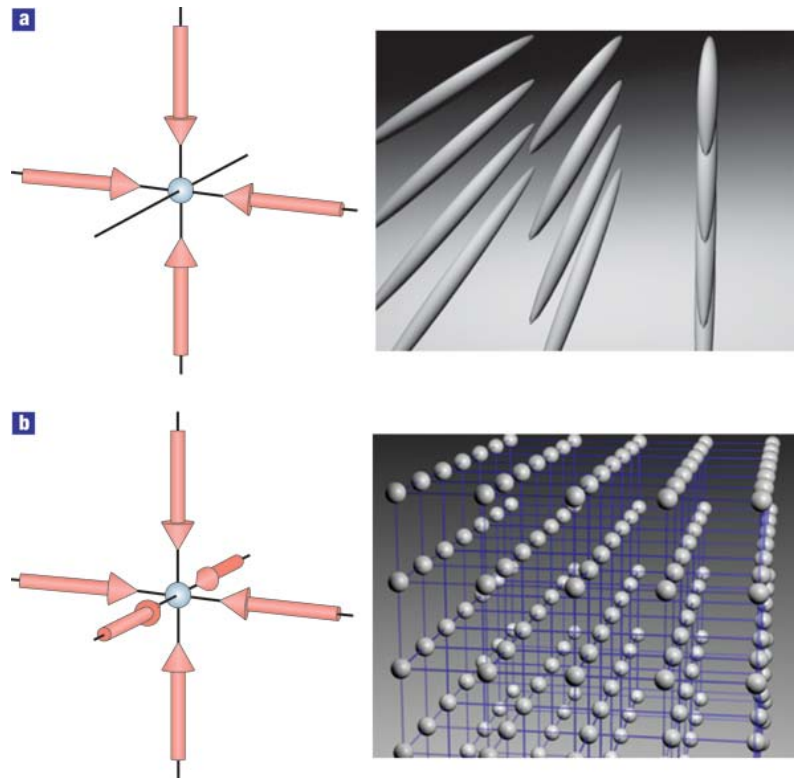


Figure 1.3: Schematical drawing of the multidimensional optical lattice potential formed by superimposing counter-propagating laser beams. (a) Two standing waves orthogonal to each other forms an array of tightly confined potential tubes, which is a 2D optical lattice. (b) A 3D lattice potential is created by superimposing three standing waves to form a 3D simple cubic array of tightly confined harmonic oscillator potentials at each lattice site. Reprinted from Macmillan Publishers Ltd: [Bloch, Nat. Phys. **1**, 23 (2005)], copyright © 2005.

the scattering of atoms from the lattice sites, an envelope confining potential is used. In general, the confining potential is harmonic which arises from the combined effect of the focussed laser beams. In 2D, it is equivalent to the egg-carton-like structure with an additional harmonic confinement.

1.2.3 Band structure

One of the fundamental properties of atoms in an optical lattice is the emergence of the band structure. It is analogous to the electrons in a periodic potential where they can only move in certain energy ranges called energy band [87, 88]. The dispersion relation

is no longer continuous as in the case of a free particle, but exhibits certain forbidden regions which arise from the interaction of the electrons with the periodically arranged ions in the solid. Here, we investigate the single particle wave function and the band structure of ultracold bosons in optical lattices.

A particle in a one-dimensional periodic potential V_{latt} with periodicity a is described by the Schrödinger equation

$$H\varphi_q^{(n)}(x) = E_q^{(n)}\varphi_q^{(n)}(x), \quad (1.25)$$

where $H = \hat{p}^2/2m + V_{\text{latt}}(x)$ is the Hamiltonian with $V_{\text{latt}}(x) = V_{\text{latt}}(x + a)$ and \hat{p} and m are the momentum operator and mass. The wave functions φ are labeled by the quasi-momentum q and the band index n . The quasi-momentum characterizes the phase difference between atoms in different lattice sites. The solutions of the Schrödinger Eq. (1.25) are the Bloch functions, which can be written as products of the plane wave $\exp(iqx/\hbar)$ and a function $u_q^{(n)}$ with the same periodicity as the lattice potential

$$\varphi_q^{(n)}(x) = e^{iqx/\hbar} \cdot u_q^{(n)}(x). \quad (1.26)$$

The quasi-momentum is unique to a reciprocal lattice vector, and therefore for the first Brillouin zone, the restriction on the quasi-momentum is $-\pi/a < q \leq \pi/a$. For a given q there are many solutions to the Schrödinger equation. This equation can be seen as a set of eigenvalue problems in a fixed interval, $0 < x < a$, one eigenvalue for each q . The energy levels in a periodic potential are given in terms of a family of continuous functions $E_q^{(n)}$ each with periodicity of a reciprocal lattice vector $2\pi/a$. These are referred to as the band structure. When we substitute the experimentally relevant sinusoidal potential in Eq. (1.25), then it takes the form

$$-\frac{d^2}{dy^2}\varphi_q^{(n)}(y) + \frac{V_0}{4E_R}[2 - 2\cos(2y)]\varphi_q^{(n)}(y) = \frac{E_q^{(n)}}{E_R}\varphi_q^{(n)}(y), \quad (1.27)$$

where $E_R = \hbar^2 k_L^2/2m$ is the recoil energy and $y = k_L x$. The above equation is recognized as the Mathieu equation

$$\frac{d^2\varphi}{dy^2} + [a + 2s\cos(2y)]\varphi = 0. \quad (1.28)$$

For a fixed value of a and s , the solution of the Mathieu equation is given by the Floquet form $e^{i\nu y}P(y)$ where ν is the characteristic exponent, $a = a(\nu, s)$ is the characteristic

parameter, and $P(y)$ is a complex valued function which is periodic in y . Here, $s = V_0/4E_R$ and $a = E_q^{(n)}/E_R - V_0/2E_R$. The wave function only exists within bands. Fig. 1.4 shows the band structure of a 1D optical lattice potential for different depths.

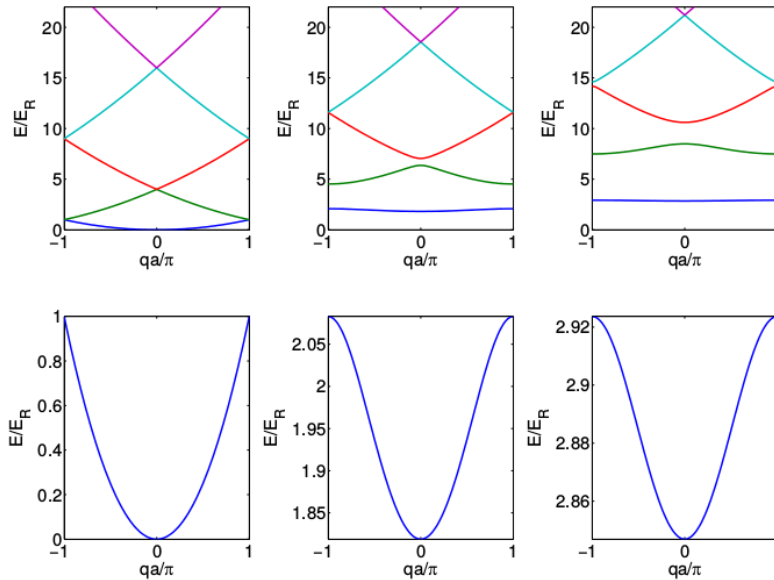


Figure 1.4: Band structure in an optical lattice for different depths $V_0 = \{0, 5, 10\} E_R$. The energies of the Bloch bands are plotted in the first Brillouin zone for different n and lattice depths. The top row shows the five lowest energy bands. The lower row shows the enlarged view of the lowest band marked in blue. The distance between bands increases with increasing lattice depths. Reprinted from the Ph.D. thesis of Andreas Nunnenkamp, St. John's College, University of Oxford, 2008.

For $V_0 = 0$, the atoms are free and therefore energy is quadratic in q . As the depth of the lattice potential increases, the band structure emerges. For small V_0 the discontinuity occurs at the edges of the first Brillouin zone (BZ) $qa = \pm\pi$, and for large depth, the band gap increases, and band width decreases. The bands get flatter with increasing depth, and corresponding effective mass of the atoms increases as it is inverse of the curvature of the band. The tunneling matrix elements J which describes the tunneling between neighbouring lattice sites is related to the width of the lowest band [89]

$$J = [\max(E_q^{(0)}) - \min(E_q^{(0)})] / 4. \quad (1.29)$$

The Bloch states are completely delocalized energy eigenstates of the Schrödinger equation for a given quasi-momentum q , and energy band n . In position space, the

Wannier function constitute an orthogonal and normalized set of wave functions which are maximally localized to the lattice sites. For shallow lattice potential, the wave functions extend to the next lattice site whereas for deep lattice potential, in the tight binding limit, the Wannier function resembles the Gaussian function.

1.3 Quantum phase transition

At zero temperature, atoms in an optical lattice can be described in two regimes. These are associated with two important energy scales involved in the system: kinetic energy or the tunneling matrix element (J) and the on-site interaction energy (U). The two regimes result from the competition of these two energy scales. When the kinetic energy dominates over the interaction energy ($J \gg U$), the system exhibits the superfluid properties. The onset of superfluidity is due to the fact that J tends to delocalize the atoms and U tends to localize them. In the SF phase, the many-body ground state is described by a macroscopic wave function. For N bosons in M lattice sites

$$|\Psi_{\text{SF}}\rangle \propto \left(\sum_{i=1}^M \hat{a}_i^\dagger \right)^N |0\rangle, \quad (1.30)$$

where $|0\rangle$ is the vacuum state. There is a macroscopic well-defined phase over the entire lattice sites, and hence the SF phase is characterized by the long-range coherence with a finite expectation value of the operator $\langle \hat{a}_i \rangle \neq 0$. The atoms are delocalized with equal relative phases between adjacent sites, they exhibit interference pattern when the lattice is switched off. As the on-site interaction increases, the average kinetic energy required by an atom to tunnel from one site to the next becomes insufficient to overcome the potential energy. This is when the quantum phase transition to MI phase occurs [90].

In the MI phase ($U \gg J$), the fluctuations in the number of atoms at a lattice site is energetically costly and the ground state of the system consists of a fixed number of atoms per site. In this phase, the expectation of the field operator vanishes $\langle \hat{a}_i \rangle = 0$. The many-body ground state is the product of Fock states in the number of atoms for each site. For a homogeneous system with commensurate filling of n atoms per lattice

site, it is given by

$$|\Psi_{\text{MI}}\rangle \propto \prod_{i=1}^M (\hat{a}_i^\dagger)^n |0\rangle. \quad (1.31)$$

The excitation spectrum of MI phase has an energy gap, which determines the energy required to create one particle-hole pair. In experiments, U and J can be tuned by changing the intensity of the laser beams used to create the optical lattices. Therefore, it is possible to drive the system from one phase to the other. When the strength of the on-site interaction relative to the tunneling energy (U/J) reaches a critical value then the system undergoes a quantum phase transition from SF to MI phase [91, 92]. This continuous phase transition is driven by quantum fluctuations and can occur at zero temperature when thermal fluctuations are absent [21, 93, 94]. The mean-field phase

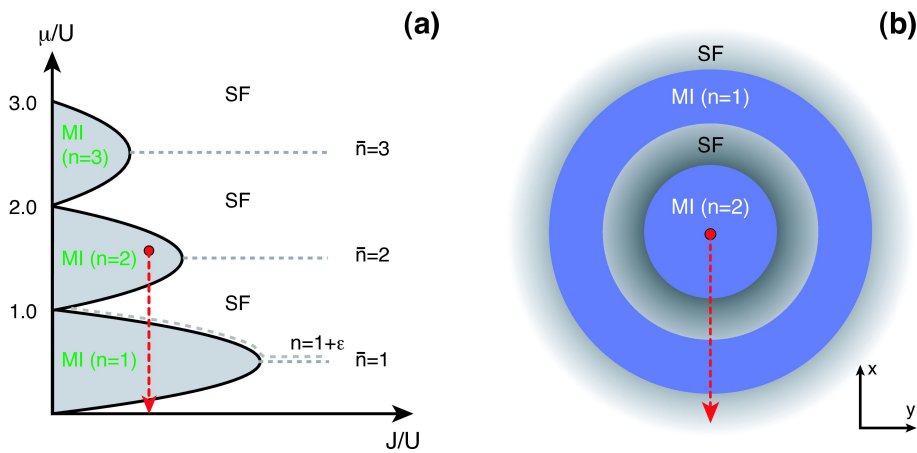


Figure 1.5: (a) Zero temperature mean-field phase diagram of SF-MI transition in a homogeneous system. The MI lobes are shown for fixed integer density $n = 1, 2, 3$. The dashed line corresponds to integer SF density $\bar{n} = 1, 2, 3$. (b) The phase diagram in a harmonic trap with MI phase for $n = 2$ in the center. A series of MI and SF phases appear from center to the edge of the cloud, where the chemical potential vanishes. This is shown by dashed red arrow. Reprinted from [Bloch et al., Rev. Mod. Phys. **80**, 885 (2008).] Copyright © 2008 by the American Physical Society.

diagram which describes the SF-MI transition in 3D homogeneous lattice is shown in Fig. 1.5(a) [21, 27]. This shows a boundary between MI and SF phase as a function of the chemical potential μ , and the tunneling matrix element J , both in units of the interaction energy U . In the MI phase each lobe is characterized by a fixed integer filling factor n . However, the structure of the lobe depends on the method used to

obtain the phase diagram, and on the dimensionality of the lattice system. The other approaches which has been applied to construct the phase diagram are multisite mean-field method [95], perturbative expansion [96], density matrix renormalization group (DMRG) [97], and quantum Monte Carlo (QMC) method [98]. The comparison of these different approaches to calculate the phase boundary of transition is investigated in Ref. [99]. The comparison of different analytical methods are made with DMRG technique for one dimension as well as QMC simulations for two and three dimensions. The results of the mean-field method agree with those obtained from other approaches in most parts of boundary that separates SF and MI phases, however the agreement becomes poor at the tip of the Mott lobes. This is due to the fact that fluctuations in the order parameter are ignored by mean-field theory and hence it yields a continuous smooth boundaries separating SF-MI phases. The multisite mean-field method include the fluctuations and provide an improvement of the results. In addition, the field-theoretic method provide better results for the SF-MI phase boundary in two and three dimensions when compared with the variational method [99]. In the MI phase, if we increase μ while keeping J fixed, there exists a point where the energy to add an extra atom, and letting it tunnel to neighbouring sites is balanced by the interaction energy. Then, an extra atom is free to move or phase coherence is restored, and the system enters the SF regime. At fixed J , the distance between the lower and upper part of the lobe in μ -axis is the energy gap. At $J = 0$, the energy gap is equal to U . The dashed lines of constant integer filling factor in the SF phase with $n = 1, 2, 3$ hit the corresponding MI phases at the tips of the lobe at a critical value of J/U , which decreases with increasing n . For $n = 1 + \varepsilon$, the line of constant filling factor remains outside the MI lobe because a fraction ε of atoms make the system superfluid even for lower values of J . Therefore, the MI phase occurs only for integer filling factor, non-integer filling factor results in the SF phase as there is always an extra atom that can tunnel without energy cost. The critical value at the tip of the Mott lobe depends on the density and the dimensionality of the lattice [100–102]. It is given by

$$(U/J)_c = z \left[2n + 1 + \sqrt{(2n + 1)^2 - 1} \right], \quad (1.32)$$

where n is the integer density of the lobe and $z = 2d$, with d as the dimensionality of the system, is the coordination number or the number of nearest neighbours.

The situation is fundamentally different for an experimentally realized inhomogeneous system with fixed total number of atoms. In the presence of an external harmonic confinement, the chemical potential at the i th lattice site is modified by the offset energy $\mu_i = \mu - \epsilon_i$ which results in a change in the filling factor. For inhomogeneous systems, the chemical potential μ is fixed, instead of the mean number of atoms at each lattice site, and the local chemical potential is changed due to redistribution of atoms over the lattice sites. This is maximum at the trap center as $\epsilon_i = 0$, and continuously decreases towards the boundary of the atomic cloud. The gradient in the local chemical potential, then, leads to a shell structure in the phase diagram with alternate shells of MI regions, and SF regions [28, 30, 103]. This configuration of the SF and MI phases is shown in Fig. 1.5(b).

1.4 Binary mixtures in optical lattices

A mixture of two BECs of different atomic species, or two isotopes or different hyperfine states of the same atomic species exhibit novel and intriguing features, and properties. The richness of the phase diagram of this system opens up a plethora of phenomena for closer inspection such as the study of the combined superfluidity of the TBEC, topology of a double MI system, influence of disorder, phase separation and quantum emulsion. Among these the phenomena of phase separation is a unique property of TBECs which spans a rich set of configurations depending on the strength of intra- or interspecies interaction that can be tuned through a magnetic Feshbach resonance. The phase separation occurs when the interspecies interaction is stronger than the geometric mean of the intraspecies interactions [104]. It must be emphasized that mixtures of ultracold quantum gases in an optical lattice is a new field of study. The novel interactions provide an ideal platform to study physics beyond the single-species Hubbard model, which is relevant to the condensed matter systems. The first experimental realization of a two-component mixture in the lattice potential was reported in 2006 [105]. This experiment dealt with the Bose-Fermi mixtures of ^{87}Rb and ^{40}K , where fermionic atoms of ^{40}K are treated as impurities in the system. The loss of phase coherence of the bosonic atoms due to increasing admixture of fermionic

atoms has been observed [106]. The other studies are related to the investigation of

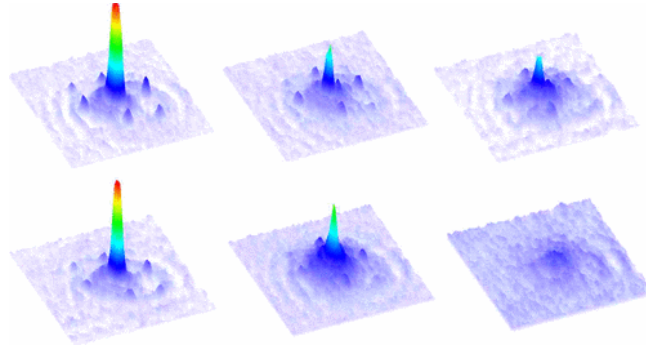


Figure 1.6: Interference pattern of ^{87}Rb for different optical lattice depths $V_0 = \{6, 11, 16\} E_R$ (left to right). The interference pattern of ^{87}Rb is shown in the absence (upper panel) and presence (lower panel) of the second species ^{41}K . Reprinted from [Catani et al. Phys. Rev. A **77**, 011603 (2008).] Copyright © 2008 by the American Physical Society.

the role of interspecies interaction on a degenerate Bose-Fermi mixtures [107, 108]. In the last decade, TBECs have been experimentally realized in two different atomic species [109, 110], and two different hyperfine states of the same species [26, 111]. These experiments have observed the reduction of phase coherence due to minor admixture of second species, as shown in Fig. 1.6 and the coexistence of the SF and MI phases in the hexagonal lattices. The loss of phase coherence is more prominent for large population imbalances and tunneling rate asymmetries of the two species [111]. In other experiments, the superexchange interactions [112], signature of Bose-glass state [113], emergence of twisted-superfluid ground state [114] and antiferromagnetic ordering [115] in binary atomic spin mixtures have been observed. It is demonstrated that the application of a magnetic field gradient to a mixture of spins enables new techniques of thermometry [116] and adiabatic cooling [117].

The introduction of a second species in the optical lattices, TBECs in optical lattices, creates a versatile model to probe diverse phenomena in physics. The second species of TBECs introduces an additional degree of freedom and provide a platform to study two-component Bose-Hubbard model [28, 118–120]. This model encompasses a remarkably rich physics, ranging from supercounterflow and antiferromagnetic phases in case of interspecies repulsion [121–123] to density-wave instabilities and pair super-

fluidity in the attractive regime [124–126]. The two-component phase diagram exhibits different combinations of SF and MI phases in coexisting or phase-separated configurations [119, 127–129]. The effect of the interspecies interactions [130], the presence of second species [131], and external harmonic potential [103] on the phase diagram has been investigated. These systems are promising candidates to explain phenomena associated with the fermionic correlations [132], and novel quantum phases in various lattice geometries [118, 121, 133]. Moreover, the effect of phase separation [134–137], hydrodynamic instability [138], quantum emulsions and coherence properties of mixtures [139–141], and nonequilibrium excitations and motion of BECs [59, 60, 67] have been explored. In addition, the influence of interspecies interaction on the transport properties has been studied [142, 143]. Recently, thermal mixing of phase-separated states [144], interspecies entanglement [145], fragmentation [146] and multicritical behaviour [147–149] were examined in binary mixture of BECs. The phenomena of phase separation, the lattice influenced geometry, and the quasiparticle spectra of TBECs are yet to be observed in experiments. Our findings of the phase separation phenomena and the finite temperature effects of TBECs provide a route towards further experimental investigations of TBECs in optical lattices.

1.5 Objectives of the present study

The Hartree-Fock approximation has been used to study the finite temperature effects in the mixture of ultracold quantum gases trapped in harmonic potential [150, 151] as well as without trapping potential [152, 153]. The ground state density profile, collective excitations [154–157] and symmetry breaking phenomena [158–161] have been explored for the TBECs. The SF phase of ultracold bosons in optical lattices has been examined in past [162, 163]. In this thesis, we use the Hartree-Fock Bogoliubov theory with the Popov (HFB-Popov) approximation in the Bose-Hubbard (BH) model to examine the equilibrium properties of the TBECs in optical lattices. The objectives of the research work done in this thesis are as follows:

- The development of the discrete nonlinear Schrödinger equation (DNLSE) using tight-binding approximation. The HFB-Popov theory to examine the ground

state density profile and the quasiparticle spectra of BEC in optical lattices at finite temperatures.

- The extension of the HFB-Popov formalism and the development of the coupled DNLSs in the BH model to study the effects of quantum and thermal fluctuations on TBECs trapped in optical lattices.
- Study of the evolution of quasiparticle modes of TBECs confined in quasi-1D optical lattices at zero temperature. We predict the emergence of an extra Goldstone mode at phase separation.
- Investigation of the role of quantum fluctuations, present at zero temperature, on the quasiparticle spectra, and the ground state density profile of TBECs in quasi-1D optical lattices. We demonstrate the hardening of the soft Kohn mode, and the topological transition of quasi-1D TBECs in the presence of the fluctuations.
- Study of the collective excitations of TBECs in quasi-2D optical lattices. We show that the lowest nonzero quasiparticle excitation, which is an out-of-phase degenerate slosh mode goes soft as the system is driven from miscible to the immiscible phase. At phase separation the slosh mode gets hardened, and degeneracy is lifted.
- Examination of the dispersion curves of the miscible and the immiscible phase of TBECs at zero temperature. These curves are explained by analyzing the structure of the mode functions in both the domains.
- Study of the quasiparticle mode evolution of TBECs at finite temperatures in the phase-separated domain. We show that the temperature of the system enhances the miscibility of the species in binary condensates.
- The first-order spatial correlation function of the TBEC is computed. The profile of the correlation function shows the decay in the coherence, and the topological transition from side-by-side geometry to the miscible type density profile of TBEC.

1.6 Overview of the chapters

The overview of the chapters in the rest of the thesis is as follows:

In **Chapter 2**, we start with the discussion on the BH Hamiltonian which is obtained using the tight-binding approximation in the many-body Hamiltonian. The equilibrium properties of the bosonic atoms in the SF regime of the optical lattice is described by DNLSE. The DNLSE is valid at zero temperature, and neglects the quantum fluctuations. However, in order to include the effects of quantum and thermal fluctuations in the weakly-interacting limit, we use Bogoliubov approximation. We discuss the HFB-Popov formalism to address the finite temperature effects on the ground state of BEC in optical lattices. This theory is extended to the TBECs of dilute atomic gases in optical lattices. At the end, the generalized coupled DNLSEs and the HFB-Popov formalism in quasi-2D optical lattices are discussed.

In **Chapter 3**, we use the coupled DNLSEs and the HFB-Popov formalism in the BH model to study the ground state density profile, and the quasiparticle mode evolution of TBECs in quasi-1D optical lattices at zero temperature. We discuss two system of relevance: two different isotopes of Rb, and the mixtures of ^{133}Cs and ^{87}Rb condensates. We examine the position exchange of the ^{87}Rb - ^{85}Rb system in the phase-separated domain. Furthermore, we investigate the role of quantum fluctuations on the ground state, and demonstrate the mode hardening at phase separation.

In **Chapter 4**, we explore the ground state density profile, and the quasiparticle mode evolution of TBECs in quasi-2D optical lattices. The quasiparticles are examined by analyzing the mode functions. In addition, we also study the dispersion curves of ^{87}Rb - ^{85}Rb TBEC in the miscible and immiscible domain. We show that the breaking of rotational symmetry, and the resulting mode mixing destroy the discernible trend of the dispersion curves in the immiscible domain.

In **Chapter 5**, we examine the role of thermal fluctuations in the TBECs trapped in quasi-2D optical lattices. We demonstrate the fluctuations induced enhancement in the miscibility, and the bifurcation in the mode evolution of a TBEC. The miscibility of the condensates is measured using the overlap integral. At the topological transition from immiscible side-by-side geometry to the miscible phase, the low-lying modes like slosh mode becomes degenerate. Furthermore, we compute the equal-time first-order

spatial correlation functions to examine the temperature driven topological transition and the decay in the phase coherence.

Finally in **Chapter 6**, we present the brief summary of the results and the future directions. At the end, the numerical details of the computations are provided in the the appendix.

Chapter 2

Finite temperature theory of bosons in optical lattices

The equilibrium properties of an ultracold quantum gas of bosonic atoms in an optical lattice is well described by the Bose-Hubbard (BH) model where the parameters of the system are controlled by laser beams [28]. For ultracold atoms trapped in optical lattices, the ratio of the interaction energy (on-site repulsion) to the kinetic energy (inter-site tunneling) of the atoms can be manipulated with the depth of the lattice. When atoms are loaded in shallow lattices, the system is in the weakly interacting regime and most of the atoms are in Bose-Einstein condensate state. This state is referred to as a superfluid (SF) phase where every atom is maximally delocalized over the entire lattice. In contrast, when the atoms are loaded in deep lattices, then the phase coherence of the atoms is lost, and the system is in the Mott insulator (MI) phase. The quantum phase transition [94] from superfluid to an insulating phase is described by the BH model. The condensate in the superfluid phase is well described by the Gross-Pitaevskii equation (GPE), and has been applied to the lattice potential whose depth is smaller than the chemical potential of the system [164–169].

In this Chapter, we begin with an introduction of the Hartree-Fock-Bogoliubov formalism of the ultracold bosons confined in harmonic trapping potential and we then use discrete nonlinear Schrödinger equation (DNLSE), which is a discrete form of the GPE, to describe bosons in optical lattices at zero temperature. The DNLSE is valid for a system, where the depth of the lattice potential is larger than the chemical potential of

the condensate. In the same way, a coupled DNLSEs is introduced to study the binary mixture of condensates in optical lattices. The DNLSE, however, does not account for the quantum fluctuations. To incorporate the quantum fluctuations in the weakly interacting system, we use Bogoliubov approximation. For this we use the second quantized grand canonical Hamiltonian of a dilute Bose gas, and employ tight-binding approximation to obtain BH Hamiltonian. Based on the Bogoliubov approximation, we derive the generalized DNLSE and the coupled Bogoliubov-de Gennes equations. For systems at finite temperatures, we develop Hartree-Fock-Bogoliubov equations with Popov approximation for single and two-species Bose-Einstein condensates.

2.1 Hartree-Fock-Bogoliubov theory

Consider a system of interacting ultracold dilute atomic Bose gas confined in a harmonic confining potential. The static and dynamical properties of such a system is described by the second quantized form of the many-body grand canonical Hamiltonian as

$$\begin{aligned} \hat{H} = & \int d\mathbf{r} \hat{\Psi}^\dagger(\mathbf{r}, t) \left[\hat{h}(\mathbf{r}, t) - \mu \right] \hat{\Psi}(\mathbf{r}, t) \\ & + \frac{1}{2} \int d\mathbf{r} d\mathbf{r}' \hat{\Psi}^\dagger(\mathbf{r}, t) \hat{\Psi}^\dagger(\mathbf{r}', t) U_{\text{int}}(\mathbf{r} - \mathbf{r}') \hat{\Psi}(\mathbf{r}', t) \hat{\Psi}(\mathbf{r}, t), \end{aligned} \quad (2.1)$$

where $\hat{h}(\mathbf{r}, t) = -(\hbar^2/2m)\nabla^2 + V_{\text{HO}}(\mathbf{r}, t)$, m is the mass of the atomic species, and μ is the chemical potential that acts as a Lagrange multiplier to fix the number of atoms in the grand canonical ensemble. Here $\hat{\Psi}(\hat{\Psi}^\dagger)$ is the bosonic annihilation (creation) field operator which satisfies the equal time Bose commutation relations,

$$[\hat{\Psi}(\mathbf{r}), \hat{\Psi}(\mathbf{r}')] = 0, \quad [\hat{\Psi}^\dagger(\mathbf{r}), \hat{\Psi}^\dagger(\mathbf{r}')] = 0, \quad [\hat{\Psi}(\mathbf{r}), \hat{\Psi}^\dagger(\mathbf{r}')] = \delta(\mathbf{r} - \mathbf{r}'). \quad (2.2)$$

In Hamiltonian given in Eq. (2.1), $V_{\text{HO}} = m(\omega_x^2 x^2 + \omega_y^2 y^2 + \omega_z^2 z^2)/2$ is the external harmonic trapping potential with $\omega_i (i = x, y, z)$ as the trapping frequency along the i -axis. In weakly interacting or dilute limit, when the scattering length a_s is much smaller than the average interatomic separation, then only the binary collisions are important, and the other higher-order interatomic interactions can be neglected. In experiments, a_s can be tuned using Feshbach resonances [170] by applying an additional

magnetic field. With this experimental technique a_s can be changed over several orders of magnitude including change in sign [171]. For negative a_s , the condensate becomes unstable above certain number of atoms [172]. In this thesis, we consider only $a_s > 0$, which corresponds to the repulsive interatomic interactions. The interatomic interaction potential is then given by $U_{\text{int}}(\mathbf{r} - \mathbf{r}') = g\delta(\mathbf{r} - \mathbf{r}')$ with $g = 4\pi\hbar^2 a_s/m$. Thus, in this limit the Hamiltonian in Eq. (2.1) becomes

$$\hat{H} = \int d\mathbf{r} \hat{\Psi}^\dagger(\mathbf{r}, t) \left[\hat{h}(\mathbf{r}) - \mu \right] \hat{\Psi}(\mathbf{r}, t) + \frac{g}{2} \int d\mathbf{r} \hat{\Psi}^\dagger(\mathbf{r}, t) \hat{\Psi}^\dagger(\mathbf{r}, t) \hat{\Psi}(\mathbf{r}, t) \hat{\Psi}(\mathbf{r}, t). \quad (2.3)$$

Using the variational principle, the minimization of the above Hamiltonian under the restriction that the total number of atoms is conserved yields

$$\left[-\frac{\hbar^2}{2m} \nabla^2 + V_{\text{HO}}(\mathbf{r}) + g|\psi(\mathbf{r})|^2 \right] \psi(\mathbf{r}, t) = i\hbar \frac{\partial \psi(\mathbf{r}, t)}{\partial t}. \quad (2.4)$$

This equation is referred to as the time-dependent Gross-Pitaevskii equation (GPE) [31, 173–175]. Here ψ is the order parameter or the condensate wave function, which is normalized to the total number of trapped atoms.

In BEC due to the macroscopic occupation of the ground state, the Bose field operator is separable into condensate and noncondensate part of the system. The condensate part is the ensemble average of the Bose field operator, and the fluctuation operator, representing the noncondensate part, is treated as a perturbation to the condensate field operator. The field operator is accordingly expanded as

$$\hat{\Psi}(\mathbf{r}, t) = \sum_{i=0}^{\infty} \hat{\alpha}_i(t) \psi_i(\mathbf{r}) = \hat{\alpha}_0(t) \psi_0(\mathbf{r}) + \sum_{i=1}^{\infty} \hat{\alpha}_i(t) \psi_i(\mathbf{r}), \quad (2.5)$$

where $\{\psi_i(\mathbf{r})\}$ is a complete set of single-particle wave functions and $\hat{\alpha}_i(t)$ is the annihilation operator of the i th state of the harmonic confining potential which obeys the equal time Bose commutation relations,

$$[\hat{\alpha}_i(t), \hat{\alpha}_j(t)] = [\hat{\alpha}_i^\dagger(t), \hat{\alpha}_j^\dagger(t)] = 0, \quad [\hat{\alpha}_i(t), \hat{\alpha}_j^\dagger(t)] = \delta_{ij}. \quad (2.6)$$

In the Bogoliubov approximation [176], we replace the operators $\hat{\alpha}_0$ and $\hat{\alpha}_0^\dagger$ by a c -number, i.e., $\hat{\alpha}_0 = \hat{\alpha}_0^\dagger = \sqrt{N_0}$, where N_0 is the number of condensate atoms. We assume $N_0 \pm 1 \approx N_0$ as the number of condensate atoms N_0 is very large and the ratio N_0/N remains finite in the thermodynamic limit, where N is the total number of

atoms. The field operator, then, assumes the form

$$\hat{\Psi}(\mathbf{r}, t) = \sqrt{N_0}\psi(\mathbf{r})e^{-i\mu t/\hbar} + \tilde{\psi}(\mathbf{r}, t), \quad (2.7)$$

where the first term on the right hand side is the condensate part and second term $\tilde{\psi}(\mathbf{r}, t) = \sum_{i=1}^{\infty} \hat{\alpha}_i(t)\psi_i(\mathbf{r})$ is the fluctuation operator corresponding to the noncondensate atoms. Thus, to study the static properties of the condensate we can write $\hat{\Psi} = \psi + \tilde{\psi}$ provided the ensemble average of the fluctuation operator $\langle \tilde{\psi} \rangle$ is zero. Using this decomposition of the field operator in the Hamiltonian given in Eq. (2.3), we obtain

$$\begin{aligned} \hat{H} = & \int d\mathbf{r} \psi^*(\mathbf{r}) \left[\hat{h}(\mathbf{r}) - \mu + \frac{g}{2}n_c(\mathbf{r}) \right] \psi(\mathbf{r}) + \int d\mathbf{r} \tilde{\psi}^\dagger(\mathbf{r}) \hat{\mathcal{L}} \tilde{\psi}(\mathbf{r}) \\ & + \frac{g}{2} \int d\mathbf{r} [\psi^2(\mathbf{r}) + \tilde{m}(\mathbf{r})] \tilde{\psi}^\dagger(\mathbf{r})\tilde{\psi}(\mathbf{r}) + \frac{g}{2} \int d\mathbf{r} [\psi^{*2}(\mathbf{r}) + \tilde{m}^*(\mathbf{r})] \tilde{\psi}^\dagger(\mathbf{r})\tilde{\psi}(\mathbf{r}), \end{aligned} \quad (2.8)$$

where $\hat{\mathcal{L}} = \hat{h}(\mathbf{r}) - \mu + 2gn(\mathbf{r})$ and $n(\mathbf{r}) = n_c(\mathbf{r}) + \tilde{n}(\mathbf{r})$ is the total density of the system with n_c and \tilde{n} as the condensate and noncondensate atomic density, respectively. Here we have used the Wick's theorem [177] to reduce the third and fourth order fluctuation operators into the quadratic form. In the mean-field approximation, these terms are $\tilde{\psi}^\dagger\tilde{\psi}\tilde{\psi} \approx 2\tilde{n}\tilde{\psi} + \tilde{m}\tilde{\psi}^\dagger$ and $\tilde{\psi}^\dagger\tilde{\psi}^\dagger\tilde{\psi}\tilde{\psi} \approx 4\tilde{n}\tilde{\psi}^\dagger\tilde{\psi} + \tilde{m}^*\tilde{\psi}\tilde{\psi} + \tilde{m}\tilde{\psi}^\dagger\tilde{\psi}^\dagger - (2\tilde{n}^2 + |\tilde{m}|^2)$, where $\tilde{n}(\mathbf{r}) = \langle \tilde{\psi}^\dagger(\mathbf{r})\tilde{\psi}(\mathbf{r}) \rangle$, and $\tilde{m}(\mathbf{r}) = \langle \tilde{\psi}(\mathbf{r})\tilde{\psi}(\mathbf{r}) \rangle$ is the anomalous average of the system. The minimization of the Hamiltonian leads to the generalized GPE which describes the condensate in the presence of the quantum or thermal fluctuations. It is given by

$$\left[\hat{h}(\mathbf{r}) - \mu \right] \psi(\mathbf{r}) + g [n_c(\mathbf{r}) + 2\tilde{n}(\mathbf{r})] \psi(\mathbf{r}) + g\tilde{m}(\mathbf{r})\psi^*(\mathbf{r}) = 0. \quad (2.9)$$

To diagonalize the Hamiltonian we use Bogoliubov transformation, which defines the fluctuation operator in terms of the quasiparticle basis or excited states of the condensates

$$\tilde{\psi}(\mathbf{r}, t) = \sum_j [\hat{\alpha}_j(t)u_j(\mathbf{r}) - \hat{\alpha}_j^\dagger(t)v_j^*(\mathbf{r})], \quad (2.10a)$$

$$\tilde{\psi}^\dagger(\mathbf{r}, t) = \sum_j [\hat{\alpha}_j^\dagger(t)u_j^*(\mathbf{r}) - \hat{\alpha}_j(t)v_j(\mathbf{r})], \quad (2.10b)$$

where $\hat{\alpha}_j(\mathbf{r}, t) = \hat{\alpha}_j e^{-iE_j t/\hbar}$ is the quasiparticle operator. Here u_j and v_j are the complex functions and referred to as the Bogoliubov quasiparticle amplitudes correspond-

ing to the j th quasiparticle mode with excitation energy E_j . The normalization conditions of these amplitudes are

$$\int d\mathbf{r} [u_j(\mathbf{r})u_{j'}^*(\mathbf{r}) - v_j(\mathbf{r})v_{j'}^*(\mathbf{r})] = \delta_{jj'}, \quad (2.11a)$$

$$\int d\mathbf{r} [u_j^*(\mathbf{r})v_{j'}^*(\mathbf{r}) - v_j^*(\mathbf{r})u_{j'}^*(\mathbf{r})] = 0, \quad (2.11b)$$

$$\int d\mathbf{r} [u_j(\mathbf{r})v_{j'}(\mathbf{r}) - v_j(\mathbf{r})u_{j'}(\mathbf{r})] = 0. \quad (2.11c)$$

We use Bogoliubov transformation in the Hamiltonian given in Eq. (2.8), and the resulting diagonal Hamiltonian is

$$\hat{H} = \int d\mathbf{r} \psi^*(\mathbf{r}) \left[\hat{h}(\mathbf{r}) - \mu + \frac{g}{2}n_c(\mathbf{r}) \right] \psi(\mathbf{r}) + \sum_j E_j \left[\hat{\alpha}_j^\dagger \hat{\alpha}_j - \int d\mathbf{r} |v_j(\mathbf{r})|^2 \right], \quad (2.12)$$

where the first term corresponds to the condensate part. In the second term, the first part is the Hamiltonian for the non-interacting quasiparticles with energy E_j which represents the quantum and thermal fluctuations of the system, and the second part is a constant energy shift in the Hamiltonian. The prefactors of $e^{-iE_j t/\hbar}$ and $e^{iE_j t/\hbar}$ are the Hartree-Fock-Bogoliubov (HFB) equations and these determine the quasiparticle amplitudes and the energies

$$\hat{\mathcal{L}}u_j(\mathbf{r}) - g [\psi^2(\mathbf{r}) + \tilde{m}(\mathbf{r})] v_j(\mathbf{r}) = E_j u_j(\mathbf{r}), \quad (2.13a)$$

$$-\hat{\mathcal{L}}v_j(\mathbf{r}) + g [\psi^{*2}(\mathbf{r}) + \tilde{m}^*(\mathbf{r})] u_j(\mathbf{r}) = E_j v_j(\mathbf{r}). \quad (2.13b)$$

The above eigenvalue equations along with the generalized GPE in Eq. (2.9) are solved self-consistently to study the effect of the fluctuations in the system. The density of the noncondensate atoms is

$$\tilde{n} \equiv \langle \tilde{\psi}^\dagger \tilde{\psi} \rangle = \sum_j [(|u_j|^2 + |v_j|^2) N_j + |v_j|^2], \quad (2.14)$$

where $N_j \equiv \langle \hat{\alpha}_j^\dagger \hat{\alpha}_j \rangle = (e^{\beta E_j} - 1)^{-1}$ with $\beta = (k_B T)^{-1}$ is the Bose-Einstein weight factor for a state with energy E_j at temperature T . At zero temperature, N_j vanishes and only last term representing the quantum fluctuations contributes.

In the HFB theory, the presence of the anomalous average \tilde{m} results in a gapped excitation spectrum. However, following Hugenholtz-Pines theorem [178] the excitation spectrum of the Bose gas should be gapless, to restore this property we use Popov

approximation. In this approximation, the anomalous average \tilde{m} is neglected. The generalized GPE and the HFB-Popov equations are

$$\left[\hat{h}(\mathbf{r}) - \mu \right] \psi(\mathbf{r}) + g [n_c(\mathbf{r}) + 2\tilde{n}(\mathbf{r})] \psi(\mathbf{r}) = 0, \quad (2.15a)$$

$$\hat{\mathcal{L}}u_j(\mathbf{r}) - g\psi^2(\mathbf{r})v_j(\mathbf{r}) = E_j u_j(\mathbf{r}), \quad (2.15b)$$

$$-\hat{\mathcal{L}}v_j(\mathbf{r}) + g\psi^{*2}(\mathbf{r})u_j(\mathbf{r}) = E_j v_j(\mathbf{r}). \quad (2.15c)$$

The self-consistent solutions of the above equations are then employed to study the effects of the quantum and thermal fluctuations in BEC [179–181].

2.2 Single-component BEC

2.2.1 Optical lattice and tight-binding approximation

We consider a BEC in an optical lattice superimposed on a harmonic oscillator potential. The lattice potential is created by two or more counter-propagating laser beams. So, the net external potential confining the BEC is

$$\begin{aligned} V(\mathbf{r}) &= V_{\text{HO}}(\mathbf{r}) + V_{\text{latt}}(\mathbf{r}) \\ &= \frac{m}{2}(\omega_x^2 x^2 + \omega_y^2 y^2 + \omega_z^2 z^2) \\ &\quad + V_0 \left[\sin^2 \left(\frac{2\pi x}{\lambda_L} \right) + \sin^2 \left(\frac{2\pi y}{\lambda_L} \right) + \sin^2 \left(\frac{2\pi z}{\lambda_L} \right) \right], \end{aligned} \quad (2.16)$$

where $V_0 = sE_R$ is the depth of the lattice potential, which is measured in terms of the recoil energy $E_R = \hbar^2 k_L^2 / 2m$, and s is a dimensionless scaling parameter. The wave number of the laser beam is $k_L = 2\pi/\lambda_L$, and λ_L is the wavelength used to create the periodic lattice potential. Thus, the lattice constant of the system is $a = \lambda_L/2$. If $V_{\text{HO}} = 0$, then the system is referred to as “translationally-invariant lattice” system, however, in this thesis we consider the experimentally relevant system of combined harmonic trap and optical lattice potential. Another important point to be mentioned is that we consider cubic or the equivalent in lower dimensions is the square geometry of the lattice potential [29, 182]. We begin the analysis by considering the second quantized grand canonical Hamiltonian, which describes a system of interacting bosonic atoms at zero temperature

$$\hat{H} = \int d\mathbf{r} \hat{\Psi}^\dagger(\mathbf{r}) \left[-\frac{\hbar^2}{2m} \nabla^2 + V(\mathbf{r}) - \mu + \frac{g}{2} \hat{\Psi}^\dagger(\mathbf{r}) \hat{\Psi}(\mathbf{r}) \right] \hat{\Psi}(\mathbf{r}), \quad (2.17)$$

where $\hat{\Psi}$ ($\hat{\Psi}^\dagger$) is the annihilation (creation) Bose field operator of single-component BEC [177], which obeys the Bose commutation relations. The GP Eq. (2.4) describes the BEC of dilute atomic gases in shallow lattice potentials at $T = 0$ K. However, the many-body properties of the cold atoms in deep lattice potential ($V_0 \gg \mu$) is described by the Bose-Hubbard Hamiltonian. In case of deep lattice, the BEC is separated into condensates localized at each lattice site, and these are coupled through quantum tunnelling. Therefore, to study the ground state properties of the system in periodic potentials we apply tight-binding approximation.

A non-interacting ultracold atoms in an optical lattice can move only in certain energy bands, which are called Bloch bands. The Bloch function which describes such systems are the complete set of solutions in momentum space and is defined as

$$\varphi_q^{(n)}(\mathbf{r}) = e^{iq\mathbf{r}/\hbar} u_q^{(n)}(\mathbf{r}), \quad (2.18)$$

where $u_q^{(n)}(\mathbf{r})$ is a periodic function which has the same periodicity as the optical lattice potential, i.e., $u_q^{(n)}(\mathbf{r}) = u_q^{(n)}(\mathbf{r} + a)$ with q and n as the quasi-momentum and band index, respectively. The quasi-momentum is the characteristic of the translational symmetry of the lattice potential.

As mentioned in the previous chapter, for deep lattice potential the band gap between different Bloch bands is large compared to the interaction energy. In this limit, all atoms in the periodic potential is assumed to occupy lowest band only, and we neglect the coupling between different bands. The basis functions in the position space are chosen as Wannier functions, which are a set of orthonormalized wave functions that describes atoms in a single band, and localized at the lattice sites. The Wannier functions in the lowest band are defined as [183]

$$w_0(\mathbf{r} - \mathbf{r}_i) = \frac{1}{\sqrt{L}} \sum_q e^{-iq\mathbf{r}_i/\hbar} \varphi_q^{(0)}(\mathbf{r}), \quad (2.19)$$

where L is the total number of lattice sites and \mathbf{r}_i is the position of the i th lattice site. Thus, the basis set in position space or the Wannier functions are obtained by the Fourier transform of the Bloch functions. These functions provide a natural position-space description of the system as the lattice depth is increased and atoms get localized to the individual lattice sites. In contrast to shallow lattices where the atoms can be described by a macroscopic wave function, the width of the single wave function in deep

lattices is smaller than the lattice constant. In tight-binding approximation (TBA), the overlap between the Wannier functions at different lattice sites is minimum and for deep lattice potential, the ground state of these functions resemble a Gaussian function. In this thesis, we use Gaussian function, which has width smaller than the lattice constant, as the basis function. The field operator in terms of the basis function can be written as [184]

$$\hat{\Psi}(\mathbf{r}) = \sum_{\xi} \hat{a}_{\xi} \phi_{\xi}(\mathbf{r}), \quad \text{and} \quad \hat{\Psi}^{\dagger}(\mathbf{r}) = \sum_{\xi} \hat{a}_{\xi}^{\dagger} \phi_{\xi}^*(\mathbf{r}), \quad (2.20)$$

where \hat{a}_{ξ} is the annihilation operator at site ξ which satisfies the bosonic commutation relations : $[\hat{a}_{\xi}, \hat{a}_{\xi'}^{\dagger}] = \delta_{\xi\xi'}$, $[\hat{a}_{\xi}, \hat{a}_{\xi'}] = 0$, and $[\hat{a}_{\xi}^{\dagger}, \hat{a}_{\xi'}^{\dagger}] = 0$. Here ξ is the unique combination of the lattice index along x , y and z directions. The basis function $\phi_{\xi}(\mathbf{r})$ are the orthonormalized Gaussian wave functions localized at the ξ th lattice site. The sum is taken over all the lattice sites. When the above definition of the field operator is used in the Hamiltonian given in Eq. (2.17), and only nearest neighbour tunnelling of the atoms is considered, we obtain Bose-Hubbard (BH) Hamiltonian.

2.2.2 Bose-Hubbard Hamiltonian

We consider a gas of ultracold bosonic atoms, held within a highly anisotropic cigar-shaped harmonic potential with trapping frequencies $\omega_x = \omega_y = \omega_{\perp} \gg \omega_z$. With this choice of trapping frequencies, the excitations along the x and y directions are of higher energy, and the system remains in the ground state at temperatures $T \ll \hbar\omega_{\perp}/k_B$. Therefore, for such system we can integrate out the condensate wave function along the radial direction and reduce it to a quasi-1D condensate. Thus, there are no excitations along the radial direction and the degree of freedom is frozen along this direction. In TBA, the BH Hamiltonian [27] which describes the quasi-1D system is obtained by using Eq. (2.20) in the many-body Hamiltonian given in Eq. (2.17). It is given by

$$\hat{H} = -J \sum_{\langle j, j' \rangle} \hat{a}_j^{\dagger} \hat{a}_{j'} + \sum_j \left[(\epsilon_j - \mu) \hat{a}_j^{\dagger} \hat{a}_j + \frac{U}{2} \hat{a}_j^{\dagger} \hat{a}_j^{\dagger} \hat{a}_j \hat{a}_j \right], \quad (2.21)$$

where j is the lattice site index, $\langle j, j' \rangle$ represents the nearest-neighbour, i.e., $(j, j-1)$ and $(j, j+1)$. The operator \hat{a}_j (\hat{a}_j^{\dagger}) is the bosonic annihilation (creation) of the atoms at

the j th lattice site. The parameters relevant to the lattice system are defined as follows,

$$J = - \int dz \phi_{j+1}^*(z) \left[-\frac{\hbar^2}{2m} \frac{\partial^2}{\partial z^2} + V_0 \sin^2 \left(\frac{2\pi z}{\lambda_L} \right) \right] \phi_j(z), \quad (2.22a)$$

$$\epsilon_j = \int dz V_{\text{HO}}(z) |\phi_j(z)|^2, \quad (2.22b)$$

$$U = \frac{2\sqrt{\lambda\kappa}\hbar^2 N a_s}{m} \int dz |\phi_j(z)|^4. \quad (2.22c)$$

Here J is the tunneling matrix element between nearest neighbours. The next-to-nearest neighbour tunneling amplitudes are two orders of magnitude smaller than J , and therefore to a good approximation they can be neglected [28]. The first term in the Eq. (2.21) is proportional to J , and is measure of the kinetic energy of the system. The second term is the offset energy at the site j due to the presence of the external harmonic potential. It can also be expressed as $\epsilon_j = j^2\Omega$ with $\Omega = m\omega_z^2 a^2/2$ as the strength of the harmonic potential. The chemical potential μ is a Lagrange multiplier to fix the number of atoms in the grand canonical ensemble. The last term in Eq. (2.21) determines the interaction energy of the system. The parameter U is the on-site interaction, which is the measure of the repulsion of two atoms at site j . In Eq. (2.22c), $\lambda = \omega_x/\omega_z$ and $\kappa = \omega_y/\omega_z$ are the anisotropy parameters along the x and y directions, respectively. The on-site interaction term complements J as it localizes an atom at a specific lattice site. The parameters J and U can be controlled by adjusting the intensity of the laser beam. The atoms get more localized at the lattice sites as the laser intensity is increased, and consequentially the tunneling amplitude J decreases exponentially. The on-site interaction U increases with the power law of the depth of the lattice potential, $U \propto V_0^{d/4}$, where d is the dimensionality of the lattice system.

2.2.3 Bogoliubov approximation

In the weakly-interacting limit, the annihilation operator of the BH Hamiltonian at each lattice site can be replaced by a c -number or complex amplitude, which describes the condensate at zero temperature [176, 185, 186]. In order to include the effects of the quantum or thermal fluctuations in the system the BH annihilation operator can be written as

$$\hat{a}_j = (c_j + \hat{\varphi}_j) e^{-i\mu t/\hbar}, \quad (2.23)$$

with $\langle \hat{\varphi}_j \rangle = 0$. The creation operator is the Hermitian conjugate of the above definition. Here c_j is the complex amplitude describing the condensate or the coherent part and $\hat{\varphi}_j$ is the fluctuation operator which represents the quantum and thermal fluctuations present in the system. It is important to note that the assumption of replacing condensate component by a c -number or $\langle \hat{a}_j \rangle = c_j$ is inaccurate near the edge of the condensate, where the condensate density is small, and below the critical temperature the fluctuations are dominant in such regions [163]. The condensate wave function is obtained by expanding the complex amplitude in the localized Gaussian basis functions

$$\psi(z) = \sum_j c_j \phi_j(z). \quad (2.24)$$

The condensate wave function has a well-defined phase which results from the broken global $U(1)$ gauge symmetry of the Hamiltonian. We apply the Bogoliubov approximation to the BH Hamiltonian and derive the Bogoliubov-de Gennes (BdG) equations.

2.2.4 Bogoliubov-de Gennes (BdG) equations

The effects of the quantum and the thermal fluctuations at finite temperatures are incorporated in the system through the use of Bogoliubov approximation. It must, however, be mentioned that the quantum fluctuations are present at zero temperature as well. When the expression of \hat{a}_j in Eq. (2.23) is inserted into the BH Hamiltonian, Eq. (2.21), we get

$$\begin{aligned} \hat{H} = & - J \sum_{\langle j,j' \rangle} \left(c_j^* c_{j'} + \hat{\varphi}_{j'} c_j^* + \hat{\varphi}_j^\dagger c_{j'} + \hat{\varphi}_j^\dagger \hat{\varphi}_{j'} \right) \\ & + \sum_j (\epsilon_j - \mu) \left(|c_j|^2 + \hat{\varphi}_j c_j^* + \hat{\varphi}_j^\dagger c_j + \hat{\varphi}_j^\dagger \hat{\varphi}_j \right) \\ & + \sum_j \frac{U}{2} \left(|c_j|^4 + 2|c_j|^2 c_j^* \hat{\varphi}_j + 2|c_j|^2 c_j \hat{\varphi}_j^\dagger + 4|c_j|^2 \hat{\varphi}_j^\dagger \hat{\varphi}_j \right. \\ & \left. + c_j^{*2} \hat{\varphi}_j \hat{\varphi}_j + c_j^2 \hat{\varphi}_j^\dagger \hat{\varphi}_j^\dagger + 2c_j \hat{\varphi}_j^\dagger \hat{\varphi}_j^\dagger \hat{\varphi}_j + 2c_j^* \hat{\varphi}_j^\dagger \hat{\varphi}_j \hat{\varphi}_j + \hat{\varphi}_j^\dagger \hat{\varphi}_j^\dagger \hat{\varphi}_j \hat{\varphi}_j \right). \quad (2.25) \end{aligned}$$

We decompose the Hamiltonian into terms of different order of the fluctuation operators as

$$\hat{H} = H_0 + \hat{H}_1 + \hat{H}_2 + \hat{H}_3 + \hat{H}_4, \quad (2.26)$$

with

$$H_0 = - J \sum_{\langle j,j' \rangle} c_j^* c_{j'} + \sum_j \left[(\epsilon_j - \mu) |c_j|^2 + \frac{U}{2} |c_j|^4 \right], \quad (2.27a)$$

$$\hat{H}_1 = - J \sum_{\langle j,j' \rangle} c_j^* \hat{\varphi}_{j'} + \sum_j (\epsilon_j - \mu + U |c_j|^2) c_j^* \hat{\varphi}_j + \text{h.c.}, \quad (2.27b)$$

$$\begin{aligned} \hat{H}_2 = & - J \sum_{\langle j,j' \rangle} \hat{\varphi}_j^\dagger \hat{\varphi}_{j'} + \sum_j (\epsilon_j - \mu) \hat{\varphi}_j^\dagger \hat{\varphi}_j \\ & + \frac{U}{2} \sum_j \left(c_j^2 \hat{\varphi}_j^{\dagger 2} + c_j^{*2} \hat{\varphi}_j^2 + 4 |c_j|^2 \hat{\varphi}_j^\dagger \hat{\varphi}_j \right), \end{aligned} \quad (2.27c)$$

$$\hat{H}_3 = U \sum_j c_j \hat{\varphi}_j^\dagger \hat{\varphi}_j^\dagger \hat{\varphi}_j + \text{h.c.}, \quad (2.27d)$$

$$\hat{H}_4 = \frac{U}{2} \sum_j \hat{\varphi}_j^\dagger \hat{\varphi}_j^\dagger \hat{\varphi}_j \hat{\varphi}_j, \quad (2.27e)$$

where the subscript of the various terms indicates the number of the fluctuation operators and h.c. stands for the Hermitian conjugate. We first neglect the higher-order terms and consider terms up to second order in the fluctuation operators. The lowest order Hamiltonian describes the condensate part of the system as it does not contain $\hat{\varphi}_j$. The minimization of H_0 with respect to the variation in the complex amplitude c_j^* gives the time-independent DNLSE, which can be written as

$$\mu c_j = -J(c_{j-1} + c_{j+1}) + (\epsilon_j + U n_j^c) c_j, \quad (2.28)$$

and c_j s are the stationary solution of the DNLSE. Here, $n_j^c = |c_j|^2$ is the condensate density of the system at zero temperature. The variation of \hat{H}_1 vanishes as c_j is a stationary solution and $\langle \hat{\varphi}_j \rangle = 0$. Thus the quadratic Hamiltonian \hat{H}_2 is the leading-order term which contributes to the noncondensate atoms of the system. At zero temperature, it has to be taken into account self-consistently to include the effects of the quantum fluctuations in the system. Apart from interaction between condensate atoms, this Hamiltonian also includes two other type of interactions, (i) interaction between condensate and noncondensate atoms, and (ii) interaction between two condensate atoms which are excited into noncondensate states after the interaction. The minimization of the \hat{H}_2 with the variation of $\hat{\varphi}_j^\dagger$ yields the governing equation for the noncondensate atoms

$$\mu \hat{\varphi}_j = -J(\hat{\varphi}_{j-1} + \hat{\varphi}_{j+1}) + (\epsilon_j + 2U n_j^c) \hat{\varphi}_j + U c_j^2 \hat{\varphi}_j^\dagger. \quad (2.29)$$

It is important to note that the quadratic Hamiltonian \hat{H}_2 is not diagonal in the fluctuation operator $\hat{\varphi}_j$, which can be diagonalized using the Bogoliubov transformation. It involves a linear canonical transformation of the creation and annihilation operators \hat{a}_j^\dagger and \hat{a}_j , respectively, into quasiparticle operators. In this transformation, the fluctuation operator is defined as the linear combination of the normal or the quasiparticle modes and is given by

$$\hat{\varphi}_j = \sum_l \left[u_j^l \hat{\alpha}_l e^{-i\omega_l t} - v_j^{*l} \hat{\alpha}_l^\dagger e^{i\omega_l t} \right], \quad (2.30a)$$

$$\hat{\varphi}_j^\dagger = \sum_l \left[u_j^{*l} \hat{\alpha}_l^\dagger e^{i\omega_l t} - v_j^l \hat{\alpha}_l e^{-i\omega_l t} \right], \quad (2.30b)$$

where u_j^l and v_j^l are the quasiparticle amplitudes corresponding to the j th lattice site, $\omega_l = E_l/\hbar$ is the l th quasiparticle mode frequency with E_l as the mode energy, and $\hat{\alpha}_l$ ($\hat{\alpha}_l^\dagger$) is the quasiparticle annihilation (creation) operator, which satisfies the Bose commutation relations. It is worth mentioning that in the above transformation $l \neq 0$, as it corresponds to the zero energy Goldstone mode associated with the breaking of the $U(1)$ gauge symmetry. The zero energy mode is non-perturbative, and neglected in the calculation of the excited or noncondensate atoms.

The Bogoliubov transformation represents the bosonic quasiparticle and satisfies the canonical commutation relations. These relations lead to the following orthonormalization conditions of the quasiparticle amplitudes

$$\sum_j \left(u_j^{*l} u_j^{l'} - v_j^{*l} v_j^{l'} \right) = \delta_{ll'}, \quad (2.31a)$$

$$\sum_j \left(u_j^l v_j^{l'} - v_j^{*l} u_j^{*l'} \right) = 0. \quad (2.31b)$$

We apply the Bogoliubov transformation [Eq. (2.30)] in the quadratic Hamiltonian \hat{H}_2 [Eq. (2.27c)], using the above orthonormality conditions, we get the following Bogoliubov-de Gennes (BdG) equations [33, 162]

$$E_l u_j^l = -J(u_{j-1}^l + u_{j+1}^l) + [2Un_j^c + (\epsilon_j - \mu)] u_j^l - Uc_j^2 v_j^l, \quad (2.32a)$$

$$E_l v_j^l = J(v_{j-1}^l + v_{j+1}^l) - [2Un_j^c + (\epsilon_j - \mu)] v_j^l + Uc_j^{*2} u_j^l. \quad (2.32b)$$

This set of coupled equations describes the quasiparticles of the condensate in the optical lattices at zero temperature. It is important to note that BdG equations do

not take into account the effect of the quantum or thermal fluctuations present in the system. To incorporate these fluctuation effects we include cubic and quartic terms in the Hamiltonian self-consistently.

2.2.5 Hartree-Fock-Bogoliubov (HFB) equations

To introduce the effects of quantum and thermal fluctuations we include \hat{H}_3 and \hat{H}_4 , higher-order terms of the fluctuation operator, in the Hamiltonian. In the mean-field approximation, the terms with higher-order fluctuation operator are factorized into the pairs [187]

$$\hat{\varphi}_j^\dagger \hat{\varphi}_j \hat{\varphi}_j \approx 2\tilde{n}_j \hat{\varphi}_j + \tilde{m}_j \hat{\varphi}_j^\dagger, \quad (2.33a)$$

$$\hat{\varphi}_j^\dagger \hat{\varphi}_j^\dagger \hat{\varphi}_j \hat{\varphi}_j \approx 4\tilde{n}_j \hat{\varphi}_j^\dagger \hat{\varphi}_j + \tilde{m}_j \hat{\varphi}_j^\dagger \hat{\varphi}_j^\dagger + \tilde{m}_j^* \hat{\varphi}_j \hat{\varphi}_j - (2\tilde{n}_j^2 + |\tilde{m}_j|^2), \quad (2.33b)$$

where $\tilde{n}_j = \langle \hat{\varphi}_j^\dagger \hat{\varphi}_j \rangle$ and $\tilde{m}_j = \langle \hat{\varphi}_j \hat{\varphi}_j \rangle$ represent the noncondensate density or depletion and the anomalous average at the j th lattice site, respectively. We use the above factorization to reduce \hat{H}_3 and \hat{H}_4 into quadratic form. The c -number term in Eq. (2.33b) is included as a shift in the energy functional H_0 . The modified higher-order Hamiltonians are

$$\hat{H}_3 = U \sum_j \left(2\tilde{n}_j \hat{\varphi}_j + \tilde{m}_j \hat{\varphi}_j^\dagger \right) c_j + \text{h.c.}, \quad (2.34a)$$

$$\hat{H}_4 = \frac{U}{2} \sum_j \left(2\tilde{n}_j \hat{\varphi}_j^\dagger \hat{\varphi}_j + \tilde{m}_j \hat{\varphi}_j^\dagger \hat{\varphi}_j^\dagger \right) + \text{h.c.}, \quad (2.34b)$$

and as mentioned, with an energy shift in H_0

$$\Delta H_0 = \frac{U}{2} (2\tilde{n}_j^2 + |\tilde{m}_j|^2). \quad (2.35)$$

The minimization of the Hamiltonian with the higher-order terms leads to the modified DNLSSE, which is given by

$$\mu' c_j = -J(c_{j-1} + c_{j+1}) + [\epsilon_j + U(n_j^c + 2\tilde{n}_j + \tilde{m}_j)] c_j, \quad (2.36)$$

where μ' is the modified chemical potential. The total atomic density $n = \sum_j \langle \hat{a}_j^\dagger \hat{a}_j \rangle = \sum_j (n_j^c + \tilde{n}_j)$. The diagonalization of the modified Hamiltonian yields the following HFB equations

$$E_l u_j^l = -J(u_{j-1}^l + u_{j+1}^l) + [2U(n_j^c + \tilde{n}_j) + (\epsilon_j - \mu')] u_j^l$$

$$- U(c_j^2 + \tilde{m}_j)v_j^l, \quad (2.37a)$$

$$E_l v_j^l = J(v_{j-1}^l + v_{j+1}^l) - [2U(n_j^c + \tilde{n}_j) + (\epsilon_j - \mu^l)] v_j^l \\ + U(c_j^{*2} + \tilde{m}_j^*)u_j^l, \quad (2.37b)$$

with the density of noncondensate atoms at the j th lattice site

$$\tilde{n}_j = \sum_l [(|u_j^l|^2 + |v_j^l|^2)N_l + |v_j^l|^2], \quad (2.38)$$

where $N_l = \langle \hat{\alpha}_l^\dagger \hat{\alpha}_l \rangle = (e^{\beta E_l} - 1)^{-1}$ with $\beta = (k_B T)^{-1}$ is the Bose factor, and E_l is the energy of l th quasiparticle mode. It is important to note that, at zero temperature, N_l in the above equation vanishes. Then, the noncondensate density is due to the quantum fluctuations, and it is given by

$$\tilde{n}_j = \sum_l |v_j^l|^2. \quad (2.39)$$

Therefore, we solve the HFB equations self-consistently in the presence of the quantum fluctuations. The anomalous average is given by

$$\tilde{m}_j = - \sum_l u_j^l v_j^{*l} [2N_l + 1]. \quad (2.40)$$

The HFB equations [Eq. (2.37)] can be written in the matrix form as,

$$E_l \begin{pmatrix} \mathbf{u}^l \\ \mathbf{v}^l \end{pmatrix} = \begin{pmatrix} \mathcal{L} & \mathcal{M} \\ -\mathcal{M}^* & -\mathcal{L} \end{pmatrix} \begin{pmatrix} \mathbf{u}^l \\ \mathbf{v}^l \end{pmatrix}, \quad (2.41)$$

where the eigenstates of the matrix with $\mathbf{u}^l = (u_1^l, u_2^l, \dots)$, $\mathbf{v}^l = (v_1^l, v_2^l, \dots)$ are the quasiparticle amplitudes with quasiparticle energy E_l as the eigenvalue. The matrix elements of \mathcal{L} and \mathcal{M} are

$$\mathcal{L}_{ij} = -J \sum_{\langle i,k \rangle} \delta_{ik} \delta_{kj} + \delta_{ij} [2U(n_j^c + \tilde{n}_j) + \epsilon_j - \mu^l], \quad (2.42a)$$

$$\mathcal{M}_{ij} = -U(c_j^2 + \tilde{m}_j) \delta_{ij}. \quad (2.42b)$$

This is a sparse matrix which is non-Hermitian and non-symmetric. The dimension of the matrix is $2(N_{\text{latt}} + 1) \times 2(N_{\text{latt}} + 1)$ with N_{latt} as the number of lattice sites in the system. The solutions of the diagonalized HFB matrix E_l appear in pairs with positive and negative energies. In other words, if E_l is the eigenvalue for quasiparticle amplitude $(\mathbf{u}^l, \mathbf{v}^l)$ then $-E_l$ is the eigenvalue for the amplitude $(\mathbf{u}^{*l}, \mathbf{v}^{*l})$. There is

one solution with $E_l = 0$ or the Goldstone mode, and the corresponding quasiparticle amplitude is proportional to the complex amplitude of the condensate, i.e., $(\mathbf{u}^0, \mathbf{v}^0) \propto (c, c)$. The matrix eigenvalue Eq. (2.41) along with the modified DNLSE [Eq. (2.36)] are solved iteratively until the solutions attain desired convergence in terms of the number of condensate and noncondensate atoms.

2.2.6 HFB-Popov approximation

The HFB equations give a gapped excitation spectrum of the Bose gas, and violate Hugenholtz-Pines theorem [178]. This theorem implies that in the presence of the condensate, as mentioned earlier, the $U(1)$ global gauge symmetry is broken, and therefore, the energy spectrum of the Bose gas must be gapless. The gapless spectrum refers to a quasiparticle with energy tending to zero as the momentum tends to zero. The Popov approximation addresses the energy gap problem by ignoring \tilde{n}_j . It is first proposed by Popov [188], and is better than HFB as it gives a gapless energy spectrum. Under this approximation the modified DNLSE and the HFB-Popov equations are

$$\mu c_j = -J(c_{j-1} + c_{j+1}) + [\epsilon_j + U(n_j^c + 2\tilde{n}_j)] c_j, \quad (2.43)$$

$$E_l u_j^l = -J(u_{j-1}^l + u_{j+1}^l) + [2U(n_j^c + \tilde{n}_j) + (\epsilon_j - \mu')] u_j^l - U c_j^2 v_j^l, \quad (2.44)$$

$$E_l v_j^l = J(v_{j-1}^l + v_{j+1}^l) - [2U(n_j^c + \tilde{n}_j) + (\epsilon_j - \mu')] v_j^l + U c_j^{*2} u_j^l. \quad (2.45)$$

The DNLSE and coupled HFB-Popov equations are solved self-consistently to get converged solutions of c_j , and the noncondensate density \tilde{n}_j . The order parameter and the noncondensate density \tilde{n} are further obtained by the expanding the complex amplitude and the quasiparticle amplitudes u_j^l and v_j^l in terms of the localized orthonormalized Gaussian basis.

2.3 Two-component BEC

In this section, we generalize the theory introduced in the previous section for an interacting two-component BEC (TBEC). We consider a mixture of binary condensates or a TBEC held in an optical lattice with a harmonic potential as an external envelope

potential. In the mean-field regime, the second quantized grand canonical Hamiltonian governing this system at zero temperature is

$$\begin{aligned} \hat{H} = & \sum_{k=1}^2 \int d\mathbf{r} \hat{\Psi}_k^\dagger(\mathbf{r}) \left[-\frac{\hbar^2 \nabla^2}{2m_k} + V_k(\mathbf{r}) - \mu_k + \frac{g_{kk}}{2} \hat{\Psi}_k^\dagger(\mathbf{r}) \hat{\Psi}_k(\mathbf{r}) \right] \hat{\Psi}_k(\mathbf{r}) \\ & + g_{12} \int d\mathbf{r} \hat{\Psi}_1^\dagger(\mathbf{r}) \hat{\Psi}_2^\dagger(\mathbf{r}) \hat{\Psi}_1(\mathbf{r}) \hat{\Psi}_2(\mathbf{r}), \end{aligned} \quad (2.46)$$

where $k = 1, 2$ is the species index, m_k is the atomic mass of the k th species, and $\hat{\Psi}_k$, μ_k , and $g_{kk} = 4\pi\hbar^2 a_{kk}/m_k$ are the bosonic field operator, chemical potential, and intraspecies interaction strength of the k th species, respectively, with a_{kk} as the scattering length of the k th species. The parameter $g_{12} = 2\pi\hbar^2 a_{12}/m_r$ is the interspecies interaction strength with a_{12} and m_r as the interspecies scattering length, and the reduced mass of the TBEC, respectively. The external harmonic trapping potential V_k is considered to be same for both the condensates. Like in the previous section, we use the TBA to describe TBEC in deep lattice potential ($V_0 \gg \mu_k$). This is valid as the bosonic atoms of both the species occupy the lowest vibrational band, and interband transitions are suppressed. In this approximation, the field operator of the species can be expanded as

$$\hat{\Psi}_k(\mathbf{r}) = \sum_{\xi} \hat{a}_{k\xi} \phi_{k\xi}(\mathbf{r}), \quad (2.47)$$

where $\hat{a}_{k\xi}$ is the annihilation operator of the k th species at the lattice site with identification index ξ , which is a unique combination of the lattice index along x , y and z axes. The basic element of TBA lies in the definition of $\phi_{k\xi}(\mathbf{r})$, these are orthonormalized on-site Gaussian wave functions localized at the ξ th lattice site. The width of the basis function depends on the mass of the species, and frequency of the lattice potential. For the present study, the frequency plays a dominant role over the mass of the constituent species. Since we consider same lattice potential for both the species, hence the width is considered to be identical for the two species, even when the mass difference of the TBEC is large. For each of the species, it is chosen such that its spatial extent is much less than the lattice constant, and thereby the overlap between the basis function of adjacent sites is small. Using the above definition of $\hat{\Psi}_k(\mathbf{r})$ in Eq. (2.46), we get the Bose-Hubbard (BH) Hamiltonian of the system.

2.3.1 Two-component Bose-Hubbard Hamiltonian

As mentioned earlier, consider a binary condensate mixture of dilute atomic gases confined in an optical lattice potential with a harmonic potential as an envelope potential. For a quasi-1D system where the trapping frequencies satisfy the condition $\omega_x = \omega_y = \omega_\perp \gg \omega_z$, using the TBA, and considering the nearest neighbour tunneling, the BH Hamiltonian at zero temperature is [28, 118, 119, 121, 138, 189, 190]

$$\begin{aligned} \hat{H} = & \sum_{i=1}^2 \left[-J_i \sum_{\langle jj' \rangle} \hat{a}_{ij}^\dagger \hat{a}_{ij'} + \sum_j (\epsilon_j^{(i)} - \mu_i) \hat{a}_{ij}^\dagger \hat{a}_{ij} \right] \\ & + \frac{1}{2} \sum_{i=1}^2 U_{ii} \sum_j \hat{a}_{ij}^\dagger \hat{a}_{ij}^\dagger \hat{a}_{ij} \hat{a}_{ij} + U_{12} \sum_j \hat{a}_{1j}^\dagger \hat{a}_{1j} \hat{a}_{2j}^\dagger \hat{a}_{2j}, \end{aligned} \quad (2.48)$$

where $i = 1, 2$ denotes the species index. The operator $\hat{a}_{ij} (\hat{a}_{ij}^\dagger)$ is the bosonic annihilation (creation) operator of the i th species at the j th lattice site, J_i s are the tunneling matrix elements, $\epsilon_j^{(i)}$ is the offset energy arising from the envelope harmonic confining potential. The parameters U_{ii} and U_{12} are the intraspecies and the interspecies on-site interactions, respectively, which depend on the interaction strength, and the width of the basis function. In this thesis, we consider the superfluid phase of the binary mixture of ultracold bosons in the lattice potential, where the tunneling strength and the on-site interactions satisfy $J_i \gg \nu U_{ii}, \nu U_{12}$. Here, ν is the filling factor, which is defined as the ratio of the number of atoms to the number of lattice sites.

2.3.2 HFB-Popov approximation for the TBEC

In the mean-field approximation, like single-component BEC, we employ the Bogoliubov approximation to define the BH annihilation operators

$$\hat{a}_{1j} = (c_j + \hat{\varphi}_{1j}) e^{-i\mu_1 t/\hbar}, \quad (2.49a)$$

$$\hat{a}_{2j} = (d_j + \hat{\varphi}_{2j}) e^{-i\mu_2 t/\hbar}, \quad (2.49b)$$

where c_j and d_j are the complex amplitudes associated with the condensate wave functions of each species. They satisfy the normalization conditions $\sum_j |c_j|^2 = \sum_j |d_j|^2 = 1$. The operators, $(\hat{\varphi}_{1j}$ or $\hat{\varphi}_{2j})$ are the perturbations to the c -numbers, and identify with the quantum and thermal fluctuations in the system. We use these definitions in the

two-component BH Hamiltonian [Eq. (2.48)], and then decompose the Hamiltonian into terms of different orders in the fluctuation operators as $\hat{H} = \sum_{i=1}^2 \sum_{n=0}^4 \hat{H}_n^i$. The different terms of the modified BH Hamiltonian are

$$\begin{aligned}
H_0^1 &= - J_1 \sum_{\langle jj' \rangle} c_j^* c_{j'} + \sum_j \left[(\epsilon_j^{(1)} - \mu_1) |c_j|^2 + \frac{1}{2} (U_{11} |c_j|^4 + U_{12} |c_j|^2 |d_j|^2) \right], \\
H_0^2 &= - J_2 \sum_{\langle jj' \rangle} d_j^* d_{j'} + \sum_j \left[(\epsilon_j^{(2)} - \mu_2) |d_j|^2 + \frac{1}{2} (U_{22} |d_j|^4 + U_{12} |c_j|^2 |d_j|^2) \right], \\
\hat{H}_1^1 &= - J_1 \sum_{\langle jj' \rangle} c_j^* \hat{\varphi}_{1j} + \sum_j \left(\epsilon_j^{(1)} - \mu_1 + U_{11} |c_j|^2 + U_{12} |d_j|^2 \right) c_j^* \hat{\varphi}_{1j} + \text{h.c.}, \\
\hat{H}_1^2 &= - J_2 \sum_{\langle jj' \rangle} d_j^* \hat{\varphi}_{2j} + \sum_j \left(\epsilon_j^{(2)} - \mu_2 + U_{22} |d_j|^2 + U_{12} |c_j|^2 \right) d_j^* \hat{\varphi}_{2j} + \text{h.c.}, \\
\hat{H}_2^1 &= - J_1 \sum_{\langle jj' \rangle} \hat{\varphi}_{1j}^\dagger \hat{\varphi}_{1j'} + \sum_j \left[(\epsilon_j^{(1)} - \mu_1) + 2U_{11} |c_j|^2 + U_{12} |d_j|^2 \right] \hat{\varphi}_{1j}^\dagger \hat{\varphi}_{1j} \\
&\quad + \sum_j \left[\frac{U_{11}}{2} (c_j^2 \hat{\varphi}_{1j}^{\dagger 2} + c_j^{*2} \hat{\varphi}_{1j}^2) + \frac{U_{12}}{2} (c_j^* d_j^* \hat{\varphi}_{1j} \hat{\varphi}_{2j} + c_j^* d_j \hat{\varphi}_{1j} \hat{\varphi}_{2j}^\dagger \right. \\
&\quad \left. + c_j d_j^* \hat{\varphi}_{1j}^\dagger \hat{\varphi}_{2j} + c_j d_j \hat{\varphi}_{1j}^\dagger \hat{\varphi}_{2j}^\dagger) \right], \\
\hat{H}_2^2 &= - J_2 \sum_{\langle jj' \rangle} \hat{\varphi}_{2j}^\dagger \hat{\varphi}_{2j'} + \sum_j \left[(\epsilon_j^{(2)} - \mu_2) + 2U_{22} |d_j|^2 + U_{12} |c_j|^2 \right] \hat{\varphi}_{2j}^\dagger \hat{\varphi}_{2j} \\
&\quad + \sum_j \left[\frac{U_{22}}{2} (d_j^2 \hat{\varphi}_{2j}^{\dagger 2} + d_j^{*2} \hat{\varphi}_{2j}^2) + \frac{U_{12}}{2} (c_j^* d_j^* \hat{\varphi}_{1j} \hat{\varphi}_{2j} + c_j^* d_j \hat{\varphi}_{1j} \hat{\varphi}_{2j}^\dagger \right. \\
&\quad \left. + c_j d_j^* \hat{\varphi}_{1j}^\dagger \hat{\varphi}_{2j} + c_j d_j \hat{\varphi}_{1j}^\dagger \hat{\varphi}_{2j}^\dagger) \right], \\
\hat{H}_3^1 &= \sum_j \left[U_{11} c_j \hat{\varphi}_{1j}^\dagger \hat{\varphi}_{1j}^\dagger \hat{\varphi}_{1j} + \frac{U_{12}}{2} (c_j \hat{\varphi}_{1j}^\dagger \hat{\varphi}_{2j}^\dagger \hat{\varphi}_{2j} + d_j \hat{\varphi}_{1j}^\dagger \hat{\varphi}_{2j}^\dagger \hat{\varphi}_{1j}) \right] + \text{h.c.}, \\
\hat{H}_3^2 &= \sum_j \left[U_{22} d_j \hat{\varphi}_{2j}^\dagger \hat{\varphi}_{2j}^\dagger \hat{\varphi}_{2j} + \frac{U_{12}}{2} (c_j \hat{\varphi}_{1j}^\dagger \hat{\varphi}_{2j}^\dagger \hat{\varphi}_{2j} + d_j \hat{\varphi}_{1j}^\dagger \hat{\varphi}_{2j}^\dagger \hat{\varphi}_{1j}) \right] + \text{h.c.}, \\
\hat{H}_4^1 &= \sum_j \left(\frac{U_{11}}{2} \hat{\varphi}_{1j}^\dagger \hat{\varphi}_{1j}^\dagger \hat{\varphi}_{1j} \hat{\varphi}_{1j} + \frac{U_{12}}{2} \hat{\varphi}_{1j}^\dagger \hat{\varphi}_{2j}^\dagger \hat{\varphi}_{1j} \hat{\varphi}_{2j} \right), \\
\hat{H}_4^2 &= \sum_j \left(\frac{U_{22}}{2} \hat{\varphi}_{2j}^\dagger \hat{\varphi}_{2j}^\dagger \hat{\varphi}_{2j} \hat{\varphi}_{2j} + \frac{U_{12}}{2} \hat{\varphi}_{1j}^\dagger \hat{\varphi}_{2j}^\dagger \hat{\varphi}_{1j} \hat{\varphi}_{2j} \right). \tag{2.50}
\end{aligned}$$

The lowest order Hamiltonian is an energy functional which describes the condensate part of the TBECs at zero temperature. The minimization of the energy functional with respect to the variation in the complex amplitudes leads to a set of time-independent coupled DNLSs [191–193]. These equations describe the equilibrium properties of

the system at zero temperature, and are given by

$$\mu_1 c_j = - J_1(c_{j-1} + c_{j+1}) + \left[\epsilon_j^{(1)} + U_{11}n_{1j}^c + U_{12}n_{2j}^c \right] c_j, \quad (2.51a)$$

$$\mu_2 d_j = - J_2(d_{j-1} + d_{j+1}) + \left[\epsilon_j^{(2)} + U_{22}n_{2j}^c + U_{12}n_{1j}^c \right] d_j, \quad (2.51b)$$

where $n_{1j}^c = |c_j|^2$ and $n_{2j}^c = |d_j|^2$ are the condensate densities of the first and second species at the j th lattice site, respectively. The equation for the noncondensate part of the TBEC is obtained by the minimization of the quadratic Hamiltonians \hat{H}_2^1 and \hat{H}_2^2 .

These are given by

$$\begin{aligned} \mu_1 \hat{\varphi}_{1j} = & - J_1(\hat{\varphi}_{1,j-1} + \hat{\varphi}_{1,j+1}) + \left[\epsilon_j^{(1)} + 2U_{11}n_{1j}^c + U_{12}n_{2j}^c \right] \hat{\varphi}_{1j} \\ & + U_{11}c_j^2 \hat{\varphi}_{1j}^\dagger + U_{12}(c_j d_j^* \hat{\varphi}_{2j} + c_j d_j \hat{\varphi}_{2j}^\dagger), \end{aligned} \quad (2.52a)$$

$$\begin{aligned} \mu_2 \hat{\varphi}_{2j} = & - J_2(\hat{\varphi}_{2,j-1} + \hat{\varphi}_{2,j+1}) + \left[\epsilon_j^{(2)} + 2U_{22}n_{2j}^c + U_{12}n_{1j}^c \right] \hat{\varphi}_{2j} \\ & + U_{22}d_j^2 \hat{\varphi}_{2j}^\dagger + U_{12}(c_j^* d_j \hat{\varphi}_{1j} + c_j d_j \hat{\varphi}_{1j}^\dagger). \end{aligned} \quad (2.52b)$$

The next step is to include the effect of the quantum and thermal fluctuations in the description of the TBECs. To diagonalize the Hamiltonian in terms of the quasiparticle basis \mathbf{u}^l 's and \mathbf{v}^l 's, we use Bogoliubov transformation. It represents the fluctuation operator in terms of the quasiparticle modes, and is given by

$$\hat{\varphi}_{ij} = \sum_l \left[u_{ij}^l \hat{\alpha}_l e^{-i\omega_l t} - v_{ij}^{*l} \hat{\alpha}_l^\dagger e^{i\omega_l t} \right], \quad (2.53a)$$

$$\hat{\varphi}_{ij}^\dagger = \sum_l \left[u_{ij}^{*l} \hat{\alpha}_l^\dagger e^{i\omega_l t} - v_{ij}^l \hat{\alpha}_l e^{-i\omega_l t} \right], \quad (2.53b)$$

where u_{ij}^l and v_{ij}^l are the quasiparticle amplitudes for the i th species in quasi-1D optical lattice potential, and the other symbols are as defined earlier in the section on single-component BEC. Here, the quasiparticle operator $\hat{\alpha}_l$ and $\hat{\alpha}_l^\dagger$ are taken to be same for both the species, and they satisfy the Bose commutation relations. The quasiparticle amplitudes satisfy the following normalization condition

$$\sum_{ij} \left(u_{ij}^{*l} u_{ij}^{l'} - v_{ij}^{*l} v_{ij}^{l'} \right) = \delta_{ll'}. \quad (2.54)$$

Now we make use of the Wick's theorem [177] to include the third and fourth order fluctuation operators in the Hamiltonian, where the product of the fluctuation operators are replaced by the expectation of the pairs of the fluctuation operators [187]. In this

approximation the terms with three fluctuation operators $\hat{\varphi}_{ij}^\dagger \hat{\varphi}_{ij} \hat{\varphi}_{ij} \approx 2\tilde{n}_{ij} \hat{\varphi}_{ij} + \tilde{m}_{ij} \hat{\varphi}_{ij}^\dagger$, $\hat{\varphi}_{1j}^\dagger \hat{\varphi}_{2j}^\dagger \hat{\varphi}_{2j} \approx \tilde{n}_{2j} \hat{\varphi}_{1j}^\dagger$, and $\hat{\varphi}_{1j}^\dagger \hat{\varphi}_{2j}^\dagger \hat{\varphi}_{1j} \approx \tilde{n}_{1j} \hat{\varphi}_{2j}^\dagger$, where $\tilde{n}_{ij} = \langle \hat{\varphi}_{ij}^\dagger \hat{\varphi}_{ij} \rangle$, and $\tilde{m}_{ij} = \langle \hat{\varphi}_{ij} \hat{\varphi}_{ij} \rangle$ are the noncondensate density and the anomalous average of the i th species at the j th lattice site, respectively. Here, for the fluctuation operators of two different species $i \neq i'$, we use the approximation $\langle \hat{\varphi}_{ij}^\dagger \hat{\varphi}_{i'j} \rangle = \langle \hat{\varphi}_{ij} \hat{\varphi}_{i'j} \rangle = 0$. Using these factorization of the third order fluctuation operators into the quadratic Hamiltonians, and the minimization of the energy functional leads to the modified coupled DNLSs

$$\begin{aligned} \mu_1 c_j = & - J_1(c_{j-1} + c_{j+1}) + \left[\epsilon_j^{(1)} + U_{11}(n_{1j}^c + 2\tilde{n}_{1j}) + U_{12}(n_{2j}^c + \tilde{n}_{2j}) \right] c_j \\ & + U_{11}\tilde{m}_1 c_j^*, \end{aligned} \quad (2.55a)$$

$$\begin{aligned} \mu_2 d_j = & - J_2(d_{j-1} + d_{j+1}) + \left[\epsilon_j^{(2)} + U_{22}(n_{2j}^c + 2\tilde{n}_{2j}) + U_{12}(n_{1j}^c + \tilde{n}_{1j}) \right] d_j \\ & + U_{22}\tilde{m}_2 d_j^*, \end{aligned} \quad (2.55b)$$

and furthermore, the modified equations for the noncondensate atoms are

$$\begin{aligned} \mu_1 \hat{\varphi}_{1j} = & - J_1(\hat{\varphi}_{1,j-1} + \hat{\varphi}_{1,j+1}) + \left[\epsilon_j^{(1)} + 2U_{11}(n_{1j}^c + \tilde{n}_{1j}) + U_{12}(n_{2j}^c + \tilde{n}_{2j}) \right] \hat{\varphi}_{1j} \\ & + U_{11}(c_j^2 + \tilde{m}_1) \hat{\varphi}_{1j}^\dagger + U_{12}(c_j d_j^* \hat{\varphi}_{2j} + c_j d_j \hat{\varphi}_{2j}^\dagger), \end{aligned} \quad (2.56a)$$

$$\begin{aligned} \mu_2 \hat{\varphi}_{2j} = & - J_2(\hat{\varphi}_{2,j-1} + \hat{\varphi}_{2,j+1}) + \left[\epsilon_j^{(2)} + 2U_{22}(n_{2j}^c + \tilde{n}_{2j}) + U_{12}(n_{1j}^c + \tilde{n}_{1j}) \right] \hat{\varphi}_{2j} \\ & + U_{22}(d_j^2 + \tilde{m}_2) \hat{\varphi}_{2j}^\dagger + U_{12}(c_j^* d_j \hat{\varphi}_{1j} + c_j d_j \hat{\varphi}_{1j}^\dagger). \end{aligned} \quad (2.56b)$$

These are coupled equations for the condensate [Eq. (2.55)] and the noncondensate [Eq. (2.56)] part of the TBECs held in the optical lattice potential. These equations do take into account the effect of the quantum fluctuations at zero temperature, and the thermal fluctuation at a finite temperature T . The use of the Bogoliubov approximation into the modified quadratic Hamiltonian leads to the HFB equations for the TBECs. These are given by

$$\begin{aligned} E_l u_{1,j}^l = & - J_1(u_{1,j-1}^l + u_{1,j+1}^l) + \left[2U_{11}n_{1j} + U_{12}n_{2j} + (\epsilon_j^{(1)} - \mu_1) \right] u_{1,j}^l \\ & - U_{11}m_{1j} v_{1,j}^l + U_{12}c_j (d_j^* u_{2,j}^l - d_j v_{2,j}^l), \end{aligned} \quad (2.57a)$$

$$\begin{aligned} E_l v_{1,j}^l = & J_1(v_{1,j-1}^l + v_{1,j+1}^l) - \left[2U_{11}n_{1j} + U_{12}n_{2j} + (\epsilon_j^{(1)} - \mu_1) \right] v_{1,j}^l \\ & + U_{11}m_{1j}^* u_{1,j}^l - U_{12}c_j^* (d_j v_{2,j}^l - d_j^* u_{2,j}^l), \end{aligned} \quad (2.57b)$$

$$\begin{aligned} E_l u_{2,j}^l = & - J_2(u_{2,j-1}^l + u_{2,j+1}^l) + \left[2U_{22}n_{2j} + U_{12}n_{1j} + (\epsilon_j^{(2)} - \mu_2) \right] u_{2,j}^l \\ & - U_{22}m_{2j} v_{2,j}^l + U_{12}d_j (c_j^* u_{1,j}^l - c_j v_{1,j}^l), \end{aligned} \quad (2.57c)$$

$$\begin{aligned}
E_l v_{2,j}^l = & J_2(v_{2,j-1}^l + v_{2,j+1}^l) - \left[2U_{22}n_{2j} + U_{12}n_{1j} + (\epsilon_j^{(2)} - \mu_2) \right] v_{2,j}^l \\
& + U_{22}m_{2j}^* u_{2,j}^l - U_{12}d_j^* (c_j v_{1,j}^l - c_j^* u_{1,j}^l), \tag{2.57d}
\end{aligned}$$

where for notational simplicity we have defined the total density of the i th species at the j th lattice site $n_{ij} = n_{ij}^c + \tilde{n}_{ij}$ and $m_{1j} = c_j^2 + \tilde{m}_{1j}$, and $m_{2j} = d_j^2 + \tilde{m}_{2j}$. It is important to note that if the on-site interaction of the bosons of two different species U_{12} is set to zero ($U_{12} \rightarrow 0$) then the equations for the complex amplitudes c_j and d_j , and the quasiparticle amplitudes $u_{i,j}^l$ and $v_{i,j}^l$ are decoupled. The decoupled equations correspond to two independent single-component BEC in optical lattices.

To get a gapless spectrum for a TBEC, we use the Popov approximation, and set the anomalous average term \tilde{m}_{ij} to zero. Under HFB-Popov approximation, the coupled DNLSs can be written as

$$\mu_1 c_j = -J_1(c_{j-1} + c_{j+1}) + \left[\epsilon_j^{(1)} + U_{11}(n_{1j}^c + 2\tilde{n}_{1j}) + U_{12}(n_{2j}^c + \tilde{n}_{2j}) \right] c_j, \tag{2.58a}$$

$$\mu_2 d_j = -J_2(d_{j-1} + d_{j+1}) + \left[\epsilon_j^{(2)} + U_{22}(n_{2j}^c + 2\tilde{n}_{2j}) + U_{12}(n_{1j}^c + \tilde{n}_{1j}) \right] d_j. \tag{2.58b}$$

The HFB-Popov equations have the form

$$\begin{aligned}
E_l u_{1,j}^l = & - J_1(u_{1,j-1}^l + u_{1,j+1}^l) + \mathcal{U}_1 u_{1,j}^l - U_{11}c_j^2 v_{1,j}^l + U_{12}c_j(d_j^* u_{2,j}^l - d_j v_{2,j}^l), \tag{2.59a}
\end{aligned}$$

$$\begin{aligned}
E_l v_{1,j}^l = & J_1(v_{1,j-1}^l + v_{1,j+1}^l) + \underline{\mathcal{U}}_1 v_{1,j}^l + U_{11}c_j^{*2} u_{1,j}^l - U_{12}c_j^*(d_j v_{2,j}^l - d_j^* u_{2,j}^l), \tag{2.59b}
\end{aligned}$$

$$\begin{aligned}
E_l u_{2,j}^l = & - J_2(u_{2,j-1}^l + u_{2,j+1}^l) + \mathcal{U}_2 u_{2,j}^l - U_{22}d_j^2 v_{2,j}^l + U_{12}d_j(c_j^* u_{1,j}^l - c_j v_{1,j}^l), \tag{2.59c}
\end{aligned}$$

$$\begin{aligned}
E_l v_{2,j}^l = & J_2(v_{2,j-1}^l + v_{2,j+1}^l) + \underline{\mathcal{U}}_2 v_{2,j}^l + U_{22}d_j^{*2} u_{2,j}^l - U_{12}d_j^*(c_j v_{1,j}^l - c_j^* u_{1,j}^l), \tag{2.59d}
\end{aligned}$$

where $\mathcal{U}_1 = 2U_{11}n_{1j} + U_{12}n_{2j} + (\epsilon_j^{(1)} - \mu_1)$, $\mathcal{U}_2 = 2U_{22}n_{2j} + U_{12}n_{1j} + (\epsilon_j^{(2)} - \mu_2)$ with $\underline{\mathcal{U}}_i = -\mathcal{U}_i$. The condensate wave function and the quasiparticle amplitudes of the TBEC is obtained by expanding the condensate complex amplitudes (c_j, d_j) , and the quasiparticle amplitudes $(u_{i,j}^l, v_{i,j}^l)$ in terms of the localized orthonormalized Gaussian basis function

$$\psi_1(z) = \sum_j c_j \phi_j(z), \quad \psi_2(z) = \sum_j d_j \phi_j(z), \tag{2.60a}$$

$$u_i^l(z) = \sum_j u_{i,j}^l \phi_j(z), \quad v_i^l(z) = \sum_j v_{i,j}^l \phi_j(z). \quad (2.60b)$$

The quasiparticle amplitudes calculated from the diagonalization of the HFB Eqs. (2.59) are then used to obtain the density of the noncondensate atoms at the j th lattice site

$$\tilde{n}_{ij} = \sum_l [(|u_{ij}^l|^2 + |v_{ij}^l|^2)N_l + |v_{ij}^l|^2]. \quad (2.61)$$

The last term in \tilde{n}_{ij} is independent of the Bose factor, $N_l = (e^{\beta E_l} - 1)^{-1}$, and hence represents the quantum fluctuations of the system at zero temperature.

The HFB-Popov equations can be written in the matrix form

$$E_l \begin{pmatrix} \mathbf{u}_1^l \\ \mathbf{v}_1^l \\ \mathbf{u}_2^l \\ \mathbf{v}_2^l \end{pmatrix} = \begin{pmatrix} \mathcal{L}^{(1)} & \mathcal{M}^{(1)} & \mathcal{P} & \mathcal{Q} \\ -\mathcal{M}^{*(1)} & -\mathcal{L}^{(1)} & \mathcal{R} & \mathcal{S} \\ -\mathcal{S} & \mathcal{Q} & \mathcal{L}^{(2)} & \mathcal{M}^{(2)} \\ \mathcal{R} & -\mathcal{P} & -\mathcal{M}^{*(2)} & -\mathcal{L}^{(2)} \end{pmatrix} \begin{pmatrix} \mathbf{u}_1^l \\ \mathbf{v}_1^l \\ \mathbf{u}_2^l \\ \mathbf{v}_2^l \end{pmatrix}, \quad (2.62)$$

where the eigenstates \mathbf{u}_i^l , and \mathbf{v}_i^l are the set of quasiparticle amplitudes at different sites of i th species with eigenvalue E_l or quasiparticle energy. The matrix elements are given by

$$\begin{aligned} \mathcal{L}_{ij}^{(1)} &= -J_1 \sum_{\langle i,k \rangle} \delta_{ik} \delta_{kj} + \delta_{ij} \left(2U_{11}n_{1j} + U_{12}n_{2j} + \epsilon_j^{(1)} - \mu_1 \right), \\ \mathcal{M}_{ij}^{(1)} &= -U_{11} c_j^2 \delta_{ij}, \\ \mathcal{P}_{ij} &= U_{12} c_j d_j^* \delta_{ij}, \\ \mathcal{Q}_{ij} &= -U_{12} c_j d_j \delta_{ij}, \\ \mathcal{R}_{ij} &= U_{12} c_j^* d_j^* \delta_{ij}, \\ \mathcal{S}_{ij} &= -U_{12} c_j^* d_j \delta_{ij}, \\ \mathcal{L}_{ij}^{(2)} &= -J_2 \sum_{\langle i,k \rangle} \delta_{ik} \delta_{kj} + \delta_{ij} \left(2U_{22}n_{2j} + U_{12}n_{1j} + \epsilon_j^{(2)} - \mu_2 \right), \\ \mathcal{M}_{ij}^{(2)} &= -U_{22} d_j^2 \delta_{ij}. \end{aligned}$$

The matrix is non-Hermitian and non-symmetric with a dimension of $4(N_{\text{latt}} + 1) \times 4(N_{\text{latt}} + 1)$ with N_{latt} as the number of lattice sites in the system. Here, the number of orthonormalized Gaussian basis is equal to the number of lattice sites chosen for the system. The diagonalization of the matrix gives an equal number of positive and negative energy eigenvalues corresponding to the quasiparticle and quasihole amplitudes, respectively.

2.3.3 TBEC in quasi-2D optical lattices

We consider a binary BEC confined in an optical lattice with pancake shaped configuration of background harmonic trapping potential. Thus, the trapping frequencies satisfy the condition $\omega_{\perp} \ll \omega_z$ with $\omega_x = \omega_y = \omega_{\perp}$. In this system, the excitations along the axial direction are of higher energy and the degree of freedom in this direction is frozen. The excitations, both the quantum and thermal fluctuations, are considered only along the radial direction. In the TBA [183, 184], the BH Hamiltonian [27, 138, 190] which describes the system is

$$\begin{aligned} \hat{H} = & \sum_{k=1}^2 \left[-J_k \sum_{\langle \xi \xi' \rangle} \hat{a}_{k\xi}^{\dagger} \hat{a}_{k\xi'} + \sum_{\xi} (\epsilon_{\xi}^{(k)} - \mu_k) \hat{a}_{k\xi}^{\dagger} \hat{a}_{k\xi} \right] \\ & + \frac{1}{2} \sum_{k=1, \xi}^2 U_{kk} \hat{a}_{k\xi}^{\dagger} \hat{a}_{k\xi}^{\dagger} \hat{a}_{k\xi} \hat{a}_{k\xi} + U_{12} \sum_{\xi} \hat{a}_{1\xi}^{\dagger} \hat{a}_{1\xi} \hat{a}_{2\xi}^{\dagger} \hat{a}_{2\xi}, \end{aligned} \quad (2.63)$$

where $k = 1, 2$ is the species index, μ_k is the chemical potential of the k th species, and $\hat{a}_{k\xi}$ ($\hat{a}_{k\xi}^{\dagger}$) is the annihilation (creation) operator of the two different species at ξ th lattice site. The index is such that $\xi \equiv (i, j)$ with i and j as the lattice site index along x and y directions, respectively. The summation index $\langle \xi \xi' \rangle$, as mentioned earlier, represents the sum over nearest-neighbour to ξ th site. The possible values of ξ' in $\langle \xi \xi' \rangle$ are $(i-1, j)$, $(i+1, j)$, $(i, j-1)$, and $(i, j+1)$. The TBA is valid when the depth of the lattice potential is much larger than the chemical potential, $V_0 \gg \mu_k$, the BH Hamiltonian then describes the system when the bosonic atoms occupy the lowest energy band. In the BH Hamiltonian, J_k s are the tunneling matrix elements, $\epsilon_{\xi}^{(k)}$ is the offset energy arising due to background harmonic potential, and U_{kk} (U_{12}) is the intraspecies (interspecies) interaction strength.

In the weakly interacting regime, under the Bogoliubov approximation [162, 187], the annihilation operators at each lattice site can be decomposed as $\hat{a}_{1\xi} = (c_{\xi} + \hat{\varphi}_{1\xi})e^{-i\mu_1 t/\hbar}$, $\hat{a}_{2\xi} = (d_{\xi} + \hat{\varphi}_{2\xi})e^{-i\mu_2 t/\hbar}$, where c_{ξ} and d_{ξ} are the complex amplitudes describing the condensate phase of the two species. The operators $\hat{\varphi}_{1\xi}$ and $\hat{\varphi}_{2\xi}$ represent the quantum or thermal fluctuation part of the field operators. From the equation of motion of the field operators with the Bogoliubov approximation, the equilibrium

properties of a TBEC is governed by the DNLSs

$$\mu_1 c_\xi = - J_1 \sum_{\xi'} c_{\xi'} + \left[\epsilon_\xi^{(1)} + U_{11}(n_{1\xi}^c + 2\tilde{n}_{1\xi}) + U_{12}n_{2\xi} \right] c_\xi, \quad (2.64a)$$

$$\mu_2 d_\xi = - J_2 \sum_{\xi'} d_{\xi'} + \left[\epsilon_\xi^{(2)} + U_{22}(n_{2\xi}^c + 2\tilde{n}_{2\xi}) + U_{12}n_{1\xi} \right] d_\xi, \quad (2.64b)$$

where $n_{1\xi}^c = |c_\xi|^2$ and $n_{2\xi}^c = |d_\xi|^2$ are the condensate, $\tilde{n}_{k\xi} = \langle \hat{\varphi}_{k\xi}^\dagger \hat{\varphi}_{k\xi} \rangle$ are the non-condensate, and $n_{k\xi} = n_{k\xi}^c + \tilde{n}_{k\xi}$ are the total density of the species. The fluctuation operators are defined in terms of the quasiparticle basis through the Bogoliubov transformation

$$\hat{\varphi}_{k\xi} = \sum_l \left[u_{k\xi}^l \hat{\alpha}_l e^{-i\omega_l t} - v_{k\xi}^{*l} \hat{\alpha}_l^\dagger e^{i\omega_l t} \right], \quad (2.65)$$

where $\hat{\alpha}_l$ ($\hat{\alpha}_l^\dagger$) is the quasiparticle annihilation (creation) operator, which satisfies the Bose commutation relations, l is the quasiparticle mode index, $u_{k\xi}^l$ and $v_{k\xi}^l$ are the quasiparticle amplitudes for the k th species, and $\omega_l = E_l/\hbar$ is the frequency of the l th quasiparticle mode with energy E_l .

Using the Bogoliubov transformation, we obtain the following HFB-Popov equations [194]:

$$E_l u_{1,\xi}^l = - J_1 (u_{1,\xi-1}^l + u_{1,\xi+1}^l) + \mathcal{U}_1 u_{1,\xi}^l - U_{11} c_\xi^2 v_{1,\xi}^l + U_{12} c_\xi (d_\xi^* u_{2,\xi}^l - d_\xi v_{2,\xi}^l), \quad (2.66a)$$

$$E_l v_{1,\xi}^l = J_1 (v_{1,\xi-1}^l + v_{1,\xi+1}^l) + \underline{\mathcal{U}}_1 v_{1,\xi}^l + U_{11} c_\xi^{*2} u_{1,\xi}^l - U_{12} c_\xi^* (d_\xi v_{2,\xi}^l - d_\xi^* u_{2,\xi}^l), \quad (2.66b)$$

$$E_l u_{2,\xi}^l = - J_2 (u_{2,\xi-1}^l + u_{2,\xi+1}^l) + \mathcal{U}_2 u_{2,\xi}^l - U_{22} d_\xi^2 v_{2,\xi}^l + U_{12} d_\xi (c_\xi^* u_{1,\xi}^l - c_\xi v_{1,\xi}^l), \quad (2.66c)$$

$$E_l v_{2,\xi}^l = J_2 (v_{2,\xi-1}^l + v_{2,\xi+1}^l) + \underline{\mathcal{U}}_2 v_{2,\xi}^l + U_{22} d_\xi^{*2} u_{2,\xi}^l - U_{12} d_\xi^* (c_\xi v_{1,\xi}^l - c_\xi^* u_{1,\xi}^l), \quad (2.66d)$$

where $\mathcal{U}_1 = 2U_{11}(n_{1\xi}^c + \tilde{n}_{1\xi}) + U_{12}(n_{2\xi}^c + \tilde{n}_{2\xi}) + (\epsilon_\xi^{(1)} - \mu_1)$, $\mathcal{U}_2 = 2U_{22}(n_{2\xi}^c + \tilde{n}_{2\xi}) + U_{12}(n_{1\xi}^c + \tilde{n}_{1\xi}) + (\epsilon_\xi^{(2)} - \mu_2)$ with $\underline{\mathcal{U}}_k = -\mathcal{U}_k$. To solve the above eigenvalue equations, we use a basis set of on-site Gaussian wave functions, and define the quasiparticle amplitude as linear combination of the basis functions. The condensate and noncondensate densities are then computed through the self-consistent solution of Eqs. (2.64)

and (2.66). The noncondensate atomic density at the ξ th lattice site is

$$\tilde{n}_{k\xi} = \sum_l [(|u_{k\xi}^l|^2 + |v_{k\xi}^l|^2) N_l + |v_{k\xi}^l|^2], \quad (2.67)$$

where $N_l = (e^{\beta E_l} - 1)^{-1}$ with $\beta = (k_B T)^{-1}$ is the Bose-Einstein distribution factor of the l th quasiparticle mode with energy E_l at temperature T . The last term in $\tilde{n}_{k\xi}$ is independent of the temperature and hence represents the quantum fluctuations of the system.

Chapter 3

Topological transition of quasi-1D binary condensates

The phenomenon of *spontaneous symmetry breaking* (SSB) is ubiquitous in nature. In condensed matter physics, it is responsible for the paramagnetic to ferromagnetic phase transition [195] and in high energy physics, it underlies our understanding of the fundamental interactions and the origin of masses of elementary particles [196–198]. Apart from these, it also plays a key role in other fields of physics, in particular, cosmology [199], liquid crystals [200], and superfluid helium [201]. In these scenarios, a small fluctuations break the underlying symmetry of the system and thus determines its dynamical evolution and the final state. In general, the symmetry breaking occurs when a parameter of the system, such as temperature, is changed across a certain value. The BECs provide unprecedented possibilities to study the symmetry breaking processes [202]. This is due to its experimental flexibility with almost all parameters can be precisely controlled. Moreover, the symmetry breaking phenomena is important in understanding the BECs and their coherence properties [203, 204]. When SSB occurs, a gapless mode known as Nambu-Goldstone (NG) mode must appear in the long-wavelength limit of the excitation spectrum. This is referred to as Goldstone’s theorem [205–207]. In a single-component BEC, the appearance of the order parameter is associated with a gapless NG mode corresponding to SSB of the global U(1) gauge symmetry. This mode is known as a phonon mode with linear dispersion relation. The first excited mode ($l = 1$) is the dipole mode, also known as the Kohn mode,

corresponds to the oscillatory motion of the center of mass when the system is perturbed. Decrease in the Kohn mode frequency due to an increase in the effective mass is reported in previous theoretical [208, 209] and experimental study [210]. The $l = 2$ mode is known as the quadrupole mode, and the higher modes ($l = 3, 4$) represent more complicated collective excitations [162]. As example we have computed the low-lying quasiparticle mode functions for ^{87}Rb condensate using the HFB theory, and these are shown in Fig. 3.1. The parameters used were $U/J = 0.2$, $\Omega = 3.48 \times 10^{-2} E_R$, and $N = 100$.

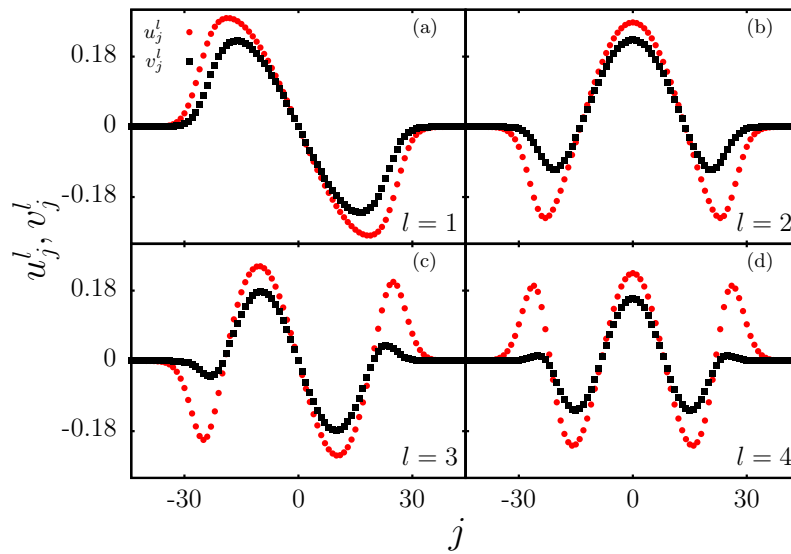


Figure 3.1: The low-lying quasiparticle amplitudes corresponding to the (a) dipole mode, (b) quadrupole mode and (c-d) other higher-energies excited modes are shown for ^{87}Rb condensate trapped in quasi-1D optical lattice. Here l and j represent the quasiparticle mode and lattice site index.

The nature of the ground state of TBECs is determined by the balance between the on-site interactions. If the intraspecies interactions dominate then the energy of the system is minimized by the overlap of the species. However, if the interspecies interaction dominate then the energy is minimized by the phase separation, where an additional Goldstone mode may appear in quasi-1D condensates. The approach of counting the NG modes and generalization of the NG theorem in non-relativistic system is proposed in Refs. [211–217]. The detailed analysis for the NG modes in the phase-separated BECs can be found in Refs. [218, 219]. Experimentally, it is possible to vary the on-site interactions through the Feshbach resonance [220–222], and drive

the TBEC from the miscible to the immiscible phase or vice versa. The experiments with harmonic trapping potential have examined the phase separation [46, 48–50, 61], and other unique phenomenon which are associated with the TBECs. Among the various lines of investigation, the theoretical studies of phase separation and the collective modes [154–157, 160, 223–226] are noteworthy. In the context of lattice systems, the phase separation of two-species Bose mixtures in 1D optical lattices has been investigated using mean-field theory [134] and DMRG technique [135, 136, 227]. In these studies, both SF and MI phases are considered, and the phase separation results into several new phases such as 2SF, phase-separated SF and phase-separated MI. The recent experimental realizations of TBECs in optical lattices [26, 109–111] provide the motivation to examine the phase separation phenomena for the superfluid bosonic mixtures in lattice systems.

In this chapter, we consider a mixture of two dilute atomic Bose gases confined in optical lattices at zero temperature. The parameters are chosen such that the system is quasi-1D, and the mean-field description like HFB-Popov is applicable. The low-dimensional BECs are important to study because the role of quantum fluctuations are more pronounced in these systems [24, 228–230]. According to Mermin-Wagner-Hohenberg theorem [231–233], in a translationally invariant system no continuous symmetry can be spontaneously broken at finite temperatures for $d \leq 2$, where d is the dimensionality of the system. Therefore, BEC does not exist in one or two dimensions, but in traps the situation is different as the confining potential modifies the density of states [234]. To obtain a system with effective lower dimensions or the motion of the atoms to be frozen out in a particular direction, the energy difference between states must be much greater than the thermal energy $k_B T$. In quasi-1D optical lattices we use HFB-Popov theory to study the ground state density profiles, and the quasiparticle spectrum of TBECs at zero temperature. The evolution of the quasiparticle modes are examined as the TBEC is driven from the miscible to the immiscible phase. This transition is achieved through the variation of intra- (inter) species on-site interaction in the BH model for ^{87}Rb - ^{85}Rb (^{133}Cs - ^{87}Rb) TBEC. We demonstrate a key feature of the ^{87}Rb - ^{85}Rb TBEC, which is the exchange of the positions of the species at same on-site intraspecies interactions. Furthermore, the interaction and the quantum

fluctuation-induced effects on the topology of the ground state and the quasiparticle spectra of the TBECs are examined. It is important to note that in this chapter the term topology refers to the geometry of the ground state density distributions of TBECs in optical lattices. This is characterized by the gauge symmetry possessed by the mixture of BECs.

3.1 Zero temperature mode evolution of trapped TBEC

The excitation spectrum shows a distinct feature when the critical point of the quantum phase transition is crossed. Under the HFB-Popov approximation, the excitation spectrum of TBEC in optical lattice is gapless for the superfluid (SF) phase, while it exhibits a finite gap for the Mott insulator (MI) phase [29]. In the MI phase, this energy gap corresponds to the particle-hole excitation, and is responsible for the insulating properties of the system. The SF phase also referred to as the ordered phase where the order parameter takes on a nonzero value at the minimum of the potential. The phase of the atoms thereby acquires a definite value through SSB of the $U(1)$ global gauge symmetry. In the SF phase of TBEC, the SSB at condensation results in two Goldstone modes, one each for the two species. The number of Goldstone modes, however, depends on whether the system is in miscible or immiscible phase, and geometry of the density distributions. To explore different possibilities, as mentioned earlier, we consider two different TBEC systems. These are binary mixtures which can be driven from the miscible to the immiscible phase through the variation of intra- or interspecies interaction using the Feshbach resonance. In particular, we consider ^{87}Rb - ^{85}Rb [50, 51] and ^{133}Cs - ^{87}Rb [45, 46] binary condensates as examples of the two cases, and study the mode evolution as the system approaches the immiscible regime from the miscible regime. These are examples of two systems with negligible and large difference in the masses of two species, respectively. Another basic difference is the transition of miscible to the immiscible phase is achieved through the variation of (intra-) interspecies on-site interaction in the $(^{87}\text{Rb}$ - $^{85}\text{Rb})$ ^{133}Cs - ^{87}Rb TBEC.

3.1.1 Third Goldstone mode in ^{87}Rb - ^{85}Rb TBEC

To examine the mode evolution with the tuning of the intraspecies interaction, we consider a quasi-1D TBEC consisting of two different isotopes of Rubidium: ^{87}Rb and ^{85}Rb [50, 51]. In this system, we consider ^{87}Rb and ^{85}Rb as the first and second species, respectively. The axial trapping frequency of the harmonic potential for both the species is $\omega_z = 2\pi \times 80$ Hz with the anisotropy parameters along the x and y directions as 12.33. The anisotropy parameter is the ratio of the radial trapping frequency (ω_x and ω_y) to the axial trapping frequency ω_z . The wavelength of the laser beam that is used to create the optical lattice potential is $\lambda_L = 775$ nm. The number of atoms in each of the species are $N_1 = N_2 = 100$, which are confined in 100 lattice sites superimposed on a harmonic potential. We choose the depth of the lattice potential $V_0 = 5E_R$ and corresponding to this depth the tunneling matrix elements for the two species are $J_1 = 0.66E_R$ and $J_2 = 0.71E_R$, the intraspecies interaction U_{11} is $0.05E_R$ and the interspecies interaction U_{12} is $0.1E_R$. The difference in the values of J_1 and J_2 arises from the mass difference of the species in the TBEC system. This set of DNLSE parameters is calculated by considering the scattering lengths $a_{11} = 99a_0$ and $a_{12} = 214a_0$, where a_0 is the Bohr radius and the width of the Gaussian basis as $0.3a$. To compute the value of DNLSE parameters we use the definitions of the tunneling matrix element and the on-site interaction described in Chapter 2 [Eqs. (2.22)].

Since the scattering length of ^{85}Rb is tunable with the Feshbach resonance [50], we study the excitation spectrum with the variation in U_{22} . The solution of the mean-field model [100, 102] predicts that the critical value of $\nu U_{ii}/J_i$ at which the SF-MI phase transition occurs, depends on the density and the dimensionality of the lattice. However, for the value of U 's and J 's considered here, the TBEC remains in the SF phase. In the computations the characteristic length and energy are the lattice spacing and the recoil energy of the first species, respectively. To examine the ground state density, and the quasiparticle spectra at zero temperature, the coupled DNLSEs [Eq. (2.55)] and BdG equations [Eqs. (2.59)] are solved. It is important to note that the quantum fluctuations are ignored for these calculations. The diagonalization of the BdG matrix results into eigenvalues and eigenstates as the quasiparticle mode energies and quasiparticle amplitudes, respectively. The quasiparticle mode energies with the variation

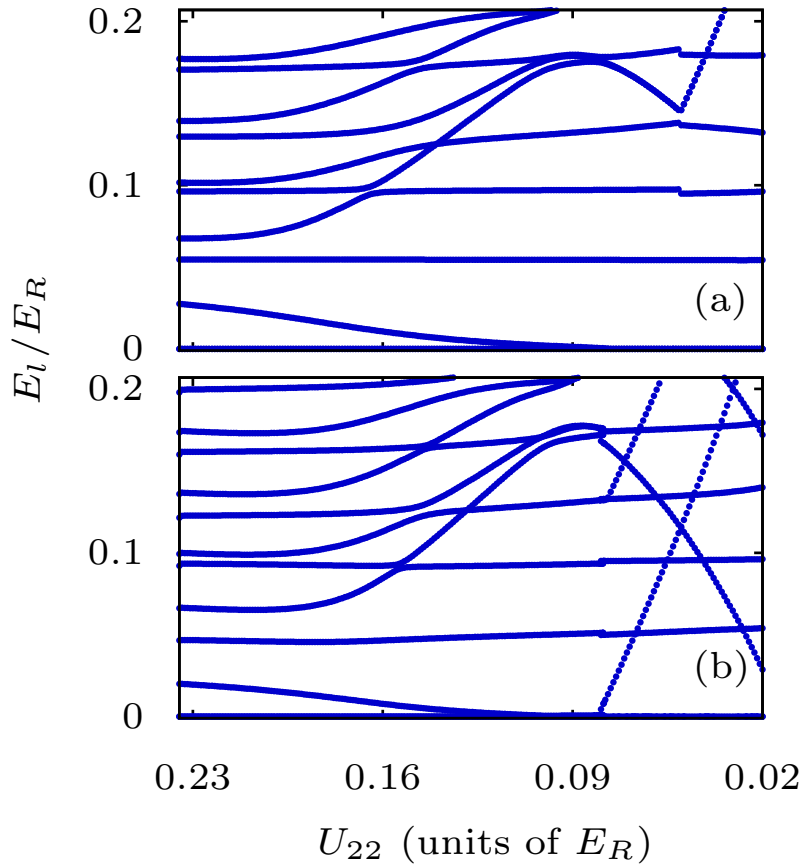


Figure 3.2: The evolution of the low-lying mode energies as a function of the intraspecies interaction of the ^{85}Rb (U_{22}) in the ^{87}Rb - ^{85}Rb TBEC held in quasi-1D optical lattices. Excitation spectrum is shown (a) for zero temperature and (b) for zero temperature in the presence of the quantum fluctuations. Here U_{22} is in units of the recoil energy E_R .

in U_{22} at zero temperature are shown in Fig. 3.2(a). The two zero energy mode are the NG modes associated with SSB of each of the condensate. The lowest energy modes with nonzero excitation energies, are the Kohn modes ($l = 1$) of the two species of ^{87}Rb - ^{85}Rb TBEC. At $U_{22} = 0.25E_R$, these modes have energies $0.029E_R$ and $0.054E_R$ for ^{85}Rb and ^{87}Rb , respectively. The energy of the ^{85}Rb Kohn mode decreases, whereas that of ^{87}Rb Kohn mode remains steady with the decrease in U_{22} . According to Kohn's theorem, for a BEC confined in a harmonic trap, the center of mass oscillates with the harmonic trapping frequency [235]. The excitation energy of the Kohn mode in a harmonic potential with frequency ω is $\hbar\omega$ which is independent of the strength and type of the two-body interaction [236]. In the BH model, the Kohn mode energy deviates

from this universal value due to the presence of the optical lattice. Recently, it has been predicted that the Kohn theorem is also violated in the vicinity of a Feshbach resonance for harmonically trapped BEC [237]. At lower U_{22} , the energy of ^{85}Rb Kohn mode decreases further, and for $U_{22} \leq 0.062E_R$ the mode continues as the third Goldstone mode. To gain further insight into the structure of Kohn modes we investigate

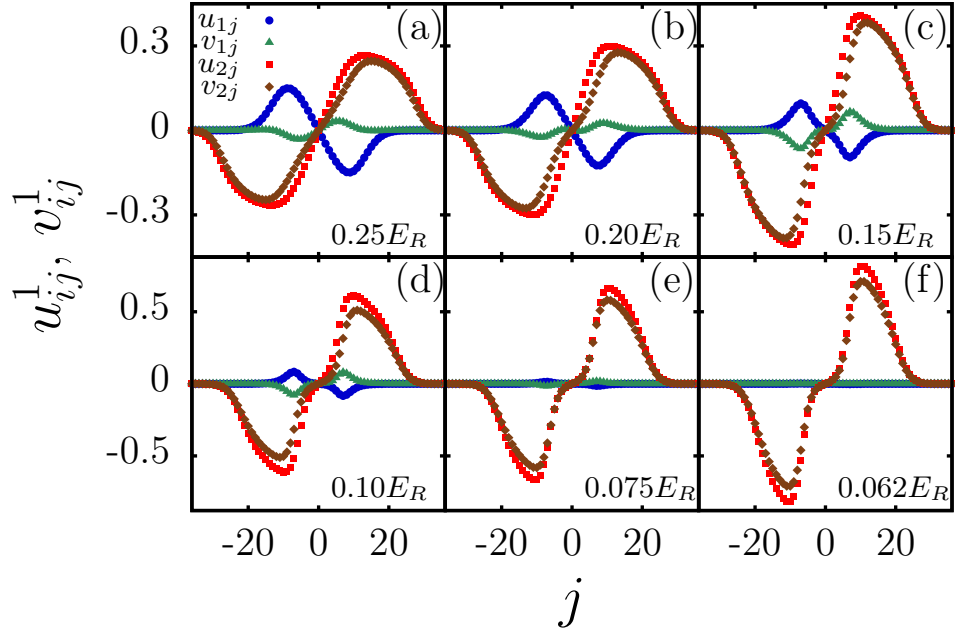


Figure 3.3: The evolution of the quasiparticle amplitudes corresponding to the Kohn mode as the intraspecies interaction of ^{85}Rb (U_{22}) is decreased from $0.25E_R$ to $0.062E_R$. (a), (b) When $U_{22} \geq 0.18E_R$, the system is in the miscible phase and the Kohn mode ($l = 1$) has contributions from both the species. (c)-(e) When system is on the verge of phase separation, then the Kohn mode of ^{85}Rb goes soft. (f) At phase separation $U_{22} \leq 0.065E_R$ the Kohn mode transforms into a Goldstone mode. Here i and j are the index for the species and the lattice site, respectively. The quasiparticle amplitudes (u_{ij}, v_{ij}) of the first species ($i = 1$) are shown by blue filled circles (\bullet) and green triangles (\blacktriangle), and for the second species ($i = 2$) these are shown by red squares (\blacksquare) and brown diamonds (\blacklozenge).

the quasiparticle amplitudes or mode functions corresponding to the Kohn modes of ^{87}Rb and ^{85}Rb . The evolution of the Kohn mode functions with the variation of U_{22} is shown in Fig. 3.3. The modes of the species evolves differently as U_{22} is decreased and mode mixing occurs for nonzero U_{12} . For $0.18 \leq U_{22} \leq 0.25E_R$, the system is

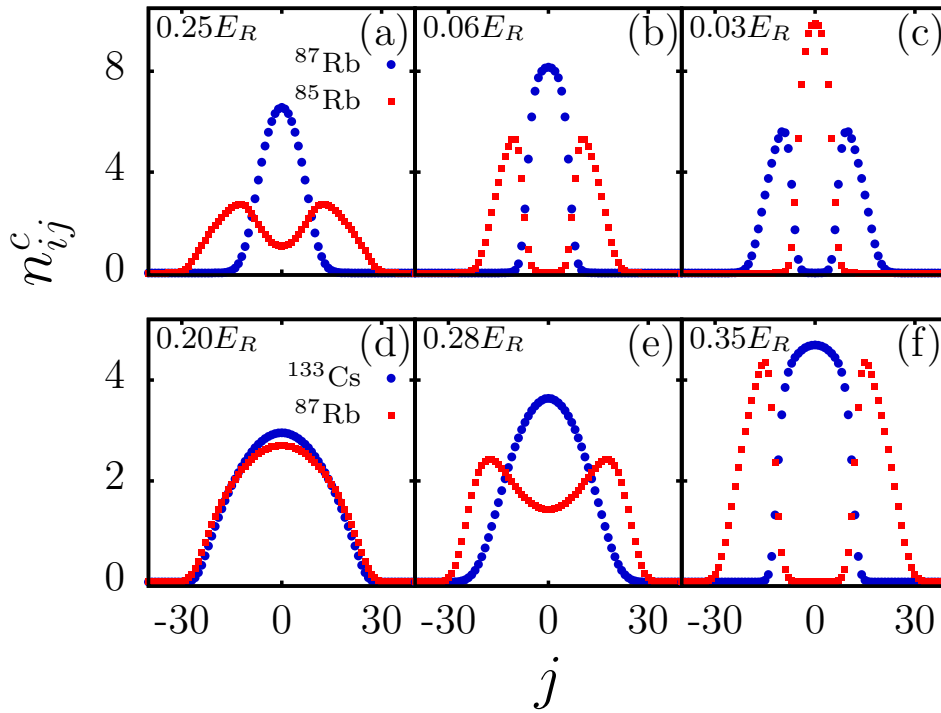


Figure 3.4: The geometry of the condensate density profiles and its transition from the miscible to the immiscible regime. (a)-(c) The transition from the miscible to the sandwich profile for the ^{87}Rb - ^{85}Rb TBEC with change in the intraspecies interaction U_{22} at $T = 0$ K. The position exchange (c) in the sandwich profile occurs at $U_{11} = U_{22} = 0.05E_R$. (d)-(f) Show similar condensate density profiles for the Cs-Rb TBEC with change in the interspecies interaction U_{12} at $T = 0$ K. In this system the transition to the sandwich geometry occurs at $U_{12}^c = 0.3E_R$. The density profiles of first and second species at each lattice site j are shown by blue circles (\bullet) and red squares (\blacksquare).

in the miscible domain, and the Kohn mode function of the TBEC is a linear combination of the mode functions of ^{87}Rb and ^{85}Rb species. As we approach the phase separation by reducing the value of U_{22} , we observe a decrease in the amplitude of the Kohn mode function of ^{87}Rb , and the mode component of ^{85}Rb goes soft at $0.062E_R$. The softening of the mode is also evident from the evolution of the mode energies as shown in Fig. 3.2(a). The emergence of the third Goldstone mode is associated with a change in the ground state geometry of the system; the density changes from the overlapping to a sandwich profile as shown in Figs. 3.4(a-c). The structure of the Kohn mode at $U_{22} = 0.062E_R$, as shown in Fig. 3.3(f), is similar to the condensate density profile of ^{85}Rb in the immiscible domain with opposite phase [Fig. 3.4(b)]. In the

phase-separated domain, the sandwich profile of the binary condensate is equivalent to three distinct sub-components, where one species is flanked by the other. This is in contrast to the mode evolution with harmonic potential only. In continuum, for TBECs with near equal masses and low number of atoms the energetically preferred ground state geometry is of side-by-side type [219, 238]. The softening of the Kohn mode has been studied for single-species BEC confined in a double-well potential [239]. An important aspect which deserves to be mention is that the phase separation criteria for the homogeneous system predicts the transition at $U_{22}^c \leq U_{12}^2/U_{11}$. This condition is not valid for the present study as the confining potential, and the contributions of the kinetic energy impact the criteria of the immiscibility [240].

3.1.2 Third Goldstone mode in ^{133}Cs - ^{87}Rb TBEC

For mode evolution with the tuning of interspecies interaction, we consider the binary system of ^{133}Cs - ^{87}Rb [45, 46]. Here, we consider Cs and Rb as the first and second species, respectively. To study the mode evolution as the system undergoes the transition from miscible to the immiscible phase, the interspecies interaction U_{12} is varied, which is possible using the magnetic Feshbach resonance [222]. The parameters of the system considered are $N_1 = N_2 = 100$ with the similar trapping frequencies as in the case of the ^{87}Rb - ^{85}Rb mixture. The lattice parameters are chosen as $J_1 = 0.92E_R$, $J_2 = 1.95E_R$, $U_{11} = 0.40E_R$, and $U_{22} = 0.21E_R$. These parameters correspond to the scattering lengths $a_{11} = 280a_0$, and $a_{22} = 99a_0$ and the same width of the Gaussian basis function is considered as in the previous case. For this system, the difference in the tunneling matrix elements of the species is large, as compared to the case of ^{87}Rb - ^{85}Rb TBEC. This is due to large mass difference of the constituent species of ^{133}Cs - ^{87}Rb TBEC.

At $U_{12} = 0$, the quasiparticle spectrum of the TBEC is independent as the two condensates are decoupled. The TBEC has two Goldstone modes, one corresponding to each of the two species. At low values of U_{12} , in the miscible regime, the condensate density profile of both the species overlap as shown in Fig. 3.4(d). As we increase U_{12} , the Kohn mode of ^{133}Cs remains steady in energy whereas that of ^{87}Rb gradually decreases, and goes soft at a critical value $U_{12}^c = 0.3E_R$. This Kohn mode of

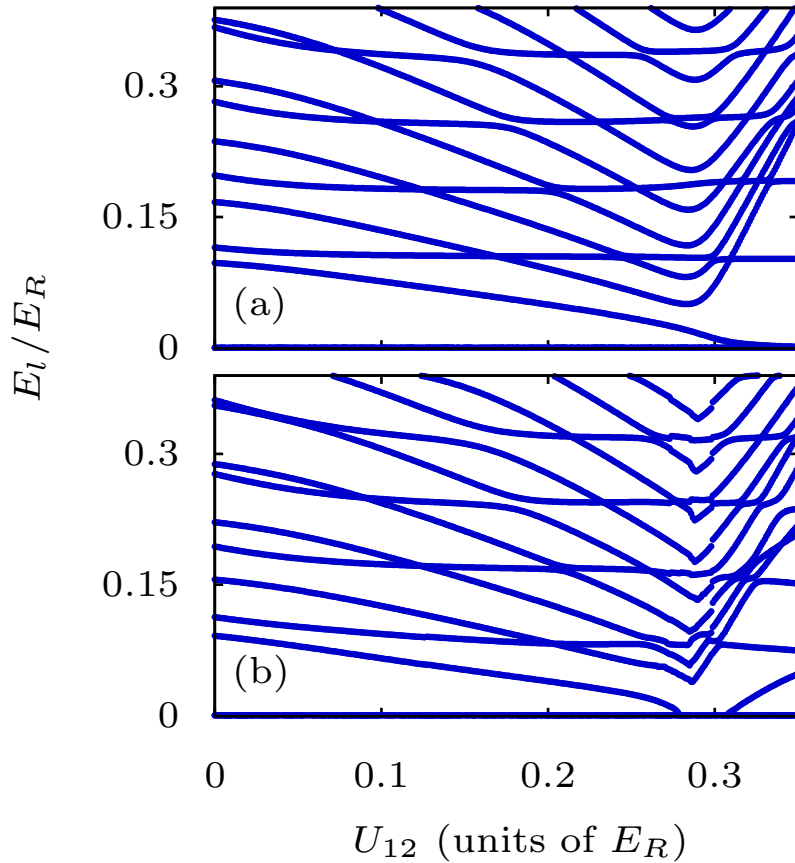


Figure 3.5: The evolution of the energies of the low-lying modes as a function of the interspecies interaction (U_{12}) in Cs-Rb TBEC held in a quasi-1D lattice potential. The excitation spectrum is shown (a) at $T = 0$ K, and (b) after including the quantum fluctuations. Here U_{12} is in units of the recoil energy E_R .

Rb remains soft for $U_{12} \geq 0.3E_R$ and is transformed into the third Goldstone mode. For $U_{12}^c < U_{12}$, the geometry of the condensate density profile changes, and acquires a sandwich structure in which the Cs condensate (higher mass) is at the center, and flanked by the Rb condensate (lower mass) at the edges as shown in Fig. 3.4(f). This is also evident from the evolution of the low-lying modes, shown in Fig. 3.5(a), and is reflected in the structural evolution of the quasiparticle amplitudes shown in Fig. 3.6. Hence, the system gains an extra Goldstone mode after transition from a miscible to a sandwich type density profile. The general trend of the mode evolution is that the mode energies decrease with increase in U_{12} , reach minimal values at the phase separation and then, increase in the immiscible domain. Here, the control parameter, which is the interspecies interaction is analogous to the barrier height in case of BEC in a

double-well potential. When the U_{12} or the barrier height is zero then the energy of the lowest excitation remains steady, whereas it decreases as the U_{12} or the barrier height is increased [241]. Another key feature is that the avoided crossing of the excitations are present in the quasiparticle mode evolution as U_{12} is varied to higher values [219, 242]. We find that the mass difference of the species does not play an important role in determining the topology of the TBECs in quasi-1D optical lattice.

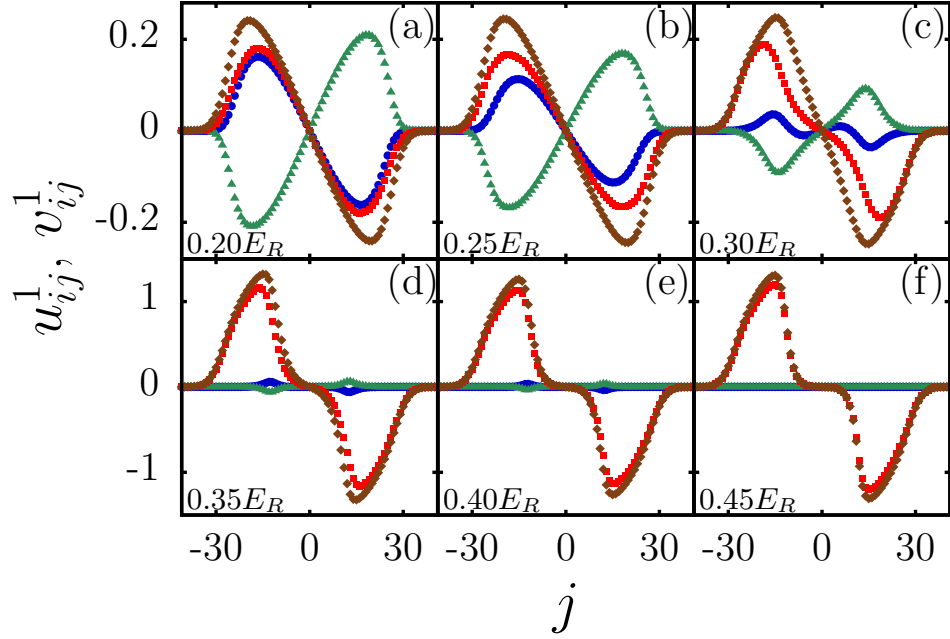


Figure 3.6: The evolution of the quasiparticle amplitudes corresponding to the Kohn mode as the interspecies interaction is increased from $0.2E_R$ to $0.35E_R$ for a Cs-Rb TBEC in quasi-1D lattice potential at $T = 0$ K. (a)-(c) In miscible regime, the Kohn mode has contributions from both the species. (d)-(f) For $U_{22} \geq 0.3E_R$ the Kohn mode of ^{87}Rb goes soft, whereas that of ^{133}Cs decreases in amplitude.

3.2 Position exchange of species

A mixture of two BECs are ideal systems to understand the development of the hydrodynamical instability [77, 243]. Recently, there has been a surge of interest in the study of the instability at the interface separating the immiscible components [78, 244–249]. Among these the Rayleigh-Taylor instability (RTI) [250, 251] ubiquitous in nature where the excess potential energy is transformed into the kinetic energy by means of

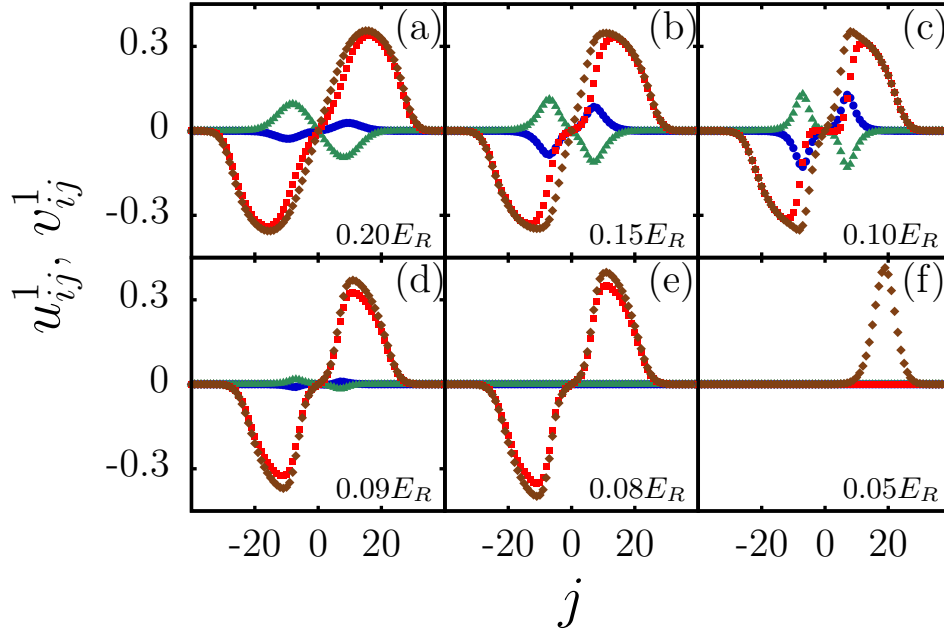


Figure 3.7: The evolution of the quasiparticle amplitudes corresponding to the Kohn mode for ^{87}Rb - ^{85}Rb TBEC in the presence of the fluctuations as the intraspecies interaction of ^{85}Rb (U_{22}) is decreased from $0.2E_R$ to $0.05E_R$. (a)-(e) The Kohn mode of ^{85}Rb goes soft, whereas that of ^{87}Rb decreases in amplitude and finally vanishes in (e). (f) The sloshing mode, which emerges after phase separation as the sandwich density profile transforms into a side-by-side profile.

the interfacial waves, and these waves grow into mushroom-shaped bubbles. In the classical hydrodynamical system, the RTI develops when a lighter fluid supports a heavier one in a gravitational field. In such a case the two immiscible fluids, with negligible diffusion, exchange positions, and reduce the potential energy with the onset of RTI. In quantum systems, the potential energy may transform into the kinetic energy with the interpenetrations of the condensates. The position exchange of two immiscible harmonically trapped BECs by the virtue of an external magnetic field is demonstrated in Refs. [252–254]. In the present work, we observe the exchange of the positions of the condensates for equilibrium case in quasi-1D optical lattice. A remarkable feature in the evolution of the condensate density profiles of ^{87}Rb - ^{85}Rb TBEC with the variation of U_{22} is the observation of the position exchange in the immiscible domain. This is absent when the trapping potential consists of only a harmonic potential (continuous system), and is the result of the discrete symmetry associated with the optical lattice.

As discussed earlier, in this system, we fix U_{11} and U_{12} , and vary U_{22} (intraspecies interaction of ^{85}Rb). At higher values of U_{22} the TBEC is in the miscible phase, and as we decrease U_{22} , at the critical value $U_{22}^c = 0.17E_R$ the TBEC enters the immiscible domain. The geometry of the density profiles is of sandwich type and the component with smaller U_{ii} is at the center. An example of a condensate density profile in this domain, $U_{22} = 0.06E_R$, is shown in Fig. 3.4(b). In the figure, the species with smaller intraspecies interaction (^{87}Rb) is at the center, and ^{85}Rb is at the edges. As U_{22} is further decreased, the system continues to be in the same phase. During evolution, an instability arises when both the intraspecies interactions are same ($U_{11} = U_{22} = 0.05E_R$). At this value of U_{22} the components exchange their positions in the trap. This is also reflected in the excitation spectrum; a discontinuity at $U_{22} = 0.05E_R$ in the plot of the quasiparticle mode evolution shown in Fig. 3.2(a) is a signature of the instability. On further decrease of U_{22} , we enter the $U_{22} < U_{11}$ domain and ^{85}Rb occupies the center of the trap. An example of the density profiles in this domain, $U_{22} = 0.03E_R$, is shown in Fig. 3.4(c). The position exchange, however, does not occur in the Cs-Rb system as in that case we vary U_{12} .

3.3 Effect of quantum fluctuations

The NG modes resulting from the SSB play crucial role in determining the low-energy behaviour of various systems from the condensed matter to the high energy physics. In previous section, we have discussed that the Kohn mode goes soft in the phase-separated domain, and emerges as an extra Goldstone mode. The soft mode gain energy in the presence of quantum fluctuations at $T = 0$ K. In the context of gauge theories, the symmetry breaking of the ground state was proposed by Weinberg and these modes were referred to as quasi-NG modes [255, 256]. At zero temperature, the quasi-NG modes behave like Goldstone mode but gain energy due to finite fluctuations. Recently, the hardening of the Goldstone mode in spinor BECs due to quantum fluctuations has been predicted [257]. We compute the condensate profiles and the quasiparticle modes for ^{87}Rb - ^{85}Rb TBEC, including the effect of quantum fluctuations. We, however, encounter severe oscillations in the number of atoms during the

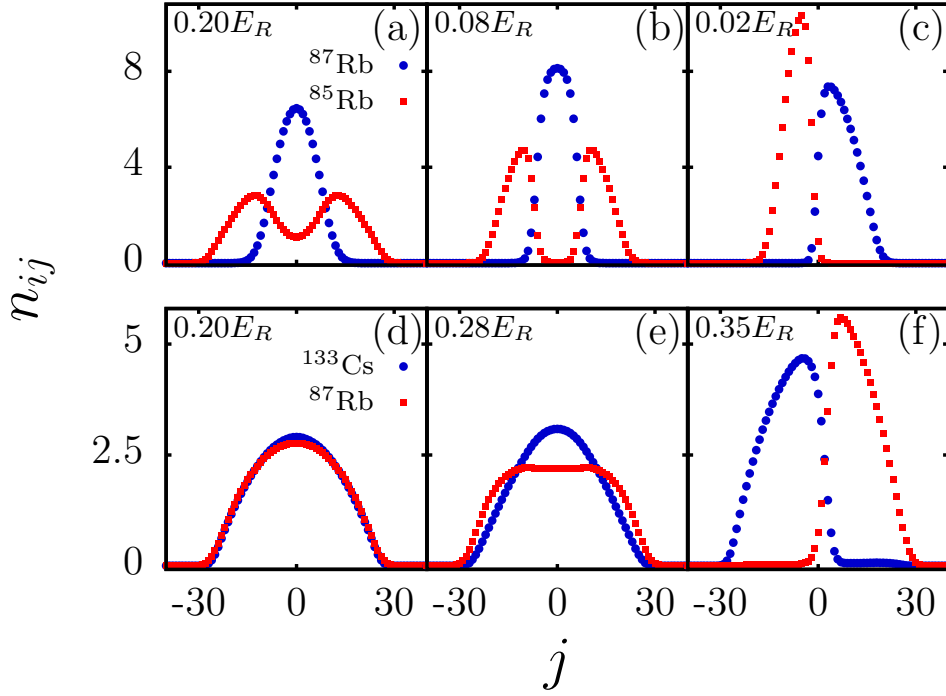


Figure 3.8: The fluctuation-induced transition in the geometry of the total density profile (condensate + quantum fluctuations) of a TBEC at $T = 0$ K in a quasi-1D lattice potential. (a)-(c) The transition in the ^{87}Rb - ^{85}Rb system from the miscible to the sandwich and finally to the side-by-side profile with the change in the intraspecies interaction. (d)-(e) The transition in the Cs-Rb TBEC from the miscible to the side-by-side profile with change in the interspecies interaction U_{12} . The geometry of the ground state of both systems in the immiscible regime is different from that at zero temperature in the absence of the fluctuations, shown in Fig. 3.4.

iterations to solve the DNLSEs self-consistently and there is no convergence. To mitigate this, we use a successive under-relaxation technique with $r^{\text{un}} = 0.6$. The details of the relaxation technique used to get converged solutions is given in the appendix of the thesis. For computations, we consider the same set of parameters as in the case of zero temperature without fluctuations. The generalized DNLSEs [Eq. (2.55)] and the HFB-Popov equations [Eqs. (2.59)] are then solved self-consistently to get the ground state density and the quasiparticle spectra. We observe that the fluctuations break the spatial symmetry of the system as we vary the intraspecies interaction of ^{85}Rb (U_{22}). In the immiscible domain, the condensate density profile changes from the sandwich to the side-by-side configuration at $0.078E_R$. The system acquires a new stable ground

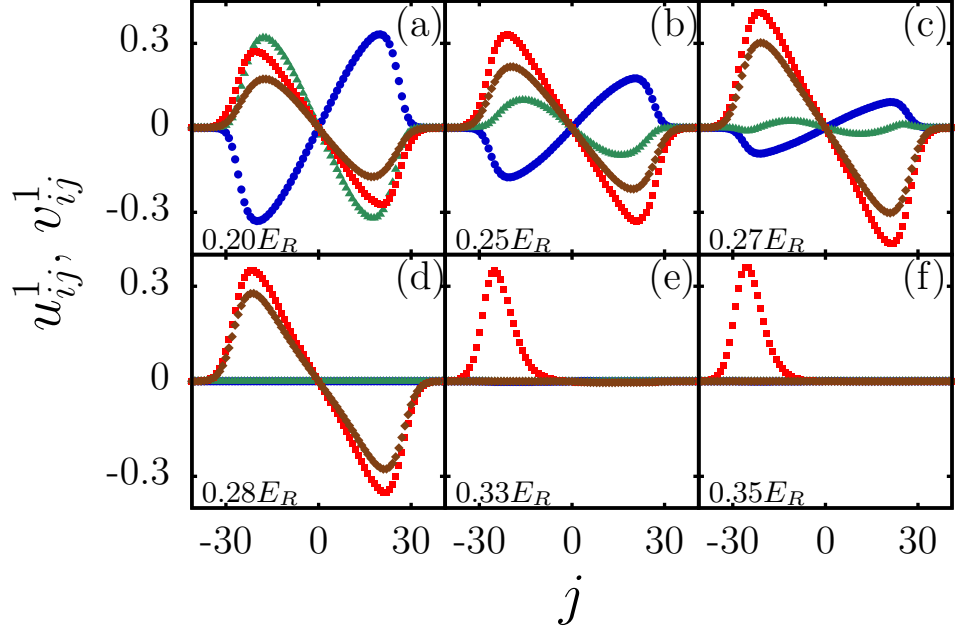


Figure 3.9: The evolution of the quasiparticle amplitudes corresponding to the Kohn mode for the Cs-Rb TBEC in the presence of quantum fluctuations at $T = 0$ K. (a)-(d) The Kohn mode evolves as the interspecies interaction is increased. (e), (f) It is transformed into a sloshing mode as the TBEC acquires the side-by-side density profile after phase separation.

state as the chemical potential of the system decreases from $0.92E_R$ to $0.80E_R$. With the inclusion of fluctuations, the evolution of the mode energies as a function of U_{22} is shown in Fig. 3.2(b). It is evident that when $U_{22} = 0.078E_R$, the ^{85}Rb Kohn mode goes soft, and emerges as a slosh mode. We refer this hardened mode as the sloshing mode because it appears on the right of the trap center whereas the ^{85}Rb condensate is left to the trap center. So, unlike in the absence of the fluctuations, there are only two Goldstone modes in the system. The transformations in the mode functions as U_{22} is decreased about this point are shown in Fig. 3.7. This topological phase transition is evident from the density profiles of the TBEC in the presence of the quantum fluctuations as shown in Figs. 3.8(a-c).

In the Cs-Rb system, due to quantum fluctuations, the Kohn mode of ^{87}Rb goes soft at a lower value of U_{12} compared to the value without fluctuations. This is evident in the mode evolution with quantum fluctuations as shown in Fig. 3.5(b). The discontinuity in the spectrum is the signature of the transition from the miscible to the immiscible

regime. The soft Kohn mode gains energy and gets hardened at $0.31E_R$. This mode hardening is due to the topological change in the ground state density profile from the miscible to the side-by-side profile, shown in Figs. 3.8(d-f). The lowest mode with nonzero excitation energy corresponding to the side-by-side profile is shown in Figs. 3.9(e,f). Another recent study reported the effect of quantum fluctuations on the nature of SF-MI quantum phase transitions [258] of a two-species bosonic system in an optical lattice potential. The quantum fluctuations also stabilize the attractive Bose-Bose mixture, which leads to the formation of the quantum droplets [259, 260].

3.4 Conclusions

We have studied the ground state density profiles and the excitation spectrum of TBEC in quasi-1D optical lattices. We observe that the system gains an additional Goldstone mode at phase separation at zero temperature. Furthermore, in a TBEC where a miscible to immiscible transition is driven through the variation of the intraspecies interaction (^{87}Rb - ^{85}Rb), a finite discontinuity in the excitation energy spectra is observed, which is due to the exchange of the position of the species at equal intraspecies interaction strengths. In the presence of quantum fluctuations, on varying the intraspecies interaction of ^{85}Rb , in the immiscible regime, the ground state density profiles transform from sandwich to side-by-side geometry. This is characterized by the hardening of the Kohn mode which emerges as a slosh mode. The fluctuation-induced topological transition from a completely miscible to a side-by-side ground state density profile is also evident in a ^{133}Cs - ^{87}Rb mixture. Our study shows that the geometry of the density profiles with and without quantum fluctuations is different. Since quantum fluctuations are present in experiments, it is crucial to include quantum fluctuations to obtain correct density profiles of TBECs in the optical lattices in the phase-separated domain.

Chapter 4

Quasiparticle spectra and dispersion curves of quasi-2D binary BECs

The experimental realization of ultracold atoms in optical lattices has opened up a plethora of new possibilities to study interacting quantum many-body systems. The optical lattices, filled with bosons [139, 261] or fermions [262, 263] provide unprecedented precision, tunability of interactions, possibility to generate different geometries and mimic the external gauge fields to study many-body systems [264]. The presence of the lattice potential leads to a variety of condensed matter effects associated with the coherent motion of the atoms in a periodic potential. The acceleration of the lattice onset the Bloch oscillations [265, 266] and reducing the potential depth results into a breakdown of these oscillations due to Landau-Zener tunneling [267–269]. The measurement of the energy of collective excitations has emerged as a fundamental and precise tool to investigate the quantum many-body physics. An example of the synergy between theory and experiment in this field is the study of the effect of tunneling and the mean-field interaction of trapped two-dimensional (2D) optical lattices on the collective excitation. The energies of the excitations are modified due to the effective mass acquired by the bosons in the lattice potential [270], which is observed in experiments [271]. A detailed understanding of the excitations of the SF phase in optical lattices is possible with controlled variation of the lattice potential and these excitations are excellent proxies to probe the properties of more complex condensed matter counterparts. The experimental realizations of the binary BECs in

harmonic potential have examined phase separation and other phenomena which are unique to binary BECs. The phenomenon of phase separation and transition from miscible to immiscible or vice versa has also been the subject of several theoretical studies [150, 161, 226, 238, 272]. These recent developments are motivation to probe the rich physics associated with TBECs in optical lattices. To study the effects of fluctuations, either quantum or thermal, in optical lattices filled with TBECs it is essential to have a comprehensive understanding of the quasiparticle spectra. Another important measure is the dispersion relations which are important to characterize the response of the system in the many-body physics. For SFs the dispersion relation is used to estimate the breakdown of the superfluidity as an object moves through the BEC [273]. The criteria of superfluidity has also been predicted for ultracold quantum gases [274] and was observed in experiment [275].

In the present chapter, we study the quasiparticle spectrum of TBECs with tight-binding approximation and the condensate density is described through a set of coupled DNLSes. We examine the evolution of the quasiparticle modes of TBECs in quasi-2D optical lattices at zero temperature. For this we use HFB formalism with Popov approximation and tune one of the interatomic interactions to drive the TBEC from the miscible to the immiscible phase. In the immiscible domain, we show that the ground state has a side-by-side density profile. This is in contrast to the case of quasi-1D system, as discussed in Chapter 3, where the ground state has a sandwich density profile at zero temperature. To identify the geometry of the ground state, we examine the quasiparticle spectra using Bogoliubov-de Gennes (BdG) analysis. For a stable ground state configuration, the eigenenergies are real, but complex for metastable states. Following BdG analysis, we further examine the dispersion relation of a binary system in optical lattices. This relation is used to understand the structure of the lower- and higher-energy excitations for miscible and immiscible domains of TBEC. The dispersion relations are important to understand the nature of the excitations [225, 276, 277] and Bragg spectroscopy [278] of ultracold quantum gases. These spectroscopic studies present full momentum-resolved measurements of the band structure and the associated interaction effects at several lattice depths [279]. In fact, these relations have proved the presence of the rotonlike excitation in trapped dipolar BECs [280–283].

4.1 Mode evolution of trapped TBEC at $T = 0$ K

To examine the evolution of the quasiparticle modes of quasi-2D TBEC in optical lattices, we consider two cases from the experimentally realized TBECs, ^{87}Rb - ^{85}Rb [50] and ^{133}Cs - ^{87}Rb [45, 46]. The former and latter are examples of TBECs with negligible, and large mass differences between the species, respectively. Another basic difference is, starting from miscible phase, the passage to the immiscible phase. In the ^{87}Rb - ^{85}Rb TBEC, the background scattering length of ^{85}Rb is negative, and hence to obtain stable ^{85}Rb condensate [284] it is essential to render it repulsive using magnetic Feshbach resonance [220, 221]. The same can be employed to drive the system from miscible to immiscible domain. On the other hand, in the ^{133}Cs - ^{87}Rb TBEC, the interspecies scattering length is tuned through a magnetic Feshbach resonance [222] to steer the TBEC from miscible to immiscible domain or vice versa.

For the ^{87}Rb - ^{85}Rb TBEC, we assume ^{87}Rb and ^{85}Rb as the first and second species, respectively. For simplicity, and ease of comparison without affecting the results, the radial trapping frequency of the two species are chosen to be identical $\omega_{\perp} = 2\pi \times 50$ Hz, with $\omega_z/\omega_{\perp} = 20.33$. The wavelength of the laser beam to create the 2D lattice potential and lattice depth are $\lambda_L = 1064$ nm and $V_0 = 5E_R$, respectively. This choice of parameters is consistent with the experimental realization of the TBEC of different hyperfine states of ^{87}Rb in optical lattices [111]. To improve convergence, and have a good description of the optical lattice properties, we take the total number of atoms as $N_1 = N_2 = 300$ confined in a 30×30 lattice system. For these set of parameters the system is quasi-2D, where the excitations are along the radial direction. However, for this work, we study the system at $T = 0$ K and ignore the quantum fluctuations. We use these set of parameters to study the ^{133}Cs - ^{87}Rb TBEC as well.

To solve the coupled DNLSs we consider Gaussian basis function of width $0.3a$, where a is the lattice constant, to evaluate the lattice parameters. The correct estimation of the width is based on the minimum overlap of the orthonormal Gaussian orbitals at each lattice site. In the case of ^{87}Rb - ^{85}Rb TBEC, the tunneling matrix elements are $J_1 = 0.66E_R$ and $J_2 = 0.71E_R$, and $U_{11} = 0.07E_R$ and $U_{12} = 0.15E_R$ are the intraspecies and interspecies interactions, respectively. Following the same steps, the parameters for the ^{133}Cs - ^{87}Rb TBEC are taken as $J_1 = 0.66E_R$, $J_2 = 1.70E_R$, $U_{11} =$

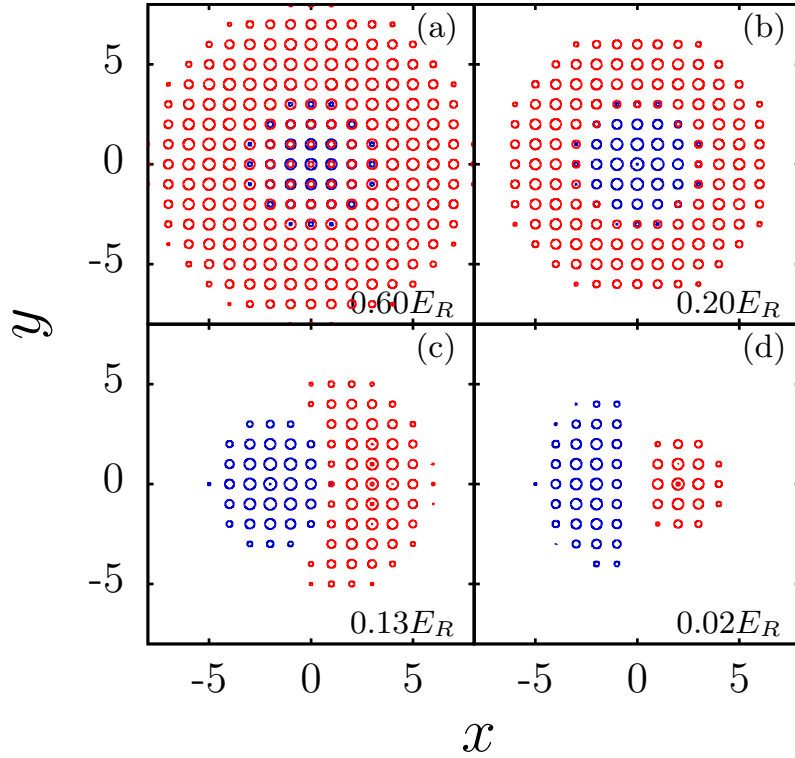


Figure 4.1: The geometry of the condensate density profiles and its transition from the miscible to the immiscible domain for the ^{87}Rb - ^{85}Rb TBEC. (a) At higher U_{22} , the density of both species partially overlap; (b) as we decrease U_{22} it changes into a sandwich type profile. At a critical value of U_{22} ($0.16E_R$), both condensate segregate and rotational symmetry is broken, which results in a side-by-side density profile in the immiscible domain shown in (c,d). The species labeled 1(2) is shown as blue (red) contours. Here x and y are in units of the lattice constant a .

$0.96E_R$ and $U_{22} = 0.42E_R$. This set of parameters are obtained from the expressions of J 's and U 's defined in Chapter 2. In both the cases, we drive the system from miscible to immiscible phase, and examine the evolution of the quasiparticle modes in detail.

4.1.1 ^{87}Rb - ^{85}Rb TBEC

For the zero temperature computation, we begin by neglecting the noncondensate density $\tilde{n}_{k\xi}$ at each lattice site and solve the DNLSEs in imaginary-time propagation using fourth order Runge-Kutta method. The initial guess values of the complex amplitudes are chosen as side-by-side profile, since the Gaussian profile gives complex eigenvalues in the diagonalization of the BdG matrix. As mentioned earlier U_{22} , the

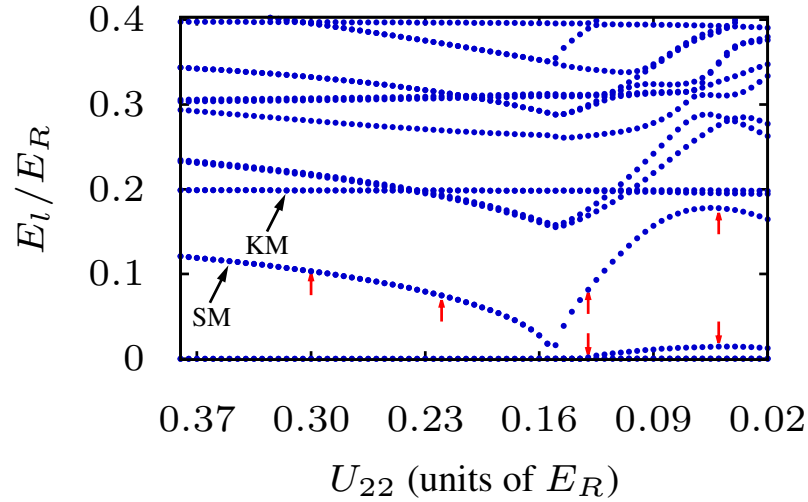


Figure 4.2: The evolution of the low-lying quasiparticle mode energies as a function of the intraspecies interaction U_{22} for the ^{87}Rb - ^{85}Rb TBEC held in quasi-2D optical lattices. The slosh mode (SM) and Kohn mode (KM) are marked by the black arrows. The critical value of miscible-to-immiscible transition is $U_{22}^c = 0.16E_R$. The energies marked by red arrows correspond to the quasiparticle amplitudes shown in Figs. 4.3 and 4.4. In the plot U_{22} is in units of the recoil energy E_R .

intraspecies interaction of ^{85}Rb , is decreased to drive the TBEC from miscible to immiscible domain. The changes in the ground state density profile with decrease in U_{22} is shown in Fig. 4.1. In the miscible domain, when $U_{22} > U_{22}^c$, the density profiles of the BECs overlap and there is a shift in the position of the density maxima as U_{22} is decreased [Fig. 4.1(a,b)]. At a critical value U_{22}^c , the two species undergo phase separation with side-by-side density profiles and break the rotational symmetry. It must be noted that, as shown in Fig. 4.1(b), the density profiles are shell structured or rotationally symmetric for intermediate values of U_{22} . However, there is a sharp transition to side-by-side density profile as phase separation occurs when U_{22} is lowered. The features of the quasiparticles too change in tandem with the density profile, and the variation of the excitation energies with U_{22} are shown in Fig. 4.2. Unlike in quasi-1D, in this system the intermediate sandwich profile is not equivalent to three distinct BECs and does not contribute to an extra Goldstone mode in the quasiparticle excitation spectra. To obtain the mode evolution curves, we do a series of computations starting from the miscible domain of the system (higher U_{22}), and decrease U_{22} to values below U_{22}^c .

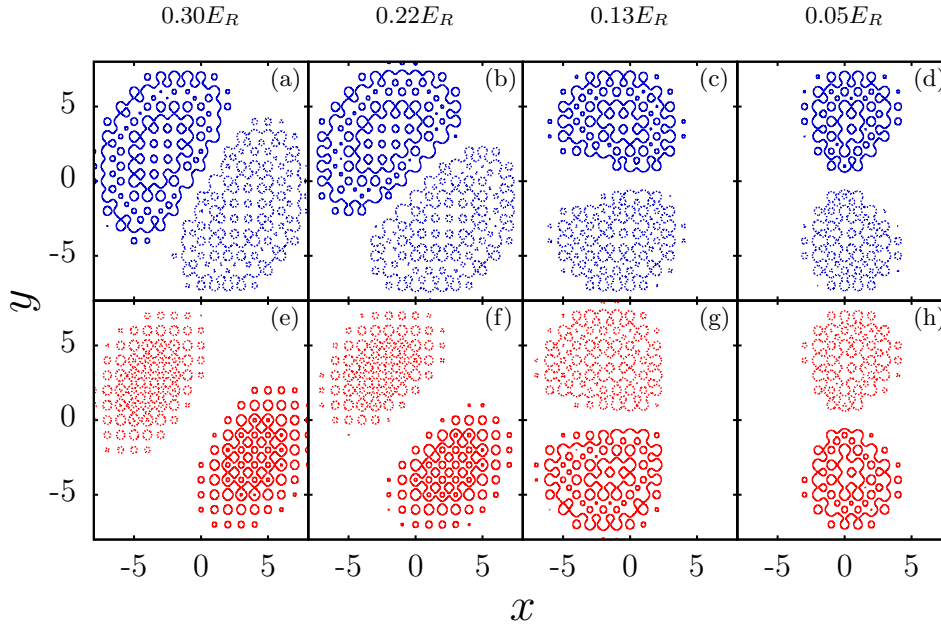


Figure 4.3: The evolution of the quasiparticle amplitudes corresponding to the slosh mode of (a)-(d) the first species and (e)-(h) the second species of the ^{87}Rb - ^{85}Rb TBEC as U_{22} is decreased from $0.30E_R$ to $0.05E_R$. The value of U_{22} is shown at the top of the figures. The blue (red) contours represent the quasiparticle amplitude u_1 (u_2). The density perturbation is from dotted contours to the solid contours. Here x and y are in units of the lattice constant a .

In the miscible domain, all the excitation modes are doubly degenerate. As U_{22} is lowered, eigenenergies of modes with different phases of the quasiparticle amplitudes of two species u_1 and u_2 , or out-of-phase modes, decrease in energy and degeneracy is lifted when U_{22} is below U_{22}^c . For binary BECs in quasi-2D optical lattices, the slosh and Kohn modes are the two lowest energy excitations in the miscible domain, and are associated with the out-of-phase and in-phase modes, respectively. The in-phase and the out-of-phase modes correspond to the excitations with the density flow in the same and different directions, respectively. The structure of the two degenerate slosh modes in the miscible domain are shown in Figs. 4.3(a,b,e,f) and Figs. 4.4(a,b,e,f), respectively. In general, the doubly degenerate modes are $\pi/2m$ rotation of each other, where m is the azimuthal quantum number. For the slosh modes ($m = 1$) this property is evident from the figures. One of the degenerate slosh modes goes soft at the phase separation $U_{22}^c = 0.16E_R$ (specifically, it is the one that is in phase with the condensate

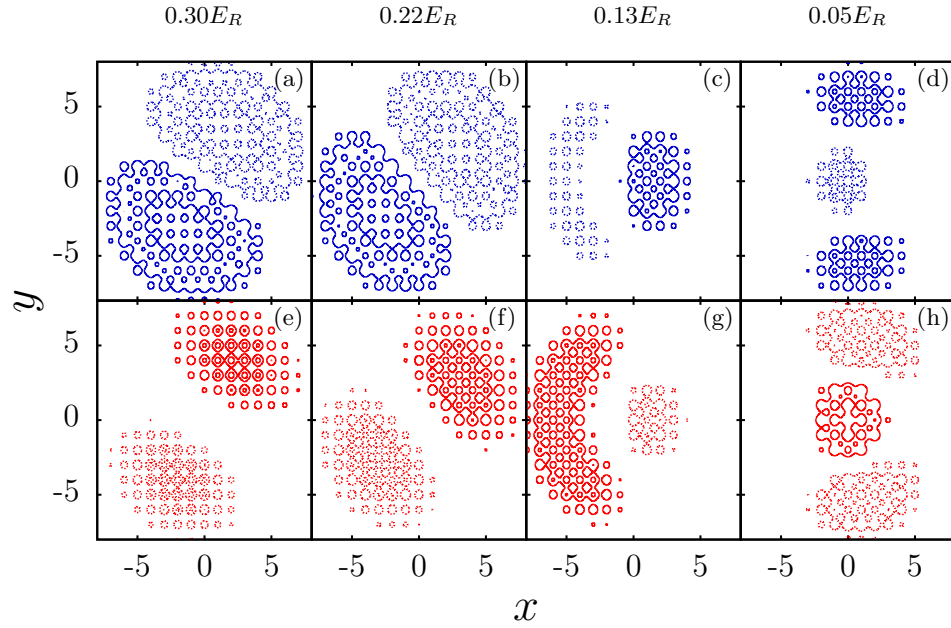


Figure 4.4: The evolution of the quasiparticle amplitudes corresponding to the other slosh mode, which is degenerate to the mode shown in Fig. 4.3 in the miscible domain. These amplitudes correspond to (a)-(d) the first species and (e)-(h) the second species of the ^{87}Rb - ^{85}Rb TBEC with the change in U_{22} , which is shown at the top of the figures. (d) and (h) At a critical value of U_{22} , this mode hardens and gets transformed into an interface mode. The blue (red) contours represent the quasiparticle amplitude of first (second) species. Here x and y are in units of the lattice constant a .

density), but the other slosh mode gains energy at phase separation. Thus, below U_{22}^c the degeneracy of the slosh modes is lifted. On further decrease of U_{22} one striking effect of the optical lattice potential is observed: the soft slosh mode gains energy and is transformed into an interface mode, where the mode functions or the excitations are more prominent at the interface regions of the species. This is in stark contrast to the case without the lattice potential, where the mode remains soft [224]. This is also apparent from the nature of the quasiparticle amplitudes shown in Figs. 4.3(c,d,g,h) and Figs. 4.4(c,d,g,h). The Kohn mode, on the other hand, remains steady with an energy of $0.2E_R$. However, this value violates the Kohn's theorem due to the presence of the optical lattice potential.

Considering the general trend, there are only mode crossings in the miscible domain, however, both mode crossings and avoided crossings occur in the phase-separated

domain. Prior to phase separation, out-of-phase modes decrease in energy as U_{22} is lowered, but the in-phase modes remain steady. So no mode mixing occurs when modes of the former type encounters the latter, and they cross each other. However, when U_{22} is below the critical value, degeneracies are lifted, and mode mixing can occur. This explains the presence of avoided crossings in the phase-separated domain. The energies of the out-of-phase modes decrease monotonically with decreasing U_{22} as it favours phase separation. After phase separation, these modes get hardened due to rotational symmetry breaking.

4.1.2 ^{133}Cs - ^{87}Rb TBEC

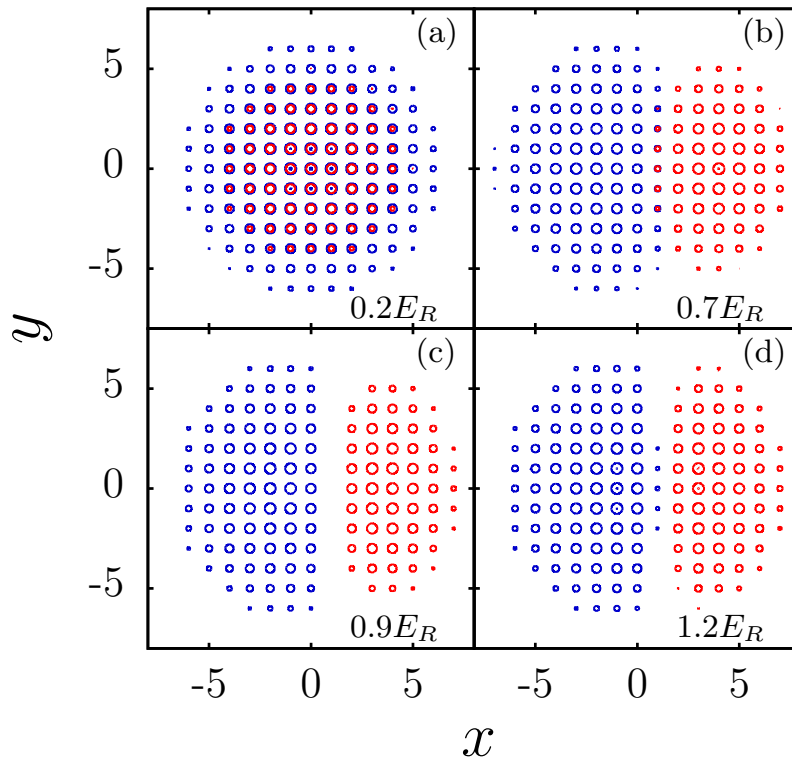


Figure 4.5: The geometry of the condensate density profiles and its transition from the miscible to the immiscible domain in the ^{133}Cs - ^{87}Rb TBEC. The species labeled 1(2) is shown as blue (red) contours. Here x and y are in units of the lattice constant a .

For the ^{133}Cs - ^{87}Rb TBEC, as mentioned earlier, we vary interspecies interaction U_{12} to induce the miscible to the immiscible phase transition. The density profiles, as the miscible to immiscible transition occurs, are shown in Fig. 4.5. The change, except for the curvature at the interface, are similar to the case of ^{87}Rb - ^{85}Rb TBEC

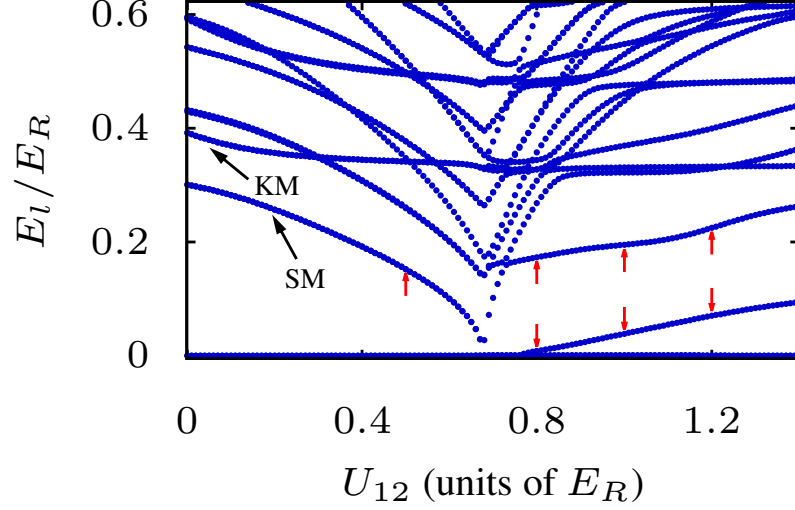


Figure 4.6: The evolution of the low-lying mode energies as a function of the interspecies interaction in the ^{133}Cs - ^{87}Rb TBEC held in quasi-2D optical lattices. The slosh mode (SM) and Kohn mode (KM) are marked by the black arrows. The critical value of miscible-to-immiscible transition is $U_{12}^c = 0.68E_R$. The energies marked by red arrows correspond to the quasiparticle amplitudes shown in Figs. 4.7 and 4.8. Here U_{12} is in units of the recoil energy E_R .

shown in Fig. 4.1. The evolution of the quasiparticle mode energies before, during and after the transition are shown in Fig. 4.6. Like in the previous case, ^{87}Rb - ^{85}Rb TBEC, the slosh mode is degenerate in the miscible domain [shown in Figs. 4.7(a,e) and Figs. 4.8(a,e)]. It goes soft at the critical value $U_{12}^c = 0.68E_R$, and the degeneracy is lifted. As shown in Figs. 4.7(b,c,d,f,g,h) and Figs. 4.8(b,c,d,f,g,h), the evolution of the nondegenerate modes are qualitatively similar to that of ^{87}Rb - ^{85}Rb TBEC. One key feature in the general trend of the mode evolution is that in the miscible domain all the mode energies decrease with increase in U_{12} . However, as discussed earlier, in ^{87}Rb - ^{85}Rb TBEC the energies of all the in-phase modes (modes with same phase of u_1 and u_2) remain steady. As an example, the Kohn mode decrease in energy for low values of U_{12} whereas it remains steady for ^{87}Rb - ^{85}Rb TBEC. At phase separation, the mode energies reach minimal values and then, increase with increasing U_{12} in the immiscible domain. To gain insight into these trends, we examine the dependence on various parameters with a series of computations.

Based on the results, we observe that the form of the interaction, interspecies or

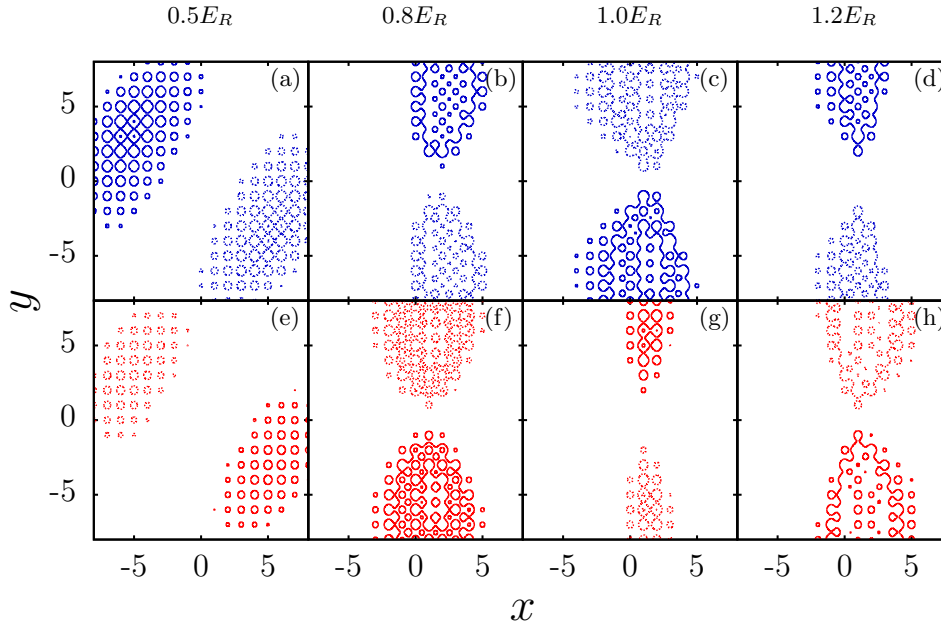


Figure 4.7: The evolution of the quasiparticle amplitudes corresponding to the slosh mode of (a)-(d) the first species and (e)-(h) the second species of the ^{133}Cs - ^{87}Rb TBEC as U_{12} is increased from $0.5E_R$ to $1.2E_R$. The value of U_{12} is shown at the top of the figures. The blue (red) contours represent the quasiparticle amplitude of ^{133}Cs (^{87}Rb). The density perturbation is from dotted contours to the solid contours. Here x and y are in units of the lattice constant a .

intraspecies, which is tuned to drive the system from the miscible to the immiscible regime, has an impact on the trends of the mode evolution. An important observation is that for high U_{kk}/J_k all the modes decrease in energy, in the miscible domain, when the interspecies interaction is tuned. However, when the intraspecies interaction is tuned all the in-phase modes remain steady. Thus, we attribute the difference in the trends to the geometry of the interface at phase separation. When the interspecies interaction is tuned, as in the ^{133}Cs - ^{87}Rb TBEC, the interface at phase separation is linear as is evident from Fig. 4.5(c). Thus, it can align with the nodes of the mode functions, and decrease all the mode energies. This is not possible in the other case, tuning intraspecies interaction in ^{87}Rb - ^{85}Rb , as the interface is curved as shown in Fig. 4.1(c). The mode evolution of two cases suggest that the mass difference of the species does not play a key role in determining the ground state configurations.

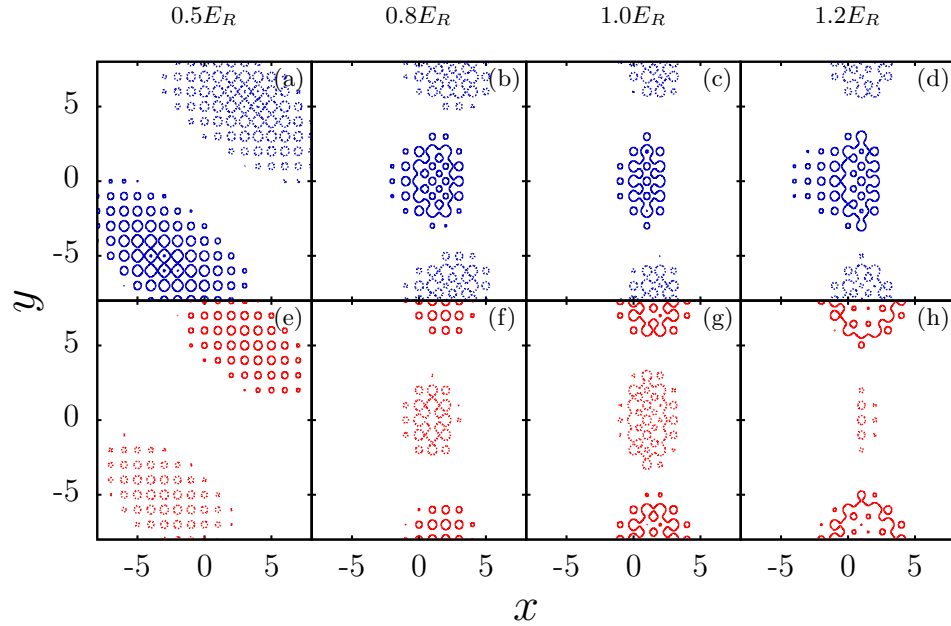


Figure 4.8: The evolution of the quasiparticle amplitudes corresponding to the slosh mode, which is degenerate with the mode shown in Fig. 4.7 in the miscible domain. These amplitudes correspond to (a)-(d) the first species and (e)-(h) the second species of the ^{133}Cs - ^{87}Rb TBEC as U_{12} is increased from $0.5E_R$ to $1.2E_R$. The value of U_{12} is shown at the top of the figures. At a critical value of U_{12} , the energy of the mode increases and it gets transformed into an interface mode. The blue (red) contours represent the quasiparticle amplitude of ^{133}Cs (^{87}Rb). Here x and y are in units of the lattice constant a .

4.2 Dispersion relations

We now examine the nature of quasiparticle excitations in the trapped binary condensates in quasi-2D optical lattices. The dispersion relations, in general, determine how a system responds to external perturbations. So, in TBECs in optical lattices as well it is important to examine the dispersion relations to understand how the system evolves after applying an external perturbation. Examples of current interest are topological defects generated through phase imprinting, evacuating single or multiple lattice sites, and tuning the lattice or harmonic potential parameters. To study the dispersion relation of the quasiparticles in optical lattices with a background trapping potential, we follow the definition in Ref. [280]. Then we take the Fourier transform of the quasiparticle amplitudes and compute the expectation value of the linear momentum

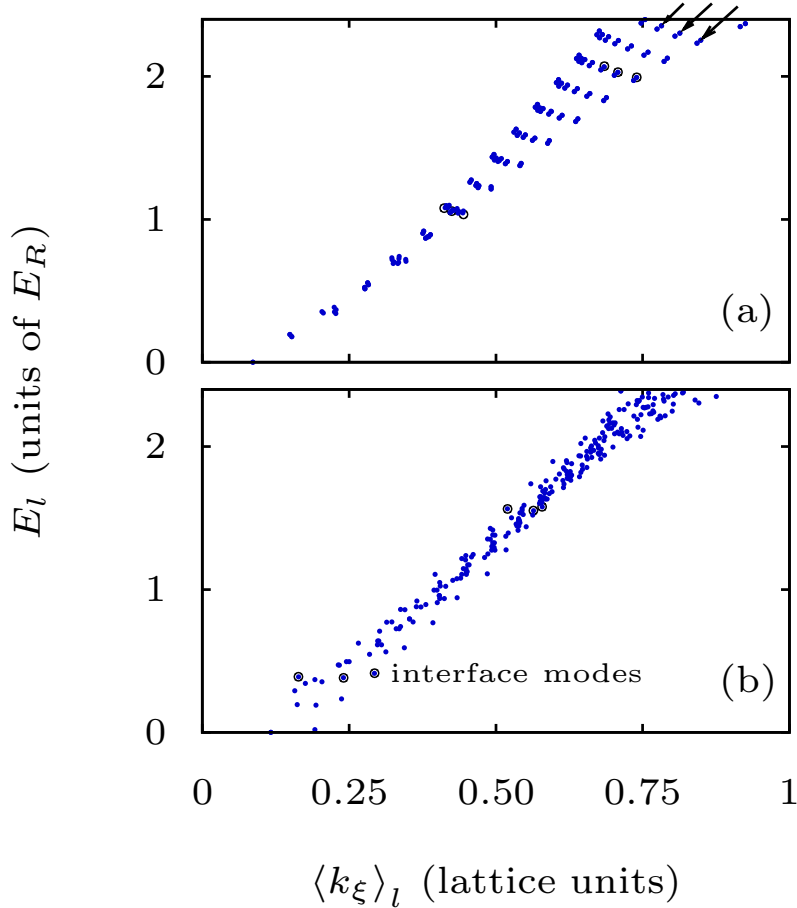


Figure 4.9: The discrete BdG quasiparticle dispersion curve in (a) the miscible and (b) the immiscible domain of the ^{87}Rb - ^{85}Rb TBEC with $J_1 = J_2 = 0.66E_R$, and $U_{11} = U_{22} = 0.01E_R$. The interspecies on-site interaction U_{12} is (a) $0.003E_R$ and (b) $0.08E_R$. The excitation energy E_l is in units of the recoil energy E_R .

$\langle k_\xi \rangle \equiv \sqrt{\langle k_\xi^2 \rangle}$ of each quasiparticle. Thus, in the momentum-space representation, for the l th quasiparticle

$$\langle k_\xi \rangle_l = \left[\frac{\sum_{\alpha, \mathbf{k}_\xi} k_\xi^2 [|\tilde{u}_\alpha^l(\mathbf{k}_\xi)|^2 + |\tilde{v}_\alpha^l(\mathbf{k}_\xi)|^2]}{\sum_{\alpha, \mathbf{k}_\xi} [|\tilde{u}_\alpha^l(\mathbf{k}_\xi)|^2 + |\tilde{v}_\alpha^l(\mathbf{k}_\xi)|^2]} \right]^{1/2}, \quad (4.1)$$

where $k_\xi = (k_i, k_j)$ is the lattice-site-dependent wave number and $\alpha = 1, 2$ is the index for the species. Here $\tilde{u}_\alpha^l(\mathbf{k}_\xi) = \mathcal{F}[u_\alpha^l(\xi)]$, and $\tilde{v}_\alpha^l(\mathbf{k}_\xi) = \mathcal{F}[v_\alpha^l(\xi)]$ are the lattice site dependent quasiparticle amplitudes in momentum space, with \mathcal{F} representing the Fourier transform. We then determine the discrete form of the dispersion relation by associating $\langle k_\xi \rangle_l$ to the excitation energies E_l . For TBECs in the harmonic potential

the dispersion curves were examined in a previous work, and reported unique trends in the miscible and immiscible regimes [225]. In comparison, the presence of the optical lattice potential is expected to modify the dispersive properties of the systems in the present study. To examine the differences and identify unique trends we compute $\langle k_\xi \rangle_l$ of the l th quasiparticle and study the dispersion curves in miscible and immiscible domains. By associating $\langle k_\xi \rangle_l$ with the quasiparticle mode energies, we obtain the dispersion curves. To highlight trends in the dispersion curves dependent on angular momentum, we choose parameters different from what we have considered so far. Furthermore, we restrict ourselves to the case of the ^{87}Rb - ^{85}Rb TBEC, where the trends in dispersion curves are more prominent due to weaker interatomic interactions, and small mass difference. In particular, we consider a system of ^{87}Rb - ^{85}Rb TBEC with DNLSE parameters $J_1 = J_2 = 0.66E_R$, and $U_{11} = U_{22} = 0.01E_R$. For the interspecies on-site interactions U_{12} , to explore the dispersion relations in the miscible and immiscible domains we set it to $0.003E_R$ and $0.08E_R$, respectively. All the other parameters are retained with the same values as mentioned earlier. One important point to be emphasized is, unlike the parameters in the mode evolutions studies, the current choice of DNLSE parameters correspond to two different sets of number of atoms N_1 and N_2 . In binary condensates, the dispersion relation depends on the interspecies on-site interaction and therefore can be classified into two regimes.

4.2.1 Miscible domain

The ground state of the system has rotational symmetry in this domain. Hence, the azimuthal quantum number (m) is a good quantum number and finite interspecies interaction mixes modes with same m arising from each of the two species. This is reflected in the branch like structures in the dispersion curve as shown in Fig. 4.9(a). To understand the physics behind the structure of the dispersion curves, we examine the structure of the quasiparticle modes. For this, let us focus on modes that lie on three branches, marked by arrows, in Fig. 4.9(a). Each of the modes can be identified based on the value of m . As an example, three from the low energies ($\approx 1E_R$) and another three from higher energies ($\approx 2E_R$) are shown in Fig. 4.10.

The energies of the first three quasiparticle modes in Figs. 4.10(a-c) are out-of-

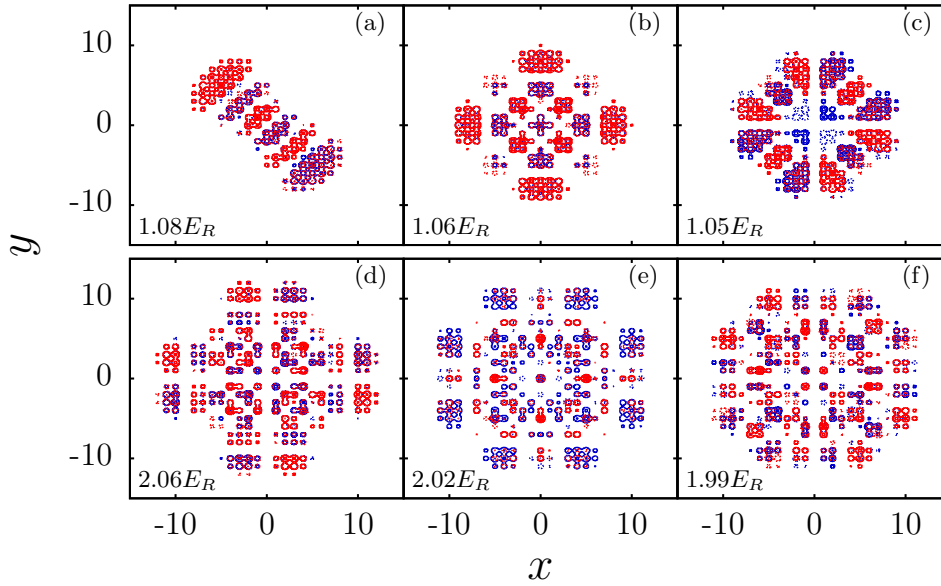


Figure 4.10: The quasiparticle amplitudes in the miscible domain of a TBEC. (a)-(c) Show the quasiparticle amplitudes with excitation energy ($\approx 1E_R$) and (d)-(f) show the quasiparticle amplitudes with excitation energy ($\approx 2E_R$). These quasiparticles are indicated in the dispersion plot [Fig. 4.9(a)] by black circles. The excitation energy corresponding to each quasiparticle is written in the lower left corner of each plot in units of the recoil energy. The excitations corresponding to species 1 (2) are shown with blue (red) contours. Here x and y are in units of the lattice constant a .

phase type and the values of m are 1, 4 and 6. Among these modes, the first two modes have $\langle k_\xi \rangle_l \approx 0.42$, and are phononlike as these lie on the linear part of the dispersion curve. However, the mode in Fig. 4.10(c) with $\langle k_\xi \rangle_l \approx 0.44$ and $m = 6$ is a surface mode, which is evident from the structure of the mode function. The same observation is confirmed from the exponential decay in the numerical values of the quasiparticle mode functions u_α ($\alpha = 1, 2$) towards the center. These three modes show that within the same energy range ($\approx 1E_R$), phononlike and surface excitation co-exist. One discernible trend is that the modes with higher m and $\langle k_\xi \rangle_l$ have extrema located farther from the center of the trap and turn into surface modes. The quasiparticle amplitudes with higher excitation energies ($\approx 2E_R$), shown in Figs. 4.10(d-f), have intricate structures. This is as expected arising from the larger mode mixing due to higher density of states and nonzero U_{12} and it is harder to identify the m of these modes. However, based on the number of minima and maxima at the outer edges, we

compute the azimuthal quantum number of these mode functions as $m \sim 4, 6, 8$. Thus, the quasiparticle modes of this domain preserve the rotational symmetry.

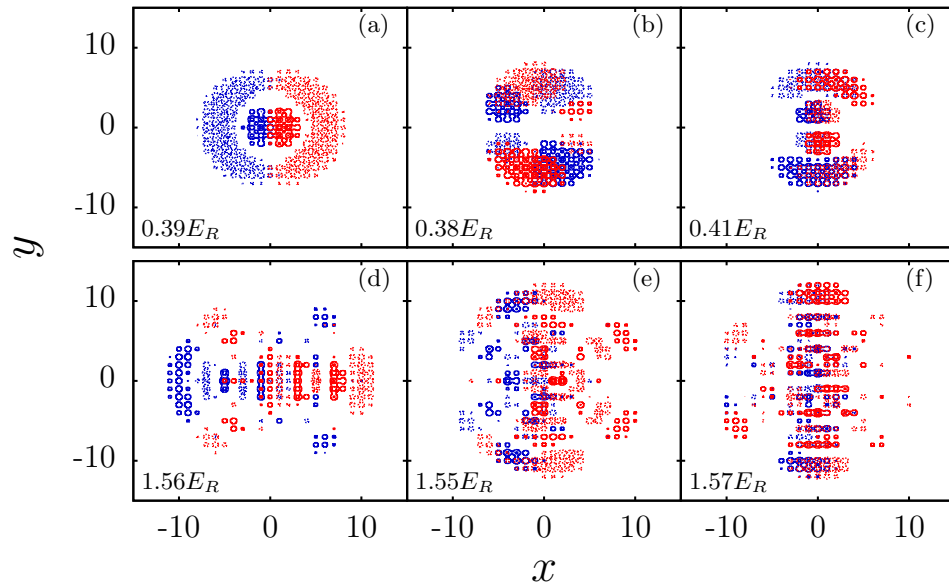


Figure 4.11: The quasiparticle amplitudes in the immiscible domain of a TBEC. (a)-(c) Show the quasiparticle amplitudes with excitation energy ($\approx 0.4E_R$) and (d)-(f) show the quasiparticle amplitudes with excitation energy ($\approx 1.5E_R$). These quasiparticles are indicated in the dispersion plot [Fig. 4.9(b)] by black circles. The excitation energy corresponding to each quasiparticle is written in the lower left corner of each plot in units of the recoil energy. The excitations corresponding to species 1 (2) are shown with blue (red) contours. Here x and y are in units of the lattice constant a .

4.2.2 Immiscible domain

For the immiscible domain, the dispersion curve is shown in Fig. 4.9(b) and there are no discernible trends. The reason is, in this domain the condensate density profile does not have rotational symmetry and hence there is mixing between quasiparticle modes with different m values. To examine the structure of the mode functions we consider three modes each with energies $\approx 0.4E_R$ and $\approx 1.55E_R$; these are shown in Figs. 4.11(a-c), and Figs. 4.11(d-f), respectively. Consider the modes with energies $0.39E_R$ and $0.38E_R$ as shown in Fig. 4.11(a), and (b), the flow patterns in these excitations are equivalent to the breathing and slosh modes in single-species condensates, respectively. There is, however, one important difference: the density flow involves

both the species, and have different velocity fields. The mode with energy $0.41E_R$, shown in Fig. 4.11(c), is out of phase in nature and has a different configuration compared to the two previous ones. That is, the mode functions are prominent around the interface region and are negligible in the region where the condensate densities are maximal. In continuum case, modes with a similar structure (interface mode) has been reported [224, 225]. The mode with higher energies have enhanced mode mixing due to higher density of states, which is evident from the structure of the modes with $\approx 1.55E_R$ shown in Figs. 4.11(d-f). Hence, it is nontrivial to classify the modes like in the case of modes with energies $\approx 0.4E_R$. In terms of the geometrical structures, the modes in Figs. 4.11(d-f) have extrema coincident with the condensates, an interlaced distribution, and are localized in the interface region, respectively. Thus, within a range of excitation energies, there exists modes with diverse characters.

4.3 Conclusions

We have examined the configurations of the ground state and the quasiparticle spectra of TBECs in quasi-2D optical lattices. Our results are relevant to the SF phase ($J > U$) of ultracold atoms in an optical lattice and with the lattice constant much smaller than the oscillator length of the background harmonic oscillator trapping potential ($a \ll a_{\text{osc}} = \sqrt{\hbar/(m_1\omega_\perp)}$). Our study shows that introduction of an optical lattice potential modifies the geometry of condensate density distribution of TBECs at the phase separation. The sandwich or shell structured density profiles are no longer energetically favourable, and the side-by-side geometry emerges as the only stable ground state density profile. This arises from the higher interface energy due to the local density enhancements at lattice sites. This result matches the ground state of TBECs obtained using QMC simulations studied in Ref. [137]. The other important observation is that as the TBEC is tuned from miscible to immiscible phase, the evolution of the quasiparticle spectra can be grouped into two. The first group has quasiparticles that exhibit a decrease in the mode energies as we approach phase separation and reach minimal values at the critical interaction strength. However, the mode energies increase after crossing into the domain of phase separation. The second group,

on the other hand, remains steady as the interaction strength is tuned across the critical value. Furthermore, we have examined the dispersion curves for miscible and immiscible domains of TBECs. The curves in the miscible domain show discernible trends associated with the azimuthal quantum number of the quasiparticle mode. However, in the immiscible domain there are no discernible trends associated with the azimuthal quantum number. This is due to the rotational symmetry breaking of the condensate density profiles and the resulting mixing of modes with different azimuthal quantum numbers.

Chapter 5

Thermal fluctuations enhanced miscibility of condensate mixtures

Ultracold atomic gases in an optical lattice has proven to be a rich ground for exploring the quantum phenomena in condensed matter physics [29, 261, 285, 286]. In particular, the multicomponent quantum fluids due to their tunable interactions using magnetic and optical Feshbach resonances creates the numerous possibilities and enriches the field of ultracold atoms.

The phenomenon of phase separation is ubiquitous in nature, and has been a long-standing topic of the interest in chemistry and physics. For repulsive on-site interactions, the transition to the phase-separated domain or immiscibility is determined by the parameter $\Delta = U_{11}U_{22}/U_{12}^2 - 1$, where U_{11} and U_{22} are the intraspecies on-site interactions and U_{12} is the interspecies on-site interaction. When $\Delta < 0$, an immiscible phase occurs in which, the atoms of species 1 and 2 have relatively strong repulsion, whereas $\Delta \geq 0$ implies a miscible phase [159, 287, 288]. This criterion is applicable for the homogeneous system at zero temperature. The presence of an external trapping potential modifies this condition as the trap introduces an additional energy cost for the species to spatially separate [240]. However, the experiments are performed at finite temperatures in trapped systems, and therefore, the deviation from the criterion is to be expected. In experiments, the unique feature of the phase separation has been successfully observed in TBECs with harmonic trapping potential [46, 50, 61]. Previously, in the context of superfluid helium at zero temperature, the phase separation of the

bosonic mixtures of isotopes of different masses has been predicted [289, 290]. The finite temperature properties of the TBECs [151, 153, 291], and the fluctuation-induced suppression of phase separation [292] in the harmonic trapping potential have been explored. The recent experimental realizations of TBECs in optical lattices provides the motivation to study the finite temperature effects in the lattice systems. One of the fundamental questions to be addressed is how the presence of thermal fluctuations affects the phenomena of phase separation of TBECs in optical lattices. The phase diagram of the binary mixture at finite temperature with rotation has been studied using large-scale Monte Carlo simulations of a two component Ginzburg-Landau model [144]. The finite temperature effects on the immiscible phase of TBECs in both the homogeneous and trapped lattice system has been investigated using QMC simulations [293]. The objectives of the present chapter is to study the role of thermal fluctuations on the collective modes and associated ground state density transformation using HFB-Popov formalism. The BEC and hence, the coherence in a system of bosons depends on the interplay between various parameters, such as the temperature, interaction strength, confinement, and dimensionality [294]. In particular, in the low-dimensional trapped Bose gases, the coherence can only be maintained across the entire spatial extent at a temperature much below the critical temperature [188]. The coherence property has already been observed in experiments [295–299].

In this chapter, we study the finite temperature effects of quasi-2D trapped TBEC in optical lattices. We address the immiscible-miscible phase transition in the ^{87}Rb - ^{85}Rb TBEC with temperature as a control parameter in the domain $T < T_c$, where T_c is the critical temperature of either of the species of the mixture. We study the evolution of the quasiparticle modes of the TBEC in quasi-2D optical lattices with temperature. For this work, we use Hartree-Fock-Bogoliubov (HFB) formalism with the Popov approximation as described in Chapter 2, and starting from phase-separated domain at zero temperature we vary the temperature. We observe that there is an immiscible to miscible transition of the TBEC at a characteristic temperature. This transition is accompanied by a discontinuity in the quasiparticle excitation spectrum, and in addition, the slosh mode corresponding to each of the species becomes degenerate. Furthermore, we compute the equal-time first-order spatial correlation function

which is the measure of the coherence, and phase fluctuations present in the system. It describes off-diagonal long-range order which is the defining feature of the BEC [32]. This is an important theoretical tool to study the many-body effects in atomic physics [300, 301], and is measured in experiments through interference and time-of-flight techniques [299, 302, 303]. At finite temperature, the decay in the coherence of the TBEC is examined using the first-order correlation function.

5.1 Overlap integral and correlation function

The condensate and noncondensate density distributions can be used to quantify the degree of phase separation. In order to examine the role of temperature on the miscibility of the condensates we define the overlap integral

$$\Lambda = \frac{[\int n_1(\mathbf{r})n_2(\mathbf{r})d\mathbf{r}]^2}{[\int n_1^2(\mathbf{r})d\mathbf{r}] [\int n_2^2(\mathbf{r})d\mathbf{r}]} \quad (5.1)$$

Here, $n_k(\mathbf{r})$ is the total density of the k th species at position $\mathbf{r} \equiv (x, y)$. The overlap integral is normalized such that $0 \leq \Lambda \leq 1$. If the two condensates of the TBEC have complete overlap to each other then the system is in the miscible phase with $\Lambda = 1$, whereas for the completely phase-separated case $\Lambda = 0$.

Another quantity of interest is the first-order correlation function $g_k^{(1)}(\mathbf{r}, \mathbf{r}')$, which is the measure of the coherence or the phase fluctuations of the species in the TBEC. The correlation function can be expressed as the expectations of the product of the field operators at different positions and times [304–307]. These functions are normalized to obtain unit modulus in the case of perfect coherence or a system consisting of only condensate atoms. Here, we restrict ourselves to the ordered spatial correlation functions at a fixed and equal time. In terms of the quantum Bose field operator $\hat{\Psi}_k$, the first-order spatial correlation function of the k th species is

$$g_k^{(1)}(\mathbf{r}, \mathbf{r}') = \frac{\langle \hat{\Psi}_k^\dagger(\mathbf{r})\hat{\Psi}_k(\mathbf{r}') \rangle}{\sqrt{\langle \hat{\Psi}_k^\dagger(\mathbf{r})\hat{\Psi}_k(\mathbf{r}) \rangle \langle \hat{\Psi}_k^\dagger(\mathbf{r}')\hat{\Psi}_k(\mathbf{r}') \rangle}}, \quad (5.2)$$

where $k = 1, 2$ is the species index and $\langle \dots \rangle$ represents the thermal average. It is important to note that the local first-order unnormalized correlation function is equal to the density, i.e., $g_k^{(1)}(\mathbf{r}, \mathbf{r}) = n_k(\mathbf{r})$. The expression of $g_k^{(1)}(\mathbf{r}, \mathbf{r}')$ can also be written

in terms of the condensate and noncondensate density correlations as

$$g_k^{(1)}(\mathbf{r}, \mathbf{r}') = \frac{n_k^c(\mathbf{r}, \mathbf{r}') + \tilde{n}_k(\mathbf{r}, \mathbf{r}')}{\sqrt{n_k(\mathbf{r})n_k(\mathbf{r}')}}, \quad (5.3)$$

where

$$\begin{aligned} n_k^c(\mathbf{r}, \mathbf{r}') &= \psi_k^*(\mathbf{r})\psi_k(\mathbf{r}'), \\ \tilde{n}_k(\mathbf{r}, \mathbf{r}') &= \sum_l [\{u_k^{*l}(\mathbf{r})u_k^l(\mathbf{r}') + v_k^{*l}(\mathbf{r})v_k^l(\mathbf{r}')\} N_l + v_k^{*l}(\mathbf{r})v_k^l(\mathbf{r}')], \\ n_k(\mathbf{r}) &= n_k^c(\mathbf{r}) + \tilde{n}_k(\mathbf{r}) \end{aligned}$$

are the condensate density correlation, noncondensate density correlation and the total density of the k th species, respectively. Here, $\psi_k(\mathbf{r})$ is the condensate wave function or the order parameter, $u_k^l(\mathbf{r})$ and $v_k^l(\mathbf{r})$ are the quasiparticle amplitudes of the k th species, and N_l is the Bose factor of l th quasiparticle mode with energy E_l . The factor $N_l \neq 0$ for finite temperature T . In the above expressions $n_k^c(\mathbf{r}, \mathbf{r}')$ and $\tilde{n}_k(\mathbf{r}, \mathbf{r}')$ are obtained by expanding the complex amplitudes (c_ξ, d_ξ), and the quasiparticle amplitudes ($u_{k,\xi}^l, v_{k,\xi}^l$) in the localized Gaussian basis. At zero temperature, the entire condensate cloud has complete coherence, and therefore $g_k^{(1)} = 1$ within the condensate region. In TBECs, the transition from phase-separated to the miscible domain at $T \neq 0$ has characteristic signature in the spatial structure of $g_k^{(1)}(\mathbf{r}, \mathbf{r}')$.

5.2 Quasiparticle spectra of trapped TBEC

To examine the effects of thermal fluctuations on the quasiparticle spectra we consider the ^{87}Rb - ^{85}Rb TBEC with ^{87}Rb labeled as species 1 and ^{85}Rb labeled as species 2. The radial trapping frequencies of the harmonic potential are $\omega_x = \omega_y = 2\pi \times 50$ Hz with the anisotropy parameter $\omega_z/\omega_\perp = 20.33$, and these parameters, as mentioned earlier, are chosen based on the experimental work of Gadway et al. [111] on the TBEC of two hyperfine states of ^{87}Rb in optical lattices. It is important to note that we consider equal background trapping potential for both the species. We emphasize here that, the results are equally applicable to the case of the TBEC consisting of two hyperfine states of ^{87}Rb , however, we have chosen ^{87}Rb - ^{85}Rb to highlight that the small mass difference has no influence on the geometry of the ground state. The laser wavelength

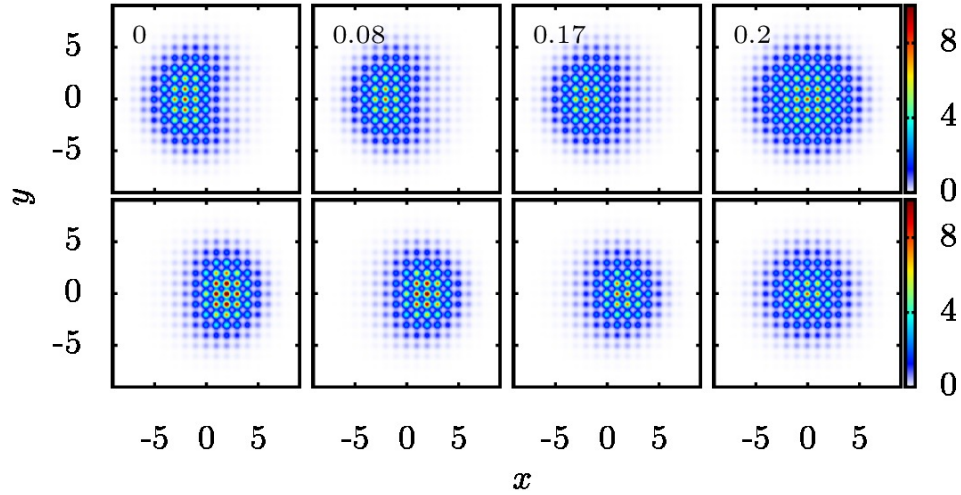


Figure 5.1: The condensate density profiles at different temperatures in the phase-separated domain of ^{87}Rb - ^{85}Rb TBEC. The condensate density distribution of the first species (upper panel) and the second species (lower panel) are shown at $T/T_c = 0, 0.08, 0.17,$ and 0.2 , which correspond to $T = 0, 30, 60,$ and 70 nK. Here x and y are measured in units of the lattice constant a .

used to create the 2D lattice potential and the lattice depth are $\lambda_L = 1064$ nm and $V_0 = 5E_R$, respectively. We then take the total number of atoms as $N_1 = N_2 = 100$, which are confined in a 40×40 quasi-2D lattice system. It must be mentioned that, the number of lattice sites considered is much larger than the spatial extent of the condensate cloud. Albeit the computations require longer time with the larger lattice size, we chose it to ensure that the spatial extent of the thermal component is confined well within the lattice sites considered. The tunneling matrix elements are $J_1 = 0.66E_R$ and $J_2 = 0.71E_R$, which correspond to an optical lattice potential with a depth of $5E_R$. The intraspecies and interspecies on-site interactions are set as $U_{11} = 0.07E_R$, $U_{22} = 0.02E_R$ and $U_{12} = 0.15E_R$, respectively. For this set of parameters the ground state density distribution of ^{87}Rb - ^{85}Rb TBEC is phase-separated with side-by-side geometry. This is a symmetry-broken profile where one species is placed to the left, and other to the right of trap center along y -axis. The evolution of the ground state from miscible to the side-by-side density profile due to decrease in the U_{22} is described in Chapter 4. In the present work, we demonstrate the role of the temperature in the phase-separated domain of the binary condensate.

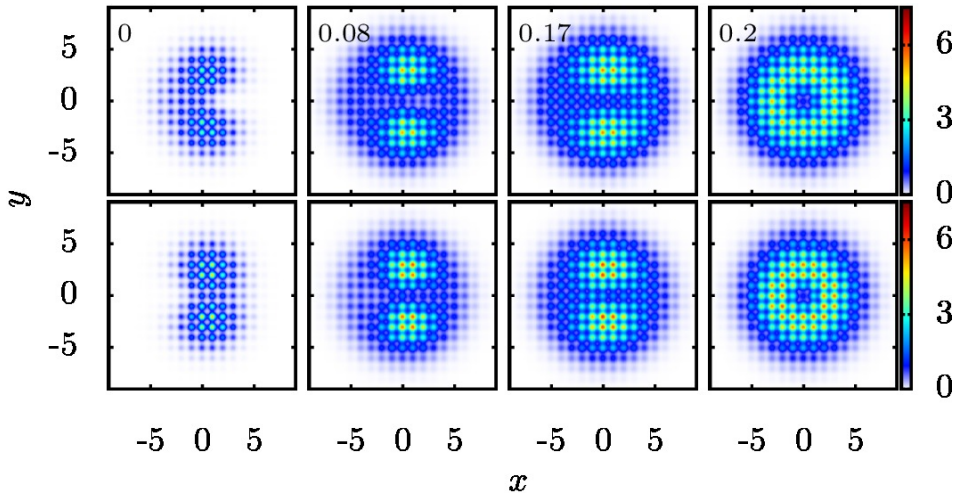


Figure 5.2: The noncondensate density profile at different temperatures in the phase-separated domain of ^{87}Rb - ^{85}Rb TBEC. The density distribution of the noncondensate atoms of first species (upper panel) and the second species (lower panel) are shown at $T/T_c = 0, 0.08, 0.17,$ and 0.2 , which correspond to $T = 0, 30, 60,$ and 70 nK. Here x and y are measured in units of the lattice constant a .

5.2.1 Zero temperature

At zero temperature, in the phase-separated domain, the energetically preferable ground state of TBEC is the side-by-side geometry, which is reported in the Chapter 4. Unlike in one-dimensional system [308] in quasi-2D system the presence of the quantum fluctuations does not alter the ground state. We start with the phase-separated ^{87}Rb - ^{85}Rb TBEC, which has the overlap integral $\Lambda = 0.10$. The density distributions of the condensate and noncondensate atoms of the two species at zero temperature are shown in Figs. 5.1 and 5.2. It is a symmetry broken side-by-side geometry with noncondensate atoms more localized at the edges of the condensate along y -axis.

5.2.2 Finite temperatures

For finite temperature computations we solve the coupled DNLSEs [Eq. (2.64)], and the HFB-Popov Eqs. (2.66) self-consistently. In the process, we encounter oscillations in the number of atoms, and face the convergence issue. To mitigate this, we use successive under and over relaxation techniques. At $T \neq 0$, in addition to the quantum fluctuations, which are present even at zero temperature, the thermal cloud also con-

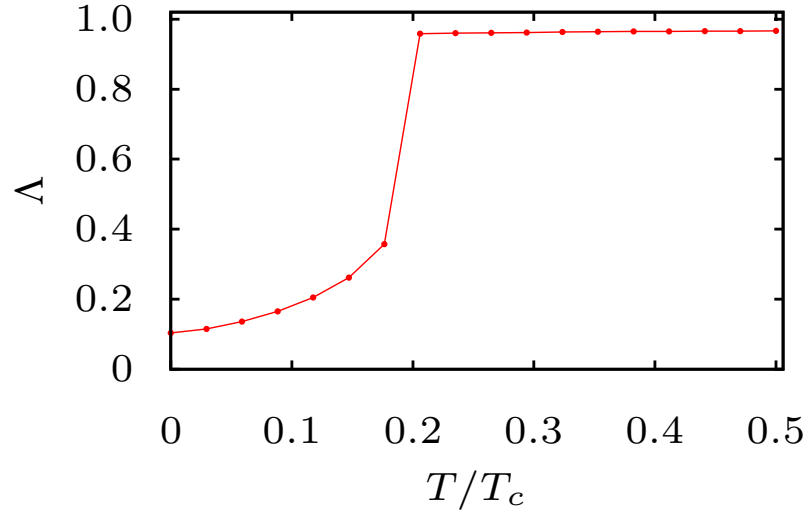


Figure 5.3: The overlap integral as a function of the temperature. A sharp increase in the value of Λ is the signature of the miscibility of the TBEC at $T/T_c = 0.185$. The temperature is scaled by the critical temperature of the ^{87}Rb species.

tribute to the noncondensate density. As shown in Figs. 5.1 and 5.2, at $T = 30$ nK, the condensate density profiles of both the species begin to overlap, or in other words, the two species are partly miscible. This is also evident from the value of $\Lambda = 0.16$, which shows a marginal increase compared to the value of 0.10 at zero temperature. Upon further increase in the temperature, at $T = 60$ nK, $\Lambda = 0.36$, this indicates an increase in the miscibility of the two species. Another important feature at 30 and 60 nK is the localization of the noncondensate atoms at the interface. This is due to the repulsion from the condensate atoms, and lower thermal energy which is insufficient to overcome the energy of repulsion. At higher temperatures, the extent of the overlap between the condensate density profiles increases, and the TBEC is completely miscible at $T = 70$ nK. This is reflected in the value of $\Lambda = 0.95$, and the condensate as well as the noncondensate densities acquire rotational symmetry. The condensate fraction of the species decreases rapidly at $T/T_c = 0.185$, and this results into a sharp increase in the miscibility of the species. This is evident from Fig. 5.3, which shows the overlap integral as a function of the temperature.

The transition from the phase-separated into miscible domain can further be examined from the evolution of the quasiparticle modes as a function of the temperature [309]. The evolution of the few low-lying mode energies with temperature is

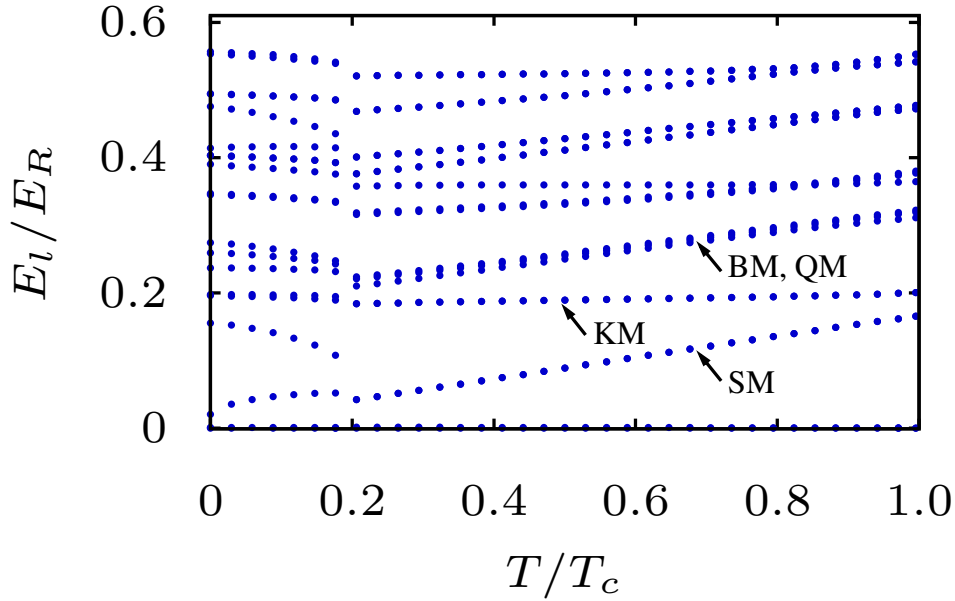


Figure 5.4: The quasiparticle energies of the low-lying modes as a function of the temperature in the phase-separated domain of ^{87}Rb - ^{85}Rb TBEC. At $T/T_c = 0.185$ the slosh and higher modes energy becomes degenerate and the system transforms from side-by-side to the miscible density profile. In the figure, the slosh mode (SM), Kohn mode (KM), breathing mode (BM), and quadrupole mode (QM) are marked by the black arrows. Here the excitation energy E_l and the temperature T are scaled with respect to the recoil energy E_R and the critical temperature T_c of the ^{87}Rb , respectively.

shown in Fig. 5.4 where the temperature is defined in the units of the critical temperature T_c of the ^{87}Rb atoms, which for the parameters considered is 338 nK. It is evident from the figure that there are mode energy bifurcations with the increase in the temperature. These are associated with the restoration of the rotational symmetry when the TBEC is rendered miscible through an increase in the temperature.

As to be expected the two lowest energy modes are the zero energy or the NG modes, which are the result of the SSB associated with the condensation of the TBEC. In the phase-separated domain, these modes correspond to one each for each of the two species. The first two excited modes are the nondegenerate slosh modes of the two species, and these remain nondegenerate in the domain $T/T_c < 0.185$. The structure of these modes are shown in Figs. 5.5 and 5.6. When $T/T_c \geq 0.185$ the TBEC acquires a rotational symmetry, and the slosh modes becomes degenerate. In addition to this, the slosh mode start rotating as T is increased above the characteristic temperature,

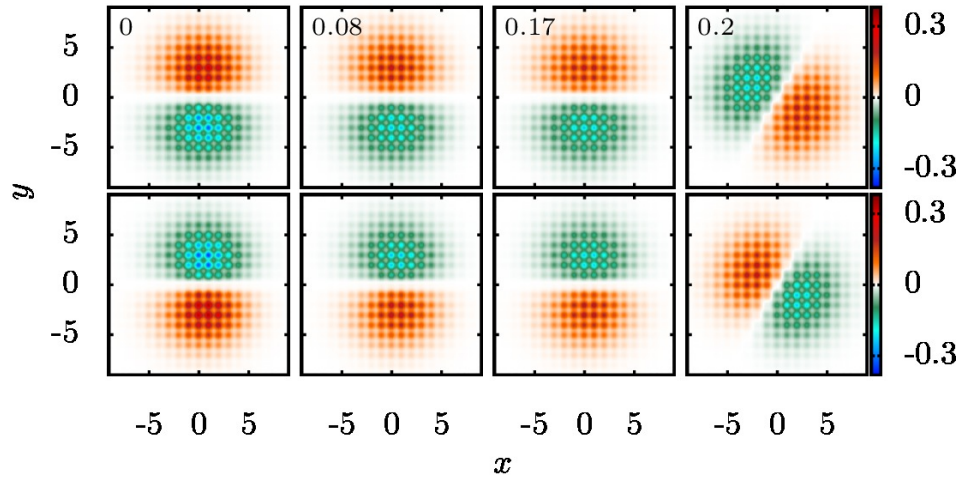


Figure 5.5: The mode function of the first excited mode (slosh mode) as a function of the temperature in the phase-separated domain of ^{87}Rb - ^{85}Rb TBEC. The slosh mode is an out-of-phase mode, where the density flow of the first species (upper panel) is in opposite direction to the flow of the second species (lower panel). The value of T/T_c is shown at the upper left corner of each plot in the upper panel. These values correspond to $T = 0, 30, 60,$ and 70 nK. Here x and y are in units of the lattice constant a .

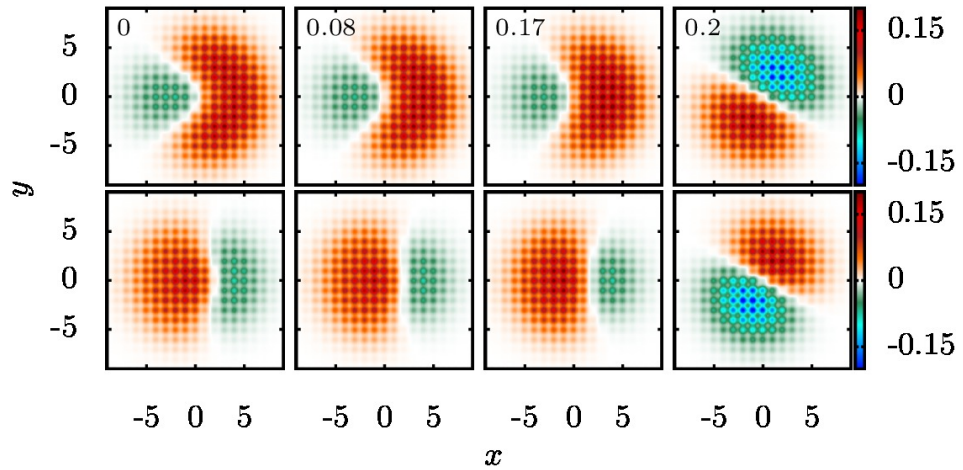


Figure 5.6: The mode function of the second excited mode (slosh mode) for ^{87}Rb - ^{85}Rb TBEC, which at $T/T_c \geq 0.185$ becomes degenerate to the mode shown in Fig. 5.5. Here, the density flow of the first species (upper panel) is out of phase to the flow of the second species (lower panel). The value of T/T_c is shown at the upper left corner of each plot in the upper panel. These values correspond to $T = 0, 30, 60,$ and 70 nK. Here x and y are in units of the lattice constant a .

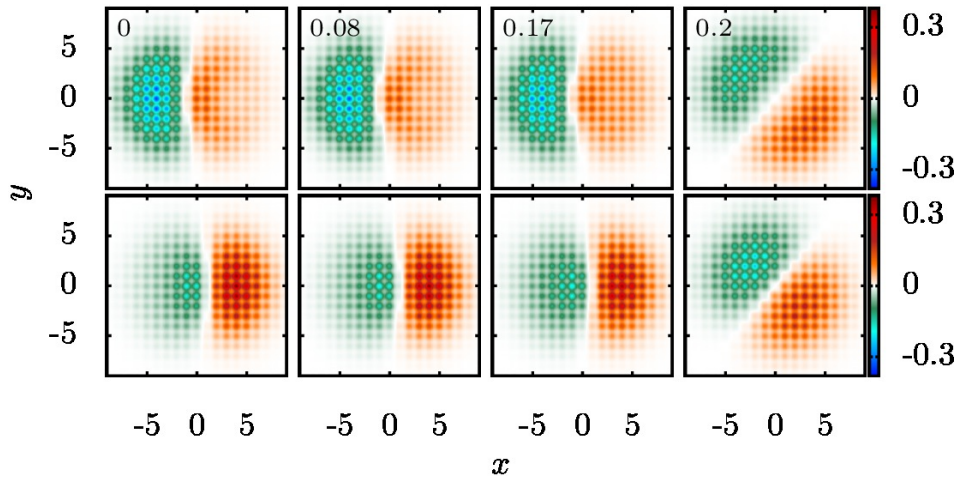


Figure 5.7: The mode function corresponding to the Kohn mode as a function of the temperature in the phase-separated domain of ^{87}Rb - ^{85}Rb TBEC. The Kohn mode is an in-phase mode, where the density flow of the first species (upper panel) and the second species (lower panel) is in the same direction. The value of T/T_c is shown at the upper left corner of each plot in the upper panel. These values correspond to $T = 0, 30, 60,$ and 70 nK. Here x and y are in units of the lattice constant a .

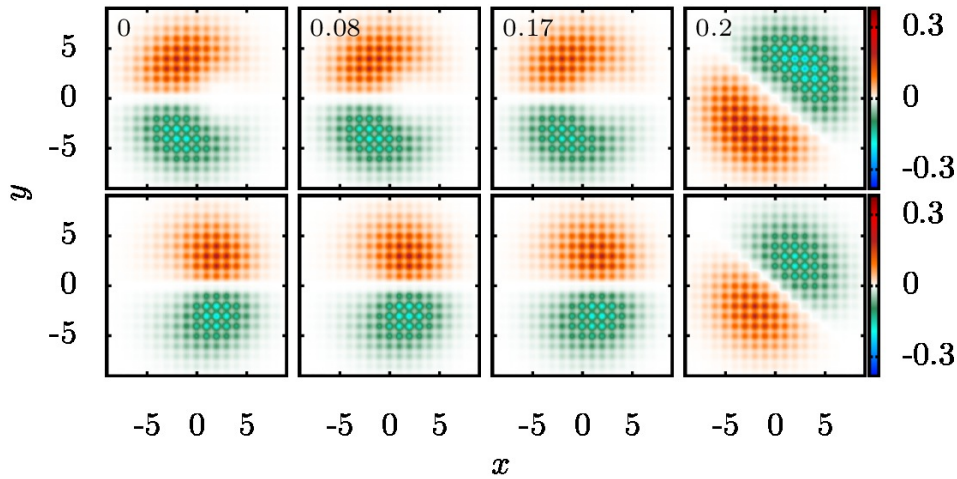


Figure 5.8: The mode function of the Kohn mode for ^{87}Rb - ^{85}Rb TBEC, which is degenerate to the mode shown in Fig. 5.7. The value of T/T_c is shown at the upper left corner of each plot in the upper panel. These values correspond to $T = 0, 30, 60,$ and 70 nK. Here x and y are in units of the lattice constant a .

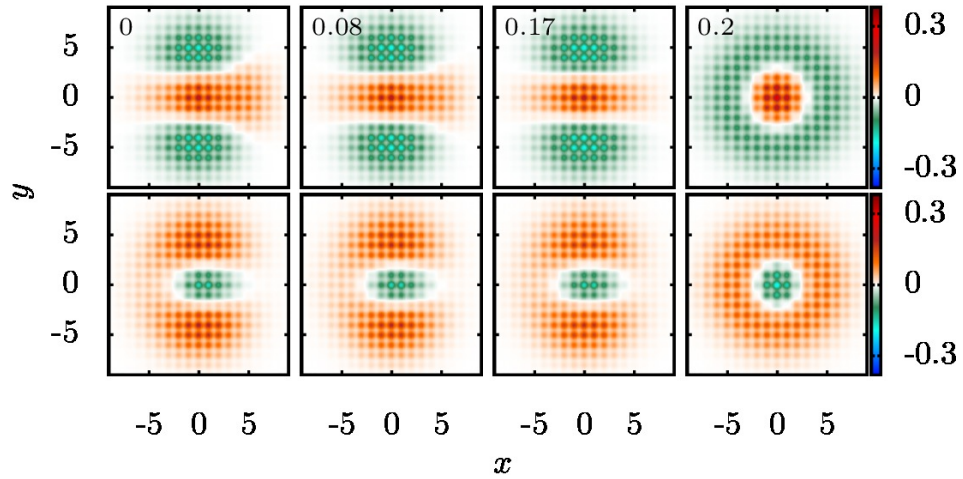


Figure 5.9: The evolution of the interface mode in the phase-separated domain of ^{87}Rb - ^{85}Rb TBEC with temperature. At $T/T_c \geq 0.185$, this mode transformed into the breathing mode as the system acquires the rotational symmetry. These are out-of-phase modes as the density flow of the first species (upper panel) is in opposite direction to the the second species (lower panel). The value of T/T_c is shown at the upper left corner of each plot in the upper panel. Here x and y are in units of the lattice constant a .

which for the parameters considered is 66 nK. In general, in the miscible domain the degenerate quasiparticle modes are related by a rotation of $\pi/2m$ angle with m as the azimuthal quantum number. For the slosh modes ($m = 1$), this property is evident from the mode functions in the figures. A key feature in the quasiparticle mode evolution is that the energy of all the out-of-phase mode increases for $T/T_c \geq 0.185$, whereas all the in-phase mode remains steady. Here, out-of-phase and in-phase mean the amplitudes u_1 and u_2 of a quasiparticle are of different and same phases, respectively. Among the low-energy modes, the Kohn mode is an in phase whereas the breathing and quadrupole modes are out of phase in nature. The quasiparticle mode functions corresponding to the Kohn modes are shown in Figs. 5.7 and 5.8. One unique feature of the TBEC in the immiscible phase is the presence of the interface modes, which have amplitudes prominent around the interface region. The existence of these modes is reported in Chapter 4, and were investigated in other works [224, 225] for TBECs confined in harmonic potential alone at zero temperature. One of the low-energy interface mode is shown in Fig. 5.9. It is evident from the figure that the mode is out-of-phase

in nature, and it is transformed into the breathing mode of the miscible domain when $T/T_c \geq 0.185$. In the miscible domain, the breathing mode becomes degenerate with the quadrupole mode and gains energy. The quasiparticles of the miscible domain have well-defined azimuthal quantum number, and thereby modes undergo rotations as T is further increased. The rotations of the slosh, and the Kohn modes after the immiscible-miscible transition is evident from the structure of the modes [Figs. 5.5-5.8].

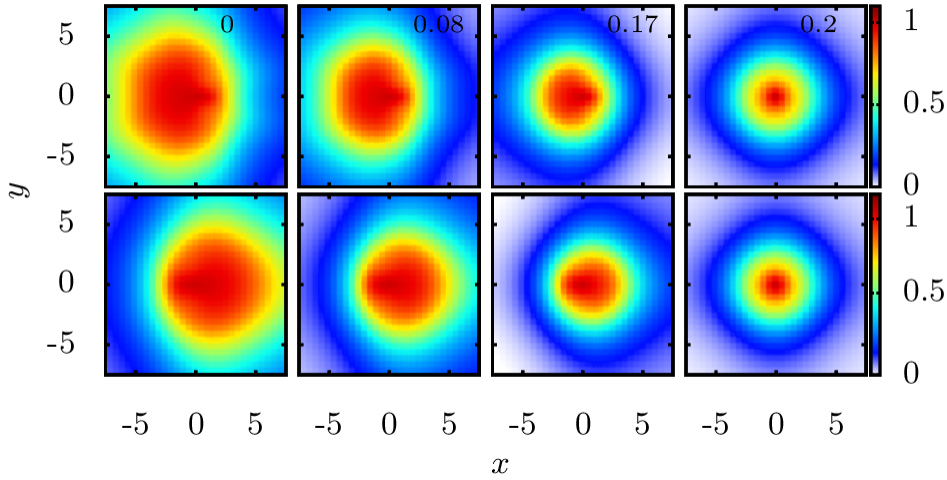


Figure 5.10: The normalized first-order off-diagonal correlation function $g_k^{(1)}(0, \mathbf{r})$ of ^{87}Rb (upper panel) and ^{85}Rb (lower panel) at $T/T_c = 0, 0.08, 0.17$, and 0.2 , which correspond to $T = 0, 30, 60$, and 70 nK. Here x and y are measured in units of the lattice constant a .

5.3 Correlation function of TBEC

The correlation function is an important tool to examine the coherence properties of the system. The experiment on TBEC in optical lattice has observed the loss of SF coherence of the heavier species in the presence of a lighter species. This decrease in coherence is independent of the sign of the interaction, and exist even for small overlap of the two species [109]. In another recent experiment, the reduction of the coherence has been observed for the large atom number imbalance, and the tunneling rate asymmetry [111]. In this work, we study the loss of coherence with increase in the temperature. To investigate the spatial coherence of TBEC at equilibrium, we examine

the trends in $g_k^{(1)}(0, \mathbf{r})$ defined earlier in Eq. (5.3), and are shown in Fig. 5.10 for various temperatures [309]. The profile of the correlation function depends on the interplay of the on-site interaction and the temperature. As mentioned earlier, at zero temperature, $n_k(\mathbf{r}) \approx n_k^c(\mathbf{r})$ have complete phase coherence, and therefore, $g_k^{(1)} = 1$ within the extent of the condensates, this is shown in Fig. 5.10. At zero temperature or in the limit $\tilde{n}_k \equiv 0$ the correlation function, Eq. (5.3), resemble a Heaviside function, and the negligible contribution from the quantum fluctuations smooth out the sharp edges as $g_k^{(1)}$ drops to zero. More importantly, in the numerical computations this causes a loss of numerical accuracy as it involves division of two small numbers in Eq. (5.3) [310]. However, at finite temperature the presence of the noncondensate atoms modify the nature of the spatial coherence present in the system. At lower temperatures, the off-diagonal long-range order dominates due to large condensate fraction. In contrast, at higher temperatures, close to the critical temperature T_c , the thermal component is much more significant compared to the condensate, which results in the loss of coherence at T_c . The decay rate of the correlation function increases with the temperature, and this is evident from Fig. 5.10, which shows $g_k^{(1)}(0, \mathbf{r})$ at $T = 30, 60,$ and 70 nK. In addition to this, the transition from phase-separated to the miscible phase of TBEC is also reflected in the decay trends of $g_k^{(1)}(0, \mathbf{r})$.

5.4 Conclusions

We have examined the finite temperature effects on the phenomenon of phase separation in TBECs confined in quasi-2D optical lattices. As the temperature is increased the phase-separated side-by-side ground state geometry is transformed into miscible phase. For the case of TBEC comprising of ^{87}Rb and ^{85}Rb , the transformation occurs at $T/T_c \approx 0.185$. This demonstrates the importance of the thermal fluctuations which can make TBECs miscible albeit the interaction parameters satisfy the criterion of the phase separation. The other key observation is that the transition from phase-separated domain to the miscible domain is associated with a change in the nature of the quasiparticle energies. The low-lying out-of-phase mode, in particular, the slosh mode becomes degenerate and increase in energy. On the other hand, the in-phase

mode, such as Kohn mode, remains steady as temperature ($T < T_c$) is increased. The interface mode, which is unique to the phase-separated domain, in addition to change in energy, is geometrically transformed into the rotationally symmetric breathing mode in the miscible domain. The temperature driven immiscible to the miscible transition is also evident in the profile of the correlation function of TBEC.

Chapter 6

Summary and future directions

In this thesis, we have described the coupled DNLSs, and the HFB-Popov theory in the two-component Bose-Hubbard model to examine the configurations of the ground state, evolution of the quasiparticle modes and the structure of the mode functions of TBECs. We have shown that the lowest excited mode with nonzero energy, which is Kohn mode, goes soft at the phase separation, and emerges as an additional Goldstone mode in the immiscible phase of TBECs in quasi-1D optical lattices. In the immiscible phase, the ground state acquires a sandwich type density profile, which is equivalent to three coupled condensates of a TBEC. In the presence of the quantum fluctuations, the soft Kohn mode, which appears at phase separation, gets hardened and consequently a symmetry broken side-by-side type density profile appears as the ground state in the immiscible phase. In other words, the fluctuations break the symmetry of the ground-state after phase separation at zero temperature.

We have observed that the sandwich or shell-structured density distribution of quasi-2D TBECs is not energetically favourable, and the side-by-side geometry emerges as a stable ground state. The quasiparticles of the miscible phase of TBECs are degenerate, and the degeneracies of these modes are lifted at the phase separation. The dispersion curves of the miscible domain show discernible trends associated with the azimuthal quantum number of the quasiparticle. On the contrary, in the immiscible domain there are no clear structures in the dispersion curves. This is due to the rotational symmetry breaking, and the resulting mixing of the modes with different azimuthal quantum numbers.

We have investigated the role of the finite temperatures on the evolution of the quasiparticle modes in the immiscible phase of TBEC. As the temperature is increased, a phase-separated side-by-side geometry is transformed into the miscible phase. This immiscible-miscible transition is associated with a discontinuity in the quasiparticle spectra. In addition, the low-lying out-of-phase modes, such as slosh mode become degenerate, and increase in energy whereas the in-phase mode, such as Kohn mode remains steady with temperature. In future, we shall study the static and dynamical properties of TBECs in more complex lattice geometries such as triangular and hexagonal. Another question is the quasiparticle spectra of TBECs in the presence of the topological defects like solitons and vortices in optical lattices, which can be examined in our future research. The extension of the DNLSs to describe dipolar atoms in optical lattice is also an agenda of our future investigations.

Appendix A

Numerical Details

We solve the scaled coupled DNLSEs using fourth order Runge-Kutta (RK4) method to find the equilibrium state of the harmonically trapped binary condensates in optical lattices. We start the calculations for zero temperature by ignoring the quantum fluctuations at each lattice site. We choose the initial guess values of the complex amplitudes as Gaussian or the side-by-side envelope profile such that the quasiparticle energy eigenvalues are real. We then use imaginary-time propagation of the DNLSEs to find the stationary ground state of the TBEC. In the tight-binding limit, we take a basis set consisting of the orthonormalized Gaussian functions localized at each lattice site [183]. The width of the function is a crucial parameter as it affects the overlap of the Gaussian orbitals at each lattice site. The correct estimation of the width is required in order to obtain orthonormal basis functions. The width depends on the mass of the species and the frequency of the lattice potential. In the present study, the frequency plays a dominant role over the mass of the constituent species. Therefore, the widths of the Gaussian basis functions are taken to be identical for both the species of a TBEC. Furthermore, to study the excitation spectrum, we cast the set of BdG or HFB-Popov equations as a matrix eigenvalue equation. The matrix is non-Hermitian, non-symmetric and may have complex eigenvalues. To diagonalize the matrix and find the quasiparticle energies and amplitudes, we use the routine ZGEEV from the LAPACK library [311]. We solve the modified DNLSEs and the HFB-Popov equations self-consistently to investigate the role of quantum fluctuations in quasi-1D lattices and thermal fluctuations induced effects in quasi-2D lattices. For these computations, we

iterate the solution until we reach desired convergence in the number of condensate and noncondensate atoms. In this process, sometimes, we encounter severe oscillations in the number of atoms. To damp these oscillations and accelerate convergence we employ a successive over (under) relaxation technique for updating the condensate (noncondensate) atom densities [312]. After the iteration cycle (IC), the updated values of the complex amplitudes associated with the condensate wave functions and the noncondensate densities of quasi-1D TBEC are given by

$$\begin{aligned} c_{j,\text{IC}}^{\text{new}} &= r^{\text{ov}} c_{j,\text{IC}} + (1 - r^{\text{ov}}) c_{j,\text{IC}-1}, \\ d_{j,\text{IC}}^{\text{new}} &= r^{\text{ov}} d_{j,\text{IC}} + (1 - r^{\text{ov}}) d_{j,\text{IC}-1}, \\ \tilde{n}_{ij,\text{IC}}^{\text{new}} &= r^{\text{un}} \tilde{n}_{ij,\text{IC}} + (1 - r^{\text{un}}) \tilde{n}_{ij,\text{IC}-1}, \end{aligned}$$

where $i = 1, 2$ is the species index, j is the lattice site index, and $r^{\text{ov}} > 1$ ($r^{\text{un}} < 1$) is the over- (under-) relaxation parameter. During computation, we ensure that the eigenvalues of the BdG or HFB-Popov matrix are real as there are no topological defects present in the system. To compute the dispersion curves of quasi-2D TBEC, we use FFTW library [313] in Intel MKL to transform the quasiparticle amplitudes into the momentum space.

Bibliography

- [1] M. H. Anderson, J. R. Ensher, M. R. Matthews, C. E. Wieman, and E. A. Cornell, *Observation of Bose-Einstein condensation in a dilute atomic vapor*, Science **269**, 198 (1995).
- [2] K. B. Davis, M. O. Mewes, M. R. Andrews, N. J. van Druten, D. S. Durfee, D. M. Kurn, and W. Ketterle, *Bose-Einstein condensation in a gas of sodium atoms*, Phys. Rev. Lett. **75**, 3969 (1995).
- [3] C. C. Bradley, C. A. Sackett, J. J. Tollett, and R. G. Hulet, *Evidence of Bose-Einstein condensation in an atomic gas with attractive interactions*, Phys. Rev. Lett. **75**, 1687 (1995).
- [4] S. Chu, *Nobel lecture: The manipulation of neutral particles*, Rev. Mod. Phys. **70**, 685 (1998).
- [5] C. N. Cohen-Tannoudji, *Nobel lecture: Manipulating atoms with photons*, Rev. Mod. Phys. **70**, 707 (1998).
- [6] W. D. Phillips, *Nobel lecture: Laser cooling and trapping of neutral atoms*, Rev. Mod. Phys. **70**, 721 (1998).
- [7] W. Ketterle, *Happy birthday BEC*, Nat. Phys. **11**, 982 (2015).
- [8] B. P. Anderson and M. A. Kasevich, *Macroscopic quantum interference from atomic tunnel arrays*, Science **282**, 1686 (1998).
- [9] M. Kozuma, L. Deng, E. W. Hagley, J. Wen, R. Lutwak, K. Helmerson, S. L. Rolston, and W. D. Phillips, *Coherent splitting of Bose-Einstein condensed atoms with optically induced Bragg diffraction*, Phys. Rev. Lett. **82**, 871 (1999).

- [10] J. Stenger, S. Inouye, A. P. Chikkatur, D. M. Stamper-Kurn, D. E. Pritchard, and W. Ketterle, *Bragg spectroscopy of a Bose-Einstein condensate*, Phys. Rev. Lett. **82**, 4569 (1999).
- [11] Y. B. Ovchinnikov, J. H. Müller, M. R. Doery, E. J. D. Vredenburg, K. Helmerston, S. L. Rolston, and W. D. Phillips, *Diffraction of a released Bose-Einstein condensate by a pulsed standing light wave*, Phys. Rev. Lett. **83**, 284 (1999).
- [12] E. W. Hagley, L. Deng, M. Kozuma, M. Trippenbach, Y. B. Band, M. Edwards, M. Doery, P. S. Julienne, K. Helmerston, S. L. Rolston, and W. D. Phillips, *Measurement of the coherence of a Bose-Einstein condensate*, Phys. Rev. Lett. **83**, 3112 (1999).
- [13] B. DeMarco and D. S. Jin, *Onset of Fermi degeneracy in a trapped atomic gas*, Science **285**, 1703 (1999).
- [14] S. Jochim, M. Bartenstein, A. Altmeyer, G. Hendl, S. Riedl, C. Chin, J. Hecker Denschlag, and R. Grimm, *Bose-Einstein condensation of molecules*, Science **302**, 2101 (2003).
- [15] M. W. Zwierlein, C. A. Stan, C. H. Schunck, S. M. F. Raupach, S. Gupta, Z. Hadzibabic, and W. Ketterle, *Observation of Bose-Einstein condensation of molecules*, Phys. Rev. Lett. **91**, 250401 (2003).
- [16] M. Greiner, C. A. Regal, and D. S. Jin, *Emergence of a molecular Bose-Einstein condensate from a Fermi gas*, Nature (London) **426**, 537 (2003).
- [17] O. Morsch and M. Oberthaler, *Dynamics of Bose-Einstein condensates in optical lattices*, Rev. Mod. Phys. **78**, 179 (2006).
- [18] M. Bartenstein, A. Altmeyer, S. Riedl, S. Jochim, C. Chin, J. H. Denschlag, and R. Grimm, *Crossover from a molecular Bose-Einstein condensate to a degenerate Fermi gas*, Phys. Rev. Lett. **92**, 120401 (2004).
- [19] J. Kinast, S. L. Hemmer, M. E. Gehm, A. Turlapov, and J. E. Thomas, *Evidence for superfluidity in a resonantly interacting Fermi gas*, Phys. Rev. Lett. **92**, 150402 (2004).

- [20] G. B. Partridge, K. E. Strecker, R. I. Kamar, M. W. Jack, and R. G. Hulet, *Molecular probe of pairing in the BEC-BCS crossover*, Phys. Rev. Lett. **95**, 020404 (2005).
- [21] I. Bloch, J. Dalibard, and W. Zwerger, *Many-body physics with ultracold gases*, Rev. Mod. Phys. **80**, 885 (2008).
- [22] M. Lewenstein, A. Sanpera, and V. Ahufinger, *Ultracold Atoms in Optical Lattices: Simulating quantum many-body systems* (Oxford University Press, Oxford, 2012).
- [23] M. Lewenstein, A. Sanpera, V. Ahufinger, B. Damski, A. Sen(De), and U. Sen, *Ultracold atomic gases in optical lattices: mimicking condensed matter physics and beyond*, Adv. Phys. **56**, 243 (2007).
- [24] M. A. Cazalilla, R. Citro, T. Giamarchi, E. Orignac, and M. Rigol, *One dimensional bosons: From condensed matter systems to ultracold gases*, Rev. Mod. Phys. **83**, 1405 (2011).
- [25] C. Becker, P. Soltan-Panahi, J. Kronjäger, S. Dörscher, K. Bongs, and K. Sengstock, *Ultracold quantum gases in triangular optical lattices*, New J. Phys. **12**, 065025 (2010).
- [26] P. Soltan-Panahi, J. Struck, P. Hauke, A. Bick, W. Plenkers, G. Meineke, C. Becker, P. Windpassinger, M. Lewenstein, and K. Sengstock, *Multi-component quantum gases in spin-dependent hexagonal lattices*, Nat. Phys. **7**, 434 (2011).
- [27] M. P. A. Fisher, P. B. Weichman, G. Grinstein, and D. S. Fisher, *Boson localization and the superfluid-insulator transition*, Phys. Rev. B **40**, 546 (1989).
- [28] D. Jaksch, C. Bruder, J. I. Cirac, C. W. Gardiner, and P. Zoller, *Cold bosonic atoms in optical lattices*, Phys. Rev. Lett. **81**, 3108 (1998).
- [29] M. Greiner, O. Mandel, T. Esslinger, T. W. Hänsch, and I. Bloch, *Quantum phase transition from a superfluid to a Mott insulator in a gas of ultracold atoms*, Nature (London) **415**, 39 (2002).

- [30] M. Greiner, *Ultracold quantum gases in three-dimensional optical lattice potentials*, Ph.D. thesis, Ludwig Maximilian University of Munich, Germany (2003).
- [31] C. Pethick and H. Smith, *Bose-Einstein Condensation in Dilute Gases* (Cambridge University Press, 2008).
- [32] O. Penrose and L. Onsager, *Bose-Einstein condensation and liquid helium*, Phys. Rev. **104**, 576 (1956).
- [33] L. Pitaevskii and S. Stringari, *Bose-Einstein Condensation* (Clarendon, Oxford, 2003).
- [34] A. Griffin, D. W. Snoke, and S. Stringari, *Bose-Einstein Condensation* (Cambridge University Press, 1996).
- [35] V. V. Tolmachev, *Superconducting Bose-Einstein condensates of Cooper pairs interacting with electrons*, Phys. Lett. A **266**, 400 (2000).
- [36] I. Sapina and T. Dahm, *Interaction of a Bose-Einstein condensate and a superconductor via eddy currents*, New J. Phys. **15**, 073035 (2013).
- [37] A. Retzker, J. I. Cirac, M. B. Plenio, and B. Reznik, *Methods for detecting acceleration radiation in a Bose-Einstein condensate*, Phys. Rev. Lett. **101**, 110402 (2008).
- [38] P. R. Anderson, R. Balbinot, A. Fabbri, and R. Parentani, *Hawking radiation correlations in Bose-Einstein condensates using quantum field theory in curved space*, Phys. Rev. D **87**, 124018 (2013).
- [39] J. Steinhauer, *Observation of self-amplifying Hawking radiation in an analogue black-hole laser*, Nat. Phys. **10**, 864 (2014).
- [40] T. Fukuyama and M. Morikawa, *Stagflation: Bose-Einstein condensation in the early universe*, Phys. Rev. D **80**, 063520 (2009).
- [41] B. Opanchuk, R. Polkinghorne, O. Fialko, J. Brand, and P. D. Drummond, *Quantum simulations of the early universe*, Ann. phys. (Berlin) **525**, 866 (2013).

- [42] E. A. Calzetta and B. L. Hu, *Early universe quantum processes in BEC collapse experiments*, Int. J. Theor. Phys. **44**, 1691 (2005).
- [43] C. J. Myatt, E. A. Burt, R. W. Ghrist, E. A. Cornell, and C. E. Wieman, *Production of two overlapping Bose-Einstein condensates by sympathetic cooling*, Phys. Rev. Lett. **78**, 586 (1997).
- [44] G. Modugno, M. Modugno, F. Riboli, G. Roati, and M. Inguscio, *Two atomic species superfluid*, Phys. Rev. Lett. **89**, 190404 (2002).
- [45] A. Lercher, T. Takekoshi, M. Debatin, B. Schuster, R. Rameshan, F. Ferlaino, R. Grimm, and H.-C. Nägerl, *Production of a dual-species Bose-Einstein condensate of Rb and Cs atoms*, Eur. Phys. J. D **65**, 3 (2011).
- [46] D. J. McCarron, H. W. Cho, D. L. Jenkin, M. P. Köppinger, and S. L. Cornish, *Dual-species Bose-Einstein condensate of ^{87}Rb and ^{133}Cs* , Phys. Rev. A **84**, 011603 (2011).
- [47] B. Pasquiou, A. Bayerle, S. M. Tzanova, S. Stellmer, J. Szczepkowski, M. Parigger, R. Grimm, and F. Schreck, *Quantum degenerate mixtures of strontium and rubidium atoms*, Phys. Rev. A **88**, 023601 (2013).
- [48] L. Wacker, N. B. Jørgensen, D. Birkmose, R. Horchani, W. Ertmer, C. Klempt, N. Winter, J. Sherson, and J. J. Arlt, *Tunable dual-species Bose-Einstein condensates of ^{39}K and ^{87}Rb* , Phys. Rev. A **92**, 053602 (2015).
- [49] F. Wang, X. Li, D. Xiong, and D. Wang, *A double species ^{23}Na and ^{87}Rb Bose-Einstein condensate with tunable miscibility via an interspecies Feshbach resonance*, J. Phys. B **49**, 015302 (2016).
- [50] S. B. Papp, J. M. Pino, and C. E. Wieman, *Tunable miscibility in a dual-species Bose-Einstein condensate*, Phys. Rev. Lett. **101**, 040402 (2008).
- [51] S. Händel, T. P. Wiles, A. L. Marchant, S. A. Hopkins, C. S. Adams, and S. L. Cornish, *Magnetic merging of ultracold atomic gases of ^{85}Rb and ^{87}Rb* , Phys. Rev. A **83**, 053633 (2011).

- [52] S. Sugawa, R. Yamazaki, S. Taie, and Y. Takahashi, *Bose-Einstein condensate in gases of rare atomic species*, Phys. Rev. A **84**, 011610 (2011).
- [53] D. S. Hall, M. R. Matthews, J. R. Ensher, C. E. Wieman, and E. A. Cornell, *Dynamics of component separation in a binary mixture of Bose-Einstein condensates*, Phys. Rev. Lett. **81**, 1539 (1998).
- [54] D. M. Stamper-Kurn, M. R. Andrews, A. P. Chikkatur, S. Inouye, H.-J. Miesner, J. Stenger, and W. Ketterle, *Optical confinement of a Bose-Einstein condensate*, Phys. Rev. Lett. **80**, 2027 (1998).
- [55] J. Stenger, S. Inouye, D. M. Stamper-Kurn, H.-J. Miesner, A. P. Chikkatur, and W. Ketterle, *Spin domains in ground-state Bose-Einstein condensates*, Nature (London) **396**, 345 (1998).
- [56] P. Maddaloni, M. Modugno, C. Fort, F. Minardi, and M. Inguscio, *Collective oscillations of two colliding Bose-Einstein condensates*, Phys. Rev. Lett. **85**, 2413 (2000).
- [57] G. Delannoy, S. G. Murdoch, V. Boyer, V. Josse, P. Bouyer, and A. Aspect, *Understanding the production of dual Bose-Einstein condensation with sympathetic cooling*, Phys. Rev. A **63**, 051602 (2001).
- [58] L. E. Sadler, J. M. Higbie, S. R. Leslie, M. Vengalattore, and D. M. Stamper-Kurn, *Spontaneous symmetry breaking in a quenched ferromagnetic spinor Bose-Einstein condensate*, Nature (London) **443**, 312 (2006).
- [59] K. M. Mertes, J. W. Merrill, R. Carretero-González, D. J. Frantzeskakis, P. G. Kevrekidis, and D. S. Hall, *Nonequilibrium dynamics and superfluid ring excitations in binary Bose-Einstein condensates*, Phys. Rev. Lett. **99**, 190402 (2007).
- [60] R. P. Anderson, C. Ticknor, A. I. Sidorov, and B. V. Hall, *Spatially inhomogeneous phase evolution of a two-component Bose-Einstein condensate*, Phys. Rev. A **80**, 023603 (2009).

- [61] S. Tojo, Y. Taguchi, Y. Masuyama, T. Hayashi, H. Saito, and T. Hirano, *Controlling phase separation of binary Bose-Einstein condensates via mixed-spin-channel Feshbach resonance*, Phys. Rev. A **82**, 033609 (2010).
- [62] S. Ronen, J. L. Bohn, L. E. Halmó, and M. Edwards, *Dynamical pattern formation during growth of a dual-species Bose-Einstein condensate*, Phys. Rev. A **78**, 053613 (2008).
- [63] M. A. Hoefer, J. J. Chang, C. Hamner, and P. Engels, *Dark-dark solitons and modulational instability in miscible two-component Bose-Einstein condensates*, Phys. Rev. A **84**, 041605 (2011).
- [64] C. Hamner, J. J. Chang, P. Engels, and M. A. Hoefer, *Generation of dark-bright soliton trains in superfluid-superfluid counterflow*, Phys. Rev. Lett. **106**, 065302 (2011).
- [65] S. De, D. L. Campbell, R. M. Price, A. Putra, B. M. Anderson, and I. B. Spielman, *Quenched binary Bose-Einstein condensates: Spin-domain formation and coarsening*, Phys. Rev. A **89**, 033631 (2014).
- [66] Y. Eto, M. Takahashi, K. Nabeta, R. Okada, M. Kunimi, H. Saito, and T. Hirano, *Bouncing motion and penetration dynamics in multicomponent Bose-Einstein condensates*, Phys. Rev. A **93**, 033615 (2016).
- [67] Y. Eto, M. Takahashi, M. Kunimi, H. Saito, and T. Hirano, *Nonequilibrium dynamics induced by miscible-immiscible transition in binary Bose-Einstein condensates*, New J. Phys. **18**, 073029 (2016).
- [68] E. Nicklas, M. Karl, M. Höfer, A. Johnson, W. Muessel, H. Strobel, J. Tomkovič, T. Gasenzer, and M. K. Oberthaler, *Observation of scaling in the dynamics of a strongly quenched quantum gas*, Phys. Rev. Lett. **115**, 245301 (2015).
- [69] P. K. Molony, P. D. Gregory, Z. Ji, B. Lu, M. P. Köppinger, C. R. Le Sueur, C. L. Blackley, J. M. Hutson, and S. L. Cornish, *Creation of ultracold $^{87}\text{Rb}^{133}\text{Cs}$*

- molecules in the rovibrational ground state*, Phys. Rev. Lett. **113**, 255301 (2014).
- [70] M. Guo, B. Zhu, B. Lu, X. Ye, F. Wang, R. Vexiau, N. Bouloufa-Maafa, G. Quéméner, O. Dulieu, and D. Wang, *Creation of an ultracold gas of ground-state dipolar $^{23}\text{Na}^{87}\text{Rb}$ molecules*, Phys. Rev. Lett. **116**, 205303 (2016).
- [71] S. A. Will, J. W. Park, Z. Z. Yan, H. Loh, and M. W. Zwierlein, *Coherent microwave control of ultracold $^{23}\text{Na}^{40}\text{K}$ molecules*, Phys. Rev. Lett. **116**, 225306 (2016).
- [72] P. Mason and A. Aftalion, *Classification of the ground states and topological defects in a rotating two-component Bose-Einstein condensate*, Phys. Rev. A **84**, 033611 (2011).
- [73] A. Aftalion, P. Mason, and J. Wei, *Vortex-peak interaction and lattice shape in rotating two-component Bose-Einstein condensates*, Phys. Rev. A **85**, 033614 (2012).
- [74] J. Hofmann, S. S. Natu, and S. Das Sarma, *Coarsening dynamics of binary Bose condensates*, Phys. Rev. Lett. **113**, 095702 (2014).
- [75] I.-K. Liu, R. W. Pattinson, T. P. Billam, S. A. Gardiner, S. L. Cornish, T.-M. Huang, W.-W. Lin, S.-C. Gou, N. G. Parker, and N. P. Proukakis, *Stochastic growth dynamics and composite defects in quenched immiscible binary condensates*, Phys. Rev. A **93**, 023628 (2016).
- [76] K. Kasamatsu and M. Tsubota, *Multiple domain formation induced by modulation instability in two-component Bose-Einstein condensates*, Phys. Rev. Lett. **93**, 100402 (2004).
- [77] H. Takeuchi, S. Ishino, and M. Tsubota, *Binary quantum turbulence arising from countersuperflow instability in two-component Bose-Einstein condensates*, Phys. Rev. Lett. **105**, 205301 (2010).

- [78] N. Suzuki, H. Takeuchi, K. Kasamatsu, M. Tsubota, and H. Saito, *Crossover between Kelvin-Helmholtz and counter-superflow instabilities in two-component Bose-Einstein condensates*, Phys. Rev. A **82**, 063604 (2010).
- [79] S. Chu, J. E. Bjorkholm, A. Ashkin, and A. Cable, *Experimental observation of optically trapped atoms*, Phys. Rev. Lett. **57**, 314 (1986).
- [80] A. Ashkin, *Optical trapping and manipulation of neutral particles using lasers*, Proc. Natl. Acad. Sci. **94**, 4853 (1997).
- [81] H. Metcalf and P. van der Straten, *Laser Cooling and Trapping* (Springer New York, 2001).
- [82] J. E. Bjorkholm, R. R. Freeman, A. Ashkin, and D. B. Pearson, *Observation of focusing of neutral atoms by the dipole forces of resonance-radiation pressure*, Phys. Rev. Lett. **41**, 1361 (1978).
- [83] R. Grimm, M. Weidemüller, and Y. B. Ovchinnikov, *Optical dipole traps for neutral atoms*, Adv. At. Mol. Opt. Phys. **42**, 95 (2000).
- [84] W. Alt, *Optical control of single neutral atoms*, Ph.D. thesis, University of Bonn, Germany (2004).
- [85] A. Corney, *Atomic and Laser Spectroscopy* (Clarendon, Oxford, 2006).
- [86] I. Bloch, *Ultracold quantum gases in optical lattices*, Nat. Phys. **1**, 23 (2005).
- [87] N. W. Ashcroft and N. D. Mermin, *Solid State Physics* (Holt, Rinehart and Winston, 1976).
- [88] C. Kittel, *Introduction to Solid State Physics* (Wiley, 2004).
- [89] D. Jaksch, *Bose-Einstein condensation and applications*, Ph.D. thesis, University of Innsbruck, Austria (1999).
- [90] N. F. Mott, *Metal-insulator transition*, Rev. Mod. Phys. **40**, 677 (1968).
- [91] S. L. Sondhi, S. M. Girvin, J. P. Carini, and D. Shahar, *Continuous quantum phase transitions*, Rev. Mod. Phys. **69**, 315 (1997).

- [92] D. Jaksch, *Optical lattices, ultracold atoms and quantum information processing*, Contemp. Phys. **45**, 367 (2004).
- [93] V. I. Yukalov, *Cold bosons in optical lattices*, Laser Phys. **19**, 1 (2009).
- [94] S. Sachdev, *Quantum Phase Transitions* (Cambridge University Press, New York, 2011).
- [95] T. McIntosh, P. Pisarski, R. J. Gooding, and E. Zaremba, *Multisite mean-field theory for cold bosonic atoms in optical lattices*, Phys. Rev. A **86**, 013623 (2012).
- [96] J. K. Freericks and H. Monien, *Strong-coupling expansions for the pure and disordered Bose-Hubbard model*, Phys. Rev. B **53**, 2691 (1996).
- [97] T. D. Kühner and H. Monien, *Phases of the one-dimensional Bose-Hubbard model*, Phys. Rev. B **58**, R14741 (1998).
- [98] B. Capogrosso-Sansone, N. V. Prokof'ev, and B. V. Svistunov, *Phase diagram and thermodynamics of the three-dimensional Bose-Hubbard model*, Phys. Rev. B **75**, 134302 (2007).
- [99] F. E. A. dos Santos and A. Pelster, *Quantum phase diagram of bosons in optical lattices*, Phys. Rev. A **79**, 013614 (2009).
- [100] W. Krauth, M. Caffarel, and J.-P. Bouchaud, *Gutzwiller wave function for a model of strongly interacting bosons*, Phys. Rev. B **45**, 3137 (1992).
- [101] K. Sheshadri, H. R. Krishnamurthy, R. Pandit, and T. V. Ramakrishnan, *Superfluid and insulating phases in an interacting-boson model: Mean-field theory and the RPA*, EPL **22**, 257 (1993).
- [102] L. Amico and V. Penna, *Time-dependent mean-field theory of the superfluid-insulator phase transition*, Phys. Rev. B **62**, 1224 (2000).
- [103] R. V. Pai, J. M. Kurdestany, K. Sheshadri, and R. Pandit, *Bose-Hubbard models in confining potentials: Inhomogeneous mean-field theory*, Phys. Rev. B **85**, 214524 (2012).

- [104] T.-L. Ho and V. B. Shenoy, *Binary mixtures of Bose condensates of alkali atoms*, Phys. Rev. Lett. **77**, 3276 (1996).
- [105] S. Ospelkaus, C. Ospelkaus, O. Wille, M. Succo, P. Ernst, K. Sengstock, and K. Bongs, *Localization of bosonic atoms by fermionic impurities in a three-dimensional optical lattice*, Phys. Rev. Lett. **96**, 180403 (2006).
- [106] K. Günter, T. Stöferle, H. Moritz, M. Köhl, and T. Esslinger, *Bose-Fermi mixtures in a three-dimensional optical lattice*, Phys. Rev. Lett. **96**, 180402 (2006).
- [107] T. Best, S. Will, U. Schneider, L. Hackermüller, D. van Oosten, I. Bloch, and D.-S. Lühmann, *Role of interactions in ^{87}Rb - ^{40}K Bose-Fermi mixtures in a 3D optical lattice*, Phys. Rev. Lett. **102**, 030408 (2009).
- [108] S. Sugawa, K. Inaba, S. Taie, R. Yamazaki, M. Yamashita, and Y. Takahashi, *Interaction and filling-induced quantum phases of dual Mott insulators of bosons and fermions*, Nat. Phys. **7**, 642 (2011).
- [109] J. Catani, L. De Sarlo, G. Barontini, F. Minardi, and M. Inguscio, *Degenerate Bose-Bose mixture in a three-dimensional optical lattice*, Phys. Rev. A **77**, 011603 (2008).
- [110] G. Thalhammer, G. Barontini, L. De Sarlo, J. Catani, F. Minardi, and M. Inguscio, *Double species Bose-Einstein condensate with tunable interspecies interactions*, Phys. Rev. Lett. **100**, 210402 (2008).
- [111] B. Gadway, D. Pertot, R. Reimann, and D. Schneble, *Superfluidity of interacting bosonic mixtures in optical lattices*, Phys. Rev. Lett. **105**, 045303 (2010).
- [112] S. Trotzky, P. Cheinet, S. Fölling, M. Feld, U. Schnorrberger, A. M. Rey, A. Polkovnikov, E. A. Demler, M. D. Lukin, and I. Bloch, *Time-resolved observation and control of superexchange interactions with ultracold atoms in optical lattices*, Science **319**, 295 (2008).
- [113] B. Gadway, D. Pertot, J. Reeves, M. Vogt, and D. Schneble, *Glassy behavior in a binary atomic mixture*, Phys. Rev. Lett. **107**, 145306 (2011).

- [114] P. Soltan-Panahi, D.-S. Luhmann, J. Struck, P. Windpassinger, and K. Sengstock, *Quantum phase transition to unconventional multi-orbital superfluidity in optical lattices*, Nat. Phys. **8**, 71 (2012).
- [115] B. Gadway, D. Pertot, J. Reeves, and D. Schneble, *Probing an ultracold-atom crystal with matter waves*, Nat. Phys. **8**, 544 (2012).
- [116] D. M. Weld, P. Medley, H. Miyake, D. Hucul, D. E. Pritchard, and W. Ketterle, *Spin gradient thermometry for ultracold atoms in optical lattices*, Phys. Rev. Lett. **103**, 245301 (2009).
- [117] P. Medley, D. M. Weld, H. Miyake, D. E. Pritchard, and W. Ketterle, *Spin gradient demagnetization cooling of ultracold atoms*, Phys. Rev. Lett. **106**, 195301 (2011).
- [118] L.-M. Duan, E. Demler, and M. D. Lukin, *Controlling spin exchange interactions of ultracold atoms in optical lattices*, Phys. Rev. Lett. **91**, 090402 (2003).
- [119] E. Altman, W. Hofstetter, E. Demler, and M. D. Lukin, *Phase diagram of two-component bosons on an optical lattice*, New J. Phys. **5**, 113 (2003).
- [120] W. Wang, V. Penna, and B. Capogrosso-Sansone, *Analysis and resolution of the ground-state degeneracy of the two-component Bose-Hubbard model*, Phys. Rev. E **90**, 022116 (2014).
- [121] A. B. Kuklov and B. V. Svistunov, *Counterflow superfluidity of two-species ultracold atoms in a commensurate optical lattice*, Phys. Rev. Lett. **90**, 100401 (2003).
- [122] U. Shrestha, *Antiferromagnetism in a bosonic mixture of rubidium (^{87}Rb) and potassium (^{41}K)*, Phys. Rev. A **82**, 041603 (2010).
- [123] M. Guglielmino, V. Penna, and B. Capogrosso-Sansone, *Ising antiferromagnet with ultracold bosonic mixtures confined in a harmonic trap*, Phys. Rev. A **84**, 031603 (2011).
- [124] L. Mathey, *Commensurate mixtures of ultracold atoms in one dimension*, Phys. Rev. B **75**, 144510 (2007).

- [125] A. Hu, L. Mathey, I. Danshita, E. Tiesinga, C. J. Williams, and C. W. Clark, *Counterflow and paired superfluidity in one-dimensional Bose mixtures in optical lattices*, Phys. Rev. A **80**, 023619 (2009).
- [126] C. Menotti and S. Stringari, *Detection of pair-superfluidity for bosonic mixtures in optical lattices*, Phys. Rev. A **81**, 045604 (2010).
- [127] A. Isacsson, M.-C. Cha, K. Sengupta, and S. M. Girvin, *Superfluid-insulator transitions of two-species bosons in an optical lattice*, Phys. Rev. B **72**, 184507 (2005).
- [128] M. Iskin, *Strong-coupling expansion for the two-species Bose-Hubbard model*, Phys. Rev. A **82**, 033630 (2010).
- [129] D. Benjamin and E. Demler, *Variational polaron method for Bose-Bose mixtures*, Phys. Rev. A **89**, 033615 (2014).
- [130] G.-H. Chen and Y.-S. Wu, *Quantum phase transition in a multicomponent Bose-Einstein condensate in optical lattices*, Phys. Rev. A **67**, 013606 (2003).
- [131] M. Guglielmino, V. Penna, and B. Capogrosso-Sansone, *Mott-insulator-to-superfluid transition in Bose-Bose mixtures in a two-dimensional lattice*, Phys. Rev. A **82**, 021601 (2010).
- [132] B. Paredes and J. I. Cirac, *From Cooper pairs to Luttinger liquids with bosonic atoms in optical lattices*, Phys. Rev. Lett. **90**, 150402 (2003).
- [133] L. He, Y. Li, E. Altman, and W. Hofstetter, *Quantum phases of Bose-Bose mixtures on a triangular lattice*, Phys. Rev. A **86**, 043620 (2012).
- [134] O. E. Alon, A. I. Streltsov, and L. S. Cederbaum, *Demixing of bosonic mixtures in optical lattices from macroscopic to microscopic scales*, Phys. Rev. Lett. **97**, 230403 (2006).
- [135] T. Mishra, R. V. Pai, and B. P. Das, *Phase separation in a two-species Bose mixture*, Phys. Rev. A **76**, 013604 (2007).

- [136] F. Zhan and I. P. McCulloch, *Comment on “Phase separation in a two-species Bose mixture”*, Phys. Rev. A **89**, 057601 (2014).
- [137] F. Lingua, M. Guglielmino, V. Penna, and B. Capogrosso Sansone, *Demixing effects in mixtures of two bosonic species*, Phys. Rev. A **92**, 053610 (2015).
- [138] E. Lundh and J.-P. Martikainen, *Kelvin-Helmholtz instability in two-component Bose gases on a lattice*, Phys. Rev. A **85**, 023628 (2012).
- [139] M. Greiner, I. Bloch, O. Mandel, T. W. Hänsch, and T. Esslinger, *Exploring phase coherence in a 2D lattice of Bose-Einstein condensates*, Phys. Rev. Lett. **87**, 160405 (2001).
- [140] T. Roscilde and J. I. Cirac, *Quantum emulsion: A glassy phase of bosonic mixtures in optical lattices*, Phys. Rev. Lett. **98**, 190402 (2007).
- [141] P. Buonsante, S. M. Giampaolo, F. Illuminati, V. Penna, and A. Vezzani, *Mixtures of strongly interacting bosons in optical lattices*, Phys. Rev. Lett. **100**, 240402 (2008).
- [142] S. Hooley and K. A. Benedict, *Dynamical instabilities in a two-component Bose-Einstein condensate in a one-dimensional optical lattice*, Phys. Rev. A **75**, 033621 (2007).
- [143] J. Ruostekoski and Z. Dutton, *Dynamical and energetic instabilities in multicomponent Bose-Einstein condensates in optical lattices*, Phys. Rev. A **76**, 063607 (2007).
- [144] P. N. Galteland, E. Babaev, and A. Sudb, *Thermal remixing of phase-separated states in two-component bosonic condensates*, New J. Phys. **17**, 103040 (2015).
- [145] W. Wang, V. Penna, and B. Capogrosso-Sansone, *Inter-species entanglement of Bose-Bose mixtures trapped in optical lattices*, New J. Phys. **18**, 063002 (2016).
- [146] H. Shim and T. Bergeman, *Phase coherence and fragmentation of two-component Bose-Einstein condensates loaded in state-dependent optical lattices*, Phys. Rev. A **94**, 043631 (2016).

- [147] G. Ceccarelli, J. Nespolo, A. Pelissetto, and E. Vicari, *Bose-Einstein condensation and critical behavior of two-component bosonic gases*, Phys. Rev. A **92**, 043613 (2015).
- [148] G. Ceccarelli, J. Nespolo, A. Pelissetto, and E. Vicari, *Phase diagram and multicritical behaviors of mixtures of three-dimensional bosonic gases*, Phys. Rev. A **93**, 033647 (2016).
- [149] S. Anufriiev and T. A. Zaleski, *Multicriticality and interaction-induced first-order phase transitions in mixtures of ultracold bosons in an optical lattice*, Phys. Rev. A **94**, 043613 (2016).
- [150] P. Öhberg and S. Stenholm, *Hartree-Fock treatment of the two-component Bose-Einstein condensate*, Phys. Rev. A **57**, 1272 (1998).
- [151] K. Nho and D. P. Landau, *Finite-temperature properties of binary mixtures of two Bose-Einstein condensates*, Phys. Rev. A **76**, 053610 (2007).
- [152] C.-H. Zhang and H. A. Fertig, *Collective excitations of a two-component Bose-Einstein condensate at finite temperature*, Phys. Rev. A **75**, 013601 (2007).
- [153] H. Shi, W.-M. Zheng, and S.-T. Chui, *Phase separation of Bose gases at finite temperature*, Phys. Rev. A **61**, 063613 (2000).
- [154] E. V. Goldstein and P. Meystre, *Quasiparticle instabilities in multicomponent atomic condensates*, Phys. Rev. A **55**, 2935 (1997).
- [155] H. Pu and N. P. Bigelow, *Collective excitations, metastability, and nonlinear response of a trapped two-species Bose-Einstein condensate*, Phys. Rev. Lett. **80**, 1134 (1998).
- [156] R. Graham and D. Walls, *Collective excitations of trapped binary mixtures of Bose-Einstein condensed gases*, Phys. Rev. A **57**, 484 (1998).
- [157] D. Gordon and C. M. Savage, *Excitation spectrum and instability of a two-species Bose-Einstein condensate*, Phys. Rev. A **58**, 1440 (1998).

- [158] B. D. Esry, *Impact of spontaneous spatial symmetry breaking on the critical atom number for two-component Bose-Einstein condensates*, Phys. Rev. A **58**, R3399 (1998).
- [159] B. D. Esry and C. H. Greene, *Spontaneous spatial symmetry breaking in two-component Bose-Einstein condensates*, Phys. Rev. A **59**, 1457 (1999).
- [160] J. G. Kim and E. K. Lee, *Characteristic features of symmetry breaking in two-component Bose-Einstein condensates*, Phys. Rev. E **65**, 066201 (2002).
- [161] A. A. Svidzinsky and S. T. Chui, *Symmetric-asymmetric transition in mixtures of Bose-Einstein condensates*, Phys. Rev. A **67**, 053608 (2003).
- [162] A. M. Rey, *Ultracold bosonic atoms in optical lattices*, Ph.D. thesis, University of Maryland, USA (2004).
- [163] D. Baillie and P. B. Blakie, *Finite-temperature theory of superfluid bosons in optical lattices*, Phys. Rev. A **80**, 033620 (2009).
- [164] D.-I. Choi and Q. Niu, *Bose-Einstein condensates in an optical lattice*, Phys. Rev. Lett. **82**, 2022 (1999).
- [165] J. C. Bronski, L. D. Carr, B. Deconinck, and J. N. Kutz, *Bose-Einstein condensates in standing waves: The cubic nonlinear Schrödinger equation with a periodic potential*, Phys. Rev. Lett. **86**, 1402 (2001).
- [166] N. H. Berry and J. N. Kutz, *Dynamics of Bose-Einstein condensates under the influence of periodic and harmonic potentials*, Phys. Rev. E **75**, 036214 (2007).
- [167] R. Zhang, R. E. Sapiro, R. R. Mhaskar, and G. Raithel, *Role of the mean field in Bloch oscillations of a Bose-Einstein condensate in an optical lattice and harmonic trap*, Phys. Rev. A **78**, 053607 (2008).
- [168] Z. X. Liang, X. Dong, Z. D. Zhang, and B. Wu, *Sound speed of a Bose-Einstein condensate in an optical lattice*, Phys. Rev. A **78**, 023622 (2008).

- [169] S.-L. Zhang, Z.-W. Zhou, and B. Wu, *Superfluidity and stability of a Bose-Einstein condensate with periodically modulated interatomic interaction*, Phys. Rev. A **87**, 013633 (2013).
- [170] A. J. Leggett, *Bose-Einstein condensation in the alkali gases: Some fundamental concepts*, Rev. Mod. Phys. **73**, 307 (2001).
- [171] S. Inouye, M. R. Andrews, J. Stenger, H.-J. Miesner, D. M. Stamper-Kurn, and W. Ketterle, *Observation of Feshbach resonances in a Bose-Einstein condensate*, Nature (London) **392**, 151 (1998).
- [172] A. Eleftheriou and K. Huang, *Instability of a Bose-Einstein condensate with an attractive interaction*, Phys. Rev. A **61**, 043601 (2000).
- [173] E. P. Gross, *Structure of a quantized vortex in boson systems*, Il Nuovo Cimento **20**, 454 (1961).
- [174] E. P. Gross, *Hydrodynamics of a superfluid condensate*, J. Math. Phys. **4**, 195 (1963).
- [175] L. P. Pitaevskii, *Vortex lines in an imperfect Bose gas*, J. Exptl. Theoret. Phys. **13**, 451 (1961).
- [176] N. N. Bogolyubov, *On the theory of superfluidity*, J. Phys. **11**, 23 (1947).
- [177] A. Fetter and J. Walecka, *Quantum Theory of Many-Particle Systems* (Dover Publications, 2012).
- [178] N. M. Hugenholtz and D. Pines, *Ground-state energy and excitation spectrum of a system of interacting bosons*, Phys. Rev. **116**, 489 (1959).
- [179] D. A. W. Hutchinson, E. Zaremba, and A. Griffin, *Finite temperature excitations of a trapped Bose gas*, Phys. Rev. Lett. **78**, 1842 (1997).
- [180] R. J. Dodd, M. Edwards, C. W. Clark, and K. Burnett, *Collective excitations of Bose-Einstein-condensed gases at finite temperatures*, Phys. Rev. A **57**, R32 (1998).

- [181] D. A. W. Hutchinson, K. Burnett, R. J. Dodd, S. A. Morgan, M. Rusch, E. Zaremba, N. P. Proukakis, M. Edwards, and C. W. Clark, *Gapless mean-field theory of Bose-Einstein condensates*, J. Phys. B **33**, 3825 (2000).
- [182] T. Stöferle, H. Moritz, C. Schori, M. Köhl, and T. Esslinger, *Transition from a strongly interacting 1D superfluid to a Mott insulator*, Phys. Rev. Lett. **92**, 130403 (2004).
- [183] M. L. Chiofalo, M. Polini, and M. P. Tosi, *Collective excitations of a periodic Bose condensate in the Wannier representation*, Eur. Phys. J. D **11**, 371 (2000).
- [184] A. Smerzi and A. Trombettoni, *Nonlinear tight-binding approximation for Bose-Einstein condensates in a lattice*, Phys. Rev. A **68**, 023613 (2003).
- [185] N. N. Bogoljubov, *On a new method in the theory of superconductivity*, Il Nuovo Cimento **7**, 794 (1958).
- [186] A. L. Fetter, *Nonuniform states of an imperfect Bose gas*, Ann. Phys. (N.Y.) **70**, 67 (1972).
- [187] A. Griffin, *Conserving and gapless approximations for an inhomogeneous Bose gas at finite temperatures*, Phys. Rev. B **53**, 9341 (1996).
- [188] V. N. Popov, J. Niederle, and L. Hlavatý, *Functional Integrals in Quantum Field Theory and Statistical Physics* (Springer Netherlands, 2001).
- [189] B. Damski, L. Santos, E. Tiemann, M. Lewenstein, S. Kotochigova, P. Julienne, and P. Zoller, *Creation of a dipolar superfluid in optical lattices*, Phys. Rev. Lett. **90**, 110401 (2003).
- [190] P. P. Hofer, C. Bruder, and V. M. Stojanović, *Superfluid drag of two-species Bose-Einstein condensates in optical lattices*, Phys. Rev. A **86**, 033627 (2012).
- [191] P. L. Christiansen, Y. B. Gaididei, K. Ø. Rasmussen, V. K. Mezentsev, and J. J. Rasmussen, *Dynamics in discrete two-dimensional nonlinear Schrödinger equations in the presence of point defects*, Phys. Rev. B **54**, 900 (1996).

- [192] E. Arévalo, *Soliton theory of two-dimensional lattices: The discrete nonlinear Schrödinger equation*, Phys. Rev. Lett. **102**, 224102 (2009).
- [193] M. D. Petrović, G. Gligorić, A. Maluckov, L. Hadžievski, and B. A. Malomed, *Interface solitons in locally linked two-dimensional lattices*, Phys. Rev. E **84**, 026602 (2011).
- [194] K. Suthar and D. Angom, *Optical-lattice-influenced geometry of quasi-two-dimensional binary condensates and quasiparticle spectra*, Phys. Rev. A **93**, 063608 (2016).
- [195] H. Stanley, *Introduction to Phase Transitions and Critical Phenomena* (Oxford University Press, 1971).
- [196] N. Turok and J. Zdrozny, *Dynamical generation of baryons at the electroweak transition*, Phys. Rev. Lett. **65**, 2331 (1990).
- [197] G. Aad *et al.*, *Observation of a new particle in the search for the Standard Model Higgs boson with the ATLAS detector at the LHC*, Phys. Lett. B **716**, 1 (2012).
- [198] S. Chatrchyan *et al.*, *Observation of a new boson at a mass of 125 GeV with the CMS experiment at the LHC*, Phys. Lett. B **716**, 30 (2012).
- [199] T. W. B. Kibble, *Topology of cosmic domains and strings*, J. Phys. A **9**, 1387 (1976).
- [200] I. Chuang, R. Durrer, N. Turok, and B. Yurke, *Cosmology in the laboratory: Defect dynamics in liquid crystals*, Science **251**, 1336 (1991).
- [201] W. H. Zurek, *Cosmological experiments in superfluid helium?* Nature (London) **317**, 505 (1985).
- [202] H. Saito, Y. Kawaguchi, and M. Ueda, *Symmetry breaking in scalar, spinor, and rotating Bose-Einstein condensates*, Nucl. Phys. A **790**, 737c (2007).
- [203] J. Javanainen and S. M. Yoo, *Quantum phase of a Bose-Einstein condensate with an arbitrary number of atoms*, Phys. Rev. Lett. **76**, 161 (1996).

- [204] J. I. Cirac, C. W. Gardiner, M. Naraschewski, and P. Zoller, *Continuous observation of interference fringes from Bose condensates*, Phys. Rev. A **54**, R3714 (1996).
- [205] Y. Nambu and G. Jona-Lasinio, *Dynamical model of elementary particles based on an analogy with superconductivity. I*, Phys. Rev. **122**, 345 (1961).
- [206] J. Goldstone, *Field theories with “superconductor” solutions*, Il Nuovo Cimento **19**, 154 (1961).
- [207] J. Goldstone, A. Salam, and S. Weinberg, *Broken symmetries*, Phys. Rev. **127**, 965 (1962).
- [208] S. Burger, F. S. Cataliotti, C. Fort, F. Minardi, M. Inguscio, M. L. Chiofalo, and M. P. Tosi, *Superfluid and dissipative dynamics of a Bose-Einstein condensate in a periodic optical potential*, Phys. Rev. Lett. **86**, 4447 (2001).
- [209] M. Krämer, C. Menotti, L. Pitaevskii, and S. Stringari, *Bose-Einstein condensates in 1D optical lattices*, Eur. Phys. J. D **27**, 247 (2003).
- [210] F. S. Cataliotti, S. Burger, C. Fort, P. Maddaloni, F. Minardi, A. Trombettoni, A. Smerzi, and M. Inguscio, *Josephson junction arrays with Bose-Einstein condensates*, Science **293**, 843 (2001).
- [211] H. B. Nielsen and S. Chadha, *On how to count Goldstone bosons*, Nucl. Phys. B **105**, 445 (1976).
- [212] I. Low and A. V. Manohar, *Spontaneously broken spacetime symmetries and Goldstone’s theorem*, Phys. Rev. Lett. **88**, 101602 (2002).
- [213] Y. Nambu, *Spontaneous breaking of Lie and current algebras*, J. Stat. Phys. **115**, 7 (2004).
- [214] H. Watanabe and T. Brauner, *Number of Nambu-Goldstone bosons and its relation to charge densities*, Phys. Rev. D **84**, 125013 (2011).
- [215] H. Watanabe and H. Murayama, *Unified description of Nambu-Goldstone bosons without Lorentz invariance*, Phys. Rev. Lett. **108**, 251602 (2012).

- [216] Y. Hidaka, *Counting rule for Nambu-Goldstone modes in nonrelativistic systems*, Phys. Rev. Lett. **110**, 091601 (2013).
- [217] D. A. Takahashi and M. Nitta, *Counting rule of Nambu-Goldstone modes for internal and spacetime symmetries: Bogoliubov theory approach*, Ann. Phys. **354**, 101 (2015).
- [218] H. Takeuchi and K. Kasamatsu, *Nambu-Goldstone modes in segregated Bose-Einstein condensates*, Phys. Rev. A **88**, 043612 (2013).
- [219] A. Roy, *Finite temperature effects in the condensates of dilute atomic gases*, Ph.D. thesis, Indian Institute of Technology, Gandhinagar (2015).
- [220] Ph. Courteille, R. S. Freeland, D. J. Heinzen, F. A. van Abeelen, and B. J. Verhaar, *Observation of a Feshbach resonance in cold atom scattering*, Phys. Rev. Lett. **81**, 69 (1998).
- [221] J. L. Roberts, N. R. Claussen, J. P. Burke, Jr., C. H. Greene, E. A. Cornell, and C. E. Wieman, *Resonant magnetic field control of elastic scattering in cold ^{85}Rb* , Phys. Rev. Lett. **81**, 5109 (1998).
- [222] K. Pilch, A. D. Lange, A. Prantner, G. Kerner, F. Ferlaino, H.-C. Nägerl, and R. Grimm, *Observation of interspecies Feshbach resonances in an ultracold Rb-Cs mixture*, Phys. Rev. A **79**, 042718 (2009).
- [223] F. Riboli and M. Modugno, *Topology of the ground state of two interacting Bose-Einstein condensates*, Phys. Rev. A **65**, 063614 (2002).
- [224] C. Ticknor, *Excitations of a trapped two-component Bose-Einstein condensate*, Phys. Rev. A **88**, 013623 (2013).
- [225] C. Ticknor, *Dispersion relation and excitation character of a two-component Bose-Einstein condensate*, Phys. Rev. A **89**, 053601 (2014).
- [226] K. L. Lee, N. B. Jørgensen, I.-K. Liu, L. Wacker, J. J. Arlt, and N. P. Proukakis, *Phase separation and dynamics of two-component Bose-Einstein condensates*, Phys. Rev. A **94**, 013602 (2016).

- [227] F. Zhan, J. Sabbatini, M. J. Davis, and I. P. McCulloch, *Miscible-immiscible quantum phase transition in coupled two-component Bose-Einstein condensates in one-dimensional optical lattices*, Phys. Rev. A **90**, 023630 (2014).
- [228] E. H. Lieb and W. Liniger, *Exact analysis of an interacting Bose gas. I. The general solution and the ground state*, Phys. Rev. **130**, 1605 (1963).
- [229] A. Görlitz, J. M. Vogels, A. E. Leanhardt, C. Raman, T. L. Gustavson, J. R. Abo-Shaeer, A. P. Chikkatur, S. Gupta, S. Inouye, T. Rosenband, and W. Ketterle, *Realization of Bose-Einstein condensates in lower dimensions*, Phys. Rev. Lett. **87**, 130402 (2001).
- [230] D. S. Petrov, D. M. Gangardt, and G. V. Shlyapnikov, *Low-dimensional trapped gases*, J. Phys. IV France **116**, 5 (2004).
- [231] P. C. Hohenberg and P. C. Martin, *Microscopic theory of superfluid helium*, Ann. Phys. **34**, 291 (1965).
- [232] N. D. Mermin and H. Wagner, *Absence of ferromagnetism or antiferromagnetism in one- or two-dimensional isotropic Heisenberg models*, Phys. Rev. Lett. **17**, 1133 (1966).
- [233] P. C. Hohenberg, *Existence of long-range order in one and two dimensions*, Phys. Rev. **158**, 383 (1967).
- [234] V. Bagnato and D. Kleppner, *Bose-Einstein condensation in low-dimensional traps*, Phys. Rev. A **44**, 7439 (1991).
- [235] W. Kohn, *Cyclotron resonance and de Haas-van Alphen oscillations of an interacting electron gas*, Phys. Rev. **123**, 1242 (1961).
- [236] J. F. Dobson, *Harmonic-potential theorem: Implications for approximate many-body theories*, Phys. Rev. Lett. **73**, 2244 (1994).
- [237] H. Al-Jibbouri and A. Pelster, *Breakdown of the Kohn theorem near a Feshbach resonance in a magnetic trap*, Phys. Rev. A **88**, 033621 (2013).

- [238] A. Roy, S. Gautam, and D. Angom, *Goldstone modes and bifurcations in phase-separated binary condensates at finite temperature*, Phys. Rev. A **89**, 013617 (2014).
- [239] L. Salasnich, A. Parola, and L. Reatto, *Bose condensate in a double-well trap: Ground state and elementary excitations*, Phys. Rev. A **60**, 4171 (1999).
- [240] L. Wen, W. M. Liu, Y. Cai, J. M. Zhang, and J. Hu, *Controlling phase separation of a two-component Bose-Einstein condensate by confinement*, Phys. Rev. A **85**, 043602 (2012).
- [241] Y. Japha and Y. B. Band, *Ground state and excitations of a Bose gas: From a harmonic trap to a double well*, Phys. Rev. A **84**, 033630 (2011).
- [242] R. S. MacKay and J. D. Meiss, *Hamiltonian Dynamical Systems* (Taylor & Francis, 1987).
- [243] K. Sasaki, N. Suzuki, and H. Saito, *Dynamics of bubbles in a two-component Bose-Einstein condensate*, Phys. Rev. A **83**, 033602 (2011).
- [244] R. Blaauwgeers, V. B. Eltsov, G. Eska, A. P. Finne, R. P. Haley, M. Krusius, J. J. Ruohio, L. Skrbek, and G. E. Volovik, *Shear flow and Kelvin-Helmholtz instability in superfluids*, Phys. Rev. Lett. **89**, 155301 (2002).
- [245] H. Saito, Y. Kawaguchi, and M. Ueda, *Ferrofluidity in a two-component dipolar Bose-Einstein condensate*, Phys. Rev. Lett. **102**, 230403 (2009).
- [246] A. Bezett, V. Bychkov, E. Lundh, D. Kobayakov, and M. Marklund, *Magnetic Richtmyer-Meshkov instability in a two-component Bose-Einstein condensate*, Phys. Rev. A **82**, 043608 (2010).
- [247] H. Takeuchi, N. Suzuki, K. Kasamatsu, H. Saito, and M. Tsubota, *Quantum Kelvin-Helmholtz instability in phase-separated two-component Bose-Einstein condensates*, Phys. Rev. B **81**, 094517 (2010).
- [248] F. Tsitoura, V. Achilleos, B. A. Malomed, D. Yan, P. G. Kevrekidis, and D. J. Frantzeskakis, *Matter-wave solitons in the counterflow of two immiscible superfluids*, Phys. Rev. A **87**, 063624 (2013).

- [249] D. Kobayakov, A. Bezett, E. Lundh, M. Marklund, and V. Bychkov, *Turbulence in binary Bose-Einstein condensates generated by highly nonlinear Rayleigh-Taylor and Kelvin-Helmholtz instabilities*, Phys. Rev. A **89**, 013631 (2014).
- [250] S. Gautam and D. Angom, *Rayleigh-Taylor instability in binary condensates*, Phys. Rev. A **81**, 053616 (2010).
- [251] T. Kadokura, T. Aioi, K. Sasaki, T. Kishimoto, and H. Saito, *Rayleigh-Taylor instability in a two-component Bose-Einstein condensate with rotational symmetry*, Phys. Rev. A **85**, 013602 (2012).
- [252] D. Kobayakov, V. Bychkov, E. Lundh, A. Bezett, V. Akkerman, and M. Marklund, *Interface dynamics of a two-component Bose-Einstein condensate driven by an external force*, Phys. Rev. A **83**, 043623 (2011).
- [253] D. Kobayakov, A. Bezett, E. Lundh, M. Marklund, and V. Bychkov, *Quantum swapping of immiscible Bose-Einstein condensates as an alternative to the Rayleigh-Taylor instability*, Phys. Rev. A **85**, 013630 (2012).
- [254] D. Kobayakov, V. Bychkov, E. Lundh, A. Bezett, and M. Marklund, *Parametric resonance of capillary waves at the interface between two immiscible Bose-Einstein condensates*, Phys. Rev. A **86**, 023614 (2012).
- [255] S. Weinberg, *Approximate symmetries and pseudo-Goldstone bosons*, Phys. Rev. Lett. **29**, 1698 (1972).
- [256] S. Uchino, M. Kobayashi, M. Nitta, and M. Ueda, *Quasi-Nambu-Goldstone modes in Bose-Einstein condensates*, Phys. Rev. Lett. **105**, 230406 (2010).
- [257] N. T. Phuc, Y. Kawaguchi, and M. Ueda, *Quantum mass acquisition in spinor Bose-Einstein condensates*, Phys. Rev. Lett. **113**, 230401 (2014).
- [258] B. Liu and J. Hu, *Quantum fluctuation-driven first-order phase transitions in optical lattices*, Phys. Rev. A **92**, 013606 (2015).
- [259] D. S. Petrov, *Quantum mechanical stabilization of a collapsing Bose-Bose mixture*, Phys. Rev. Lett. **115**, 155302 (2015).

- [260] I. Ferrier-Barbut, H. Kadau, M. Schmitt, M. Wenzel, and T. Pfau, *Observation of quantum droplets in a strongly dipolar Bose gas*, Phys. Rev. Lett. **116**, 215301 (2016).
- [261] D. Jaksch, C. Bruder, J. I. Cirac, C. W. Gardiner, and P. Zoller, *Cold bosonic atoms in optical lattices*, Phys. Rev. Lett. **81**, 3108 (1998).
- [262] M. Köhl, H. Moritz, T. Stöferle, K. Günter, and T. Esslinger, *Fermionic atoms in a three dimensional optical lattice: Observing Fermi surfaces, dynamics, and interactions*, Phys. Rev. Lett. **94**, 080403 (2005).
- [263] W. Hofstadter, J. I. Cirac, P. Zoller, E. Demler, and M. D. Lukin, *High-temperature superfluidity of fermionic atoms in optical lattices*, Phys. Rev. Lett. **89**, 220407 (2002).
- [264] J. Dalibard, F. Gerbier, G. Juzeliūnas, and P. Öhberg, *Colloquium : Artificial gauge potentials for neutral atoms*, Rev. Mod. Phys. **83**, 1523 (2011).
- [265] M. Ben Dahan, E. Peik, J. Reichel, Y. Castin, and C. Salomon, *Bloch oscillations of atoms in an optical potential*, Phys. Rev. Lett. **76**, 4508 (1996).
- [266] K. Berg-Sørensen and K. Mølmer, *Bose-Einstein condensates in spatially periodic potentials*, Phys. Rev. A **58**, 1480 (1998).
- [267] B. Wu and Q. Niu, *Nonlinear Landau-Zener tunneling*, Phys. Rev. A **61**, 023402 (2000).
- [268] J. Liu, L. Fu, B.-Y. Ou, S.-G. Chen, D.-I. Choi, B. Wu, and Q. Niu, *Theory of nonlinear Landau-Zener tunneling*, Phys. Rev. A **66**, 023404 (2002).
- [269] V. V. Konotop, P. G. Kevrekidis, and M. Salerno, *Landau-Zener tunneling of Bose-Einstein condensates in an optical lattice*, Phys. Rev. A **72**, 023611 (2005).
- [270] M. Krämer, L. Pitaevskii, and S. Stringari, *Macroscopic dynamics of a trapped Bose-Einstein condensate in the presence of 1D and 2D optical lattices*, Phys. Rev. Lett. **88**, 180404 (2002).

- [271] C. Fort, F. S. Cataliotti, L. Fallani, F. Ferlaino, P. Maddaloni, and M. Inguscio, *Collective excitations of a trapped Bose-Einstein condensate in the presence of a 1D optical lattice*, Phys. Rev. Lett. **90**, 140405 (2003).
- [272] B. D. Esry, C. H. Greene, J. P. Burke, Jr., and J. L. Bohn, *Hartree-Fock theory for double condensates*, Phys. Rev. Lett. **78**, 3594 (1997).
- [273] L. Landau, *Theory of the superfluidity of helium II*, Phys. Rev. **60**, 356 (1941).
- [274] T. Frisch, Y. Pomeau, and S. Rica, *Transition to dissipation in a model of superflow*, Phys. Rev. Lett. **69**, 1644 (1992).
- [275] C. Raman, M. Köhl, R. Onofrio, D. S. Durfee, C. E. Kuklewicz, Z. Hadzibabic, and W. Ketterle, *Evidence for a critical velocity in a Bose-Einstein condensed gas*, Phys. Rev. Lett. **83**, 2502 (1999).
- [276] D. M. Stamper-Kurn, A. P. Chikkatur, A. Görlitz, S. Inouye, S. Gupta, D. E. Pritchard, and W. Ketterle, *Excitation of phonons in a Bose-Einstein condensate by light scattering*, Phys. Rev. Lett. **83**, 2876 (1999).
- [277] J. Steinhauer, R. Ozeri, N. Katz, and N. Davidson, *Excitation spectrum of a Bose-Einstein condensate*, Phys. Rev. Lett. **88**, 120407 (2002).
- [278] X. Du, S. Wan, E. Yesilada, C. Ryu, D. J. Heinzen, Z. Liang, and B. Wu, *Bragg spectroscopy of a superfluid Bose-Hubbard gas*, New J. Phys. **12**, 083025 (2010).
- [279] P. T. Ernst, S. Götze, J. S. Krauser, K. Pyka, D.-S. Lühmann, D. Pfannkuche, and K. Sengstock, *Probing superfluids in optical lattices by momentum-resolved Bragg spectroscopy*, Nat. Phys. **6**, 56 (2010).
- [280] R. M. Wilson, S. Ronen, and J. L. Bohn, *Critical superfluid velocity in a trapped dipolar gas*, Phys. Rev. Lett. **104**, 094501 (2010).
- [281] C. Ticknor, R. M. Wilson, and J. L. Bohn, *Anisotropic superfluidity in a dipolar Bose gas*, Phys. Rev. Lett. **106**, 065301 (2011).

- [282] R. N. Bisset and P. B. Blakie, *Fingerprinting rotons in a dipolar condensate: Super-poissonian peak in the atom-number fluctuations*, Phys. Rev. Lett. **110**, 265302 (2013).
- [283] P. B. Blakie, D. Baillie, and R. N. Bisset, *Depletion and fluctuations of a trapped dipolar Bose-Einstein condensate in the roton regime*, Phys. Rev. A **88**, 013638 (2013).
- [284] S. L. Cornish, N. R. Claussen, J. L. Roberts, E. A. Cornell, and C. E. Wieman, *Stable ^{85}Rb Bose-Einstein condensates with widely tunable interactions*, Phys. Rev. Lett. **85**, 1795 (2000).
- [285] C. Orzel, A. K. Tuchman, M. L. Fenselau, M. Yasuda, and M. A. Kasevich, *Squeezed states in a Bose-Einstein condensate*, Science **291**, 2386 (2001).
- [286] I. Bloch, J. Dalibard, and S. Nascimbene, *Quantum simulations with ultracold quantum gases*, Nat. Phys. **8**, 267 (2012).
- [287] T.-L. Ho and V. B. Shenoy, *Binary mixtures of Bose condensates of alkali atoms*, Phys. Rev. Lett. **77**, 3276 (1996).
- [288] E. Timmermans, *Phase separation of Bose-Einstein condensates*, Phys. Rev. Lett. **81**, 5718 (1998).
- [289] G. V. Chester, *Statistical mechanics of mixtures of isotopes*, Phys. Rev. **100**, 446 (1955).
- [290] M. D. Miller, *Theory of boson mixtures*, Phys. Rev. B **18**, 4730 (1978).
- [291] P. Öhberg, *Two-component condensates: The role of temperature*, Phys. Rev. A **61**, 013601 (1999).
- [292] A. Roy and D. Angom, *Thermal suppression of phase separation in condensate mixtures*, Phys. Rev. A **92**, 011601 (2015).
- [293] F. Lingua, B. Capogrosso Sansone, F. Minardi, and V. Penna, *Thermometry of cold atoms in optical lattices via demixing*, arXiv:1609.08352 (2016).

- [294] N. P. Proukakis, *Spatial correlation functions of one-dimensional Bose gases at equilibrium*, Phys. Rev. A **74**, 053617 (2006).
- [295] S. Dettmer, D. Hellweg, P. Ryytty, J. J. Arlt, W. Ertmer, K. Sengstock, D. S. Petrov, G. V. Shlyapnikov, H. Kreutzmann, L. Santos, and M. Lewenstein, *Observation of phase fluctuations in elongated Bose-Einstein condensates*, Phys. Rev. Lett. **87**, 160406 (2001).
- [296] D. Hellweg, L. Cacciapuoti, M. Kottke, T. Schulte, K. Sengstock, W. Ertmer, and J. J. Arlt, *Measurement of the spatial correlation function of phase fluctuating Bose-Einstein condensates*, Phys. Rev. Lett. **91**, 010406 (2003).
- [297] S. Richard, F. Gerbier, J. H. Thywissen, M. Hugbart, P. Bouyer, and A. Aspect, *Momentum spectroscopy of 1D phase fluctuations in Bose-Einstein condensates*, Phys. Rev. Lett. **91**, 010405 (2003).
- [298] J. Esteve, J.-B. Trebbia, T. Schumm, A. Aspect, C. I. Westbrook, and I. Bouchoule, *Observations of density fluctuations in an elongated Bose gas: Ideal gas and quasicondensate regimes*, Phys. Rev. Lett. **96**, 130403 (2006).
- [299] T. Plisson, B. Allard, M. Holzmann, G. Salomon, A. Aspect, P. Bouyer, and T. Bourdel, *Coherence properties of a two-dimensional trapped Bose gas around the superfluid transition*, Phys. Rev. A **84**, 061606 (2011).
- [300] E. A. Burt, R. W. Ghrist, C. J. Myatt, M. J. Holland, E. A. Cornell, and C. E. Wieman, *Coherence, correlations, and collisions: What one learns about Bose-Einstein condensates from their decay*, Phys. Rev. Lett. **79**, 337 (1997).
- [301] B. L. Tolra, K. M. O'Hara, J. H. Huckans, W. D. Phillips, S. L. Rolston, and J. V. Porto, *Observation of reduced three-body recombination in a correlated 1D degenerate Bose gas*, Phys. Rev. Lett. **92**, 190401 (2004).
- [302] P. Cladé, C. Ryu, A. Ramanathan, K. Helmerson, and W. D. Phillips, *Observation of a 2D Bose gas: From thermal to quasicondensate to superfluid*, Phys. Rev. Lett. **102**, 170401 (2009).

- [303] S. Tung, G. Lamporesi, D. Lobser, L. Xia, and E. A. Cornell, *Observation of the presuperfluid regime in a two-dimensional Bose gas*, Phys. Rev. Lett. **105**, 230408 (2010).
- [304] R. J. Glauber, *Coherent and incoherent states of the radiation field*, Phys. Rev. **131**, 2766 (1963).
- [305] M. Naraschewski and R. J. Glauber, *Spatial coherence and density correlations of trapped Bose gases*, Phys. Rev. A **59**, 4595 (1999).
- [306] A. Bezett, E. Toth, and P. B. Blakie, *Two-point correlations of a trapped interacting Bose gas at finite temperature*, Phys. Rev. A **77**, 023602 (2008).
- [307] A. Bezett and E. Lundh, *Temporal correlations of elongated Bose gases at finite temperature*, J. Phys. B **45**, 205301 (2012).
- [308] K. Suthar, A. Roy, and D. Angom, *Fluctuation-driven topological transition of binary condensates in optical lattices*, Phys. Rev. A **91**, 043615 (2015).
- [309] K. Suthar and D. Angom, *Thermal fluctuations-enhanced miscibility of binary condensates in optical lattices*, arXiv:1608.04629 (2016).
- [310] C. Gies and D. A. W. Hutchinson, *Coherence properties of the two-dimensional Bose-Einstein condensate*, Phys. Rev. A **70**, 043606 (2004).
- [311] E. Anderson, Z. Bai, C. Bischof, S. Blackford, J. Demmel, J. Dongarra, J. D. Croz, A. Greenbaum, S. Hammarling, A. McKenney, and D. Sorensen, *LAPACK Users' Guide* (Society for Industrial and Applied Mathematics, Philadelphia, PA, 1999), 3rd ed.
- [312] T. P. Simula, S. M. M. Virtanen, and M. M. Salomaa, *Quantized circulation in dilute Bose-Einstein condensates*, Comp. Phys. Comm. **142**, 396 (2001).
- [313] M. Frigo and S. G. Johnson, *The design and implementation of FFTW3*, Proceedings of the IEEE **93**, 216 (2005). Special issue on "Program Generation, Optimization, and Platform Adaptation".

List of Publications

Publications in Journals

1. **K. Suthar**, Arko Roy, and D. Angom
Acoustic radiation from vortex-barrier interaction in atomic Bose-Einstein condensate,
J. Phys. B **47**, 135301 (2014). 9pp, arXiv:1312.7811.
2. **K. Suthar**, Arko Roy, and D. Angom
Fluctuation-driven topological transition of binary condensates in optical lattices,
Phys. Rev. A **91**, 043615 (2015). 9pp, arXiv:1412.0405.
3. **K. Suthar** and D. Angom
Optical-lattice-influenced geometry of quasi-two-dimensional binary condensates and quasiparticle spectra,
Phys. Rev. A **93**, 063608 (2016). 9pp, arXiv:1603.02455.
4. **K. Suthar** and D. Angom
Characteristic temperature for the immiscible-miscible transition of binary condensates in optical lattices,
Phys. Rev. A **95**, 043602 (2017). 9pp, arXiv:1608.04629.

Conference Paper

1. S. Gautam, **K. Suthar**, and D. Angom
Vortex reconnections between coreless vortices in binary condensates,
AIP Conf. Proc. **1582**, 46 (2014). 9pp, arXiv:1408.1573.

Publications attached with thesis

1. **K. Suthar**, Arko Roy, and D. Angom

Fluctuation-driven topological transition of binary condensates in optical lattices,

Phys. Rev. A **91**, 043615 (2015).

doi: [10.1103/PhysRevA.91.043615](https://doi.org/10.1103/PhysRevA.91.043615)

2. **K. Suthar** and D. Angom

Optical-lattice-influenced geometry of quasi-two-dimensional binary condensates and quasiparticle spectra,

Phys. Rev. A **93**, 063608 (2016).

doi: [10.1103/PhysRevA.93.063608](https://doi.org/10.1103/PhysRevA.93.063608)

3. **K. Suthar** and D. Angom

Characteristic temperature for the immiscible-miscible transition of binary condensates in optical lattices,

Phys. Rev. A **95**, 043602 (2017).

doi: [10.1103/PhysRevA.95.043602](https://doi.org/10.1103/PhysRevA.95.043602)

Fluctuation-driven topological transition of binary condensates in optical latticesK. Suthar,^{1,2} Arko Roy,^{1,2} and D. Angom¹¹*Physical Research Laboratory, Navrangpura, Ahmedabad-380009, Gujarat, India*²*Indian Institute of Technology, Gandhinagar, Ahmedabad-382424, Gujarat, India*

(Received 29 December 2014; published 13 April 2015)

We show the emergence of a third Goldstone mode in binary condensates at phase separation in quasi-one-dimensional (quasi-1D) optical lattices. We develop the coupled discrete nonlinear Schrödinger equations using Hartree-Fock-Bogoliubov theory with the Popov approximation in the Bose-Hubbard model to investigate the mode evolution at zero temperature, in particular, as the system is driven from the miscible to the immiscible phase. We demonstrate that the position exchange of the species in the ^{87}Rb - ^{85}Rb system is accompanied by a discontinuity in the excitation spectrum. Our results show that, in quasi-1D optical lattices, the presence of the fluctuations dramatically changes the geometry of the ground-state density profile of two-component Bose-Einstein condensates.

DOI: [10.1103/PhysRevA.91.043615](https://doi.org/10.1103/PhysRevA.91.043615)

PACS number(s): 67.85.Bc, 42.50.Lc, 67.85.Fg, 67.85.Hj

I. INTRODUCTION

Ultracold dilute atomic Bose gases in low dimensions have been the subject of growing interest over the last few decades. These are an ideal platform to probe many-body phenomena where quantum fluctuations play a crucial role [1,2]. In particular, optical lattices serve as an excellent and versatile tool for studying the physics of strongly correlated systems and other phenomena in condensed matter physics [3,4]. A variety of experimental techniques have been used to load and manipulate Bose-Einstein condensates (BECs) in optical lattices [5–8]. These have helped to explore quantum phase transitions [9], in particular the superfluid (SF)–Mott insulator (MI) transition [10–13]. The characteristics of the SF phase, such as coherence [14,15], collective modes [16], and transport [17,18] have also been studied. The center-of-mass dipole oscillation of a BEC in a cigar-shaped lattice potential has been experimentally studied in detail [19]. In such systems, a decrease in the Kohn mode frequency has been reported in Ref. [20] which has been justified in Ref. [21] as an increase of the effective mass due to the lattice potential. On the theoretical front, the low-lying collective excitations of a trapped Bose gas in a periodic lattice potential have been studied in Refs. [22–25] using the Bose-Hubbard (BH) model [26].

The two-component BECs (TBECs), on the other hand, exhibit a unique property that they can be phase separated [27]. There have been numerous experimental and theoretical investigations of binary mixtures of BECs over the last few years. Experimentally, it is possible to vary the interactions through the Feshbach resonance [28,29], and drive the binary mixture from the miscible to the immiscible phase or vice versa. Among the various lines of investigation, the theoretical studies of the stationary states [30], dynamical instabilities [31,32], and the collective excitations [33,34] of TBECs are noteworthy. Furthermore, in optical lattices TBECs have also been observed in recent experiments [35,36]. Theoretical studies of TBECs in optical lattices [37–40] and, in particular, phase separation [41–43] and dynamical instabilities [44] have also been carried out. Despite all these theoretical and experimental advances, the study of collective excitations of

TBECs in optical lattices is yet to be explored. This is the research gap addressed in the present work.

In this paper, we report the development of coupled discrete nonlinear Schrödinger equations (DNLSEs) of TBECs in optical lattices under the Hartree-Fock-Bogoliubov (HFB)–Popov approximation [45]. We use this theory to study the ground-state density profiles and the quasiparticle spectrum of ^{87}Rb - ^{85}Rb and ^{133}Cs - ^{87}Rb TBECs at zero temperature. We focus, in particular, on the evolution of the quasiparticle as the TBEC is driven from the miscible to the immiscible phase. This is possible by tuning either the intra- or interspecies interaction strengths. The two systems considered correspond to these possibilities. The fluctuation- and interaction-induced effects on the collective excitation spectra and topological change in the density profiles are the major findings of our present study. It deserves to be mentioned here that for systems without a lattice potential, at equilibrium, recent works have shown the existence of additional Goldstone modes in TBECs at phase separation [46] and complex eigenenergies due to quantum fluctuations [47].

The paper is organized as follows. Section II describes the tight-binding approximation for a trapped BEC in a one-dimensional (1D) lattice potential. In Sec. III we present the HFB-Popov theory to determine the quasiparticle energies and mode functions of single-component BECs and TBECs at finite temperature. The results of our studies are presented in Sec. IV. Finally, we highlight the key results of our work in Sec. V.

II. QUASI-1D OPTICAL LATTICE

We consider a Bose-Einstein condensate, held within a highly anisotropic cigar-shaped harmonic potential with trapping frequencies $\omega_x = \omega_y = \omega_\perp \gg \omega_z$. In this case we can integrate out the condensate wave function along the x and y directions and reduce it to a quasi-1D condensate. In the mean-field approximation, the grand-canonical Hamiltonian, in the second-quantized form, of the bosonic atoms in an external potential plus lattice is

given by

$$\begin{aligned} \hat{H} = & \int dz \hat{\Psi}^\dagger(z) \left(-\frac{\hbar^2}{2m} \frac{\partial^2}{\partial z^2} + V_{\text{latt}}(z) \right) \hat{\Psi}(z) \\ & + \int dz (V_{\text{ext}} - \mu) \hat{\Psi}^\dagger(z) \hat{\Psi}(z) \\ & + \frac{1}{2} \int dz dz' \hat{\Psi}^\dagger(z) \hat{\Psi}^\dagger(z') U(z-z') \hat{\Psi}(z) \hat{\Psi}(z'), \quad (1) \end{aligned}$$

where $\hat{\Psi}(z)$ and $\hat{\Psi}^\dagger(z)$ are the bosonic field operators which obey the Bose commutation relations, m is the atomic mass of the species, V_{latt} is the periodic lattice potential, V_{ext} is the external trapping potential, and μ is the chemical potential. Here, the interaction potential is given by $U(z-z') = U\delta(z-z')$, where $U = 2\sqrt{\lambda\kappa}\hbar^2 Na_s/m$, with N as the total number of atoms, and $\lambda = \omega_x/\omega_z$ and $\kappa = \omega_y/\omega_z$ are the anisotropy parameters along the x and y directions, respectively. Here a_s is the s -wave scattering length, which is repulsive ($a_s > 0$) in the present work. The net external potential is

$$V = V_{\text{ext}} + V_{\text{latt}} = \frac{1}{2} m \omega_z^2 z^2 + V_0 \sin^2(kz), \quad (2)$$

where $V_0 = sE_R$ is the optical lattice depth with s and E_R as the lattice depth scaling parameter and the recoil energy of the laser light photon, respectively. The wave number of the counterpropagating laser beams, which are used to create a periodic lattice potential, is $k = \pi/a$ with $a = \lambda_L/2$ the lattice spacing and λ_L the wavelength of the laser light. The energy barrier between adjacent lattice sites is expressed in units of the recoil energy $E_R = \hbar^2 k^2 / 2m$. In the tight-binding approximation, valid when $\mu \ll V_0$, the 1D field operator can be written as [48]

$$\hat{\Psi}(z) = \sum_j \hat{a}_j \phi_j(z), \quad (3)$$

where \hat{a}_j is the annihilation operator corresponding to the j th site, and the spatial part $\phi_j(z) = \phi(z - ja)$ is the orthonormal Gaussian orbital of the lowest vibrational band centered at the j th lattice site, with $\int dz \phi_{j\pm 1}^*(z) \phi_j(z) = 0$ and $\int dz |\phi_j(z)|^2 = 1$. By using the above ansatz in \hat{H} and considering only the nearest-neighbor tunneling we obtain the Bose-Hubbard Hamiltonian.

III. HFB-POPOV APPROXIMATION

A. Single-component BEC in optical lattices

The BH Hamiltonian describes the dynamics of 1D optical lattices when only the lowest band or the lowest vibrational level of the site is occupied. In this case the tight-binding approximation [49] is valid, and the BH Hamiltonian of the system is

$$\hat{H} = -J \sum_{\langle jj' \rangle} \hat{a}_j^\dagger \hat{a}_{j'} + \sum_j \left[(\epsilon_j - \mu) \hat{a}_j^\dagger \hat{a}_j + \frac{1}{2} U \hat{a}_j^\dagger \hat{a}_j^\dagger \hat{a}_j \hat{a}_j \right], \quad (4)$$

where the index j runs over the lattice sites, $\langle jj' \rangle$ represents the nearest-neighbor sum, and \hat{a}_j (\hat{a}_j^\dagger) is the bosonic annihilation (creation) operator of a bosonic atom at the j th lattice site. Here $J = -\int dz \phi_{j+1}^*(z) [-(\hbar^2/2m)(\partial^2/\partial z^2) + V_0 \sin^2(2\pi z/\lambda_L)] \phi_j(z)$ is the tunneling matrix element

between adjacent sites, $\epsilon_j = \int dz V_{\text{ext}}(z) |\phi_j(z)|^2$ is the energy offset of the j th lattice site, and $U = (2\sqrt{\lambda\kappa}\hbar^2 Na_s/m) \int dz |\phi_j(z)|^4$ is the on-site interaction strength of atoms occupying the j th lattice site. The offset energy can also be expressed as $\epsilon_j = j^2 \Omega$; here, $\Omega = m\omega_z^2 a^2 / 2$ is the energy cost of moving a boson from the central site to its nearest-neighbor site. To take into account the quantum fluctuations and thermal effects in the description of the system, we decompose the Bose field operator of each lattice site j in terms of a complex mean-field part c_j and a fluctuation operator $\hat{\phi}_j$, as $\hat{a}_j = (c_j + \hat{\phi}_j) e^{-i\mu t/\hbar}$. Using this field operator in the BH Hamiltonian, we get

$$\hat{H} = H_0 + \hat{H}_1 + \hat{H}_2 + \hat{H}_3 + \hat{H}_4, \quad (5)$$

with

$$H_0 = -J \sum_{\langle jj' \rangle} c_j^* c_{j'} + \sum_j \left[(\epsilon_j - \mu) |c_j|^2 + \frac{1}{2} U |c_j|^4 \right], \quad (6a)$$

$$\hat{H}_1 = -J \sum_{\langle jj' \rangle} \hat{\phi}_j c_{j'}^* + \sum_j (\epsilon_j - \mu + U |c_j|^2) c_j^* \hat{\phi}_j + \text{H.c.}, \quad (6b)$$

$$\begin{aligned} \hat{H}_2 = & -J \sum_{\langle jj' \rangle} \hat{\phi}_j^\dagger \hat{\phi}_{j'} + \sum_j (\epsilon_j - \mu) \hat{\phi}_j^\dagger \hat{\phi}_j \\ & + \frac{U}{2} \sum_j (\hat{\phi}_j^{\dagger 2} c_j^2 + \hat{\phi}_j^2 c_j^{*2} + 4|c_j|^2 \hat{\phi}_j^\dagger \hat{\phi}_j), \quad (6c) \end{aligned}$$

$$\hat{H}_3 = U \sum_j \hat{\phi}_j^\dagger \hat{\phi}_j^\dagger \hat{\phi}_j c_j + \text{H.c.}, \quad (6d)$$

$$\hat{H}_4 = \frac{U}{2} \sum_j \hat{\phi}_j^\dagger \hat{\phi}_j^\dagger \hat{\phi}_j \hat{\phi}_j, \quad (6e)$$

where the subscript of the various terms indicates the order of fluctuation operators and H.c. stands for the Hermitian conjugate. To study the system without quantum fluctuation at $T = 0$ K, we consider terms up to second order in $\hat{\phi}_j$ and neglect the higher-order terms (third and fourth order). The lowest-order term of the Hamiltonian describes the condensate part of the system. The minimization of H_0 with respect to the variation in the complex amplitude c_j^* gives the time-independent DNLS, which can be written as

$$\mu c_j = -J(c_{j-1} + c_{j+1}) + (\epsilon_j + U n_j^c) c_j, \quad (7)$$

with the condensate density $n_j^c = |c_j|^2$. The quadratic Hamiltonian \hat{H}_2 is the leading-order term which describes the noncondensate part, since the variation in \hat{H}_1 vanishes because c_j is a stationary solution of the DNLS. The minimization of \hat{H}_2 yields the governing equation for the noncondensate given by

$$\mu \hat{\phi}_j = -J(\hat{\phi}_{j-1} + \hat{\phi}_{j+1}) + (\epsilon_j + 2U n_j^c) \hat{\phi}_j + U c_j^2 \hat{\phi}_j^\dagger. \quad (8)$$

The quadratic Hamiltonian can be diagonalized using the Bogoliubov transformation

$$\hat{\phi}_j = \sum_l [u_j^l \hat{\alpha}_l e^{-i\omega_l t} - v_j^{*l} \hat{\alpha}_l^\dagger e^{i\omega_l t}], \quad (9a)$$

$$\hat{\phi}_j^\dagger = \sum_l [u_j^{*l} \hat{\alpha}_l^\dagger e^{i\omega_l t} - v_j^l \hat{\alpha}_l e^{-i\omega_l t}], \quad (9b)$$

where u_j^l and v_j^l are the quasiparticle amplitudes, $\omega_l = E_l/\hbar$ is the l th quasiparticle mode frequency with E_l as the mode energy, and $\hat{\alpha}_l$ ($\hat{\alpha}_l^\dagger$) are the quasiparticle annihilation (creation) operators, which satisfy the Bose commutation relations. The quasiparticle amplitudes satisfy the following normalization conditions:

$$\sum_j (u_j^{*l} u_j^{l'} - v_j^{*l} v_j^{l'}) = \delta_{ll'}, \quad (10a)$$

$$\sum_j (u_j^l v_j^{l'} - v_j^{*l} u_j^{*l'}) = 0. \quad (10b)$$

By using the definition of $\hat{\phi}_j$ from Eq. (9) in \hat{H}_2 [Eq. 6(c)] and the above conditions, we get the following Bogoliubov–de Gennes (BdG) equations

$$E_l u_j^l = -J(u_{j-1}^l + u_{j+1}^l) + [2Un_j^c + (\epsilon_j - \mu)]u_j^l - Uc_j^2 v_j^l, \quad (11a)$$

$$E_l v_j^l = J(v_{j-1}^l + v_{j+1}^l) - [2Un_j^c + (\epsilon_j - \mu)]v_j^l + Uc_j^{*2} u_j^l. \quad (11b)$$

This set of coupled equations describes the quasiparticles of the condensate in the optical lattice without considering the quantum fluctuations.

To investigate the effect of fluctuation and finite temperature we include the higher-order terms (\hat{H}_3 and \hat{H}_4) of the fluctuation operator in the Hamiltonian. We treat these terms in the self-consistent mean-field approximation [45] such that $\hat{\phi}_j^\dagger \hat{\phi}_j \hat{\phi}_j \approx 2\tilde{n}_j \hat{\phi}_j + \tilde{m}_j \hat{\phi}_j^\dagger$ and $\hat{\phi}_j^\dagger \hat{\phi}_j \hat{\phi}_j \hat{\phi}_j \approx 4\tilde{n}_j \hat{\phi}_j^\dagger \hat{\phi}_j + \tilde{m}_j \hat{\phi}_j^\dagger \hat{\phi}_j^\dagger + \tilde{m}_j^* \hat{\phi}_j \hat{\phi}_j - (2\tilde{n}_j^2 + |\tilde{m}_j|^2)$, where $\tilde{n}_j = \langle \hat{\phi}_j^\dagger \hat{\phi}_j \rangle$ and $\tilde{m}_j = \langle \hat{\phi}_j \hat{\phi}_j \rangle$ are the excited population (noncondensate) density and anomalous density at the j th site, respectively. In the HFB-Popov approximation, where the anomalous density is neglected, the corrections from higher-order terms yield the modified DNLS

$$\mu' c_j = -J(c_{j-1} + c_{j+1}) + [\epsilon_j + U(n_j^c + 2\tilde{n}_j)]c_j, \quad (12)$$

where μ' is the modified chemical potential. The total density is $n = \sum_j (n_j^c + \tilde{n}_j)$. The diagonalization of the modified Hamiltonian leads to the following HFB-Popov equations:

$$E_l u_j^l = -J(u_{j-1}^l + u_{j+1}^l) + [2U(n_j^c + \tilde{n}_j) + (\epsilon_j - \mu')]u_j^l - Uc_j^2 v_j^l, \quad (13a)$$

$$E_l v_j^l = J(v_{j-1}^l + v_{j+1}^l) - [2U(n_j^c + \tilde{n}_j) + (\epsilon_j - \mu')]v_j^l + Uc_j^{*2} u_j^l, \quad (13b)$$

with the noncondensate density at the j th lattice site given by

$$\tilde{n}_j = \sum_l [(|u_j^l|^2 + |v_j^l|^2)N_0(E_l) + |v_j^l|^2], \quad (14)$$

where $N_0(E_l) = \langle \hat{\alpha}_l^\dagger \hat{\alpha}_l \rangle = (e^{\beta E_l} - 1)^{-1}$ is the Bose-Einstein distribution function of the quasiparticle state with real and positive mode energy E_l . The coupled equations (12) and (13) are solved iteratively until the solutions converge to the desired accuracy. It is important to note that, at $T = 0$ K, $N_0(E_l)$ in the above equation vanishes. The noncondensate density, then, has a contribution from only the quantum fluctuations, which is given by

$$\tilde{n}_j = \sum_l |v_j^l|^2. \quad (15)$$

Therefore, we solve the equations self-consistently in the presence of the quantum fluctuations.

B. Two-component BEC in optical lattices

For a two-species condensate, the 1D second-quantized grand-canonical Hamiltonian is given by

$$\hat{H} = \sum_{i=1}^2 \int dz \hat{\Psi}_i^\dagger(z) \left[-\frac{\hbar^2}{2m_i} \frac{\partial^2}{\partial z^2} + V^i(z) - \mu_i + \frac{U_{ii}}{2} \hat{\Psi}_i^\dagger(z) \times \hat{\Psi}_i(z) \right] \hat{\Psi}_i(z) + U_{12} \int dz \hat{\Psi}_1^\dagger(z) \hat{\Psi}_2^\dagger(z) \hat{\Psi}_1(z) \hat{\Psi}_2(z), \quad (16)$$

where $i = 1, 2$ denotes the species index, the $\hat{\Psi}_i$'s are the annihilation field operators for the two different species, μ_i is the chemical potential of the i th species, U_{ii} are the intraspecies interaction parameters, and U_{12} is the interspecies interaction parameter with the m_i 's as the atomic masses of the species. Here, we consider repulsive interactions $U_{ii}, U_{12} > 0$. The external potential V^i is the sum of the harmonic and periodic optical lattice potentials. It is given by

$$V^i = V_{\text{ext}}^i + V_{\text{lat}}^i = \frac{1}{2} m_i \omega_{zi}^2 z_i^2 + V_0 \sin^2(2\pi z_i / \lambda_L). \quad (17)$$

In the present work, we consider the same external potential for both the species. The depth of the lattice potential is also the same for both species and is $V_0 = s E_R$ with $E_R = \hbar^2 k^2 / 2m_1$. If the lattice is deep enough, the tight-binding approximation is valid, and the bosons can be assumed to occupy the lowest vibrational band only. Under this approximation, the Bose field operator for the two species can be expanded as

$$\hat{\Psi}_i(z) = \sum_j \hat{a}_{ij} \phi_{ij}(z), \quad (18)$$

where the \hat{a}_{ij} 's are the annihilation operators and the $\phi_{ij}(z)$'s are the orthonormal Gaussian bases of the two species. It is worth mentioning here that the width of the basis function depends on the mass of the species and the natural frequency of the lattice potential. In the present case, the frequency plays a dominant role over the mass of the constituent species. Hence the widths of the Gaussian basis functions are taken to be identical for both species, even when m_1 and m_2 are widely different. The BH Hamiltonian for two species can be obtained by using the above ansatz in the Hamiltonian Eq. (16). We then obtain the many-body Hamiltonian governing the system of a

binary BEC in a quasi-1D optical lattice as

$$\begin{aligned} \hat{H} = & \sum_{i=1}^2 \left[- \sum_{(jj')} J_i \hat{a}_{ij}^\dagger \hat{a}_{ij'} + \sum_j (\epsilon_j^{(i)} - \mu_i) \hat{a}_{ij}^\dagger \hat{a}_{ij} \right] \\ & + \frac{1}{2} \sum_{i=1}^2 U_{ii} \sum_j \hat{a}_{ij}^\dagger \hat{a}_{ij}^\dagger \hat{a}_{ij} \hat{a}_{ij} + U_{12} \sum_j \hat{a}_{1j}^\dagger \hat{a}_{1j} \hat{a}_{2j}^\dagger \hat{a}_{2j}. \end{aligned} \quad (19)$$

Here J_i are the tunneling matrix elements, and $\epsilon_j^{(i)}$ is the offset energy of species i at the j th lattice site. In the mean-field approximation, using the Bogoliubov approximation as in a single-species condensate, we decompose the operators of both species as $\hat{a}_{1j} = (c_j + \hat{\phi}_{1j})e^{-i\mu_1 t/\hbar}$ and $\hat{a}_{2j} = (d_j + \hat{\phi}_{2j})e^{-i\mu_2 t/\hbar}$. We use these definitions in the BH Hamiltonian [Eq. (19)] and then decompose the Hamiltonian into different terms according to the order of the noncondensate operator they contain. The minimization of the lowest-order term gives the stationary-state equations or time-independent coupled DNLSes, and these are given by

$$\mu_1 c_j = -J_1(c_{j-1} + c_{j+1}) + [\epsilon_j^{(1)} + U_{11}n_{1j}^c + U_{12}n_{2j}^c]c_j, \quad (20a)$$

$$\mu_2 d_j = -J_2(d_{j-1} + d_{j+1}) + [\epsilon_j^{(2)} + U_{22}n_{2j}^c + U_{12}n_{1j}^c]d_j, \quad (20b)$$

where $n_{1j}^c = |c_j|^2$ and $n_{2j}^c = |d_j|^2$ are the condensate densities of the first and second species, respectively. The noncondensate part of the TBEC is obtained by the minimization of the quadratic Hamiltonian

$$\begin{aligned} \mu_1 \hat{\phi}_{1j} = & -J_1(\hat{\phi}_{1,j-1} + \hat{\phi}_{1,j+1}) + [\epsilon_j^{(1)} + 2U_{11}n_{1j}^c] \hat{\phi}_{1j} \\ & + U_{11}c_j^2 \hat{\phi}_{1j}^\dagger + U_{12}(n_{2j}^c \hat{\phi}_{1j} + d_j^* c_j \hat{\phi}_{2j} + d_j c_j \hat{\phi}_{2j}^\dagger), \end{aligned} \quad (21a)$$

$$\begin{aligned} \mu_2 \hat{\phi}_{2j} = & -J_2(\hat{\phi}_{2,j-1} + \hat{\phi}_{2,j+1}) + [\epsilon_j^{(2)} + 2U_{22}n_{2j}^c] \hat{\phi}_{2j} \\ & + U_{22}d_j^2 \hat{\phi}_{2j}^\dagger + U_{12}(n_{1j}^c \hat{\phi}_{2j} + c_j^* d_j \hat{\phi}_{1j} + c_j d_j \hat{\phi}_{1j}^\dagger). \end{aligned} \quad (21b)$$

The Bogoliubov transformation equations of the TBEC, which couple the positive- and negative-energy mode excitations, are

$$\hat{\phi}_{ij} = \sum_l [u_{ij}^l \hat{\alpha}_l e^{-i\omega_l t} - v_{ij}^{*l} \hat{\alpha}_l^\dagger e^{i\omega_l t}], \quad (22a)$$

$$\hat{\phi}_{ij}^\dagger = \sum_l [u_{ij}^{*l} \hat{\alpha}_l^\dagger e^{i\omega_l t} - v_{ij}^l \hat{\alpha}_l e^{-i\omega_l t}], \quad (22b)$$

where u_{ij}^l and v_{ij}^l are the quasiparticle amplitudes for the first ($i=1$) and second ($i=2$) species. The above transformation diagonalizes the quadratic Hamiltonian and gives the Bogoliubov–de Gennes equations at $T=0$ K for the two-component system. The inclusion of the higher-order terms of the perturbation or fluctuation in the quadratic Hamiltonian gives the HFB-Popov equations for the

two-component BEC,

$$\begin{aligned} E_l u_{1,j}^l = & -J_1(u_{1,j-1}^l + u_{1,j+1}^l) + \mathcal{U}_1 u_{1,j}^l - U_{11}c_j^2 v_{1,j}^l \\ & + U_{12}c_j(d_j^* u_{2,j}^l - d_j v_{2,j}^l), \end{aligned} \quad (23a)$$

$$\begin{aligned} E_l v_{1,j}^l = & J_1(v_{1,j-1}^l + v_{1,j+1}^l) + \mathcal{U}_1 v_{1,j}^l + U_{11}c_j^{*2} u_{1,j}^l \\ & - U_{12}c_j^*(d_j v_{2,j}^l - d_j^* u_{2,j}^l), \end{aligned} \quad (23b)$$

$$\begin{aligned} E_l u_{2,j}^l = & -J_2(u_{2,j-1}^l + u_{2,j+1}^l) + \mathcal{U}_2 u_{2,j}^l - U_{22}d_j^2 v_{2,j}^l \\ & + U_{12}d_j(c_j^* u_{1,j}^l - c_j v_{1,j}^l), \end{aligned} \quad (23c)$$

$$\begin{aligned} E_l v_{2,j}^l = & J_2(v_{2,j-1}^l + v_{2,j+1}^l) + \mathcal{U}_2 v_{2,j}^l + U_{22}d_j^{*2} u_{2,j}^l \\ & - U_{12}d_j^*(c_j v_{1,j}^l - c_j^* u_{1,j}^l), \end{aligned} \quad (23d)$$

where $\mathcal{U}_1 = 2U_{11}(n_{1j}^c + \tilde{n}_{1j}) + U_{12}(n_{2j}^c + \tilde{n}_{2j}) + (\epsilon_j^{(1)} - \mu_1)$ and $\mathcal{U}_2 = 2U_{22}(n_{2j}^c + \tilde{n}_{2j}) + U_{12}(n_{1j}^c + \tilde{n}_{1j}) + (\epsilon_j^{(2)} - \mu_2)$ with $\underline{\mathcal{U}}_i = -\mathcal{U}_i$. The density of the noncondensate atoms at the j th lattice site is

$$\tilde{n}_{ij} = \sum_l [(|u_{ij}^l|^2 + |v_{ij}^l|^2)N_0(E_l) + |v_{ij}^l|^2], \quad (24)$$

with $N_0(E_l)$ as the Bose factor of the system with energy E_l at temperature T . At $T=0$ K the noncondensate part reduces to the quantum fluctuations

$$\tilde{n}_{ij} = \sum_l |v_{ij}^l|^2. \quad (25)$$

If we neglect quantum fluctuations (the noncondensate part), the HFB-Popov equations (23) are the BdG equations for a binary BEC.

IV. RESULTS AND DISCUSSION

A. Numerical details

We solve the scaled coupled DNLSes using the fourth-order Runge-Kutta method to find the equilibrium state of harmonically trapped binary condensates in optical lattices. We start the calculations for $T=0$ K by ignoring the quantum fluctuations at each lattice site. The initial complex amplitudes of both species c_j and d_j are chosen as $1/\sqrt{N_{\text{latt}}}$, with N_{latt} as the total number of lattice sites. The advantage of this choice is that the amplitudes are normalized. We then use imaginary-time propagation of the DNLSes (20) to find the stationary ground-state wave function of the TBEC. In the tight-binding limit, the condensate wave function can be defined as the superposition of the basis functions as shown in Eq. (18). The basis function is chosen as the ground state, which is a Gaussian function, of the lowest-energy band [48]. The width of the function is a crucial parameter as it affects the overlap of the Gaussian orbitals at each lattice site. The correct estimation of the width is required in order to obtain orthonormal basis functions [50]. Furthermore, to study the excitation spectrum, we cast Eqs. (23) as a matrix eigenvalue equation. The matrix is $4N_{\text{latt}} \times 4N_{\text{latt}}$, non-Hermitian, nonsymmetric, and may have complex eigenvalues. To diagonalize the matrix and to find the quasiparticle energies E_l and amplitudes u_{ij}^l and v_{ij}^l , we use the routine ZGEEV from the LAPACK library [51]. In the later part of the work, when we include the effect of the

quantum fluctuations, we need to solve Eqs. (20) and (23) self-consistently. For this we iterate the solution until we reach the desired convergence in the number of condensate and noncondensate atoms. In this process, sometimes we encounter severe oscillations in the number of atoms. To damp these oscillations and accelerate convergence we employ a successive over- (under-) relaxation technique for updating the condensate (noncondensate) atom densities [52]. The new solutions after the iteration cycle (IC) are given by

$$c_{j,IC}^{\text{new}} = r^{\text{ov}} c_{j,IC} + (1 - r^{\text{ov}}) c_{j,IC-1}, \quad (26a)$$

$$\tilde{n}_{j,IC}^{\text{new}} = r^{\text{un}} \tilde{n}_{j,IC} + (1 - r^{\text{un}}) \tilde{n}_{j,IC-1}, \quad (26b)$$

where $r^{\text{ov}} > 1$ ($r^{\text{un}} < 1$) is the over- (under-) relaxation parameter. After the condensate and noncondensate densities converge, we compute low-lying mode energies and amplitudes u_{ij}^l and v_{ij}^l . During computation, we ensure that the eigenvalues of the HFB-Popov matrix are real as there are no topological defects present in the system.

B. Mode evolution of the trapped TBEC at $T = 0$ K

Under the HFB-Popov approximation, the excitation spectrum of the TBEC in an optical lattice is gapless for the SF phase, while it has a finite gap for the MI phase [10]. In the SF phase, spontaneous symmetry breaking at condensation results in two Goldstone modes, one each for the two species. The number of Goldstone modes, however, depends on whether the system is in the miscible or immiscible phase, and the geometry of the density distributions. To explore different possibilities, as mentioned earlier, we consider two different TBEC systems. These are binary mixtures which can be driven from the miscible to the immiscible phase through the variation of the intra- or interspecies interaction using the Feshbach resonance. In particular, we consider ^{87}Rb - ^{85}Rb [28,53] and ^{133}Cs - ^{87}Rb [54,55] binary condensates as examples of the two cases, and study the mode evolution as the system approaches the immiscible from the miscible regime.

1. Third Goldstone mode in the ^{87}Rb - ^{85}Rb TBEC

To examine the mode evolution with the tuning of the intraspecies interaction, we consider a quasi-1D TBEC consisting of ^{87}Rb and ^{85}Rb [28,53]. In this system, we consider ^{87}Rb and ^{85}Rb as the first and second species, respectively. The axial trapping frequency for both the species is $\omega_z = 2\pi \times 80$ Hz with 12.33 as the anisotropy parameter along the x and y directions. The laser wavelength used to create the optical lattice potential is $\lambda_L = 775$ nm. The numbers of atoms are $N_1 = N_2 = 100$, confined in 100 lattice sites superimposed on a harmonic potential. We choose the depth of the lattice potential $V_0 = 5E_R$ and set the tunneling matrix elements for the two species as $J_1 = 0.66E_R$ and $J_2 = 0.71E_R$, the intraspecies interaction U_{11} as $0.05E_R$, and the interspecies interaction U_{12} as $0.1E_R$. This set of DNLS parameters is calculated by considering the width of the Gaussian beam as $0.3a$. Since the scattering length of ^{85}Rb is tunable with the Feshbach resonance [28], we study the excitation spectrum with variation in U_{22} . The evolution of the Kohn mode functions with the variation of U_{22} is shown in Fig. 1. For

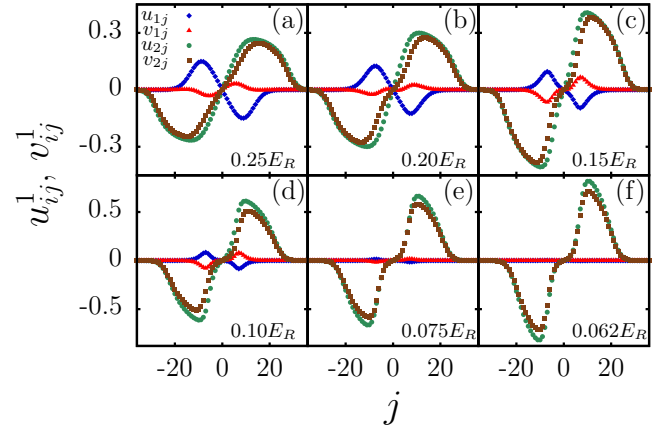


FIG. 1. (Color online) The evolution of the quasiparticle amplitudes corresponding to the ^{85}Rb Kohn mode as the intraspecies interaction of ^{85}Rb (U_{22}) is decreased from $0.25E_R$ to $0.062E_R$. (a),(b) When $U_{22} \geq 0.18E_R$, the system is in the miscible phase and the Kohn mode ($l = 1$) has contributions from both the species. (c)–(e) When the system is on the verge of phase separation, then the Kohn mode of ^{85}Rb goes soft. (f) At phase separation $U_{22} \leq 0.065E_R$ the Kohn mode transforms into a Goldstone mode.

$0.18 \leq U_{22} \leq 0.25E_R$, the system is in the miscible domain, and the Kohn mode is a linear combination of the ^{87}Rb and ^{85}Rb Kohn modes. As we approach phase separation by reducing the value of U_{22} , we observe a decrease in the Kohn mode amplitude of ^{87}Rb component and the mode function of ^{85}Rb becomes soft at $0.062E_R$. The softening of the mode is evident from the evolution of the mode energies as shown in Fig. 2(a). The figure shows that the mode continues as the third Goldstone mode for $U_{22} \leq 0.062E_R$. The emergence of the third Goldstone mode is associated with a change in the geometry of the system; the density changes from the overlapping to a sandwich profile as shown in Figs. 3(a)–3(c). Thus, as discussed in our earlier work [46], the binary condensate is separated into three distinct subcomponents.

2. Third Goldstone mode in the ^{133}Cs - ^{87}Rb TBEC

For mode evolution with tuning of the interspecies interaction, we consider the binary system of Cs-Rb [54,55]. Here, we consider ^{133}Cs and ^{87}Rb as the first and second species, respectively. To study the mode evolution as the system undergoes the transition from the miscible to the immiscible phase, the interspecies interaction U_{12} is varied, which is possible using the magnetic Feshbach resonance [56]. The parameters of the system considered are $N_1 = N_2 = 100$ with similar trapping frequencies as in the case of the ^{87}Rb - ^{85}Rb mixture. The lattice parameters are chosen as $J_1 = 0.92E_R$, $J_2 = 1.95E_R$, $U_{11} = 0.40E_R$, and $U_{22} = 0.21E_R$. At $U_{12} = 0$, the two condensates are uncoupled and have two Goldstone modes, one corresponding to each of the two species. At low values of U_{12} , in the miscible regime, the condensate density profiles of the two species overlap as shown in Fig. 3(d). As we increase U_{12} , the Kohn mode of ^{87}Rb gradually goes soft and at a critical value $U_{12}^c = 0.3E_R$ it is transformed into the third Goldstone mode. For $U_{12}^c < U_{12}$, the geometry of the condensate density profile changes and acquires a sandwich

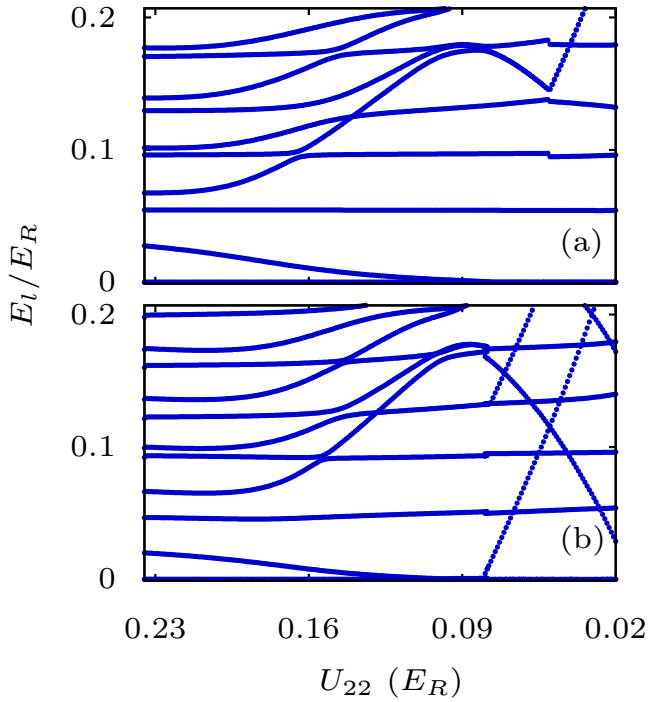


FIG. 2. (Color online) The evolution of the low-lying modes as a function of the intraspecies interaction of the ^{85}Rb (U_{22}) in the ^{87}Rb - ^{85}Rb TBEC held in quasi-1D optical lattices. Excitation spectrum (a) at zero temperature and (b) in the presence of quantum fluctuations. Here U_{22} is in units of the recoil energy E_R .

structure in which the Cs condensate (higher mass) is at the center and flanked by the Rb condensate (lower mass) at the edges as shown in Fig. 3(f). This is also evident from the evolu-

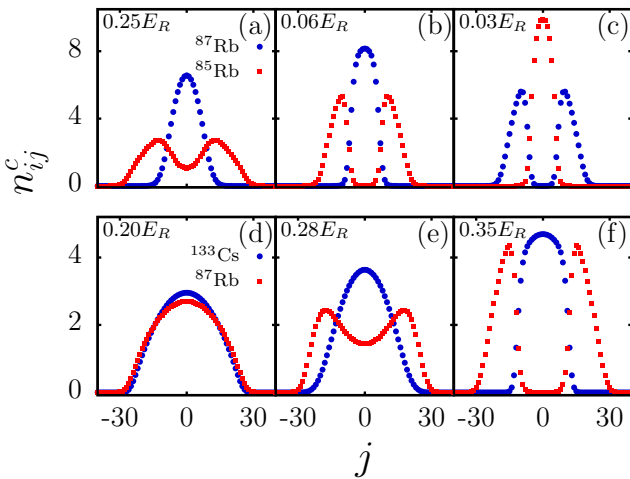


FIG. 3. (Color online) The geometry of the condensate density profiles and its transition from the miscible to the immiscible regime. (a)–(c) The transition from the miscible to the *sandwich* profile for the ^{87}Rb - ^{85}Rb TBEC with change in the intraspecies interaction U_{22} at $T = 0$ K. The position exchange (c) in the sandwich profile occurs at $U_{11} = U_{22} = 0.05E_R$. (d)–(f) show similar condensate density profiles for the Cs-Rb TBEC with change in the interspecies interaction U_{12} at $T = 0$ K. In this system the transition to the sandwich geometry occurs at $U_{12}^c = 0.3E_R$.

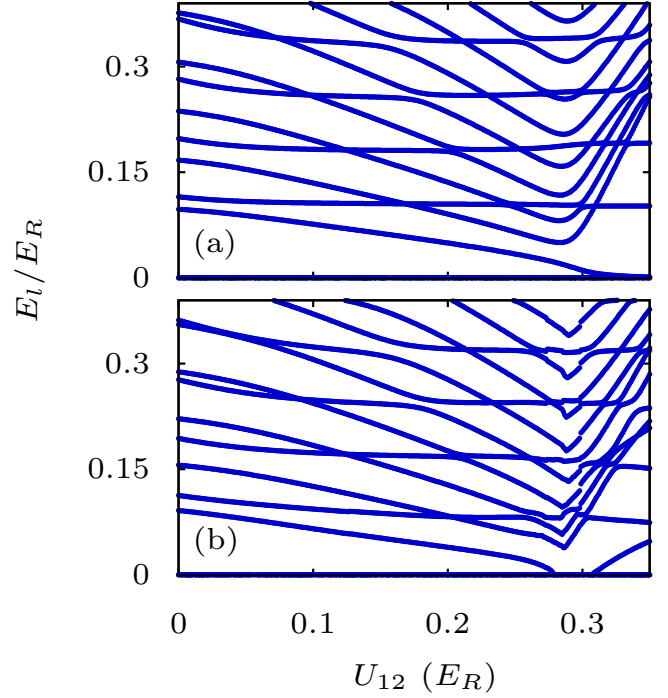


FIG. 4. (Color online) The evolution of the energies of the low-lying modes as a function of the interspecies interaction (U_{12}) in Cs-Rb TBEC held in a quasi-1D lattice potential. The excitation spectrum (a) at $T = 0$ K, and (b) after including the quantum fluctuations. Here U_{12} is in units of the recoil energy E_R .

tion of the low-lying modes, shown in Fig. 4(a), and is reflected in the structural evolution of the quasiparticle amplitudes in Fig. 5. Hence the system attains an extra Goldstone mode after transition from a miscible- to a sandwich-type profile.

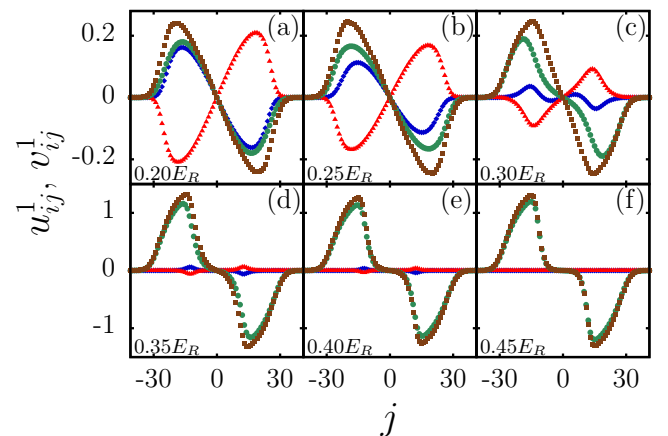


FIG. 5. (Color online) The evolution of the quasiparticle amplitudes corresponding to the Kohn mode as the interspecies interaction is increased from $0.2E_R$ to $0.35E_R$ for a Cs-Rb TBEC in a quasi-1D lattice potential at $T = 0$ K. (a)–(c) In the miscible regime, the Kohn mode has contributions from both species. (d)–(f) For $U_{12} > 0.3E_R$ the Kohn mode of ^{87}Rb goes soft, whereas that of ^{133}Cs decreases in amplitude.

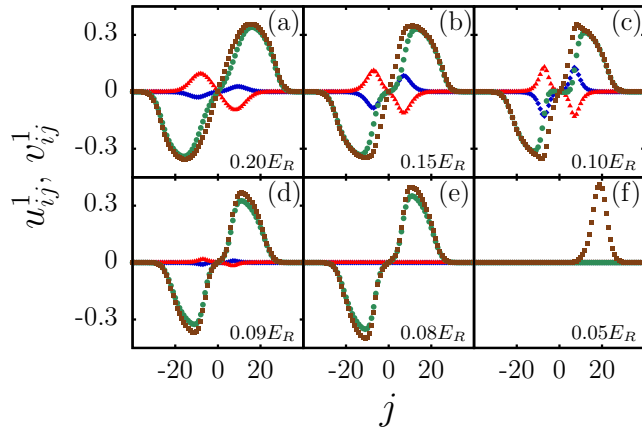


FIG. 6. (Color online) The evolution of the quasiparticle amplitudes corresponding to the Kohn mode for ^{87}Rb - ^{85}Rb TBEC in the presence of the fluctuations as the intraspecies interaction of ^{85}Rb (U_{22}) is decreased from $0.2E_R$ to $0.05E_R$. (a)–(e) The Kohn mode of ^{85}Rb goes soft, whereas that of ^{87}Rb decreases in amplitude and finally vanishes in (e). (f) The sloshing mode, which emerges after phase separation as the sandwich density profile transforms into a *side-by-side* profile.

3. Position exchange of species

A remarkable feature in the evolution of the condensate density profiles of an ^{87}Rb - ^{85}Rb TBEC with variation of U_{22} is the observation of position exchange in the immiscible domain. This is absent when the trapping potential consists of only a harmonic potential (continuous system), and is the result of the discrete symmetry associated with the optical lattice. As discussed earlier, in this system we fix U_{11} and U_{12} and vary U_{22} (the intraspecies interaction of ^{85}Rb). At higher values of U_{22} the TBEC is in the miscible phase, and as we decrease U_{22} , at the critical value $U_{22}^c = 0.17E_R$ the TBEC enters the immiscible domain. The geometry of the density profiles is of sandwich type and the component with smaller U_{ii} is at the center. An example of a condensate density profile in this domain, $U_{22} = 0.06E_R$, is shown in Fig. 3(b). In the figure, the species with smaller intraspecies interaction (^{87}Rb) is at the center and ^{85}Rb is at the edges. As U_{22} is further decreased, the system continues to be in the same phase. During evolution, an instability arises when both intraspecies interactions are the same ($U_{11} = U_{22} = 0.05$). At this value of U_{22} the components exchange their places in the trap. This is also reflected in the excitation spectrum; a discontinuity at $U_{22} = 0.05E_R$ in the plot of the mode evolution shown in Fig. 2(a) is a signature of the instability. On further decrease of U_{22} , we enter the $U_{22} < U_{11}$ domain and ^{85}Rb occupies the center of the trap. An example of the density profiles in this domain, $U_{22} = 0.03$, is shown in Fig. 3(c). The position exchange, however, does not occur in the Cs-Rb system as in that case we vary U_{12} .

C. Effect of quantum fluctuations

We compute the condensate profiles and modes for the ^{87}Rb - ^{85}Rb TBEC, including the effect of quantum fluctuations.

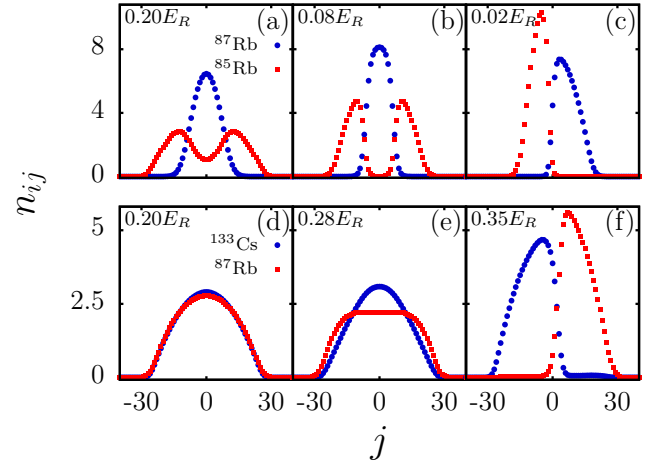


FIG. 7. (Color online) The fluctuation-induced transition in the geometry of the total density profile (condensate + quantum fluctuations) of a TBEC at $T = 0$ K in a quasi-1D lattice potential. (a)–(c) The transition in the ^{87}Rb - ^{85}Rb system from the miscible to the sandwich and finally to the side-by-side profile with change in the intraspecies interaction. (d), (e) The transition in the Cs-Rb TBEC from the miscible to the side-by-side profile with change in the interspecies interaction U_{12} . The geometry of the ground state of both systems in the immiscible regime is different from that at zero temperature in the absence of the fluctuations, Fig. 3.

We then encounter severe oscillations in the number of atoms during the iterations used to solve the DNLSEs and there is no convergence. To mitigate this, we use a successive under-relaxation technique with $r^{\text{un}} = 0.6$. For computations, we consider the same set of parameters as in the case of $T = 0$ K without fluctuations. The fluctuations break the spatial symmetry of the system as we vary the intraspecies interaction of ^{85}Rb (U_{22}). In the immiscible domain, the condensate density profile changes from the sandwich to the side-by-side profile at $0.078E_R$. The system acquires a new stable ground state as the chemical potential of the system decreases from $0.92E_R$ to $0.80E_R$. The evolution of the mode energies with U_{22} including the fluctuation is shown in Fig. 2(b). It is evident that at this value $U_{22} = 0.078E_R$, the ^{85}Rb Kohn mode goes soft and emerges as a sloshing mode. The transformations in the mode functions as U_{22} is decreased about this point are shown in Fig. 6. This topological phase transition is evident from the density profiles of the TBEC in the presence of quantum fluctuations as shown in Figs. 7(a)–7(c).

In the Cs-Rb system, due to quantum fluctuations, the Kohn mode of ^{87}Rb goes soft at a lower value of U_{12} compared to the value without fluctuations. This is evident in the mode evolution with quantum fluctuations as shown in Fig. 4(b). The discontinuity in the spectrum is the signature of the transition from the miscible to the immiscible regime. The soft Kohn mode gains energy and gets hard at $0.31E_R$. This mode hardening is due to the topological change in the ground-state density profile from the miscible to the side-by-side profile, shown in Figs. 7(d)–7(f). The lowest mode with nonzero excitation energy corresponding to the side-by-side profile is shown in Figs. 8(e) and 8(f).

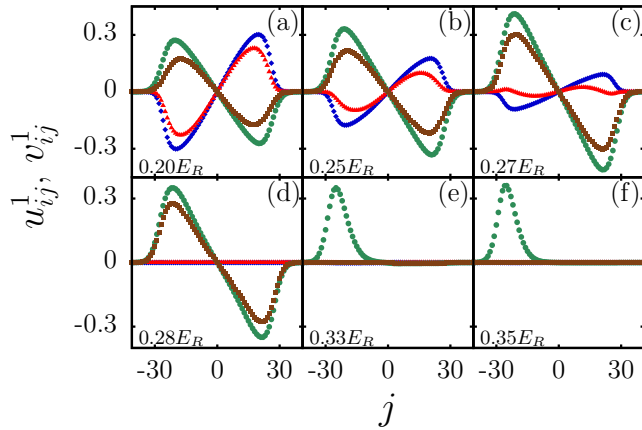


FIG. 8. (Color online) The evolution of the quasiparticle amplitude corresponding to the Kohn mode for the Cs-Rb TBEC in the presence of fluctuations. (a)–(d) The Kohn mode evolves as the interspecies interaction is increased. (e),(f) It is transformed into a sloshing mode as the TBEC acquires the side-by-side density profile after phase separation.

V. CONCLUSIONS

We have studied the ground-state density profiles and the excitation spectrum of TBECs in quasi-1D optical lattices. We observe that the system gains an additional Goldstone mode at

phase separation at zero temperature. Furthermore, in a TBEC where a miscible to immiscible transition is driven through variation of the intraspecies interaction (^{87}Rb - ^{85}Rb), a finite discontinuity in the excitation energy spectra is observed in the neighbourhood of equal intraspecies interaction strengths. In the presence of quantum fluctuations, on varying the intraspecies interaction of ^{85}Rb , in the immiscible regime, the ground-state density profiles transform from sandwich to side-by-side geometry. This is characterized by the hardening of the Kohn mode which emerges as a sloshing mode. The fluctuation-induced topological change from a completely miscible to a side-by-side ground-state density profile is also evident in a ^{133}Cs - ^{87}Rb mixture. Our current studies show that the geometry of the density profiles with and without quantum fluctuations is different. Since quantum fluctuations are present in experiments, it is crucial to include quantum fluctuations to obtain the correct density profiles of TBECs in optical lattices in the phase-separated domain.

ACKNOWLEDGMENTS

We thank S. Gautam and S. Chattopadhyay for useful discussions. The results presented in the paper are based on computations using the 3TFLOP HPC cluster at the Physical Research Laboratory, Ahmedabad, India. We also thank the anonymous referee for the thorough review and valuable comments, which contributed to improving the quality of the paper.

-
- [1] M. A. Cazalilla, R. Citro, T. Giamarchi, E. Orignac, and M. Rigol, *Rev. Mod. Phys.* **83**, 1405 (2011).
 - [2] E. H. Lieb and W. Liniger, *Phys. Rev.* **130**, 1605 (1963).
 - [3] O. Morsch and M. Oberthaler, *Rev. Mod. Phys.* **78**, 179 (2006).
 - [4] I. Bloch, J. Dalibard, and W. Zwerger, *Rev. Mod. Phys.* **80**, 885 (2008).
 - [5] S. Friebe, C. D’Andrea, J. Walz, M. Weitz, and T. W. Hänsch, *Phys. Rev. A* **57**, R20 (1998).
 - [6] L. Guidoni and P. Verkerk, *Phys. Rev. A* **57**, R1501 (1998).
 - [7] B. Paredes, A. Widera, V. Murg, O. Mandel, S. Fölling, I. Cirac, G. V. Shlyapnikov, T. W. Hänsch, and I. Bloch, *Nature (London)* **429**, 277 (2004).
 - [8] I. Bloch, *Nat. Phys.* **1**, 23 (2005).
 - [9] S. Sachdev, *Quantum Phase Transitions* (Cambridge University Press, New York, 2011).
 - [10] M. Greiner, O. Mandel, T. Esslinger, T. W. Hänsch, and I. Bloch, *Nature (London)* **415**, 39 (2002).
 - [11] H. Moritz, T. Stöferle, M. Köhl, and T. Esslinger, *Phys. Rev. Lett.* **91**, 250402 (2003).
 - [12] T. Stöferle, H. Moritz, C. Schori, M. Köhl, and T. Esslinger, *Phys. Rev. Lett.* **92**, 130403 (2004).
 - [13] B. Laburthe Tolra, K. M. O’Hara, J. H. Huckans, W. D. Phillips, S. L. Rolston, and J. V. Porto, *Phys. Rev. Lett.* **92**, 190401 (2004).
 - [14] C. Orzel, A. K. Tuchman, M. L. Fenselau, M. Yasuda, and M. A. Kasevich, *Science* **291**, 2386 (2001).
 - [15] M. Greiner, I. Bloch, O. Mandel, T. W. Hänsch, and T. Esslinger, *Phys. Rev. Lett.* **87**, 160405 (2001).
 - [16] C. Fort, F. S. Cataliotti, L. Fallani, F. Ferlaino, P. Maddaloni, and M. Inguscio, *Phys. Rev. Lett.* **90**, 140405 (2003).
 - [17] C. D. Fertig, K. M. O’Hara, J. H. Huckans, S. L. Rolston, W. D. Phillips, and J. V. Porto, *Phys. Rev. Lett.* **94**, 120403 (2005).
 - [18] L. Fallani, L. De Sarlo, J. E. Lye, M. Modugno, R. Saers, C. Fort, and M. Inguscio, *Phys. Rev. Lett.* **93**, 140406 (2004).
 - [19] S. Burger, F. S. Cataliotti, C. Fort, F. Minardi, M. Inguscio, M. L. Chiofalo, and M. P. Tosi, *Phys. Rev. Lett.* **86**, 4447 (2001).
 - [20] F. S. Cataliotti, S. Burger, C. Fort, P. Maddaloni, F. Minardi, A. Trombettoni, A. Smerzi, and M. Inguscio, *Science* **293**, 843 (2001).
 - [21] M. Krämer, C. Menotti, L. Pitaevskii, and S. Stringari, *Eur. Phys. J. D* **27**, 247 (2003).
 - [22] E. Lundh, *Phys. Rev. A* **70**, 033610 (2004).
 - [23] J.-P. Martikainen and H. T. C. Stoof, *Phys. Rev. A* **68**, 013610 (2003).
 - [24] A. M. Rey, G. Pupillo, C. W. Clark, and C. J. Williams, *Phys. Rev. A* **72**, 033616 (2005).
 - [25] A. M. Rey, Ultracold bosonic atoms in optical lattices, Ph.D. thesis, University of Maryland, 2004.
 - [26] M. P. A. Fisher, P. B. Weichman, G. Grinstein, and D. S. Fisher, *Phys. Rev. B* **40**, 546 (1989).
 - [27] R. Navarro, R. Carretero-González, and P. G. Kevrekidis, *Phys. Rev. A* **80**, 023613 (2009).
 - [28] S. B. Papp, J. M. Pino, and C. E. Wieman, *Phys. Rev. Lett.* **101**, 040402 (2008).
 - [29] S. Tojo, Y. Taguchi, Y. Masuyama, T. Hayashi, H. Saito, and T. Hirano, *Phys. Rev. A* **82**, 033609 (2010).

- [30] S. Gautam and D. Angom, *J. Phys. B* **44**, 025302 (2011).
- [31] S. Gautam and D. Angom, *Phys. Rev. A* **81**, 053616 (2010).
- [32] T. Kadokura, T. Aioi, K. Sasaki, T. Kishimoto, and H. Saito, *Phys. Rev. A* **85**, 013602 (2012).
- [33] C. Ticknor, *Phys. Rev. A* **88**, 013623 (2013).
- [34] D. Gordon and C. M. Savage, *Phys. Rev. A* **58**, 1440 (1998).
- [35] J. Catani, L. De Sarlo, G. Barontini, F. Minardi, and M. Inguscio, *Phys. Rev. A* **77**, 011603 (2008).
- [36] B. Gadway, D. Pertot, R. Reimann, and D. Schneble, *Phys. Rev. Lett.* **105**, 045303 (2010).
- [37] G.-H. Chen and Y.-S. Wu, *Phys. Rev. A* **67**, 013606 (2003).
- [38] A. B. Kuklov and B. V. Svistunov, *Phys. Rev. Lett.* **90**, 100401 (2003).
- [39] A. Kuklov, N. Prokof'ev, and B. Svistunov, *Phys. Rev. Lett.* **92**, 050402 (2004).
- [40] M.-C. Cha, *Int. J. Mod. Phys. B* **27**, 1362002 (2013).
- [41] F. Zhan and I. P. McCulloch, *Phys. Rev. A* **89**, 057601 (2014).
- [42] T. Mishra, R. V. Pai, and B. P. Das, *Phys. Rev. A* **76**, 013604 (2007).
- [43] Y.-C. Kuo and S.-F. Shieh, *J. Math. Anal. Appl.* **347**, 521 (2008).
- [44] J. Ruostekoski and Z. Dutton, *Phys. Rev. A* **76**, 063607 (2007).
- [45] A. Griffin, *Phys. Rev. B* **53**, 9341 (1996).
- [46] A. Roy, S. Gautam, and D. Angom, *Phys. Rev. A* **89**, 013617 (2014).
- [47] A. Roy and D. Angom, *Phys. Rev. A* **90**, 023612 (2014).
- [48] M. L. Chiofalo, M. Polini, and M. P. Tosi, *Eur. Phys. J. D* **11**, 371 (2000).
- [49] D. Jaksch, C. Bruder, J. I. Cirac, C. W. Gardiner, and P. Zoller, *Phys. Rev. Lett.* **81**, 3108 (1998).
- [50] G. Baym and C. J. Pethick, *Phys. Rev. Lett.* **76**, 6 (1996).
- [51] E. Anderson, Z. Bai, C. Bischof, S. Blackford, J. Demmel, J. Dongarra, J. D. Croz, A. Greenbaum, S. Hammarling, A. McKenney, and D. Sorensen, *LAPACK Users' Guide*, 3rd ed. (Society for Industrial and Applied Mathematics, Philadelphia, 1999).
- [52] T. P. Simula, S. M. M. Virtanen, and M. M. Salomaa, *Comput. Phys. Commun.* **142**, 396 (2001).
- [53] S. Händel, T. P. Wiles, A. L. Marchant, S. A. Hopkins, C. S. Adams, and S. L. Cornish, *Phys. Rev. A* **83**, 053633 (2011).
- [54] D. J. McCarron, H. W. Cho, D. L. Jenkin, M. P. Köppinger, and S. L. Cornish, *Phys. Rev. A* **84**, 011603 (2011).
- [55] A. Lercher, T. Takekoshi, M. Debatin, B. Schuster, R. Rameshan, F. Ferlaino, R. Grimm, and H.-C. Ngerl, *Eur. Phys. J. D* **65**, 3 (2011).
- [56] K. Pilch, A. D. Lange, A. Prantner, G. Kerner, F. Ferlaino, H.-C. Nägerl, and R. Grimm, *Phys. Rev. A* **79**, 042718 (2009).

Optical-lattice-influenced geometry of quasi-two-dimensional binary condensates and quasiparticle spectra

K. Suthar^{1,2} and D. Angom¹¹*Physical Research Laboratory, Navrangpura, Ahmedabad 380009, Gujarat, India*²*Indian Institute of Technology, Gandhinagar, Ahmedabad 382424, Gujarat, India*

(Received 15 March 2016; published 7 June 2016)

We explore the collective excitation of two-species Bose-Einstein condensates (TBECs) confined in quasi-two-dimensional optical lattices. For this we use a set of coupled discrete nonlinear Schrödinger equations to describe the system and we employ Hartree-Fock-Bogoliubov theory with the Popov approximation to analyze the quasiparticle spectra at zero temperature. The ground-state geometry, evolution of quasiparticle energies, structure of quasiparticle amplitudes, and dispersion relations are examined in detail. We observe that the TBEC acquires a side-by-side density profile when it is tuned from the miscible to the immiscible phase. In addition, the quasiparticle energies are softened as the system is tuned towards phase separation, but harden after phase separation and mode degeneracies are lifted. In terms of structure, in the miscible phase the quasiparticles have well-defined azimuthal quantum numbers, but that is not the case for the immiscible phase.

DOI: [10.1103/PhysRevA.93.063608](https://doi.org/10.1103/PhysRevA.93.063608)

I. INTRODUCTION

The experimental realization of ultracold atoms in optical lattices has opened up a plethora of new possibilities to study interacting quantum many-body systems. Optical lattices, filled with bosons [1,2] or fermions [3,4], provide unprecedented precision, tunability of interactions, and the possibility to generate different geometries and mimic the external gauge fields to study many-body systems [5]. These are near ideal systems to observe quantum phenomena such as superfluidity [6,7], quantum phase transitions [8,9], Bloch oscillations [10,11], Landau-Zener tunneling [12,13], and various kinds of instabilities [14,15]. In fact, the energy of collective excitations has emerged as a fundamental and versatile tool to investigate many-body physics. An example of the synergy between theory and experiment in this field is the study of the effect of tunneling and the mean-field interaction of trapped two-dimensional (2D) optical lattices on the collective excitation. Theoretically, Krämer *et al.* [16] studied it in detail and Fort *et al.* [17] verified the theoretical findings in experiments. A detailed understanding of the excitations of the superfluid phase in optical lattices is possible with controlled variation of the lattice potential; these excitations are excellent proxies to probe the properties of more complex condensed-matter counterparts. In this work we examine the quasiparticle spectrum of condensates with the tight-binding approximation and the condensate density is described through a set of coupled discrete nonlinear Schrödinger equations.

The introduction of a second species in the optical lattices, two-species Bose-Einstein condensates (TBECs) in lattices, creates a versatile model to probe diverse phenomena in physics. These are promising candidates to explain phenomena associated with fermionic correlations [18], phase separation [19], hydrodynamical instability [20], and novel phases [21,22]. One remarkable property of TBECs is the phase segregation, which occurs when the interspecies interaction is stronger than the geometric mean of the intraspecies interactions [23]. To date, TBECs in optical lattices have been experimentally realized in two different atomic species [24] and two different hyperfine states of the same

atomic species [25,26]. It must be emphasized that TBECs with harmonic potential only have been realized in two different species of alkali-metal atoms [27–30], in two different isotopes [31], and in two different hyperfine states [32–35]. These experiments have examined phase separation and other phenomena that are unique to binary BECs. The phenomenon of phase separation and transition from miscible to immiscible or vice versa has also been the subject of several theoretical studies [36–39]. These recent developments provide motivation to probe the rich physics associated with TBECs in optical lattices. In recent works we have investigated the fluctuation-induced instability of dark solitons in TBECs [40] and change in the topology of the TBECs in quasi-1D lattices [41]. However, to study the effects of fluctuations, either quantum or thermal, in optical lattices filled with TBECs it is essential to have a comprehensive understanding of the quasiparticle spectra.

In this paper we examine the evolution of the quasiparticle spectra of TBECs in quasi-2D optical lattices at zero temperature. For this we use the Hartree-Fock-Bogoliubov (HFB) formalism with the Popov approximation and tune one of the interatomic interactions to drive the TBEC from the miscible to the immiscible phase. In the immiscible domain, we show that the ground state has a side-by-side density profile. This is in contrast to the case of the quasi-1D system, where the ground state has a *sandwich* density profile. To identify the geometry of the ground state, we examine the quasiparticle spectra using Bogoliubov–de Gennes (BdG) analysis. For a stable ground-state configuration, the spectra are real, but complex for metastable states. Following BdG analysis, we further examine the dispersion relation of a binary system in optical lattices. This relation is used to understand the structure of the lower- and higher-energy excitations for miscible and immiscible domains of TBEC in lattice systems. The dispersion relations are important to understand the nature of the excitations [42–44] and Bragg spectroscopy [45] of ultracold quantum gases. These spectroscopic studies present full momentum-resolved measurements of the band structure and the associated interaction effects at several lattice depths [46]. In fact, these relations have proved

the presence of the rotonlike excitation in trapped dipolar BECs [47–50].

The paper is organized as follows. In Sec. II we describe the HFB-Popov formalism and the dispersion relations for TBECs confined in optical lattices. The quasiparticle mode evolution and characteristics of the quasiparticle excitations with dispersion curves are presented in Sec. III. Finally, we conclude with the key findings of the present work in Sec. IV.

II. THEORY AND METHODS

Consider TBECs of dilute atomic gases in an optical lattice with a harmonic-oscillator potential as a confining envelope potential. The net external potential is

$$\begin{aligned} V^k(\mathbf{r}) &= V_{\text{HO}}^k + V_{\text{latt}}^k \\ &= \frac{m_k}{2}(\omega_x^2 x^2 + \omega_y^2 y^2 + \omega_z^2 z^2) + V_0[\sin^2(2\pi x/\lambda_L) \\ &\quad + \sin^2(2\pi y/\lambda_L) + \sin^2(2\pi z/\lambda_L)], \end{aligned} \quad (1)$$

where $k = 1, 2$ denotes the species index, m_k is the atomic mass of the k th species, ω_i ($i = x, y, z$) are the frequencies of the harmonic potential along each direction, and $V_0 = sE_R$ is the depth of the lattice potential in terms of the recoil energy $E_R = \hbar^2 k_L^2 / 2m_1$ and dimensionless scale factor s . Here $k_L = 2\pi/\lambda_L$ is the wave number of the laser beam with wavelength λ_L used to generate the optical lattice and hence the lattice constant of the system is $a = \lambda_L/2$. It should be noted that we consider the same external potential for both condensates and at $T = 0$ K the grand canonical Hamiltonian of the system is

$$\begin{aligned} \hat{H} &= \sum_{k=1}^2 \int d\mathbf{r} \hat{\Psi}_k^\dagger(\mathbf{r}) \left[-\frac{\hbar^2 \nabla^2}{2m_k} + V^k(\mathbf{r}) - \mu_k \right. \\ &\quad \left. + \frac{U_{kk}}{2} \hat{\Psi}_k^\dagger(\mathbf{r}) \times \hat{\Psi}_k(\mathbf{r}) \right] \hat{\Psi}_k(\mathbf{r}) \\ &\quad + U_{12} \int d\mathbf{r} \hat{\Psi}_1^\dagger(\mathbf{r}) \hat{\Psi}_2^\dagger(\mathbf{r}) \hat{\Psi}_1(\mathbf{r}) \hat{\Psi}_2(\mathbf{r}), \end{aligned} \quad (2)$$

where $\hat{\Psi}_k$, μ_k , and U_{kk} are the bosonic field operator, chemical potential, and intraspecies interaction strength of k th species, respectively, and U_{12} is the interspecies interaction strength. In the present study we consider all the interactions to be repulsive, that is, $U_{kk}, U_{12} > 0$. If the lattice is deep, i.e., $V_0 \gg \mu_k$, the tight-binding approximation (TBA) is applicable and bosons occupy only the lowest-energy band. In this approximation, the condensate is well localized within each lattice site and the field operator for each of the species can be written as [51,52]

$$\hat{\Psi}_k(\mathbf{r}) = \sum_{\xi} \hat{a}_{k\xi} \phi_{k\xi}(\mathbf{r}), \quad (3)$$

where $\hat{a}_{k\xi}$ is the annihilation operator of the k th species at the lattice site with identification index ξ , which is a unique combination of the lattice index along the x , y , and z axes. The basic element of the TBA lies in the definition of $\phi_{k\xi}(\mathbf{r})$, which are orthonormalized on-site Gaussian wave functions localized at the ξ th lattice site. Using the above definition of $\hat{\Psi}_k(\mathbf{r})$ in Eq. (2), we get the Bose-Hubbard (BH) Hamiltonian of the system.

A. The HFB-Popov approximation for quasi-2D TBECs in optical lattices

To create a potential suitable to generate quasi-2D TBECs in optical lattices, set the frequencies to satisfy the condition $\omega_x = \omega_y = \omega_{\perp} \ll \omega_z$. The excitations along the tight or high-frequency z axis are of higher energy and we consider the condensate in the ground state along the z axis at low temperature $T \ll \hbar\omega_z/k_B$, with k_B the Boltzmann constant. Hence, the excitations of importance for quantum and thermal fluctuations are along the radial direction. In the TBA, the BH Hamiltonian that describes the system is [20,53]

$$\begin{aligned} \hat{H} &= \sum_{k=1}^2 \left[-J_k \sum_{\langle \xi \xi' \rangle} \hat{a}_{k\xi}^\dagger \hat{a}_{k\xi'} + \sum_{\xi} (\epsilon_{\xi}^{(k)} - \mu_k) \hat{a}_{k\xi}^\dagger \hat{a}_{k\xi} \right] \\ &\quad + \frac{1}{2} \sum_{k=1}^2 U_{kk} \sum_{\xi} \hat{a}_{k\xi}^\dagger \hat{a}_{k\xi}^\dagger \hat{a}_{k\xi} \hat{a}_{k\xi} + U_{12} \sum_{\xi} \hat{a}_{1\xi}^\dagger \hat{a}_{1\xi} \hat{a}_{2\xi}^\dagger \hat{a}_{2\xi}, \end{aligned} \quad (4)$$

where the index ξ covers all the lattice sites. The summation index $\langle \xi \xi' \rangle$ represents the nearest neighbor; for illustration take $\xi \equiv (i, j)$ with i and j as labels of a lattice site along the x and y axes, respectively. The possible values of ξ' in $\langle \xi \xi' \rangle$ are then $(i-1, j)$, $(i+1, j)$, $(i, j-1)$, and $(i, j+1)$. The operator $\hat{a}_{k\xi}$ ($\hat{a}_{k\xi}^\dagger$) is the bosonic annihilation (creation) operator of the k th species at the ξ th lattice site and the J_k are the tunneling matrix elements. The effect of the envelope harmonic trapping potentials is subsumed in the offset energy $\epsilon_{\xi}^{(k)} = \Omega(i^2 + j^2)$. Here $\Omega = m\omega_{\perp}^2 a^2/2$ is the strength of the harmonic confinement. For simplicity, we assume that the tunneling strengths of the two species are identical on both the x and y axes. For large tunneling strength and density $J_k \gg \nu U_{kk}, \nu U_{12}$, with ν the filling factor, the bosons remain in the superfluid phase. In the mean-field approximation, using the Bogoliubov approximation, we define the annihilation operators of the two species as

$$\hat{a}_{1\xi} = (c_{\xi} + \hat{\phi}_{1\xi}) e^{-i\mu_1 t/\hbar}, \quad (5a)$$

$$\hat{a}_{2\xi} = (d_{\xi} + \hat{\phi}_{2\xi}) e^{-i\mu_2 t/\hbar} \quad (5b)$$

and the creation operators are the Hermitian conjugates. Here $c_{\xi} \equiv c_{i,j}$ and $d_{\xi} \equiv d_{i,j}$ are the complex amplitudes associated with the condensate wave functions of each species, which satisfy the normalization conditions $\sum_{\xi} |c_{\xi}|^2 = \sum_{\xi} |d_{\xi}|^2 = 1$. The operators ($\hat{\phi}_{1\xi}$ or $\hat{\phi}_{2\xi}$) represent perturbations and identify with the quantum and thermal fluctuations in the system. These definitions, when used in Eq. (4), partition the BH Hamiltonian to terms of different orders in the fluctuation operators. The minimization of the lowest-order term leads to a set of time-independent 2D coupled discrete nonlinear Schrödinger equations (DNLSEs) [54–56], which describe the equilibrium properties of the system at $T = 0$ K. These are given by

$$\mu_1 c_{\xi} = -J_1 \sum_{\xi'} c_{\xi'} + [\epsilon_{\xi}^{(1)} + U_{11} n_{1\xi}^c + U_{12} n_{2\xi}^c] c_{\xi}, \quad (6a)$$

$$\mu_2 d_{\xi} = -J_2 \sum_{\xi'} d_{\xi'} + [\epsilon_{\xi}^{(2)} + U_{22} n_{2\xi}^c + U_{12} n_{1\xi}^c] d_{\xi}, \quad (6b)$$

where the summation ξ' is over the nearest neighbors of the site ξ , more explicitly, $\sum_{\xi'} c_{\xi'} \equiv c_{\xi-1} + c_{\xi+1} \equiv c_{i-1,j} + c_{i+1,j} + c_{i,j-1} + c_{i,j+1}$. From the definition of $\phi_{k\xi}$, in Eqs. (6) $n_{1\xi}^c = |c_\xi|^2$ and $n_{2\xi}^c = |d_\xi|^2$ are the condensate densities of the first and second species at the ξ th lattice site, respectively. In the Bogoliubov approximation, the leading-order correction terms describe the effects arising from quantum and thermal fluctuations of the system. A more detailed description of the derivation is given in one of our previous works [41]. The fluctuation operators are defined in terms of normal modes of the system or the quasiparticles through the Bogoliubov transformations

$$\hat{\phi}_{k\xi} = \sum_l [u_{k\xi}^l \hat{\alpha}_l e^{-i\omega_l t} - v_{k\xi}^{*l} \hat{\alpha}_l^\dagger e^{i\omega_l t}], \quad (7a)$$

$$\hat{\phi}_{k\xi}^\dagger = \sum_l [u_{k\xi}^{*l} \hat{\alpha}_l^\dagger e^{i\omega_l t} - v_{k\xi}^l \hat{\alpha}_l e^{-i\omega_l t}], \quad (7b)$$

where $u_{k\xi}^l$ and $v_{k\xi}^l$ are the quasiparticle amplitudes for the k th species in the quasi-2D optical lattice potential and $\omega_l = E_l/\hbar$ is the frequency of the l th quasiparticle mode, with E_l the mode excitation energy. Furthermore, the quasiparticle amplitudes satisfy the normalization condition

$$\sum_{k\xi} (u_{k\xi}^{*l} u_{k\xi}^l - v_{k\xi}^{*l} v_{k\xi}^l) = \delta_{ll'}. \quad (8)$$

Here $\hat{\alpha}_l$ and $\hat{\alpha}_l^\dagger$ are the quasiparticle annihilation and creation operators, respectively, which satisfy the Bose commutation relations. The above transformation diagonalizes the BH Hamiltonian and taking into account the higher-order terms in the fluctuation operators in the total Hamiltonian leads to the HFB-Popov equations [57,58]

$$E_l u_{1,\xi}^l = -J_1(u_{1,\xi-1}^l + u_{1,\xi+1}^l) + \mathcal{U}_1 u_{1,\xi}^l - U_{11} c_\xi^2 v_{1,\xi}^l + U_{12} c_\xi (d_\xi^* u_{2,\xi}^l - d_\xi v_{2,\xi}^l), \quad (9a)$$

$$E_l v_{1,\xi}^l = J_1(v_{1,\xi-1}^l + v_{1,\xi+1}^l) + \underline{\mathcal{U}}_1 v_{1,\xi}^l + U_{11} c_\xi^* u_{1,\xi}^l - U_{12} c_\xi^* (d_\xi v_{2,\xi}^l - d_\xi^* u_{2,\xi}^l), \quad (9b)$$

$$E_l u_{2,\xi}^l = -J_2(u_{2,\xi-1}^l + u_{2,\xi+1}^l) + \mathcal{U}_2 u_{2,\xi}^l - U_{22} d_\xi^2 v_{2,\xi}^l + U_{12} d_\xi (c_\xi^* u_{1,\xi}^l - c_\xi v_{1,\xi}^l), \quad (9c)$$

$$E_l v_{2,\xi}^l = J_2(v_{2,\xi-1}^l + v_{2,\xi+1}^l) + \underline{\mathcal{U}}_2 v_{2,\xi}^l + U_{22} d_\xi^* u_{2,\xi}^l - U_{12} d_\xi^* (c_\xi v_{1,\xi}^l - c_\xi^* u_{1,\xi}^l), \quad (9d)$$

where $\mathcal{U}_1 = 2U_{11}(n_{1\xi}^c + \tilde{n}_{1\xi}) + U_{12}(n_{2\xi}^c + \tilde{n}_{2\xi}) + (\epsilon_\xi^{(1)} - \mu_1)$ and $\mathcal{U}_2 = 2U_{22}(n_{2\xi}^c + \tilde{n}_{2\xi}) + U_{12}(n_{1\xi}^c + \tilde{n}_{1\xi}) + (\epsilon_\xi^{(2)} - \mu_2)$, with $\underline{\mathcal{U}}_k = -\mathcal{U}_k$. The density of the noncondensate atoms at the ξ th lattice site is

$$\tilde{n}_{k\xi} = \sum_l [(|u_{k\xi}^l|^2 + |v_{k\xi}^l|^2) N_0(E_l) + |v_{k\xi}^l|^2], \quad (10)$$

with $N_0(E_l)$ the Bose factor of the system with energy E_l at temperature T . The last term in $\tilde{n}_{k\xi}$ is the quantum fluctuation, which is independent of the Bose factor and hence represents the quantum fluctuation of the system.

B. Dispersion relations of binary BECs

Dispersion relations, in general, determine how a system responds to external perturbations. So, in TBECs in optical lattices as well it is important to examine the dispersion relations to understand how the system evolves after applying an external perturbation. Examples of current interest are topological defects generated through phase imprinting, evacuating single or multiple lattice sites, and tuning the lattice or harmonic potential parameters. To study the dispersion relation of the quasiparticles in optical lattices with a background trapping potential, we follow the definition in Ref. [47]. Then we take the Fourier transform of the quasiparticle amplitudes and compute the expectation value of the linear momentum $\langle k_\xi \rangle$ of each quasiparticle. Thus, in the momentum-space representation, for the l th quasiparticle

$$\langle k_\xi \rangle_l = \left[\frac{\sum_{\alpha, \mathbf{k}_\xi} k_\xi^2 [|\tilde{u}_\alpha^l(\mathbf{k}_\xi)|^2 + |\tilde{v}_\alpha^l(\mathbf{k}_\xi)|^2]}{\sum_{\alpha, \mathbf{k}_\xi} [|\tilde{u}_\alpha^l(\mathbf{k}_\xi)|^2 + |\tilde{v}_\alpha^l(\mathbf{k}_\xi)|^2]} \right]^{1/2}, \quad (11)$$

where $k_\xi = (k_i, k_j)$ is the lattice-site-dependent wave number and $\alpha = 1, 2$ is the index for the species. Here $\tilde{u}_\alpha^l(\mathbf{k}_\xi) = \mathcal{F}[u_\alpha^l(\xi)]$ and $\tilde{v}_\alpha^l(\mathbf{k}_\xi) = \mathcal{F}[v_\alpha^l(\xi)]$ are the lattice-site-dependent quasiparticle amplitudes in momentum space, with \mathcal{F} representing the Fourier transform. We then determine the discrete form of the dispersion relation by associating $\langle k_\xi \rangle_l$ with the excitation energies E_l . For TBECs in the harmonic potential the dispersion curves were examined in a previous work and reported unique trends in the miscible and immiscible regimes [44]. In comparison, the presence of the optical lattice potential is expected to modify the dispersive properties of the systems in the present study. To examine the differences and identify unique trends we compute $\langle k_\xi \rangle_l$ and study the dispersion curves in miscible and immiscible domains.

C. Numerical methods

To solve the coupled DNLSs (6) at $T = 0$ K, we first scale the equations and rewrite them in dimensionless form [41]. The equations are then solved using the fourth-order Runge-Kutta method. For the zero-temperature computations we begin by neglecting the noncondensate density $\tilde{n}_{k\xi}$ at each lattice site and choose the initial guess values of the complex amplitudes with the Gaussian or side-by-side envelope profile such that the quasiparticle energy spectrum is real. To obtain the ground state of the system, we solve the DNLSs with imaginary-time propagation. As described earlier, in the TBA, we take a basis set consisting of orthonormalized Gaussian functions localized at each lattice site. Hence, the basis set size or the number of basis functions is equal to the number of lattice sites in the system. Furthermore, to obtain the excitation spectrum we cast the HFB-Popov equations (9) as a matrix eigenvalue equation. For the computations at $T = 0$ K, the nonsymmetric matrix with complex elements is diagonalized using the routine ZGEEV from the LAPACK library [59] to obtain the quasiparticle energies E_l and amplitudes u_ξ^l and v_ξ^l . However, when $T \neq 0$ K a larger number of basis functions is required to obtain a correct description of the thermal fluctuations and this increases the dimension of the matrix corresponding to Eqs. (9). It is then better to use the

ARPACK [60] library for diagonalization as it is faster and provides the option to compute a limited set of eigenvalues and eigenfunctions. The other advantage of using ARPACK is the optimal storage of large sparse matrices. In the latter part of our work to compute the dispersion curves, which in the present approach requires quasiparticle amplitudes in the momentum representation, we use the FFTW library [61] in Intel MKL.

III. RESULTS AND DISCUSSION

To examine the mode evolution of quasi-2D TBECs in optical lattices, we consider two cases from the experimentally realized TBECs, ^{87}Rb - ^{85}Rb [31] and ^{133}Cs - ^{87}Rb [28,29], which are examples of TBECs with negligible and large mass differences between the species, respectively. Another basic difference is, starting from the miscible phase, the passage to the immiscible phase. In the ^{87}Rb - ^{85}Rb TBEC, the background scattering length of ^{85}Rb is negative and hence to obtain a stable ^{85}Rb condensate [62] it is essential to render it repulsive using a magnetic Feshbach resonance [63,64]. The same can be employed to drive the system from the miscible to the immiscible domain. On the other hand, in the ^{133}Cs - ^{87}Rb TBEC, the interspecies scattering length is tuned through a magnetic Feshbach resonance [65] to steer the TBEC from the miscible to the immiscible domain or vice versa.

For the ^{87}Rb - ^{85}Rb TBEC, we assume ^{87}Rb and ^{85}Rb as the first and second species, respectively. For simplicity and ease of comparison without affecting the results, the radial trapping frequencies of the two species are chosen to be identical $\omega_{\perp} = 2\pi \times 50$ Hz, with $\omega_z/\omega_{\perp} = 20.33$. The wavelength of the laser beam to create the 2D lattice potential and lattice depth are $\lambda_L = 1064$ nm and $V_0 = 5E_R$, respectively. To improve convergence and obtain a good description of the optical lattice properties, we take the total number of atoms $N_1 = N_2 = 300$ confined in a 30×30 lattice system. We use these set of parameters to study the ^{133}Cs - ^{87}Rb TBEC as well.

A. Mode evolution of trapped TBECs at $T = 0$ K

To solve the DNLS we consider Gaussian basis function of width $0.3a$, where a is the lattice constant, to evaluate the lattice parameters. In the case of the ^{87}Rb - ^{85}Rb TBEC, the tunneling matrix elements are $J_1 = 0.66E_R$ and $J_2 = 0.71E_R$, and $U_{11} = 0.07E_R$ and $U_{12} = 0.15E_R$ are the intraspecies and interspecies interactions, respectively. The difference in the values of J_1 and J_2 arises from the mass difference of the species in the TBEC system. Following the same steps, the parameters for the ^{133}Cs - ^{87}Rb TBEC are $J_1 = 0.66E_R$, $J_2 = 1.70E_R$, $U_{11} = 0.96E_R$, and $U_{22} = 0.42E_R$. In both cases, we drive the system from the miscible to the immiscible phase and examine the evolution of the modes in detail.

1. The ^{87}Rb - ^{85}Rb TBEC

As mentioned earlier U_{22} , the intraspecies interaction of ^{85}Rb is decreased to drive the TBEC from the miscible to the immiscible domain. The changes in the ground-state density profile are shown in Fig. 1. In the miscible domain, the profiles overlap and there is a shift in the position of the density maxima as U_{22} is decreased [Fig. 1(b)]. At a critical value U_{22}^c , the two species undergo phase separation with side-by-side density

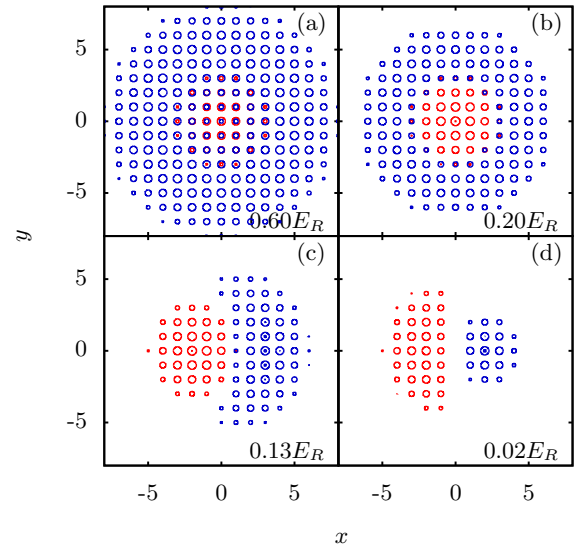


FIG. 1. Geometry of the condensate density profiles and its transition from the miscible to the immiscible domain for the ^{87}Rb - ^{85}Rb TBEC. (a) At higher U_{22} , the density of both species partially overlap; (b) as we decrease U_{22} it changes into a sandwich-type profile. At a critical value of U_{22} ($0.16E_R$), both condensates segregate and rotational symmetry is broken, which results in a side-by-side density profile in the immiscible domain shown in (c) and (d). The species labeled 1 (2) is shown as red (blue) contours. Here x and y are in units of the lattice constant a .

profiles and break the rotational symmetry. The features of the quasiparticles also change in tandem with the density profile and the variation of the excitation energies with U_{22} is shown in Fig. 2. To obtain the mode evolution curves, we do a series of computations starting from the miscible domain of the system (higher U_{22}) and decrease U_{22} to values below U_{22}^c .

In the miscible domain, all the excitation modes are doubly degenerate. As U_{22} is lowered, eigenenergies of modes with different phases of u_1 and u_2 , or out-of-phase modes, decrease in energy and degeneracy is lifted when U_{22} is below U_{22}^c . The slosh and Kohn modes are the two lowest-energy ones in

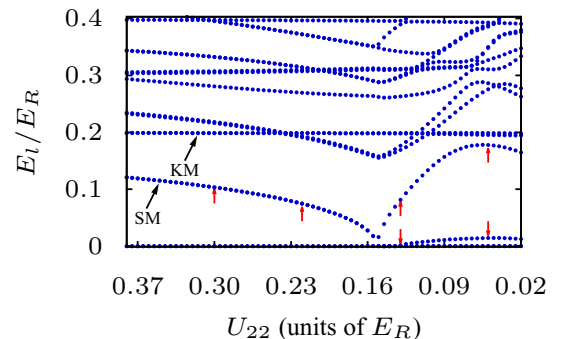


FIG. 2. Evolution of the low-lying quasiparticle modes as a function of the intraspecies interaction U_{22} for the ^{87}Rb - ^{85}Rb TBEC held in quasi-2D optical lattices. The slosh mode (SM) and Kohn mode (KM) are marked by the black arrows. The energies marked by red arrows correspond to the quasiparticle amplitudes shown in Figs. 3 and 4. In the plot U_{22} is in units of the recoil energy E_R .

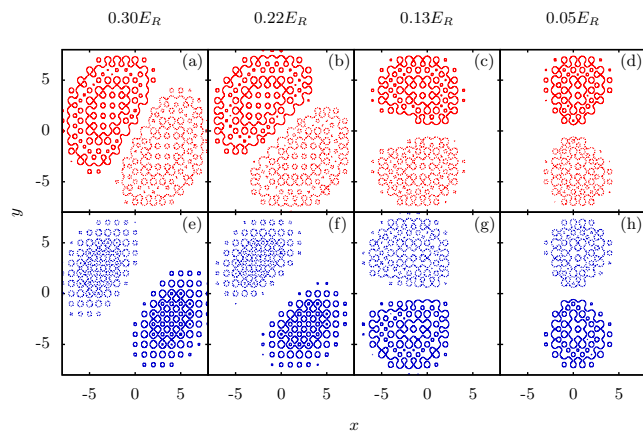


FIG. 3. Evolution of the quasiparticle amplitude corresponding to the slosh mode of (a)–(d) the first species and (e)–(h) the second species of the ^{87}Rb - ^{85}Rb TBEC as U_{22} is decreased from $0.30E_R$ to $0.05E_R$. The value of U_{22} is shown at the top of the figures. The red (blue) contours represent the quasiparticle amplitude u_1 (u_2). The density perturbation is from dotted contours to the solid contours. Here x and y are in units of the lattice constant a .

the miscible domain and are associated with the out-of-phase and in-phase modes, respectively. The structure of the two degenerate slosh modes are shown in Figs. 3(a), 3(b), 3(e), and 3(f) and Figs. 4(a), 4(b), 4(e), and 4(f), respectively. In general, the doubly degenerate modes are $\pi/2m$ rotations of each other, where m is the azimuthal quantum number. For the slosh modes this property is evident from the figures. One of the degenerate slosh modes goes soft at $U_{22}^c = 0.16$ (specifically, it is the one that is in phase with the condensate density), but the other slosh mode gains energy at phase separation. Thus, below U_{22}^c the degeneracy of the slosh modes is lifted. With

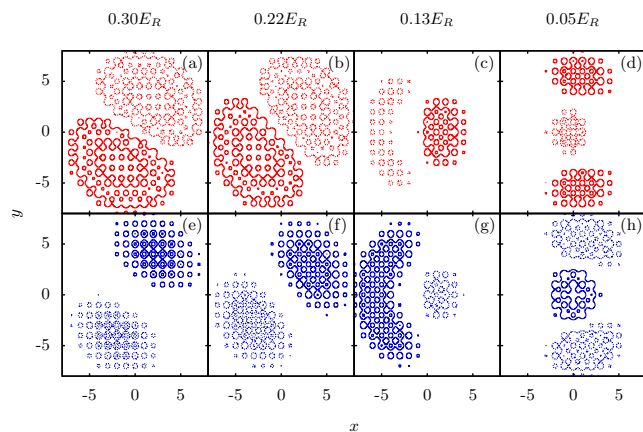


FIG. 4. Evolution of the quasiparticle amplitude corresponding to the other slosh mode, which is degenerate to the mode shown in Fig. 3 in the miscible domain. These amplitudes correspond to (a)–(d) the first species and (e)–(h) the second species of the ^{87}Rb - ^{85}Rb TBEC with the change in U_{22} , which is shown at the top of the figures. (d) and (h) At a critical value of U_{22} , this mode hardens and transforms into an interface mode. The red (blue) contours represent the quasiparticle amplitude of first (second) species. Here x and y are in units of the lattice constant a .

a further decrease of U_{22} one striking effect of the optical lattice potential is observed: The soft slosh mode gains energy and is transformed into an interface mode. This is in stark contrast to the case without the lattice potential, where the mode remains soft [66]. This is also apparent from the nature of the quasiparticle amplitudes shown in Figs. 3(c), 3(d), 3(g), and 3(h) and Figs. 4(c), 4(d), 4(g), and 4(h). The Kohn mode, on the other hand, remains steady with an energy of $0.2E_R$.

Considering the general trend, there are only mode crossings in the miscible domain, however, both mode crossings and avoided crossings occur in the phase-separated domain. Prior to phase separation, out-of-phase modes decrease in energy as U_{22} is lowered, but the in-phase modes remain steady. So no mode mixing occurs when modes of the former type encounters the latter, and they cross each other. However, when U_{22} is below the critical value, degeneracies are lifted and mode mixing can occur. This explains the presence of avoided crossings in the phase-separated domain. The energies of the out-of-phase modes decrease monotonically with decreasing U_{22} as it favors phase separation. After phase separation, these modes get hardened due to rotational symmetry breaking. It must be noted that, as shown in Fig. 1(b), the density profiles are shell structured or rotationally symmetric for intermediate values of U_{22} . However, there is a sharp transition to the side-by-side density profile as phase separation occurs when U_{22} is lowered.

2. The ^{133}Cs - ^{87}Rb TBEC

For the ^{133}Cs - ^{87}Rb TBEC, as mentioned earlier, we vary the interspecies interaction U_{12} to induce the miscible to immiscible phase transition. The density profiles, as the miscible to immiscible transition occurs, are shown in Fig. 5. The change, except for the curvature at the interface, are similar to the case of the ^{87}Rb - ^{85}Rb TBEC shown in Fig. 1. The evolution of the mode energies before, during, and after the

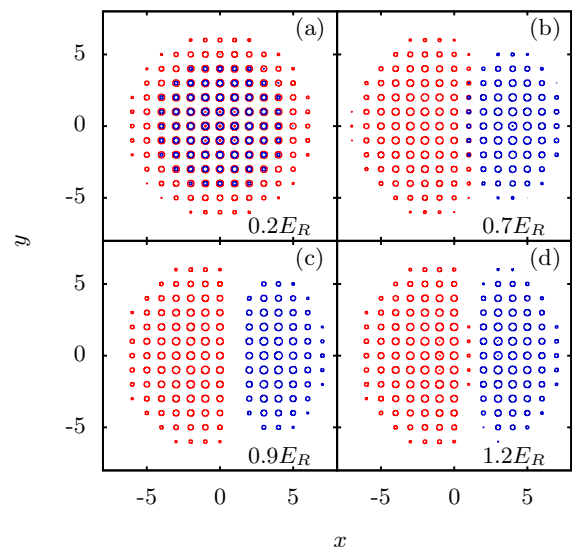


FIG. 5. Geometry of the condensate density profiles and its transition from the miscible to the immiscible domain in the ^{133}Cs - ^{87}Rb TBEC. The species labeled 1 (2) is shown as red (blue) contours. Here x and y are in units of the lattice constant a .

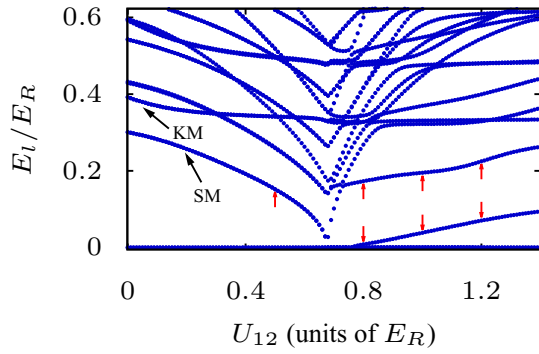


FIG. 6. Evolution of the low-lying modes as a function of the interspecies interaction in the ^{133}Cs - ^{87}Rb TBEC held in quasi-2D optical lattices. The slosh mode and Kohn mode are marked by the black arrows. The energies marked by red arrows correspond to the quasiparticle amplitudes shown in Figs. 7 and 8. Here U_{12} is in units of the recoil energy E_R .

transition are shown in Fig. 6. Like in the previous case of the ^{87}Rb - ^{85}Rb TBEC, the slosh mode is degenerate in the miscible domain [shown in Figs. 7(a), 7(e), 8(a), and 8(e)]. It goes soft at the critical value $U_{12}^c = 0.68E_R$ and the degeneracy is lifted. As shown in Figs. 7(b)–7(d), 7(f)–7(h), 8(b)–8(d), and 8(f)–8(h), the evolution of the nondegenerate modes is qualitatively similar to that of the ^{87}Rb - ^{85}Rb TBEC. One key feature in the general trend of the mode evolution is that in the miscible domain all the mode energies decrease with an increase in U_{12} . However, as discussed earlier, in the ^{87}Rb - ^{85}Rb TBEC the energies of all the in-phase modes (modes with same phase of u_1 and u_2) remain steady. At phase separation, the mode energies reach minimal values and then increase with increasing U_{12} in the immiscible domain. To gain insight into these trends, we examine the dependence on various parameters with a series of computations.

Based on the results, we observe that the form of the interaction, interspecies or intraspecies, which is tuned to

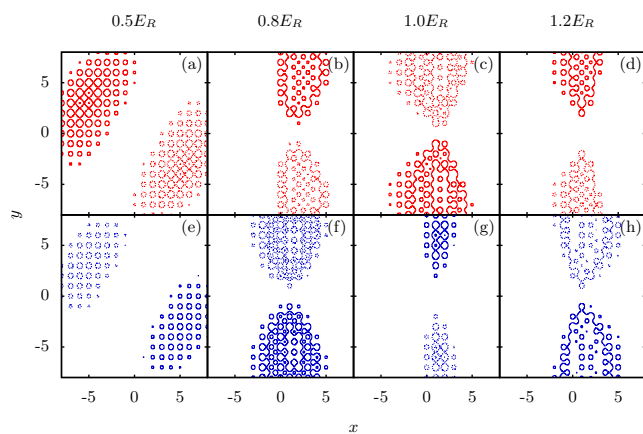


FIG. 7. Evolution of the quasiparticle amplitude corresponding to the slosh mode of (a)–(d) the first species and (e)–(h) the second species of the ^{133}Cs - ^{87}Rb TBEC as U_{12} is increased from $0.5E_R$ to $1.2E_R$. The value of U_{12} is shown at the top of the figures. The red (blue) contours represent the quasiparticle amplitude of ^{133}Cs (^{87}Rb). The density perturbation is from dotted contours to solid contours. Here x and y are in units of the lattice constant a .

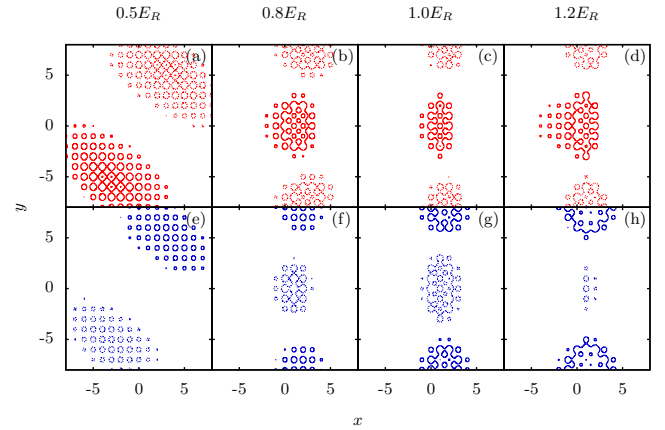


FIG. 8. Evolution of the quasiparticle amplitude corresponding to the slosh mode, which is degenerate with the mode shown in Fig. 7 in the miscible domain. These amplitudes correspond to (a)–(d) the first species and (e)–(h) the second species of the ^{133}Cs - ^{87}Rb TBEC as U_{12} is increased from $0.5E_R$ to $1.2E_R$. The value of U_{12} is shown at the top of the figures. At a critical value of U_{12} , the energy of the mode increases and transforms into an interface mode. The red (blue) contours represent the quasiparticle amplitude of ^{133}Cs (^{87}Rb). Here x and y are in units of the lattice constant a .

drive the miscible to immiscible transition, has an impact on the trends of the mode evolution. An important observation is that for high U_{kk}/J_k all the modes decrease in energy, in the miscible domain, when the interspecies interaction is tuned. However, when the intraspecies interaction is tuned all the in-phase modes remain steady. Thus, we attribute the difference in the trends to the geometry of the interface at phase separation. When the interspecies interaction is tuned, as in the ^{133}Cs - ^{87}Rb TBEC, the interface at phase separation is linear, as is evident from Fig. 5(c). Thus, it can align with the nodes of the mode functions and decrease all the mode energies. This is not possible in the other case, tuning the intraspecies interaction in the ^{87}Rb - ^{85}Rb TBEC, as the interface is curved as shown in Fig. 1(c).

B. Dispersion relations

To obtain dispersion curves, based on Eq. (11), we compute $\langle k_\xi \rangle_l$ of the l th quasiparticle and plot the mode energies. To highlight trends in the dispersion curves dependent on angular momentum, we choose parameters different from what we have considered so far. Furthermore, we restrict ourselves to the case of the ^{87}Rb - ^{85}Rb TBEC, where the trends in dispersion curves are more prominent due to weaker interatomic interactions, and small mass difference. In particular, we consider a system of the ^{87}Rb - ^{85}Rb TBEC with DNLSE parameters $J_1 = J_2 = 0.66E_R$ and $U_{11} = U_{22} = 0.01E_R$. For the interspecies on-site interactions U_{12} , to explore the dispersion relations in the miscible and immiscible domains we set it to $0.003E_R$ and $0.08E_R$, respectively. All the other parameters are retained with the same values as mentioned earlier. One important point to be emphasized is that, unlike the parameters in the mode evolutions studies, the current choice of DNLSE parameters corresponds to two different sets of N_1 and N_2 .

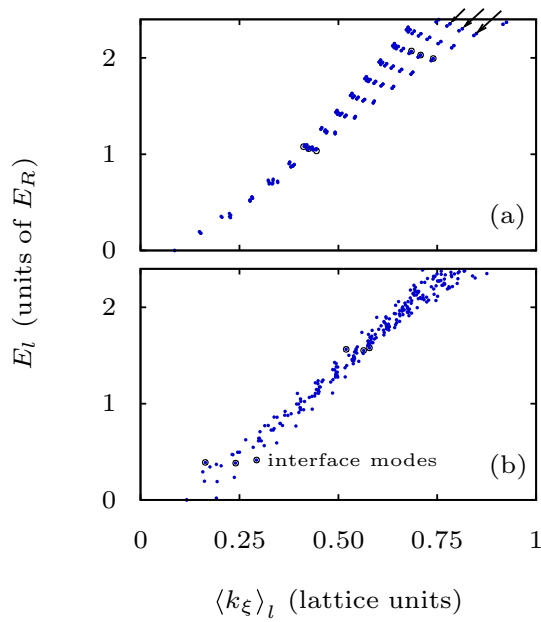


FIG. 9. Discrete BdG quasiparticle dispersion curve in (a) the miscible and (b) the immiscible domain of the ^{87}Rb - ^{85}Rb TBEC with $J_1 = J_2 = 0.66E_R$ and $U_{11} = U_{22} = 0.01E_R$. The interspecies on-site interaction U_{12} is (a) $0.003E_R$ and (b) $0.08E_R$. The excitation energy E_l is in units of the recoil energy E_R .

1. Miscible domain

The ground state of the system has rotational symmetry in this domain. Hence, the azimuthal quantum number m is a good quantum number and the finite interspecies interaction mixes modes with the same m arising from each of the two species. This is reflected in the branchlike structures in the dispersion curve as shown in Fig. 9(a). To understand the physics behind the structure of the dispersion curves, we examine the structure of the quasiparticle modes. For this, let us focus on modes that lie on three branches, marked by arrows, in Fig. 9(a). Each of the modes can be identified based on the value of m . As an example, three from the low energies ($\approx 1E_R$) and another three from higher energies ($\approx 2E_R$) are shown in Fig. 10.

The energies of the first three quasiparticle modes in Figs. 10(a)–10(c) are the out-of-phase type and the values of m are 1, 4, and 6. Among these modes, the first two modes have $\langle k_\xi \rangle_l \approx 0.42$ and are phononlike as these lie on the linear part of the dispersion curve. However, the mode in Fig. 10(c) with $\langle k_\xi \rangle_l \approx 0.44$ and $m = 6$ is a surface mode, which is evident from the structure of the mode function. The same observation is confirmed from the exponential decay in the numerical values of u towards the center. These three modes show that within the same energy range ($\approx 1E_R$), phononlike and surface excitation coexists. One discernible trend is that the modes with higher m and $\langle k_\xi \rangle_l$ have extrema located farther from the center of the trap and turn into surface modes. The quasiparticle amplitudes with higher excitation energies ($\approx 2E_R$), shown in Figs. 10(d)–10(f), have intricate structures. This is as expected arising from the larger mode mixing due to the higher density of states and nonzero U_{12} and it is harder to identify the m

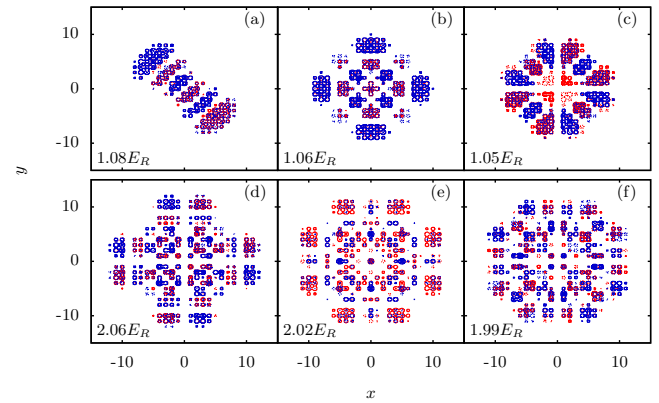


FIG. 10. Quasiparticle amplitudes in the miscible domain of a TBEC. (a)–(c) Quasiparticle amplitudes with excitation energy ($\approx 1E_R$) and (d)–(f) quasiparticle amplitudes with excitation energy ($\approx 2E_R$). These quasiparticles are indicated in the dispersion plot [Fig. 9(a)] by black circles. The excitation energy corresponding to each quasiparticle is written in the lower left corner of each plot in units of the recoil energy. The excitations corresponding to species 1 (2) are shown with red (blue) contours. Here x and y are in units of the lattice constant a .

of these modes. However, based on the number of minima and maxima at the outer edges, we compute the azimuthal quantum number of these mode functions as $m \sim 4, 6, 8$. Thus, the quasiparticle modes of this domain preserve the rotational symmetry.

2. Immiscible domain

For the immiscible domain, the dispersion curve is as shown in Fig. 9(b) and there are no discernible trends. The reason is that in this domain the condensate density profile does not have rotational symmetry and hence there is mixing between quasiparticle modes with different m values. To examine the structure of the mode functions we consider three, each with energies $\approx 0.4E_R$ and $\approx 1.55E_R$; these are shown in Figs. 11(a)–11(c) and Figs. 11(d)–11(f), respectively. Consider the modes with energies $0.39E_R$ and $0.38E_R$ as shown in Figs. 11(a) and 11(b). The flow patterns in these are equivalent to the breathing and slosh modes in single-species condensates, respectively. There is, however, one important difference: The density flow involves both species, and have different velocity fields. The mode with energy $0.41E_R$, shown in Fig. 11(c), is out of phase in nature and has a different configuration compared to the two previous ones. That is, the mode functions are prominent around the interface region and are negligible in the region where the condensate densities are maximal. In the continuum case, modes with a similar structure (interface mode) have been reported [44,66]. The mode with higher energies have enhanced mode mixing due to a higher density of states, which is evident from the structure of the modes with $\approx 1.55E_R$ shown in Figs. 11(d)–11(f). Hence, it is nontrivial to classify the modes like in the case of modes with energies $\approx 0.4E_R$. In terms of the geometrical structures, the modes in Figs. 11(d)–11(f) have extrema coincident with the condensates, an interlaced distribution, and are localized

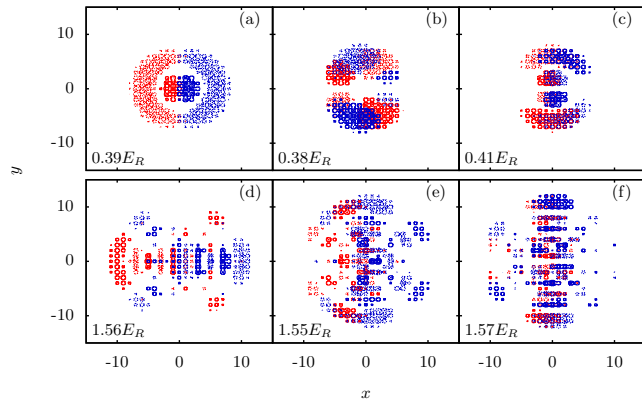


FIG. 11. Quasiparticle amplitudes in the immiscible domain of a TBEC. (a)–(c) Quasiparticle amplitudes with excitation energy ($\approx 0.4E_R$) and (d)–(f) quasiparticle amplitudes with excitation energy ($\approx 1.5E_R$). These quasiparticles are indicated in the dispersion plot [Fig. 9(b)] by black circles. The excitation energy corresponding to each quasiparticle is written in the lower left corner of each plot in units of the recoil energy. The excitations corresponding to species 1 (2) are shown with red (blue) contours. Here x and y are in units of the lattice constant a .

in the interface region, respectively. Thus, within a range of excitation energies, there exist modes with diverse characters.

IV. CONCLUSION

In this work we have examined the configurations of the ground state and the quasiparticle spectra of TBECs in quasi-2D optical lattices. Our results are relevant to the superfluid phase ($J > U$) of ultracold atoms in an optical lattice and with a lattice constant much smaller than the oscillator length of the background harmonic-oscillator trapping frequency ($a \ll$

$a_{\text{osc}} = \sqrt{\hbar/m_1\omega_{\perp}}$). Our study shows that the introduction of an optical lattice potential modifies the geometry of the condensate density distribution of TBECs at phase separation. The sandwich or shell structured density profiles are no longer energetically favorable and the side-by-side geometry emerges as the only stable ground-state density profile. This arises from the higher interface energy due to the local density enhancements at lattice sites. The other important observation is that, as the TBEC is tuned from the miscible to the immiscible phase, the evolution of the quasiparticle spectra can be grouped into two. The first group has quasiparticles that exhibit a decrease in the mode energies as we approach phase separation and reach minimal values at the critical interaction strength. However, the mode energies increase after crossing into the domain of phase separation. The second group, on the other hand, remains steady as the interaction strength is tuned across the critical value. Furthermore, we have examined the dispersion curves for miscible and immiscible domains of TBECs. The curves in the miscible domain show discernible trends associated with the azimuthal quantum number of the quasiparticle. However, in the immiscible domain there are no discernible trends associated with azimuthal quantum number. This is due to the rotational symmetry breaking of the condensate density profiles and the resulting mixing of modes with different azimuthal quantum numbers.

ACKNOWLEDGMENTS

We thank Arko Roy, S. Gautam, S. Bandyopadhyay, and R. Bai for useful discussions. The results presented in the paper are based on the computations using Vikram-100, the 100TFLOP HPC Cluster at Physical Research Laboratory, Ahmedabad, India. We also thank the anonymous referee for the thorough review and valuable comments, which contributed to improving the quality of the paper.

-
- [1] M. Greiner, I. Bloch, O. Mandel, T. W. Hänsch, and T. Esslinger, *Phys. Rev. Lett.* **87**, 160405 (2001).
 - [2] D. Jaksch, C. Bruder, J. I. Cirac, C. W. Gardiner, and P. Zoller, *Phys. Rev. Lett.* **81**, 3108 (1998).
 - [3] M. Köhl, H. Moritz, T. Stöferle, K. Günter, and T. Esslinger, *Phys. Rev. Lett.* **94**, 080403 (2005).
 - [4] W. Hofstetter, J. I. Cirac, P. Zoller, E. Demler, and M. D. Lukin, *Phys. Rev. Lett.* **89**, 220407 (2002).
 - [5] J. Dalibard, F. Gerbier, G. Juzeliūnas, and P. Öhberg, *Rev. Mod. Phys.* **83**, 1523 (2011).
 - [6] B. P. Anderson and M. A. Kasevich, *Science* **282**, 1686 (1998).
 - [7] M. P. A. Fisher, P. B. Weichman, G. Grinstein, and D. S. Fisher, *Phys. Rev. B* **40**, 546 (1989).
 - [8] M. Greiner, O. Mandel, T. Esslinger, T. W. Hansch, and I. Bloch, *Nature (London)* **415**, 39 (2002).
 - [9] E. Altman, A. Polkovnikov, E. Demler, B. I. Halperin, and M. D. Lukin, *Phys. Rev. Lett.* **95**, 020402 (2005).
 - [10] M. Ben Dahan, E. Peik, J. Reichel, Y. Castin, and C. Salomon, *Phys. Rev. Lett.* **76**, 4508 (1996).
 - [11] K. Berg-Sørensen and K. Mølmer, *Phys. Rev. A* **58**, 1480 (1998).
 - [12] B. Wu and Q. Niu, *Phys. Rev. A* **61**, 023402 (2000).
 - [13] J. Liu, L. Fu, B.-Y. Ou, S.-G. Chen, D.-I. Choi, B. Wu, and Q. Niu, *Phys. Rev. A* **66**, 023404 (2002).
 - [14] V. V. Konotop and M. Salerno, *Phys. Rev. A* **65**, 021602 (2002).
 - [15] Z. Chen and B. Wu, *Phys. Rev. A* **81**, 043611 (2010).
 - [16] M. Krämer, L. Pitaevskii, and S. Stringari, *Phys. Rev. Lett.* **88**, 180404 (2002).
 - [17] C. Fort, F. S. Cataliotti, L. Fallani, F. Ferlaino, P. Maddaloni, and M. Inguscio, *Phys. Rev. Lett.* **90**, 140405 (2003).
 - [18] B. Paredes and J. I. Cirac, *Phys. Rev. Lett.* **90**, 150402 (2003).
 - [19] O. E. Alon, A. I. Streltsov, and L. S. Cederbaum, *Phys. Rev. Lett.* **97**, 230403 (2006).
 - [20] E. Lundh and J.-P. Martikainen, *Phys. Rev. A* **85**, 023628 (2012).
 - [21] L.-M. Duan, E. Demler, and M. D. Lukin, *Phys. Rev. Lett.* **91**, 090402 (2003).
 - [22] A. B. Kuklov and B. V. Svistunov, *Phys. Rev. Lett.* **90**, 100401 (2003).
 - [23] T.-L. Ho and V. B. Shenoy, *Phys. Rev. Lett.* **77**, 3276 (1996).
 - [24] J. Catani, L. De Sarlo, G. Barontini, F. Minardi, and M. Inguscio, *Phys. Rev. A* **77**, 011603 (2008).

- [25] B. Gadway, D. Pertot, R. Reimann, and D. Schneble, *Phys. Rev. Lett.* **105**, 045303 (2010).
- [26] P. Soltan-Panahi, J. Struck, P. Hauke, A. Bick, W. Plenkers, G. Meineke, C. Becker, P. Windpassinger, M. Lewenstein, and K. Sengstock, *Nat. Phys.* **7**, 434 (2011).
- [27] G. Modugno, M. Modugno, F. Riboli, G. Roati, and M. Inguscio, *Phys. Rev. Lett.* **89**, 190404 (2002).
- [28] A. Lercher, T. Takekoshi, M. Debatin, B. Schuster, R. Rameshan, F. Ferlaino, R. Grimm, and H.-C. Nägerl, *Eur. Phys. J. D* **65**, 3 (2011).
- [29] D. J. McCarron, H. W. Cho, D. L. Jenkin, M. P. Köppinger, and S. L. Cornish, *Phys. Rev. A* **84**, 011603 (2011).
- [30] G. Thalhammer, G. Barontini, L. De Sarlo, J. Catani, F. Minardi, and M. Inguscio, *Phys. Rev. Lett.* **100**, 210402 (2008).
- [31] S. B. Papp, J. M. Pino, and C. E. Wieman, *Phys. Rev. Lett.* **101**, 040402 (2008).
- [32] C. J. Myatt, E. A. Burt, R. W. Ghrist, E. A. Cornell, and C. E. Wieman, *Phys. Rev. Lett.* **78**, 586 (1997).
- [33] D. M. Stamper-Kurn, M. R. Andrews, A. P. Chikkatur, S. Inouye, H.-J. Miesner, J. Stenger, and W. Ketterle, *Phys. Rev. Lett.* **80**, 2027 (1998).
- [34] D. S. Hall, M. R. Matthews, J. R. Ensher, C. E. Wieman, and E. A. Cornell, *Phys. Rev. Lett.* **81**, 1539 (1998).
- [35] S. Tojo, Y. Taguchi, Y. Masuyama, T. Hayashi, H. Saito, and T. Hirano, *Phys. Rev. A* **82**, 033609 (2010).
- [36] B. D. Esry, C. H. Greene, J. P. Burke, Jr., and J. L. Bohn, *Phys. Rev. Lett.* **78**, 3594 (1997).
- [37] P. Öhberg and S. Stenholm, *Phys. Rev. A* **57**, 1272 (1998).
- [38] A. A. Svidzinsky and S. T. Chui, *Phys. Rev. A* **67**, 053608 (2003).
- [39] A. Roy, S. Gautam, and D. Angom, *Phys. Rev. A* **89**, 013617 (2014).
- [40] A. Roy and D. Angom, *Phys. Rev. A* **90**, 023612 (2014).
- [41] K. Suthar, A. Roy, and D. Angom, *Phys. Rev. A* **91**, 043615 (2015).
- [42] D. M. Stamper-Kurn, A. P. Chikkatur, A. Görlitz, S. Inouye, S. Gupta, D. E. Pritchard, and W. Ketterle, *Phys. Rev. Lett.* **83**, 2876 (1999).
- [43] J. Steinhauer, R. Ozeri, N. Katz, and N. Davidson, *Phys. Rev. Lett.* **88**, 120407 (2002).
- [44] C. Ticknor, *Phys. Rev. A* **89**, 053601 (2014).
- [45] X. Du, S. Wan, E. Yesilada, C. Ryu, D. J. Heinzen, Z. Liang, and B. Wu, *New J. Phys.* **12**, 083025 (2010).
- [46] P. T. Ernst, S. Götze, J. S. Krauser, K. Pyka, D.-S. Lühmann, D. Pfannkuche, and K. Sengstock, *Nat. Phys.* **6**, 56 (2010).
- [47] R. M. Wilson, S. Ronen, and J. L. Bohn, *Phys. Rev. Lett.* **104**, 094501 (2010).
- [48] C. Ticknor, R. M. Wilson, and J. L. Bohn, *Phys. Rev. Lett.* **106**, 065301 (2011).
- [49] R. N. Bisset and P. B. Blakie, *Phys. Rev. Lett.* **110**, 265302 (2013).
- [50] P. B. Blakie, D. Baillie, and R. N. Bisset, *Phys. Rev. A* **88**, 013638 (2013).
- [51] M. L. Chiofalo, M. Polini, and M. P. Tosi, *Eur. Phys. J. D* **11**, 371 (2000).
- [52] A. Smerzi and A. Trombettoni, *Phys. Rev. A* **68**, 023613 (2003).
- [53] P. P. Hofer, C. Bruder, and V. M. Stojanović, *Phys. Rev. A* **86**, 033627 (2012).
- [54] P. L. Christiansen, Y. B. Gaididei, K. O. Rasmussen, V. K. Mezentsev, and J. J. Rasmussen, *Phys. Rev. B* **54**, 900 (1996).
- [55] E. Arévalo, *Phys. Rev. Lett.* **102**, 224102 (2009).
- [56] M. D. Petrović, G. Gligorić, A. Maluckov, L. Hadžievski, and B. A. Malomed, *Phys. Rev. E* **84**, 026602 (2011).
- [57] A. Griffin, *Phys. Rev. B* **53**, 9341 (1996).
- [58] A. M. Rey, K. Burnett, R. Roth, M. Edwards, C. J. Williams, and C. W. Clark, *J. Phys. B* **36**, 825 (2003).
- [59] E. Anderson, Z. Bai, C. Bischof, S. Blackford, J. Demmel, J. Dongarra, J. D. Croz, A. Greenbaum, S. Hammarling, A. McKenney, and D. Sorensen, *LAPACK Users' Guide*, 3rd ed. (SIAM, Philadelphia, 1999).
- [60] R. Lehoucq, D. Sorensen, and C. Yang, *ARPACK Users' Guide: Solution of Large-Scale Eigenvalue Problems with Implicitly Restarted Arnoldi Methods* (SIAM, Philadelphia, 1998).
- [61] M. Frigo and S. G. Johnson, *Proc. IEEE* **93**, 216 (2005), special issue on program generation, optimization, and platform adaptation, edited by F. T. Ulaby.
- [62] S. L. Cornish, N. R. Claussen, J. L. Roberts, E. A. Cornell, and C. E. Wieman, *Phys. Rev. Lett.* **85**, 1795 (2000).
- [63] P. Courteille, R. S. Freeland, D. J. Heinzen, F. A. van Abeelen, and B. J. Verhaar, *Phys. Rev. Lett.* **81**, 69 (1998).
- [64] J. L. Roberts, N. R. Claussen, J. P. Burke, C. H. Greene, E. A. Cornell, and C. E. Wieman, *Phys. Rev. Lett.* **81**, 5109 (1998).
- [65] K. Pilch, A. D. Lange, A. Prantner, G. Kerner, F. Ferlaino, H.-C. Nägerl, and R. Grimm, *Phys. Rev. A* **79**, 042718 (2009).
- [66] C. Ticknor, *Phys. Rev. A* **88**, 013623 (2013).

Characteristic temperature for the immiscible-miscible transition of binary condensates in optical lattices

K. Suthar^{1,2} and D. Angom^{1,*}¹*Physical Research Laboratory, Navrangpura, Ahmedabad-380009, Gujarat, India*²*Indian Institute of Technology, Gandhinagar, Ahmedabad-382424, Gujarat, India*

(Received 23 August 2016; published 4 April 2017)

We study two-species Bose-Einstein condensates confined in quasi-two-dimensional (quasi-2D) optical lattices at finite temperatures, employing the Hartree-Fock-Bogoliubov theory with the Popov approximation. We examine the role of thermal fluctuations in the ground-state density distributions and the quasiparticle mode evolution. At zero temperature, the geometry of the ground state in the immiscible domain is side by side. Our results show that the thermal fluctuations enhance the miscibility of the condensates, and at a characteristic temperature the system becomes miscible with rotationally symmetric overlapping density profiles. This immiscible-miscible transition is accompanied by a discontinuity in the excitation spectrum, and the low-lying quasiparticle modes such as slosh mode become degenerate at the characteristic temperature.

DOI: [10.1103/PhysRevA.95.043602](https://doi.org/10.1103/PhysRevA.95.043602)

I. INTRODUCTION

Ultracold atoms in an optical lattice offer fascinating prospects to investigate many-body quantum physics of strongly correlated systems in a highly controllable environment [1–4]. These systems are recognized as ideal tools to explore new quantum phases [5–7], complex phase transitions [8–11], quantum magnetism [12,13], and quantum information [14] and to simulate the transport and magnetic properties of condensed-matter systems [15,16]. Moreover, the effects of phase separation [17,18], quantum emulsions and coherence properties [19–21], and multicritical behavior [22,23] of the mixtures have been explored in the past decade.

Among the various observations made in two-species Bose-Einstein condensates (TBECs) of ultracold atomic gases, the most remarkable is the phenomenon of phase separation, and it has been a long-standing topic of interest in chemistry and physics. For repulsive on-site interactions, the transition to the phase-separated domain or immiscibility is characterized by the parameter $\Delta = U_{11}U_{22}/U_{12}^2 - 1$, where U_{11} and U_{22} are the intraspecies on-site interactions and U_{12} is the interspecies on-site interaction. When $\Delta < 0$, an immiscible phase occurs in which the atoms of species 1 and 2 show relatively strong repulsion, whereas $\Delta \geq 0$ implies a miscible phase [24–26]. It is important to note that the mention criterion is valid at zero temperature for homogeneous systems. The presence of an external trapping potential, however, modifies this condition, as the trap introduces an additional energy cost for the species to spatially separate [27]. In experiments, the unique feature of phase separation has been successfully observed in TBECs with a harmonic trapping potential [28–30]. Previously, in the context of superfluid helium at zero temperature, the phase separation of bosonic mixtures of isotopes of different masses has also been predicted in Refs. [31] and [32]. Recent experimental realizations of TBECs in optical lattices, either of two atomic species [33] or two hyperfine states of same atomic species [34,35], provide the motivation to study these systems in detail. In recent works, we have examined the

miscible-immiscible transition, and the quasiparticle spectra of the TBECs at zero temperature in quasi-one-dimensional (quasi-1D) [36] and quasi-two-dimensional (quasi-2D) [37] geometries. The finding in the latter work [37], where we examined the nature of the density profiles in the immiscible regime at zero temperature, is of relevance to the present work. In addition, we showed how the optical lattice potential influences the density profiles in the immiscible domain. The other related study is the ground-state phase diagram, and the effect of the filling factor of the TBECs on the phenomenon of phase separation, which was investigated using quantum Monte Carlo simulations [38,39]. In addition, phase separation of TBECs at various length scales has been examined using the multiorbital mean-field theory [40,41]. Among the full quantum methods the multiconfigurational time-dependent Hartree for bosons (MCTDHB) method provides a good description of the formation of interference fringes in the densities during the mixing of condensates [42,43]. This method allows the dynamical creation of quantum superposition of states in ultracold Bose gases [44]. In other theoretical studies, the finite-temperature properties of TBECs have been explored [45–47]. In continuum or TBECs with a harmonic confining potential alone, we have explored the suppression of phase separation due to the presence of thermal fluctuations [48]. However, a theoretical understanding of the finite-temperature effects on the topology and the collective excitations of TBECs in optical lattices is yet to be explored. Bose-Einstein condensation and, hence, the coherence in a system of bosons depend on the interplay between various parameters, such as the temperature, interaction strength, confinement, and dimensionality [49]. In particular, in low-dimensional Bose gases, coherence can only be maintained across the entire spatial extent at a temperature much below the critical temperature. The coherence property, in experiments, has been studied in recent works [50–54].

With attention to this unexplored physics, we study the finite-temperature effects of quasi-2D trapped TBECs in optical lattices. In the present work, we address the topological phase transition in TBECs of two isotopes of Rb with temperature as a control parameter in the domain $T < T_c$, where T_c is the critical temperature of either of the species of

*angom@prl.res.in

the mixture. Here, it must be mentioned that in our previous works [36,37], we investigated the ground-state density and quasiparticles with variation in the on-site interaction energy at zero temperature. In addition, we have examined the effect of quantum fluctuations on the ground-state geometry and collective excitations of quasi-1D TBECs. In the present work, we examine the evolution of quasiparticle modes of TBECs in quasi-2D optical lattices with variation in the temperature. For this work, we use the Hartree-Fock-Bogoliubov (HFB) formalism with the Popov approximation, and starting from the phase-separated domain at zero temperature we increase the temperature. We observe that there is an immiscible-to-miscible transition of the TBEC at a characteristic temperature. This transition is accompanied by a discontinuity in the quasiparticle excitation spectrum, and in addition, some of the modes like the slosh mode become degenerate. We then compute the equal-time first-order spatial correlation function, which is a measure of the coherence and phase fluctuations present in the system. It describes the off-diagonal long-range order, which is a defining feature of the BEC [55]. This is an important theoretical tool to study many-body effects in atomic physics experiments [56,57].

This paper is organized as follows. In Sec. II we describe the HFB-Popov formalism and the numerical techniques used in the present work. The evolution of the quasiparticle modes and density distributions with the temperature is reported in Sec. III. Finally, our main results are summarized in Sec. IV.

II. THEORY AND METHODS

A. HFB-Popov approximation for a quasi-2D TBEC

We consider a TBEC confined in an optical lattice with a pancake-shaped configuration of the background harmonic trapping potential. Thus, the trapping frequencies satisfy the condition $\omega_{\perp} \ll \omega_z$ with $\omega_x = \omega_y = \omega_{\perp}$. In this system, the excitation energies along the axial direction are high, and the degree of freedom in this direction is frozen. The excitations, both quantum and thermal fluctuations, are considered only along the radial direction. In the tight-binding approximation [58,59], the Bose-Hubbard (BH) Hamiltonian [60–62] describing this system is

$$\hat{H} = \sum_{k=1}^2 \left[-J_k \sum_{\langle \xi \xi' \rangle} \hat{a}_{k\xi}^{\dagger} \hat{a}_{k\xi'} + \sum_{\xi} (\epsilon_{\xi}^{(k)} - \mu_k) \hat{a}_{k\xi}^{\dagger} \hat{a}_{k\xi} \right] + \frac{1}{2} \sum_{k=1,2} U_{kk} \hat{a}_{k\xi}^{\dagger} \hat{a}_{k\xi}^{\dagger} \hat{a}_{k\xi} \hat{a}_{k\xi} + U_{12} \sum_{\xi} \hat{a}_{1\xi}^{\dagger} \hat{a}_{1\xi} \hat{a}_{2\xi}^{\dagger} \hat{a}_{2\xi}, \quad (1)$$

where $k = 1, 2$ is the species index, μ_k is the chemical potential of the k th species, and $\hat{a}_{k\xi}$ ($\hat{a}_{k\xi}^{\dagger}$) is the annihilation (creation) operators of the two species at the ξ th lattice site. The index is such that $\xi \equiv (i, j)$, with i and j the lattice site index along the x and y directions, respectively. The summation index $\langle \xi \xi' \rangle$ represents the sum over the nearest neighbor to the ξ th site. The tight-binding approximation is valid when the depth of the lattice potential is much larger than the chemical potential $V_0 \gg \mu_k$; the BH Hamiltonian then describes the system when the bosonic atoms occupy the lowest energy band. A detailed derivation of the BH Hamiltonian is given in our previous works [36,37]. In the BH Hamiltonian, J_k

are the tunneling matrix elements, $\epsilon_{\xi}^{(k)}$ is the offset energy arising due to the background harmonic potential, and U_{kk} (U_{12}) are the intraspecies (interspecies) interaction strengths. In the present work all the interaction strengths are considered to be repulsive, that is, $U_{kk}, U_{12} > 0$.

In the weakly interacting regime, under the Bogoliubov approximation [63,64], the annihilation operators at each lattice site can be written as $\hat{a}_{1\xi} = (c_{\xi} + \hat{\phi}_{1\xi})e^{-i\mu_1 t/\hbar}$ and $\hat{a}_{2\xi} = (d_{\xi} + \hat{\phi}_{2\xi})e^{-i\mu_2 t/\hbar}$, where c_{ξ} and d_{ξ} are the complex amplitudes describing the condensate phase of each of the species. The operators $\hat{\phi}_{1\xi}$ and $\hat{\phi}_{2\xi}$ represent the quantum or thermal fluctuation part of the field operators. Furthermore, we consider the system in the superfluid domain where the mean-field description is applicable, and accordingly, the parameters satisfy the condition $U/J \ll 16.7$ [65–67]. In this domain, the equation of motion of the condensate in an optical lattice with the tight-binding approximation is reduced to the discrete nonlinear Schrödinger equation (DNLSE). However, in the Mott-insulator phase, $U/J \geq 16.7$, the mean-field description breaks down, and a full quantum description is required [68–70]. From the equation of motion of the field operators with the Bogoliubov approximation, the equilibrium properties of a TBEC is governed by the coupled generalized DNLSEs,

$$\mu_1 c_{\xi} = -J_1 \sum_{\xi'} c_{\xi'} + [\epsilon_{\xi}^{(1)} + U_{11}(n_{1\xi}^c + 2\tilde{n}_{1\xi}) + U_{12}n_{2\xi}^c]c_{\xi}, \quad (2a)$$

$$\mu_2 d_{\xi} = -J_2 \sum_{\xi'} d_{\xi'} + [\epsilon_{\xi}^{(2)} + U_{22}(n_{2\xi}^c + 2\tilde{n}_{2\xi}) + U_{12}n_{1\xi}^c]d_{\xi}, \quad (2b)$$

where $n_{1\xi}^c = |c_{\xi}|^2$ and $n_{2\xi}^c = |d_{\xi}|^2$, $\tilde{n}_{k\xi} = \langle \hat{\phi}_{k\xi}^{\dagger} \hat{\phi}_{k\xi} \rangle$, and $n_{k\xi} = n_{k\xi}^c + \tilde{n}_{k\xi}$ are the condensate, noncondensate, and total density of the species, respectively. The fluctuation operators are defined in terms of the quasiparticles through the Bogoliubov transformation

$$\hat{\phi}_{k\xi} = \sum_l [u_{k\xi}^l \hat{\alpha}_l e^{-i\omega_l t} - v_{k\xi}^{*l} \hat{\alpha}_l^{\dagger} e^{i\omega_l t}], \quad (3)$$

where $\hat{\alpha}_l$ ($\hat{\alpha}_l^{\dagger}$) are the quasiparticle annihilation (creation) operators, which satisfy the Bose commutation relations, l is the quasiparticle mode index, $u_{k\xi}^l$ and $v_{k\xi}^l$ are the quasiparticle amplitudes for the k th species, and $\omega_l = E_l/\hbar$ is the frequency of the l th quasiparticle mode with E_l as the mode excitation energy.

Using the Bogoliubov transformation, we obtain the HFB-Popov equations [37]

$$E_l u_{1,\xi}^l = -J_1 (u_{1,\xi-1}^l + u_{1,\xi+1}^l) + \mathcal{U}_1 u_{1,\xi}^l - U_{11} c_{\xi}^2 v_{1,\xi}^l + U_{12} c_{\xi} (d_{\xi}^* u_{2,\xi}^l - d_{\xi} v_{2,\xi}^l), \quad (4a)$$

$$E_l v_{1,\xi}^l = J_1 (v_{1,\xi-1}^l + v_{1,\xi+1}^l) + \mathcal{U}_1 v_{1,\xi}^l + U_{11} c_{\xi}^{*2} u_{1,\xi}^l - U_{12} c_{\xi}^* (d_{\xi} v_{2,\xi}^l - d_{\xi}^* u_{2,\xi}^l), \quad (4b)$$

$$E_l u_{2,\xi}^l = -J_2 (u_{2,\xi-1}^l + u_{2,\xi+1}^l) + \mathcal{U}_2 u_{2,\xi}^l - U_{22} d_{\xi}^2 v_{2,\xi}^l + U_{12} d_{\xi} (c_{\xi}^* u_{1,\xi}^l - c_{\xi} v_{1,\xi}^l), \quad (4c)$$

$$E_l v_{2,\xi}^l = J_2 (v_{2,\xi-1}^l + v_{2,\xi+1}^l) + \mathcal{U}_2 v_{2,\xi}^l + U_{22} d_{\xi}^{*2} u_{2,\xi}^l - U_{12} d_{\xi}^* (c_{\xi} v_{1,\xi}^l - c_{\xi}^* u_{1,\xi}^l), \quad (4d)$$

where $\mathcal{U}_1 = 2U_{11}(n_{1\xi}^c + \tilde{n}_{1\xi}) + U_{12}(n_{2\xi}^c + \tilde{n}_{2\xi}) + (\epsilon_\xi^{(1)} - \mu_1)$ and $\mathcal{U}_2 = 2U_{22}(n_{2\xi}^c + \tilde{n}_{2\xi}) + U_{12}(n_{1\xi}^c + \tilde{n}_{1\xi}) + (\epsilon_\xi^{(2)} - \mu_2)$ with $\underline{\mathcal{U}}_k = -\mathcal{U}_k$. To solve the above eigenvalue equation, we use a basis set of on-site Gaussian wave functions and define the quasiparticle amplitude as a linear combination of the basis functions. The condensate and noncondensate densities are then computed through the self-consistent solution of Eqs. (2) and (4). The noncondensate atomic density at the ξ th lattice site is

$$\tilde{n}_{k\xi} = \sum_l [(|u_{k\xi}^l|^2 + |v_{k\xi}^l|^2)N_0(E_l) + |v_{k\xi}^l|^2], \quad (5)$$

where $N_0(E_l) = (e^{\beta E_l} - 1)^{-1}$ with $\beta = (k_B T)^{-1}$ is the Bose-Einstein distribution factor of the l th quasiparticle mode with energy E_l at temperature T . The last term in $\tilde{n}_{k\xi}$ is independent of the temperature and, hence, represents the quantum fluctuations of the system. To examine the role of temperature we define the miscibility of the condensates in terms of the overlap integral

$$\Lambda = \frac{[\int n_1(\mathbf{r})n_2(\mathbf{r})d\mathbf{r}]^2}{[\int n_1^2(\mathbf{r})d\mathbf{r}][\int n_2^2(\mathbf{r})d\mathbf{r}]}. \quad (6)$$

Here, $n_k(\mathbf{r})$ is the total density of the k th condensate at position $\mathbf{r} \equiv (x, y)$. If the two condensates of the TBEC have complete overlap with each other, then the system is in the miscible phase with $\Lambda = 1$, whereas for the completely phase-separated case $\Lambda = 0$. Using Λ as a measure we identify the miscible and immiscible domains as a function of the temperature. As we use the coupled DNLSEs to describe the TBEC, our study is valid deep within the superfluid domain, and the mean-field description would begin to deviate from the true results near the superfluid–Mott-insulator phase transition. In this regime a full quantum description [70] would be the appropriate method, and the same applies to probing the nature of the quantum phase transition [71–74]. It is well established that for some parameter regimes, TBECs in optical lattices can be either the superfluid phase of both species or the superfluid phase of one species coexisting with the Mott-insulator phase of the other [75–78].

B. Field-field correlation function

To define a measure of the coherence in the condensate we introduce the first-order correlation function $g_k^{(1)}(\mathbf{r}, \mathbf{r}')$, which can be expressed as expectations of the products of field operators at different positions and times [79–82]. These are normalized to obtain the unit modulus in the case of perfect coherence or a system consisting of only condensate atoms. Here, we restrict ourselves to ordered spatial correlation functions at a fixed and equal time. In terms of the quantum Bose field operator $\hat{\Psi}_k$ the first-order spatial correlation function is

$$g_k^{(1)}(\mathbf{r}, \mathbf{r}') = \frac{\langle \hat{\Psi}_k^\dagger(\mathbf{r})\hat{\Psi}_k(\mathbf{r}') \rangle}{\sqrt{\langle \hat{\Psi}_k^\dagger(\mathbf{r})\hat{\Psi}_k(\mathbf{r}) \rangle \langle \hat{\Psi}_k^\dagger(\mathbf{r}')\hat{\Psi}_k(\mathbf{r}') \rangle}}, \quad (7)$$

where $\langle \dots \rangle$ represents thermal average. It is important to note that the local first-order correlation function is equal to the density, i.e., $g_k^{(1)}(\mathbf{r}, \mathbf{r}) = n_k(\mathbf{r})$. The expression of $g_k^{(1)}(\mathbf{r}, \mathbf{r}')$ can

also be written in terms of condensate and noncondensate density correlations as

$$g_k^{(1)}(\mathbf{r}, \mathbf{r}') = \frac{n_k^c(\mathbf{r}, \mathbf{r}') + \tilde{n}_k(\mathbf{r}, \mathbf{r}')}{\sqrt{n_k(\mathbf{r})n_k(\mathbf{r}')}}, \quad (8)$$

where

$$\begin{aligned} n_k^c(\mathbf{r}, \mathbf{r}') &= \psi_k^*(\mathbf{r})\psi_k(\mathbf{r}'), \\ \tilde{n}_k(\mathbf{r}, \mathbf{r}') &= \sum_l [\{u_k^{*l}(\mathbf{r})u_k^l(\mathbf{r}') + v_k^{*l}(\mathbf{r})v_k^l(\mathbf{r}')\}N_0(E_l) \\ &\quad + v_k^{*l}(\mathbf{r})v_k^l(\mathbf{r}')], \\ n_k(\mathbf{r}) &= n_k^c(\mathbf{r}) + \tilde{n}_k(\mathbf{r}) \end{aligned}$$

are the condensate density correlation, noncondensate density correlation, and total density of the k th species, respectively. In the above expressions, $n_k^c(\mathbf{r}, \mathbf{r}')$ and $\tilde{n}_k(\mathbf{r}, \mathbf{r}')$ are obtained by expanding the complex amplitudes (c_ξ, d_ξ) and the quasiparticle amplitudes ($u_{k,\xi}^l, v_{k,\xi}^l$) in the localized Gaussian basis. At $T = 0$ K, the entire condensate cloud has complete coherence, and therefore $g_k^{(1)} = 1$ within the condensate region. In TBECs, the transition from the phase-separated to the miscible domain at $T \neq 0$ has characteristic signatures in the spatial structure of $g_k^{(1)}(\mathbf{r}, \mathbf{r}')$.

C. Numerical methods

To solve the coupled DNLSEs, Eqs. (2), we scale and rewrite the equations in the dimensionless form. For this we choose the characteristic length scale as the lattice constant $a = \lambda_L/2$, with λ_L the wavelength of the laser which creates the lattice potential. Similarly, the recoil energy $E_R = \hbar^2 k_L^2/2m$, with m the atomic mass of the species and $k_L = 2\pi/\lambda_L$, is chosen as the energy scale of the system. We use the fourth-order Runge-Kutta method to solve these equations for zero as well as finite temperatures. To initiate the iterative steps to solve the equations appropriate initial guess values of c_ξ and d_ξ are chosen. For the present work we chose values corresponding to the side-by-side profile, as it gives quasiparticle energies which are real and not complex. This is important, as it shows that the solution we obtain is a stable one, and not a metastable one. The stationary ground-state wave function of the TBEC is obtained through imaginary-time propagation. In the tight-binding limit, the width of the orthonormalized Gaussian basis functions localized at each lattice site is $0.3a$. Furthermore, to study the quasiparticle excitation spectrum, we cast Eqs. (4) as matrix eigenvalue equations, and diagonalize the matrix using the routine ZGEEV from the LAPACK library [83]. For finite-temperature computations, to take into account thermal fluctuations, we solve the coupled equations, Eqs. (2) and Eqs. (4), self-consistently. The solution of the DNLSEs is iterated until it satisfies the convergence criteria in terms of the number of condensate and noncondensate atoms. In general, the convergence is not smooth, and most of the time we encounter severe oscillations in the number of atoms. To remedy these oscillations and attain convergence, we damp the solution using the successive overrelaxation (underrelaxation) technique while updating the condensate (noncondensate)

atoms. Thus, the new solutions after an iteration cycle (IC) are

$$c_{\xi,IC}^{\text{new}} = r^{\text{ov}} c_{\xi,IC} + (1 - r^{\text{ov}}) c_{\xi,IC-1}, \quad (9a)$$

$$d_{\xi,IC}^{\text{new}} = r^{\text{ov}} d_{\xi,IC} + (1 - r^{\text{ov}}) d_{\xi,IC-1}, \quad (9b)$$

$$\tilde{n}_{k\xi,IC}^{\text{new}} = r^{\text{un}} \tilde{n}_{k\xi,IC} + (1 - r^{\text{un}}) \tilde{n}_{k\xi,IC-1}, \quad (9c)$$

where $r^{\text{ov}} > 1$ ($r^{\text{un}} < 1$) is the overrelaxation (underrelaxation) parameter. The choice of r^{ov} and r^{un} depend on the temperature and interaction parameters. In general, our observation is that the oscillations are more prominent at higher temperatures, and hence, lower values of r^{ov} and r^{un} must be chosen. This in turn implies that it takes a larger number of iterations to get converged solutions at higher temperatures.

III. RESULTS AND DISCUSSION

To examine the effects of thermal fluctuations on the quasiparticle spectra we consider the ^{87}Rb - ^{85}Rb TBEC with ^{87}Rb labeled species 1 and ^{85}Rb labeled species 2. The radial trapping frequencies of the harmonic potential are $\omega_x = \omega_y = \omega_{\perp} = 2\pi \times 50$ Hz with the anisotropy parameter $\omega_z/\omega_{\perp} = 20.33$, and these parameters are chosen based on the experimental work of Gadway and collaborators [34] on the TBEC of two hyperfine states of ^{87}Rb in optical lattices. It is important to note that we consider equal background trapping potentials for species 1 and 2. We emphasize here that the results are equally applicable to the case of the TBEC consisting of two hyperfine states of ^{87}Rb , however, we have chosen ^{87}Rb - ^{85}Rb to highlight that the small mass difference has no influence on the geometry of the ground state. The laser wavelength used to create the 2D lattice potential and the lattice depth are $\lambda_L = 1064$ nm and $V_0 = 5E_R$, respectively. We then take the total number of atoms as $N_1 = N_2 = 100$ confined in a 40×40 quasi-2D lattice system. It must be mentioned that the number of lattice sites considered is much larger than the spatial extent of the condensate cloud. Although the computations require a longer time with the larger lattice size, we chose it to ensure that the spatial extent of the thermal component is confined well within the lattice considered. The tunneling matrix elements are $J_1 = 0.66E_R$ and $J_2 = 0.71E_R$, which correspond to an optical lattice potential with a depth of $5E_R$. The intraspecies and interspecies on-site interactions are set as $U_{11} = 0.07E_R$, $U_{22} = 0.02E_R$, and $U_{12} = 0.15E_R$, respectively. For this set of parameters the ground-state density distribution of ^{87}Rb - ^{85}Rb TBEC is phase separated with side-by-side geometry. This is a symmetry-broken profile where one species is placed to the left and the other to the right of the trap center along the y axis. The evolution of the ground state from the miscible to the side-by-side density profile due to a decrease in the U_{22} is reported in our previous work [37]. In the present work, we demonstrate the role of temperature in the phase-separated domain of the binary condensate.

A. Zero temperature

At zero temperature, in the phase-separated domain, the energetically preferable ground state of TBEC is the side-by-side geometry, which is reported in our previous work [37].

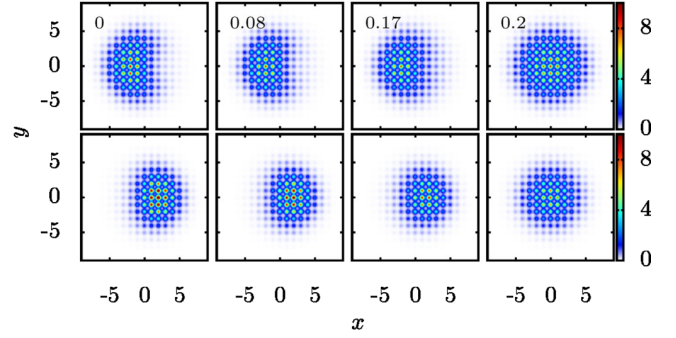


FIG. 1. Density distribution for the condensate atoms of ^{87}Rb - ^{85}Rb TBEC as a function of the temperature T/T_c . Density profiles of the ^{87}Rb (upper panel) and ^{85}Rb species (lower panel) are shown for $T/T_c = 0, 0.08, 0.17$, and 0.2 . In the phase-separated domain, the condensate density has side-by-side geometry at zero temperature, and as the temperature is increased, there is a transition to the miscible domain or the densities completely overlap at $T_{\text{ch}} = 0.185T_c$. Here x and y are measured in units of the lattice constant a .

Unlike in the 1D system [36] in the quasi-2D system the presence of the quantum fluctuations does not alter the ground state. For the parameters chosen the ^{87}Rb - ^{85}Rb TBEC is phase separated, and the overlap integral has the value $\Lambda = 0.10$. The density distributions of the condensate and noncondensate atoms of the two species at zero temperature are shown in Fig. 1 and Fig. 2. This is a symmetry-broken side-by-side geometry with noncondensate atoms more localized at the edges of the condensate along the y axis.

B. Finite temperatures

At $T \neq 0$, in addition to the quantum fluctuations, which are present at zero temperature, the thermal cloud also contributes to the noncondensate density. As shown in Figs. 1 and 2, at $T/T_c = 0.08$, the condensate density profiles of both species begin to overlap or, in other words, the two species are partly

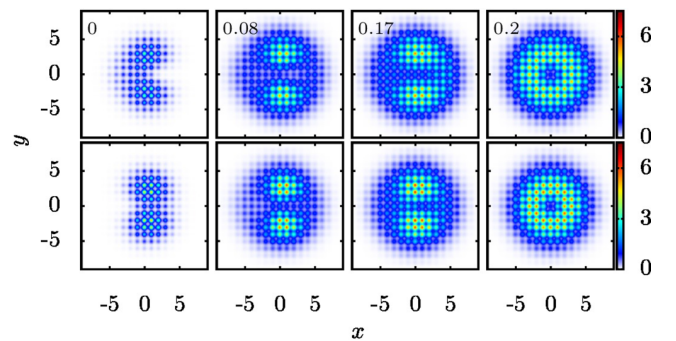


FIG. 2. Density distribution for the noncondensate atoms of ^{87}Rb - ^{85}Rb TBEC as a function of the temperature T/T_c . The noncondensate density of the ^{87}Rb (upper panel) and ^{85}Rb (lower panel) species are shown for $T/T_c = 0, 0.08, 0.17$, and 0.2 . Noncondensate atoms which are localized at the edges acquire rotational symmetry in the miscible phase, which happens at $T_{\text{ch}} = 0.185T_c$ as the temperature is increased. Here x and y are measured in units of the lattice constant a .

miscible. This is also evident from the value of $\Lambda = 0.16$, which shows a marginal increase compared to the value of 0.10 at zero temperature. In the figures, the temperature is defined in units of the critical temperature T_c of ^{87}Rb atoms, which for the parameters considered is 338 nK based on our finite-temperature computations. This value of T_c is consistent with the analytic expression for an ideal Bose gas in an optical lattice [84],

$$T_c = \frac{m\omega^2 a^2}{2\pi k_B} \left[\frac{N_k}{\zeta(3/2)} \right]^{2/3}, \quad (10)$$

where ω is the geometric mean of the three oscillator frequencies, N_k is the number of atoms of the k th species and $\zeta(3/2) = 2.612$ is the Riemann zeta function. In the presence of the harmonic confinement, the repulsive interatomic interaction reduces the density at the trap center and hence decreases T_c [84]. Upon a further increase in temperature, at $T/T_c = 0.18$, $\Lambda = 0.36$, this indicates an increase in the miscibility of the two species. Another important feature at $T/T_c = 0.08$ and 0.18 is the localization of the noncondensate atoms at the interface. This is due to repulsion from the condensate atoms and the lower thermal energy, which is insufficient to overcome this repulsion energy. The transition to the miscible domain occurs when the temperature exceeds the characteristic temperature

$$T_{\text{ch}} \approx \frac{\sqrt{n_{1\text{max}} n_{2\text{max}}} U_{12}}{k_B}, \quad (11)$$

where $n_{k\text{max}}$ is the maximum density of the k th species. At higher temperatures, the extent of overlap between the condensate density profiles increases, and the TBEC is completely miscible at $T_{\text{ch}} = 0.185T_c \approx 63$ nK. This is reflected in the value of $\Lambda = 0.95$, and the condensate as well as the noncondensate densities acquire rotational symmetry. The T_{ch} at which this transition occurs corresponds to the thermal energy $k_B T_{\text{ch}} = 0.72E_R$, which is comparable to the interspecies interaction energy of $0.66E_R$. Albeit, we discuss in detail the results for the parameters mentioned earlier, we find similar trends in the immiscible-miscible transition for different values of J 's and U 's. As is to be expected the only change is that the T_{ch} is lowered at a higher J . This is due to the higher kinetic energy associated with a higher J ; hence the atoms require less thermal energy to overcome the interspecies repulsion energy for the transition to the miscible phase. In terms of the interaction energies, the lower value of U_{kk} and higher value of U_{12} increase the T_{ch} of the TBEC.

The transition from the phase-separated to the miscible domain can further be examined from the evolution of the quasiparticle modes as a function of the temperature. The evolution of the few low-lying mode energies with temperature is shown in Fig. 3, where the temperature is defined in units of T_c . It is evident from the figure that there are mode energy bifurcations with the increase in temperature. These are associated with the restoration of rotational symmetry when the TBEC is rendered miscible through an increase in the temperature.

As is to be expected the two lowest energy modes are the zero-energy or the Goldstone modes, which are the result of the spontaneous symmetry breaking associated with

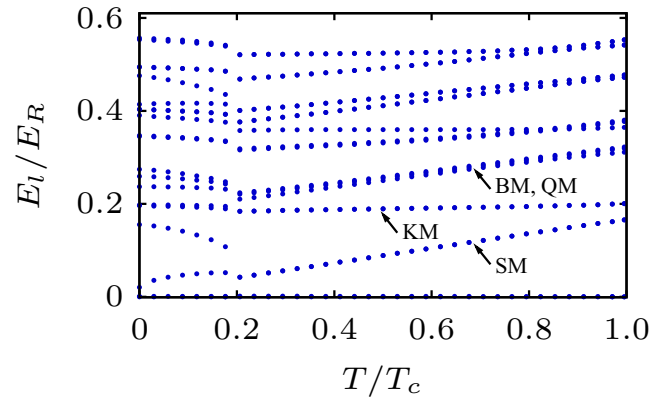


FIG. 3. Evolution of the excitation energies of the low-lying quasiparticle modes as a function of the temperature in ^{87}Rb - ^{85}Rb TBEC. The slosh and some of the other higher energy modes become degenerate at $T_{\text{ch}} = 0.185T_c$, where the density distribution is transformed from phase-separated to the miscible profile. In the plot, the slosh mode (SM), Kohn mode (KM), breathing mode (BM), and quadrupole mode (QM) are shown by the black arrows. Here, the excitation energy E_l and the temperature T are scaled with respect to the recoil energy E_R and the critical temperature T_c of the ^{87}Rb species, respectively.

condensation. In the phase-separated domain, these modes correspond to one each for each of the species. The first two excited modes are the nondegenerate Kohn or slosh modes of the two species, and these remain nondegenerate in the domain $T < T_{\text{ch}}$. The structures of these modes are shown in Figs. 4 and 5. When $T \geq T_{\text{ch}}$ as the TBEC acquires rotational symmetry, the slosh modes become degenerate with $\pi/2$ rotation. A key feature in the quasiparticle mode evolution is that the energy of all the out-of-phase modes increases for $T \geq T_{\text{ch}}$, whereas all the in-phase modes remain steady. Here, out-of-phase and in-phase means that the amplitudes u_1 and

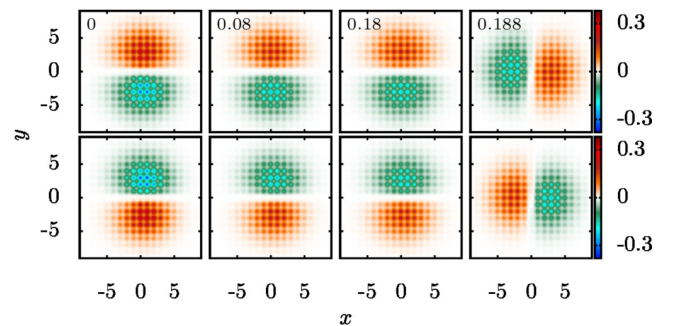


FIG. 4. Quasiparticle mode function of the first excited mode (slosh mode) as a function of the temperature for the ^{87}Rb - ^{85}Rb TBEC. The mode functions corresponding to the ^{87}Rb and ^{85}Rb species are shown in the upper and lower panels, respectively. The slosh mode is an out-of-phase mode where the density flows of the two species are in opposite directions. As the TBEC acquires rotational symmetry at $T_{\text{ch}} = 0.185T_c$, the slosh mode is rotated by an angle $\pi/2$ for $T/T_c \geq 0.185$. The value of T/T_c is shown in the top-left corner of each plot in the upper panel. The spatial coordinates x and y are in units of the lattice constant a .

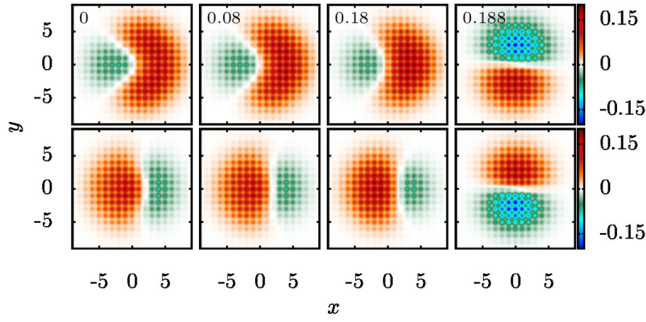


FIG. 5. Quasiparticle mode function corresponding to the second excited mode (slosh mode), which becomes degenerate with the first excited mode for $T/T_c \geq 0.185$. The mode functions of the ^{87}Rb and ^{85}Rb species are shown in the upper and lower panels, respectively. The value of T/T_c is shown in the top-left corner of each plot in the upper panel. Here x and y are in units of the lattice constant a .

u_2 of a quasiparticle are of different and the same phases, respectively. Among the low-energy modes, the Kohn mode is in-phase, whereas the breathing and quadrupole modes are out-of-phase in nature. One unique feature of the TBEC in the immiscible phase is the presence of interface modes; these have amplitudes prominent around the interface region. The existence of these modes is reported in our previous work [37] and was investigated in other works [85,86] for TBECs confined in a harmonic potential alone at zero temperature. As an example, one of the low-energy interface modes is shown in Fig. 6. It is evident from the figure that the mode is out-of-phase in nature, and it is transformed into the breathing mode in the miscible domain when $T \geq T_{\text{ch}}$. In the miscible domain, the breathing mode becomes degenerate with the quadrupole mode and gains energy. The quasiparticles of the miscible domain have a well-defined azimuthal quantum number, and modes undergo rotations as T is increased further.

To gain additional insight into the immiscible-miscible transition, we consider other TBECs. In particular, we consider

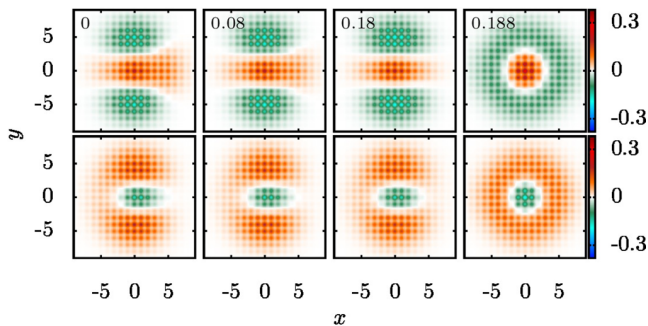


FIG. 6. The quasiparticle mode function corresponding to the interface mode in the phase-separated domain of ^{87}Rb - ^{85}Rb TBEC as a function of the temperature. This is an out-of-phase mode and the mode function is more prominent at the interface region between the condensates. For $T/T_c \geq 0.185$, when the TBEC acquires rotational symmetry, this mode is transformed into the out-of-phase breathing mode, where the mode functions are radially symmetric. The value of T/T_c is shown in the top-left corner of each plot in the upper panel. Here x and y are in units of the lattice constant a .

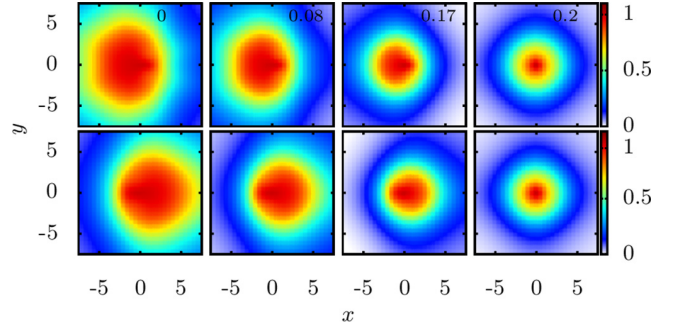


FIG. 7. Normalized first-order spatial correlation function $g_k^{(1)}(0,\mathbf{r})$ for ^{87}Rb (upper panel) and ^{85}Rb (lower panel) species at $T/T_c = 0, 0.08, 0.17,$ and 0.2 . Here x and y are measured in units of the lattice constant a .

Rb-Cs and Rb-K TBECs confined in quasi-2D optical lattices. The details of the parameters chosen and discussion are given in the Appendix. Starting from the immiscible domain we analyze the ground state and the quasiparticle mode evolution with increasing temperature. Based on the results we observe that the trend in the evolution of low-lying quasiparticle modes with the temperature is qualitatively similar to that of the ^{87}Rb - ^{85}Rb TBEC. The condensate density profiles also exhibit the same trend of transformation from immiscible side-by-side geometry to the rotationally symmetric miscible profile. As is to be expected, the value of T_{ch} depends on the mass ratio; this is due to the mass dependence of the interaction energy. In particular, for Rb-Cs and Rb-K TBECs, the T_{ch} values are $0.62T_c$ and $0.53T_c$, respectively. The thermal energies corresponding to these temperatures are $2.15E_R$ and $2.80E_R$, respectively. These are comparable to the interaction energies of the TBECs, which are $1.97E_R$ and $2.84E_R$, respectively. Here T_c is the critical temperature of condensation for the species with the lower value. In addition to the atomic mass of the condensates, as mentioned earlier, the immiscible-miscible transition also depends on the lattice parameters U and J . For these two TBECs also we have examined the density distributions with variation in the U and J parameters. We find similar trends in the value of T_{ch} as in the ^{87}Rb - ^{85}Rb TBEC. That is, a decrease in T_{ch} with an increase in J and an increase with lower and higher values of U_{kk} and U_{12} , respectively.

To investigate the spatial coherence of TBEC at equilibrium, we examine the trends in $g_k^{(1)}(0,\mathbf{r})$ defined earlier in Eq. (8) and shown in Fig. 7 for various temperatures. As mentioned earlier, at zero temperature, $n_k(\mathbf{r}) \approx n_k^c(\mathbf{r})$ has complete phase coherence, and therefore, $g_k^{(1)} = 1$ within the spatial extent of the condensates; this is shown in Fig. 7. At zero temperature or in the limit $\tilde{n}_k \equiv 0$ the correlation function, Eq. (8), resembles a Heaviside function, and the negligible contribution from the quantum fluctuations smooths out the sharp edges as $g_k^{(1)}$ drops to 0. More importantly, in the numerical computations this causes a loss of numerical accuracy, as it involves the division of two small numbers in Eq. (8) [87]. However, at a finite temperature the presence of noncondensate atoms modifies the nature of the spatial coherence present in the system. The decay rate of the correlation function increases with the temperature, and this

is evident in Fig. 7, which shows $g_k^{(1)}(0, \mathbf{r})$ at $T/T_c = 0.08$, 0.17, and 0.2. In addition to this, the transition from the phase-separated to the miscible TBEC is also reflected in the decay trends of $g_k^{(1)}(0, \mathbf{r})$.

IV. CONCLUSIONS

We have examined finite-temperature effects on the phenomenon of phase separation in TBECs confined in quasi-2D optical lattices. As the temperature is increased the phase-separated side-by-side ground-state geometry is transformed into the miscible phase. For the case of the TBEC comprised of ^{87}Rb and ^{85}Rb , the transformation occurs at the characteristic temperature. This demonstrates the importance of thermal fluctuations, which can make TBECs miscible. Based on the present work, in general, the TBEC undergoes the transition to the miscible phase at a characteristic temperature T_{ch} . This corresponds to the temperature at which the thermal energy overcomes the interspecies repulsion energy $\sqrt{n_{1\text{max}}n_{2\text{max}}}U_{12}$. The other key observation is that the transition from the phase-separated domain to the miscible domain is associated with a change in the nature of the quasiparticle energies. Low-lying out-of-phase modes, in particular, the slosh mode, become degenerate and increase in energy. On the other hand, in-phase modes, such as the Kohn mode, remain steady as the temperature ($T < T_c$) is increased. Interface modes, which are unique to the phase-separated domain, in addition to changing in energy are geometrically transformed into rotationally symmetric breathing modes in the miscible domain. The temperature-driven immiscible-to-miscible transition is also evident in the profile of the correlation functions.

ACKNOWLEDGMENTS

We thank A. Roy, S. Gautam, S. Bandyopadhyay, and R. Bai for useful discussions. The results presented in the paper are based on computations using Vikram-100, the 100TFLOP HPC Cluster at Physical Research Laboratory, Ahmedabad, India.

APPENDIX

Here, we provide brief descriptions of the computations pertaining to the Rb-Cs and Rb-K TBECs confined in quasi-2D optical lattices.

1. ^{87}Rb - ^{133}Cs TBEC

We consider a ^{87}Rb - ^{133}Cs TBEC containing 100 atoms of each species confined in a 40×40 quasi-2D optical lattice with a 1064-nm wavelength of the laser beams. The lower number of atoms is chosen to improve the convergence of finite-temperature computations, and at the same time it is sufficient to provide a good description of the superfluid phase of the TBECs. The radial trapping frequencies are $\omega_x = \omega_y = \omega_{\perp} = 2\pi \times 50$ Hz, with the anisotropy parameter 20.33 [34]. The tunneling matrix elements are $J_1 = 0.66E_R$ and $J_2 = 1.70E_R$, corresponding to a depth of the optical lattice $V_0 = 5E_R$. The lattice depth is considered such that the tight-binding limit, $V_0 \gg \mu_k$, is valid. The large difference in the values of J_k is due to the large mass difference between the atoms of the two species. The intraspecies and interspecies on-site interactions considered are $U_{11} = 0.96E_R$, $U_{22} = 0.42E_R$, and $U_{12} = 1.2E_R$. These DNLSE parameters are derived from the intra- and interspecies scattering lengths of the species, the trap parameters, and the width of the Gaussian basis, which is $0.3a$. At zero temperature, the ground state of the TBEC has side-by-side geometry with $\Lambda = 0$ [37]. As in the case of ^{87}Rb - ^{85}Rb , as the temperature of the TBEC is increased ($T < T_c$), the system is transformed into the miscible phase. In addition, we have observed a bifurcation in the energy of the slosh mode, and the mode becomes degenerate with a discontinuity in the quasiparticle spectra at $T_{\text{ch}} = 0.62T_c \approx 140$ nK.

2. ^{87}Rb - ^{41}K TBEC

In the case of the ^{87}Rb - ^{41}K TBEC, the wavelength of the laser beams and the number of atoms are considered the same as in the case of the ^{87}Rb - ^{133}Cs TBEC. The radial trapping frequencies are $\omega_x = \omega_y = \omega_{\perp} = 2\pi \times 100$ Hz, with the anisotropy parameter 1.40 [88]. The tunneling matrix elements are $J_1 = 0.66E_R$ and $J_2 = 2.84E_R$, corresponding to a $5E_R$ lattice depth. The intraspecies and interspecies on-site interactions considered are $U_{11} = 0.20E_R$, $U_{22} = 0.06E_R$, and $U_{12} = 0.60E_R$. The set of parameters is chosen such that the density profile of the TBEC is immiscible and has side-by-side geometry at zero temperature. As in the previous cases, the geometry of the TBEC is transformed from the side-by-side type to the rotationally symmetric overlapping profile and the slosh mode becomes degenerate at $T_{\text{ch}} = 0.53T_c \approx 278$ nK.

-
- [1] D. Jaksch, C. Bruder, J. I. Cirac, C. W. Gardiner, and P. Zoller, *Phys. Rev. Lett.* **81**, 3108 (1998).
 - [2] C. Orzel, A. K. Tuchman, M. L. Fenselau, M. Yasuda, and M. A. Kasevich, *Science* **291**, 2386 (2001).
 - [3] M. Greiner, O. Mandel, T. Esslinger, T. W. Hänsch, and I. Bloch, *Nature (London)* **415**, 39 (2002).
 - [4] I. Bloch, J. Dalibard, and S. Nascimbène, *Nat. Phys.* **8**, 267 (2012).
 - [5] E. Demler and F. Zhou, *Phys. Rev. Lett.* **88**, 163001 (2002).
 - [6] A. B. Kuklov and B. V. Svistunov, *Phys. Rev. Lett.* **90**, 100401 (2003).
 - [7] A. Kuklov, N. Prokof'ev, and B. Svistunov, *Phys. Rev. Lett.* **92**, 050402 (2004).
 - [8] A. Pal and D. A. Huse, *Phys. Rev. B* **82**, 174411 (2010).
 - [9] S. Choi and L. Radzihovsky, *Phys. Rev. A* **84**, 043612 (2011).
 - [10] H.-F. Lin, H.-D. Liu, H.-S. Tao, and W.-M. Liu, *Sci. Rep.* **5**, 9810 (2015).
 - [11] O. Jürgensen, K. Sengstock, and D.-S. Lühmann, *Sci. Rep.* **5**, 12912 (2015).
 - [12] S. Trotzky, P. Cheinet, S. Fölling, M. Feld, U. Schnorrberger, A. M. Rey, A. Polkovnikov, E. A. Demler, M. D. Lukin, and I. Bloch, *Science* **319**, 295 (2008).

- [13] J. Simon, W. S. Bakr, R. Ma, M. E. Tai, P. M. Preiss, and M. Greiner, *Nature (London)* **472**, 307 (2011).
- [14] I. Bloch, *Nature (London)* **453**, 1016 (2008).
- [15] M. Lewenstein, A. Sanpera, V. Ahufinger, B. Damski, A. Sen(De), and U. Sen, *Adv. Phys.* **56**, 243 (2007).
- [16] I. Bloch, J. Dalibard, and W. Zwerger, *Rev. Mod. Phys.* **80**, 885 (2008).
- [17] T. Mishra, R. V. Pai, and B. P. Das, *Phys. Rev. A* **76**, 013604 (2007).
- [18] F. Zhan and I. P. McCulloch, *Phys. Rev. A* **89**, 057601 (2014).
- [19] M. Greiner, I. Bloch, O. Mandel, T. W. Hänsch, and T. Esslinger, *Phys. Rev. Lett.* **87**, 160405 (2001).
- [20] T. Roscilde and J. I. Cirac, *Phys. Rev. Lett.* **98**, 190402 (2007).
- [21] P. Buonsante, S. M. Giampaolo, F. Illuminati, V. Penna, and A. Vezzani, *Phys. Rev. Lett.* **100**, 240402 (2008).
- [22] G. Ceccarelli, J. Nespolo, A. Pelissetto, and E. Vicari, *Phys. Rev. A* **92**, 043613 (2015).
- [23] G. Ceccarelli, J. Nespolo, A. Pelissetto, and E. Vicari, *Phys. Rev. A* **93**, 033647 (2016).
- [24] T.-L. Ho and V. B. Shenoy, *Phys. Rev. Lett.* **77**, 3276 (1996).
- [25] E. Timmermans, *Phys. Rev. Lett.* **81**, 5718 (1998).
- [26] B. D. Esry and C. H. Greene, *Phys. Rev. A* **59**, 1457 (1999).
- [27] L. Wen, W. M. Liu, Y. Cai, J. M. Zhang, and J. Hu, *Phys. Rev. A* **85**, 043602 (2012).
- [28] S. B. Papp, J. M. Pino, and C. E. Wieman, *Phys. Rev. Lett.* **101**, 040402 (2008).
- [29] S. Tojo, Y. Taguchi, Y. Masuyama, T. Hayashi, H. Saito, and T. Hirano, *Phys. Rev. A* **82**, 033609 (2010).
- [30] D. J. McCarron, H. W. Cho, D. L. Jenkin, M. P. Köppinger, and S. L. Cornish, *Phys. Rev. A* **84**, 011603 (2011).
- [31] G. V. Chester, *Phys. Rev.* **100**, 446 (1955).
- [32] M. D. Miller, *Phys. Rev. B* **18**, 4730 (1978).
- [33] J. Catani, L. De Sarlo, G. Barontini, F. Minardi, and M. Inguscio, *Phys. Rev. A* **77**, 011603 (2008).
- [34] B. Gadway, D. Pertot, R. Reimann, and D. Schneble, *Phys. Rev. Lett.* **105**, 045303 (2010).
- [35] P. Soltan-Panahi, J. Struck, P. Hauke, A. Bick, W. Plenkers, G. Meineke, C. Becker, P. Windpassinger, M. Lewenstein, and K. Sengstock, *Nat. Phys.* **7**, 434 (2011).
- [36] K. Suthar, A. Roy, and D. Angom, *Phys. Rev. A* **91**, 043615 (2015).
- [37] K. Suthar and D. Angom, *Phys. Rev. A* **93**, 063608 (2016).
- [38] F. Lingua, M. Guglielmino, V. Penna, and B. Capogrosso Sansone, *Phys. Rev. A* **92**, 053610 (2015).
- [39] P. N. Galteland, E. Babaev, and A. Sudbø, *New J. Phys.* **17**, 103040 (2015).
- [40] O. E. Alon, A. I. Streltsov, and L. S. Cederbaum, *Phys. Rev. Lett.* **97**, 230403 (2006).
- [41] O. E. Alon, A. I. Streltsov, and L. S. Cederbaum, *Phys. Rev. A* **76**, 013611 (2007).
- [42] O. E. Alon, A. I. Streltsov, and L. S. Cederbaum, *Phys. Rev. A* **76**, 062501 (2007).
- [43] O. E. Alon, A. I. Streltsov, and L. S. Cederbaum, *Phys. Rev. A* **77**, 033613 (2008).
- [44] L. S. Cederbaum, A. I. Streltsov, Y. B. Band, and O. E. Alon, *Phys. Rev. Lett.* **98**, 110405 (2007).
- [45] P. Öhberg, *Phys. Rev. A* **61**, 013601 (1999).
- [46] H. Shi, W.-M. Zheng, and S.-T. Chui, *Phys. Rev. A* **61**, 063613 (2000).
- [47] K. Nho and D. P. Landau, *Phys. Rev. A* **76**, 053610 (2007).
- [48] A. Roy and D. Angom, *Phys. Rev. A* **92**, 011601 (2015).
- [49] N. P. Proukakis, *Phys. Rev. A* **74**, 053617 (2006).
- [50] S. Dettmer, D. Hellweg, P. Ryytty, J. J. Arlt, W. Ertmer, K. Sengstock, D. S. Petrov, G. V. Shlyapnikov, H. Kreutzmann, L. Santos, and M. Lewenstein, *Phys. Rev. Lett.* **87**, 160406 (2001).
- [51] D. Hellweg, L. Cacciapuoti, M. Kottke, T. Schulte, K. Sengstock, W. Ertmer, and J. J. Arlt, *Phys. Rev. Lett.* **91**, 010406 (2003).
- [52] S. Richard, F. Gerbier, J. H. Thywissen, M. Hugbart, P. Bouyer, and A. Aspect, *Phys. Rev. Lett.* **91**, 010405 (2003).
- [53] J. Esteve, J.-B. Trebbia, T. Schumm, A. Aspect, C. I. Westbrook, and I. Bouchoule, *Phys. Rev. Lett.* **96**, 130403 (2006).
- [54] T. Plisson, B. Allard, M. Holzmann, G. Salomon, A. Aspect, P. Bouyer, and T. Bourdel, *Phys. Rev. A* **84**, 061606 (2011).
- [55] O. Penrose and L. Onsager, *Phys. Rev.* **104**, 576 (1956).
- [56] E. A. Burt, R. W. Ghrist, C. J. Myatt, M. J. Holland, E. A. Cornell, and C. E. Wieman, *Phys. Rev. Lett.* **79**, 337 (1997).
- [57] B. Laburthe Tolra, K. M. O'Hara, J. H. Huckans, W. D. Phillips, S. L. Rolston, and J. V. Porto, *Phys. Rev. Lett.* **92**, 190401 (2004).
- [58] M. L. Chiofalo, M. Polini, and M. P. Tosi, *Eur. Phys. J. D* **11**, 371 (2000).
- [59] A. Smerzi and A. Trombettoni, *Phys. Rev. A* **68**, 023613 (2003).
- [60] M. P. A. Fisher, P. B. Weichman, G. Grinstein, and D. S. Fisher, *Phys. Rev. B* **40**, 546 (1989).
- [61] E. Lundh and J.-P. Martikainen, *Phys. Rev. A* **85**, 023628 (2012).
- [62] P. P. Hofer, C. Bruder, and V. M. Stojanović, *Phys. Rev. A* **86**, 033627 (2012).
- [63] A. Griffin, *Phys. Rev. B* **53**, 9341 (1996).
- [64] A. M. Rey, Ph.D. thesis, University of Maryland, 2004.
- [65] N. Elstner and H. Monien, *Phys. Rev. B* **59**, 12184 (1999).
- [66] S. Wessel, F. Alet, M. Troyer, and G. G. Batrouni, *Phys. Rev. A* **70**, 053615 (2004).
- [67] B. Capogrosso-Sansone, Ş. G. Söyler, N. Prokof'ev, and B. Svistunov, *Phys. Rev. A* **77**, 015602 (2008).
- [68] F. Gerbier, *Phys. Rev. Lett.* **99**, 120405 (2007).
- [69] E. Toth and P. B. Blakie, *Phys. Rev. A* **83**, 021601 (2011).
- [70] S. Klaiman, A. I. Streltsov, and O. E. Alon, *Chem. Phys.* **482**, 362 (2017).
- [71] W. Krauth, M. Caffarel, and J.-P. Bouchaud, *Phys. Rev. B* **45**, 3137 (1992).
- [72] V. A. Kashurnikov and B. V. Svistunov, *Phys. Rev. B* **53**, 11776 (1996).
- [73] M. Capello, F. Becca, M. Fabrizio, and S. Sorella, *Phys. Rev. Lett.* **99**, 056402 (2007).
- [74] S. Ramanan, T. Mishra, M. S. Luthra, R. V. Pai, and B. P. Das, *Phys. Rev. A* **79**, 013625 (2009).
- [75] V. A. Kashurnikov, N. V. Prokof'ev, and B. V. Svistunov, *Phys. Rev. A* **66**, 031601 (2002).
- [76] A. Isacson, M.-C. Cha, K. Sengupta, and S. M. Girvin, *Phys. Rev. B* **72**, 184507 (2005).
- [77] R. A. Barankov, C. Lannert, and S. Vishveshwara, *Phys. Rev. A* **75**, 063622 (2007).
- [78] K. Mitra, C. J. Williams, and C. A. R. Sá de Melo, *Phys. Rev. A* **77**, 033607 (2008).
- [79] R. J. Glauber, *Phys. Rev.* **131**, 2766 (1963).
- [80] M. Naraschewski and R. J. Glauber, *Phys. Rev. A* **59**, 4595 (1999).
- [81] A. Bezett, E. Toth, and P. B. Blakie, *Phys. Rev. A* **77**, 023602 (2008).
- [82] A. Bezett and E. Lundh, *J. Phys. B* **45**, 205301 (2012).

- [83] E. Anderson, Z. Bai, C. Bischof, S. Blackford, J. Demmel, J. Dongarra, J. D. Croz, A. Greenbaum, S. Hammarling, A. McKenney, and D. Sorensen, *LAPACK Users' Guide*, 3rd ed. (Society for Industrial and Applied Mathematics, Philadelphia, PA, 1999).
- [84] D. Baillie and P. B. Blakie, *Phys. Rev. A* **80**, 031603 (2009).
- [85] C. Ticknor, *Phys. Rev. A* **88**, 013623 (2013).
- [86] C. Ticknor, *Phys. Rev. A* **89**, 053601 (2014).
- [87] C. Gies and D. A. W. Hutchinson, *Phys. Rev. A* **70**, 043606 (2004).
- [88] G. Thalhammer, G. Barontini, L. De Sarlo, J. Catani, F. Minardi, and M. Inguscio, *Phys. Rev. Lett.* **100**, 210402 (2008).

